Titre: Title:	A staggered control volume finite element method for turbulent reacting flows coupled with radiation
Auteur: Author:	Fanli Meng
Date:	1994
Type:	Mémoire ou thèse / Dissertation or Thesis
Référence: Citation:	Meng, F. (1994). A staggered control volume finite element method for turbulent reacting flows coupled with radiation [Thèse de doctorat, École Polytechnique de Montréal]. PolyPublie. https://publications.polymtl.ca/33016/

UNIVERSITE DE MONTREAL

A STAGGERED CONTROL VOLUME FINITE ELEMENT METHOD FOR TURBULENT REACTING FLOWS COUPLED WITH RADIATION

par

Fanli MENG
DEPARTEMENT DE GENIE MECANIQUE
ECOLE POLYTECHNIQUE

THESE PRESENTEE EN VUE DE L'OBTENTION
DU GRADE DE PHILOSOPHIAE DOCTOR (Ph.D.)
(GENIE MECANIQUE)
Juillet 1994

ISBN 0-315-97147-9

UNIVERSITE DE MONTREAL

ECOLE POLYTECHNIQUE

Cette thèse intitulée:

A STAGGERED CONTROL VOLUME FINITE ELEMENT METHOD FOR TURBULENT REACTING FLOWS COUPLED WITH RADIATION

présentée par: Fanli MENG

en vue de l'obtention du grade de: Philosophiae Doctor (Ph.D.)

a été dûment acceptée par le jury d'examen constitué de:

M. PELLETIER, Dominique, Ph.D., président

M. CAMARERO, Ricardo, Ph.D., membre et directeur de recherche

M. REGGIO, Marcelo, Ph.D., membre et co-directeur de recherche

M. GARON, André, Ph.D., membre interne

M. DE CHAMPLAIN, Alain, Ph.D., membre externe

Sommaire

Dans cette thèse, nous cherchons à modéliser numériquement les phénomènes de combustion dans les chambres de combustion et les brûleurs. Un nouveau schéma numérique a alors été proposé, développé puis testé pour la simulation d'écoulements bidimensionels cartésiens ou axisymétriques de fluides visqueux incompressibles en régime laminaire ou turbulent. En outre, le milieu peut être réactif ou non et éventuellement sujet à la radiation. En effet, la combustion implique les phénomènes physiques suivants: turbulence, réactions chimiques dans la flamme et transferts de chaleur par convection et radiation dus aux produits de combustion. Ces phénomènes sont gouvernés par des équations générales de conservation dont les solutions analytiques ne sont pas triviales.

L'intérêt manifesté à la simulation numérique des phénomènes de combustion est dû à la recherche accrue de l'efficacité dans la conception des brûleurs et des chambres de combustion et au besoin de contrôler la pollution. En outre, la présence sur le marché d'ordinateurs plus performants et moins chers a fait de la simulation numérique une alternative plus intéressante que l'étude expérimentale.

La base de toute la simulation numérique repose sur une bonne modélisation de l'écoulement. Pour ce faire, il est nécessaire d'utiliser une formulation appropriée de l'équation de convection-diffusion. Le problème réside alors dans la satisfaction de la contrainte d'incompressibilité ou encore le couplage vitesse-pression quand la formulation en variables primitives est utilisée.

Dans cette étude, une nouvelle méthode numérique, appelée "Staggered Control Volume Finite Element Method (SCVFEM)" est proposée et développée. C'est une méthode de volumes finis basée sur la notion de maillage décalé qui utilise la formulation en variables primitives (u,v,p). La discrétisation du domaine se fait suivant

un maillage non structuré formé de triangles à trois noeuds. Dans cette méthode, la pression est constante par élément alors que les vitesses sont stockées ou bien aux milieux des côtés ou bien aux sommets du triangle. L'élément de base utilisé ici est un élément à ordres inégaux (vitesse linéaire et pression constante). Ils est équivalent à l'élément P1 non conforme/P0 et à l'élément P1/P0 répertoriés par la méthode des éléments finis.

La méthode SCVFEM peut être considérée comme une extension de la notion de maillage décalé aux maillages non structurés. Comme nous considérons deux façons de stocker les vitesses (et toutes les autres fonctions scalaires), la volume de contrôle pour l'équation de mouvement (et toute les autre équations de transport) sera désigné par Co-Volume ou par Volume de contrôle Polygonal suivant que les vitesses sont stockées aux milieux des côtés ou aux sommets des triangles. Ainsi, la Co-Volume est construit en joignant les centroïdes des deux triangles voisins avec les extrémités de leur côté commun où la vitesse est stockée. Par ailleurs, le volume de contrôle polygonal autour de chaque sommet est obtenu en joignant les centroïdes des triangles voisins avec les milieux des côté voisins correspondants.

Les fonctions d'interpolation utilisées dans chaque élément sont la fonction exponentielle basée sur l'orientation de l'écoulement et la fonction de pondération par la masse qui utilise la différenciation amont. Ces fonctions permettent de discrétiser le terme convectif de l'équation de transport alors que la terme diffusif est approximé par une interpolation bilinéaire sur le triangle. Le volume de contrôle pour l'équation de continuité est constitué par le triangle lui-même.

La couplage vitesse-pression est effectué dans un premier temps par une intégration de l'équation de mouvement sur le Co-Volume afin d'obtenir les expressions de u et v. Ces expressions sont alors introduites dans l'équation de continuité qu'on intègre sur chaque élément et qui nous permet d'obtenir une équation pour la pression. A partir du champs de pression obtenu, on construit un champs du gradient de pression qu'on introduit dans les équations de mouvement. On peut alors

résoudre ces dernières sur le Co-Volume ou le volume de contrôle polygonal en fonction du schéma utilisé.

Toutes les équations discrétisées (pression, vitesse ou toute autre fonction scalaire) ont des propriétés conservatives. Leur résolution se fait de manière séquentielle ce qui procure des facilités pour l'extension aux écoulement 3D. En outre, l'utilisation de maillages non structurés permet une grande flexibilité dans la discrétisation de la géométrie. Dans cette thèse, la méthode SCVFEM est étendue aux écoulements turbulents réactifs avec ou sans radiation. Plusieurs modifications ont pu améliorer sensiblement la précision et la convergence.

La méthode SCVFEM a certaines propriétés qui la distinguent des autres méthodes numériques. Premièrement, pour les deux variantes (stockage aux côtés et aux sommets), il n'est pas nécessaire de spécifier les conditions frontières pour la pression ce qui évite un énorme problème. Deuxièmement, pour le schéma à stockage aux côtés, il est facile d'imposer les conditions frontières pour toutes les fonctions scalaires ainsi que l'intensité de radiation ce que évite la discontinuité engendrée par les coins. Finalement, pour un même nombre d'inconnues et une même précision recherchée, le temps CPU pour le méthode à stockage aux côtés est moindre que celui de la méthode à stockage aux sommets (voir Chapitré 5).

Pour les écoulements turbulents, de forts gradients apparaissent au niveau de la paroi. Toutefois, en ingénierie, l'intérêt est dirigé vers les propriétés de l'écoulement principal. Ainsi, un modèle basé sur les grandeurs moyennées conduit à un système d'équations différentielles pour la vitesse, la densité, les fractions de masse et l'enthalpie sous une forme conservative. Ces équations introduisent aussi des corrélations comme la correction du tenseur de Reynolds qui peut être soit prédéterminée, soit modélisée. Pour des écoulements non réactifs, les équations gouvernantes sont celles du mouvement et de la continuité; par conséquent la modélisation du tenseur de Reynolds est nécessaire pour fermer le système d'équations.

La turbulence est modélisée par le modèle à deux équations k-ϵ standard couplé avec la loi de la paroi. Toutes les variables transportées sont résolues sur un domaine de calcul séparé du domaine réel par une distance donnée et les conditions de glissement pour la vitesse sont alors imposées à la paroi. L'implantation de la loi de la paroi est basée sur l'approximation du profil de la vitesse au voisinage de la paroi par une fonction logarithmique bien connue. La détermination de la vitesse de friction ou du taux de cisaillement à la paroi est effectuée de deux manières différentes: La première est la méthode classique basée sur l'équilibre de la génération et la production de l'énergie proche de la paroi et la seconde est une méthode ou l'équation logarithmique pour la détermination de la vitesse de friction est résolue par un quasi-newton itératif.

Dans la modélisation des écoulement turbulents réactifs où la moyenne de Favre est utilisée, la corrélation pour la fluctuation de la densité n'apparait pas. Par conséquent, l'équation qui gouverne le transport de la fraction de la masse du carburant a la même forme que celle en absence de réactions chimiques. En outre, le taux de réaction chimique dans les réactions homogènes est défini comme étant le taux avec lequel l'un des réactifs forme les produits de la réaction. C'est une fonction de la température, de la pression et de la composition du mélange et elle est très influencée par la turbulence et les caractéristiques du mélange. L'objectif de la modélisation de la combustion est alors la spécification du taux de consommation du carburant, de la probabilité de réaction et des espèces chimiques.

Plusieurs modèles de combustion basés sur l'approche de conservation scalaire (conserved scalar approach) sont examinés pour les flammes de diffusion turbulentes. On cite alors le modèle à chimie rapide, modèle à taux de réaction fini, modèle d'équilibre chimique et le modèle de micro-flammes. Pour la turbulence, les deux façons de considérer la loi de la paroi sont utilisées et comparées à travers des tests

sur les quatre modèles de combustion ci-dessus. Par ailleurs, concernant les fluctuations des concentrations, les fonctions de probabilité delta et beta sont utilisées.

La contribution de la radiation à la balance énergétique est nécessaire pour compléter l'équation de conservation de l'énergie et l'équation de transfert radiatif. A cause de la nature intégro-différentielle de l'équation de radiation et de l'aspect multidimensionnel du rayonnement, le solution numérique de cette dernière équation est très complexe. Plusieurs modèles de radiation sont alors considérés pour traiter des géométries irrégulières.

Une procédure numérique est donc développée pour la résolution du transfert radiatif dans des enceintes 2D cartésiennes ou axisymétriques isotropes avec des surfaces grises. La méthode de transfert discret a été étendue aux maillages triangulaires non structurés et elle couple les équations de convection-diffusion pour les écoulement visqueux turbulents réactifs avec l'équation de radiation à travers l'équation d'énergie. La différence majeure entre la méthode actuelle et la méthode de transfert discret originale réside dans le traitement des aspects géométriques. (voir Chapitre 4). La procédure est alors utilisée pour la simulation de la combustion dans un brûleur où le modèle de l'émittance des gaz de combustion est considéré comme "three-gray plus one-clear gas".

En résumé, les objectifs principaux du présent travail sont:

- Développement de le méthode SCVFEM pour les écoulements turbulents réactifs à densité variable.
- Implantation du modèle de turbulence à deux équations k-ϵ et la loi de la paroi pour des géométries complexes.
- Investigation de différents modèles de combustion pour les flammes de diffusion turbulentes.
- Application du modèle de radiation pour des brûleurs à gaz réel.

Finalement, la validation de la méthode SCVFEM a été effectuée pour différents tests et les résultats obtenus ont été comparés aux solutions analytiques, à d'autres méthodes numériques ou à des résultats expérimentaux.

Pour des cas tests laminaires, une évaluation et une comparaison systématiques ont été effectuées concernant la précision, la convergence et la capacité de prédire les recirculations, et ce pour les deux variantes du SCVFEM. Il a été montré que les deux schémas pouvaient donner des résultats précis pour le longueur de recirculation.

Pour les cas tests turbulents, l'intérêt a été porté sur la prédiction de la longueur de recirculation dans des géométries complexes par le modèle k-ϵ, et ce pour les deux manières d'implanter la loi de la paroi qu'on appelera méthode classique et méthode du quasi-newton. Dans le cas de la marche, les résultats montrent que le modèle k-ϵ a la capacité de prédire le comportement de l'écoulement mais ne réussit pas à donner la bonne longueur de recirculation. Il a été aussi trouvé que le point de rattachement par la méthode classique était mieux que celui donné par la méthode du quasi-newton. En revanche, les profiles de vitesse fournis par cette dernière sont plus proches des résultats expérimentaux que ceux obtenus par la méthode classique.

Dans les tests turbulents réactifs, les quatre modèles de combustion ont été comparés en utilisant les deux méthodes de la loi de la paroi. Il a été trouvé que les résultats obtenus par la méthode du quasi-newton étaient beaucoup mieux. En outre, les résultats montrent que les prédictions de la distribution de la fonction de mélange utilisant les modèles PDF dans la région développée de la flamme étaient meilleurs que ceux obtenus sans PDF.

Les tests de radiation montrent que dans les problèmes à absorption dominante, l'actuelle méthode de transfert discret donne d'excellents résultats. Pour des problèmes de "scattering" purs, on obtient le même niveau de précision que d'autres méthodes. Ainsi, la présente méthode peut être utilisée pour la simulation du transfert de chaleur réactif dans des chambres de combustion à gaz avec des géométries quelconques grâce à l'économie de calcul et la précision raisonnable qu'elle procure.

Dans le test de comparaison de la flamme de diffusion turbulente couplée ou non avec la radiation, il a été trouvé que dans la région de flamme, la température maximale prédite avec radiation était de 110 °C plus basse que celle obtenue sans radiation. Il a été aussi illustré que pour de grands brûleurs et chambres de combustion, la radiation constitue un mode de transfert de chaleur très important. En outre, les résultats obtenus avec la schéma SCVFEM sont comparables aux prédictions obtenues avec la méthode des éléments finis.

Abstract

In the present study, a new numerical method, named Staggered Control-Volume Finite Element Method (SCVFEM) is proposed and developed for incompressible laminar and turbulent flows, as well as turbulent reacting flows with emphasis on radiative heat transfer. Based on the primitive variables (u,v,p) formulation, the discretisation is carried out on a triangular element, where the pressure is stored at the centroid and velocities at the midpoint of the sides or at the vertices. The element used here is an unequal-order linear velocities/constant pressure type, equivalent to the P1 non-conforming/P0 element and P1/P0 element of the finite element method. Control volumes and co-volumes constructed around each variable location leads to two different SCVFEM schemes, namely Face-centered and Vertex-centered schemes. A flow-oriented exponential function and the skewed, mass-weighted upwind interpolation function for the dependent variables are used. The pressure-velocity coupling is treated by momentum integration over the co-volume. This relation is then used to derive the pressure equation by integrating the continuity equation over each triangular element. Pressure gradients which appears in the momentum equations are evaluated by using a reconstruction method for the pressure variation. The SIMPLE segregated solution algorithm is implemented.

Turbulence is solved by using the standard k-ϵ two-equation model. Near solid walls, wall function methods are adopted. The implementation of the law-of-the-wall is based on the universality of a logarithmic velocity profile and the validity of near wall turbulent equilibrium. The determination of the friction velocity or shear stress at boundary is considered using two different methods. One is the classical approximation method, which is based on the balance of generation and dissipation of energy near the wall; another is the direct iteration method, where the logarithm law

relation for friction velocity is solved by using the quasi-newton iteration.

Based on the conserved scalar approach, several combustion models are examined for turbulent diffusion flames. These are the fast chemistry, finite reaction rate, chemical equilibrium and micro-flame models. The concentration fluctuations are accounted for by the delta and beta probability density functions.

A numerical procedure for solving radiative heat transfer in 2D cartesian and axisymmetric enclosures with a gray absorbing, emitting and isotropically scattering media is developed. The discrete transfer method is extended to an unstructured triangular mesh and coupled to the advection-diffusion equations for the viscous turbulent reacting flows through the energy equation.

Finally, validation of the proposed SCVFEM was performed on several test problems, and then applied to practical problems involving reacting flows.

Acknowledgments

I would like to express my gratitude and appreciation to Professors Ricardo Camarero and Marcelo Reggio, my supervisors, for guidance, encouragement and support during the research and the preparation of this dissertation.

Thanks are given to Dr. François McKenty for the implementation and discussion of the combustion models, and to Mr. Samir Rida for co-development of the basic SCVFEM.

Thanks also to my friend Dr. Xudong Zhang, for the numerous discussions and useful suggestions concerning the computation problems. Thanks to Mr. John C., Chai from University of Minnesota for his discussion of the radiation models and pre-reprint of his technical papers. Thanks also to members of the MIAO group of the Mechanical Engineering Department at Ecole Polytechnique.

The financial support provided by Gaz Métropolitain Inc. of Québec is highly appreciated.

Lastly and most importantly is the support and patience that I received from my family, in particular my wife Huiping and my daughter Ting-Ting.

Table of Contents

List of Figures

List of Tables

Nomenclature

A	area of an element; or coefficient of an exponential interpolation function; or eddy dissipation combustion constant
a	coefficient for an algebraic equation; or coefficient for an interpolation function of pressure
a_1,a_2,a_3	coefficients of the mass-weighted upwind interpolation function
a_{ij}	stoichiometric coefficients
B	coefficient for an exponential interpolation function
b	coefficient for an algebraic equation; or coefficient for an interpolation function of pressure
b_1,b_2,b_3	coefficients of the mass-weighted, upwind interpolation function
C	coefficient for an exponential interpolation function
C_μ,C_1,C_2	turbulence model constants
C_{g1},C_{g2}	constants for the transport equation of g
C_p	specific heat at constant pressure
c	coefficient for the interpolation function of pressure
c_1,c_2,c_3	coefficients for the mass-weighted, upwind interpolation function
D,D_0	diameters
d_1,d_2,d_3	coefficients for the mass-weighted, upwind interpolation function
E	E-factor; or turbulent roughness parameter; or emissive power
e	obstacle width
f	mixture fraction
g	square fluctuation of f
H_{fu}	heat of reaction
h	total enthalpy; or step height
I	radiant intensity

J	convection-diffusion flux
k	turbulent kinetic energy
k_a, k_s, k_e	gas absorption, scattering and extinction coefficients
L	character length
m	mass fraction
P	pressure; or variable in wall function
$P(f)$	probability density function
Pe	Peclet number
Pr	Prandtl number
$P(\vec{\Omega},\vec{\Omega}')$	phase function
q	heat flux
R	universal gas constant
R_i	radius
r	radial coordinate
S_ϕ	source term in transport equation of ϕ
s	stoichiometric mass of oxidant; or distance
T	temperature
t	time
$\vec{t},\vec{n}$	tangential and normal directions of surface
U,V	velocity components in local (X,Y) directions
W	molecular weight
u,v,w	velocity components in (x,r,θ) directions
$\dot{w}$	reaction rate
u_τ	friction velocity
y	cartesian coordinate; or distance to the wall
y^+	dimensionless distance in the normal direction to the wall
Z	exponential interpolation function

Greek Symbols

α	direction in X coordinate; or aspect ratio
α_{axi}	axisymmetric parameter
β	direction in Y coordinate; or conserved scalar
Γ	diffusion coefficient
δ	angle of the wall inclination; or gradient
ϵ	rate of dissipation of kinetic energy
ε	molar ratio of fuel/air
κ	Von Karman constant in the wall functions
λ	turbulent intensity; or lagrangian multipliers
μ	viscosity; or chemical potential
ν	coefficient of product
ξ	nondimensional mixture fraction
ρ	density
σ	Schmidt/Prandtl number; or Stefan-Boltzmans constants
τ_w	wall shear stress
θ	polar angle
ϕ	scalar variable; or azimuthal angle
φ	equivalence ratio
ω	scattering albedo
Ω	solid angle
Ω_c	control volume
$\triangleq$	equal or not

Subscripts

A	air stream
av	average value
axi	axisymmetric

c	carbon dioxide
eff	effective
F	fuel stream
fu	fuel
fu,b	fuel burnt
i	species
i,j,k	summation index
LR	direction from left element to right element
l	laminar
max	maximum
mix	mixture
n	interpolation point
nb	neighbour
t	turbulence
r	radiant
w	wall; or water vapour

Superscripts

n	time step
-	mean value
0	old value
+	leaving from the wall
-	arriving at the wall
*	modified value
'	fluctuation; or direction of rays
→	vector
·	heat rate

List of Appendices

Chapter 1

Introduction

1.1 Aims and Motivations of the Thesis

The use of CFD codes for simulating combustion phenomena is becoming a widespread tool among the scientific and industrial communities. It helps engineers to optimize the operating conditions, reduce pollutants emission, correct the measurements, and eventually, to improve the design of new combustors. Most of the commercial CFD codes, such as PHOENICS, FIDAP, FLUENT and TASCflow can be used for the simulation of the turbulent reacting flow with a moderate success. Although others commercial software such as N3S, RAMPANT are working with the triangular grid for discretization, but so far, we are unaware of any reports on the simulation of combustion by using these codes. Combustors may involve fine geometrical details, especially they may comprise the sharp angles, in this situation, the spatial discretization with unstructured triangular grid is superior to that of rectangular ones. Although the CFD codes have been well developed, there still has room for improvement. An attempt to use the unstructured triangular grid by using the control volume finite element method in conjunction with the vorticity-streamfunction formulation for the simulation of combustion has been reported (Elkaim et al., 1993). However, the method is based on the vorticity-streamfunction formulation which suffers the difficulties for boundary condition on vorticity and extension to 3D is not immediate, it is not satisfied. Alternatively, to develop an efficient CFD code using an unstructured triangular grid with primitive variable formulation applied for the simulation of combustion, is the motivation of the present work.

The primary goal of this thesis is to propose, develop and test an unequal-order, Staggered Control Volume Finite Element Method (SCVFEM) for the simulation of 2D cartesian and axisymmetric, viscous, incompressible, laminar and turbulent flows, turbulent reacting flows with and without radiation. The aim is to use this code to model the performance and techniques for flames in practical furnaces and combustors.

Stimulus for the numerical simulation of combustion is due to demands for higher efficiency furnaces and combustors and the requirement of controlling pollution formation. Because of the availability of inexpensive computer, this has become a viable alternative to experimental investigation. Combustion involves the following physical phenomena: turbulence, chemical reactions in the flame, convective heat transfer and radiative heat transfer from the products of combustion. The most basic requirement is the simulation of the laminar flow, for which it is necessary to provide the appropriate convection-diffusion formulation. The critical issue is the spurious pressure harmonics problem and the pressure-velocity coupling when the primitive variable formulation is used.

In turbulent flows, rapid fluctuations are exhibited. However, for engineering applications interest is mainly in the mean flow properties. Hence a model, based on the time-averaging, yields a set of differential equations for the mean velocities, density, mass fractions and enthalpy in the general conservation equations. These equations have additional correlation terms, such as $\overline{u_i' u_j'}$, $\overline{u_j' \phi'}$,and $\overline{\rho' u_j'}$, which must be either predetermined or modelled. For non-reacting flows, equations of interest are those governing the mass and momentum, hence, modelling of the term $\overline{u_i' u_j'}$ (Reynolds-stress) is needed in order to close this set of differential equations.

In turbulent reacting flows, when the Favre-averaging is used, the density fluctuation correlation does not appear. Hence, equations governing the transport of fuel mass fraction have a form similar to those of non-reacting flows. The chemical

reaction rate in homogeneous reactions is defined as the rate at which one of the reactants form products (Khalil, 1982). It is a function of the temperature, pressure and composition, and is strongly influenced by the turbulent and mixing characteristics of the flow. The objective of combustion modelling is to specify the rate of fuel consumption and to model probability of reaction, at last to determine the chemical species and thermal state parameters. The available combustion models will be described in Chapter 2.

In turbulent flames, besides convection, radiation also becomes important. The radiation contribution to the energy balance is needed to complete the specification of the energy conservation equation. Due to the integro-differential nature of the radiative transfer equation and the multidimensional nature of radiation itself, the numerical solution of the radiative transfer equation is very difficult. Several radiation models with emphasis on the treatment of an irregular shaped geometries are investigated.

The proposed unequal-order, SCVFEM for turbulent reacting flow uses the primitive variables, on an unstructured triangular mesh, staggered grid arrangement. It provide geometric flexibility, and ability of extension to 3D flows. In the present study, the SCVFEM (Rida, 1993) is extended to complex turbulent reacting flows with and without radiation. Further refinements have significantly improved the accuracy and convergence. In summary, the major contributions of the present work include following:

- Develop the basic SCVFEM for incompressible laminar and turbulent flows, turbulent reacting flow with variable density.
- Incorporation of the k-ϵ two-equation turbulence model and the wall function methods for turbulent flows in complex geometries.
- Investigation of the different combustion models for turbulent diffusion flames.
- Develop the radiation model for real furnace combustion gases.

1.2 Outline of the Thesis

In Chapter 2, a review of the existing numerical methods for incompressible laminar and turbulent flows, turbulent reactive flows with emphasis on radiative heat transfer is presented for combustion processes.

The governing equations for turbulent reacting flow with variable density, as well as turbulence models and combustion models will be given in Chapter 3.

Chapter 4 presents the basic Staggered Control-Volume Finite Element Method (SCVFEM). The SCVFEM involves the choice of the different type of interpolation function, the integration of the transport equations over the control volumes, the treatment of the pressure-velocity coupling, the derivation of the pressure equation, and the segregated solution algorithm, etc.. Consideration of radiative heat transfer, includes the solution procedure of radiative transfer equation and the treatment of the coupling between the energy conservation equation and the radiative transfer equation. Where, the geometric consideration in the application of the discrete transfer method are mainly addressed.

In Chapter 5, results are presented to validate the proposed SCVFEM.

Finally, conclusions concerning the computational results are discussed. Relevant recommendations related to the improvement and extension of the proposed methods are also presented.

Chapter 2

Literature Review

Numerical methods for various fluid flow and heat transfer problems range from the classical methods, such as the finite difference method (Roache, 1976, Patankar, 1980), to the more recent finite element methods (Chung, 1978, Baker, 1983), and the control volume based methods (Patankar, 1980, Baliga and Patankar, 1980). This chapter reviews the development of these different numerical methods to the solution of the fluid flow with particular attention to problems involving turbulence, combustion and radiation. The general governing equations for the scalar variables such as velocities, temperature and concentrations of chemical species can be represented as a set of transport convection-diffusion equations. The specific issues which arise in their numerical solutions are false diffusion or numerical diffusion (Raithby and Torrance, 1974), spurious pressure harmonics or checkerboard pressure fields (Patankar, 1980) and the pressure-velocity coupling when the primitive variable formulations are used.

2.1 False Diffusion

Early investigations of the numerical prediction of convection-diffusion phenomena have employed finite difference method based on the centred difference scheme (CDS). In most circumstances, CDS offers a satisfactory compromise between accuracy and computational economy when convection does not dominate diffusion. For convection dominated flow, however, central differencing results in instability or unphysical oscillatory behaviour when the grid Peclet number is greater than two.

Efforts to overcome this problem has led to the development of various upwind difference schemes. The mechanism of upwinding has been explained by Gosman et al. (1969) in their "Donor-Cell" model. While the oscillatory behaviour has been cured for high Peclet numbers, upwinding is less accurate than the CDS at low Peclet numbers. Several improvements based on the locally one-dimensional assumption have been proposed leading to the exponential difference scheme (EDS) and hybrid difference scheme (HDS) of Spalding (1972). Further refinements such as the power-law difference scheme (PLDS) of Patankar (1981) yields a better approximation to the EDS than the HDS. However, as found by Raithby (1976a), these hybrid schemes work well when the flow is steady, closely aligned with the grid lines, and possesses no strong cross flow gradients. In problems that do not conform to these conditions, the locally one-dimensional assumption used in hybrid schemes can give rise to false diffusion or numerical diffusion.

The skewed upwind difference scheme (SUDS) proposed by Raithby (1976b) is a first-order accurate scheme. It yields a significant reduction in skewness errors by using an upwind discretization in a streamwise coordinate system, in which case skewness errors are entirely absent. Leonard (1979) proposed a flow-oriented difference scheme based on a conservative quadratic upstream interpolation (QUICK) for convection terms. However, the coefficients can become negative when the convection effects are strong enough (Patel and Markatos, 1986). These lead to the development of the quadratic upstream extended (QUDSE) and quadratic upstream extended revised (QUDSER) finite difference schemes (Pollard and Siu, 1982), which ensures the coefficients are positive. In the recent evaluation of several upwind schemes, Sharif and Busnaina (1988) found that the SUDS produces the least amount of numerical or artificial diffusion, however, unacceptable numerical dispersion (over- and undershoot) is produced when the flow angle is skewed at large angles to grid lines. This is because the SUDS does not satisfy the discrete maximum principle, and the influence coefficients determined by SUDS are not guaranteed to be positive.

Busnaina et al. (1991) found that higher-order and streamwise differencing schemes produce less numerical diffusion but introduce oscillations in the solution. On the other hand, lower-order schemes produce excessive numerical diffusion but no oscillations.

Different modifications of the SUDS scheme have been proposed to improve its performance. Van Doormaal et al. (1987) proposed a physical advection correction scheme (PAC) to the SUDS, where the approximation to the convected quantity at a cell face is modified and it reflects the interactions between the physical processes of advection, diffusion and source terms. Solutions exhibit little or no spurious overshoots or undershoots. Busnaina et al. (1991) proposed a modified skew upwind weighted differencing (SUWD) scheme for discretizing the convection terms, which produces less numerical diffusion and dispersion than SUDS. Calhoon and Roach (1993) developed a new upwind procedure which seeks to include the viscous terms so that boundary and shear layer will not be over-dissipated as with standard upwind scheme. The method closely parallels the Finite Analytic method (Chen et al., 1988) which is based on a local analytic solution of the governing equation for an element in constructing an algebraic representation of the partial or ordinary differential equation and yields a fully conservative method. The difference between the finite analytic method and the exponential scheme lies in that the transient terms are considered in the finite analytic method, while it is not considered in the exponential scheme in the derivation of the local analytic solutions.

Conventional Finite Element Method (FEM) encountered difficulties similar to those that afflict central differencing schemes. Christie et al. (1976) proposed a one-dimensional upwind FEM scheme based on skewed weighting functions, which was extended to two-dimensional problems by Heinrich et al. (1977). Hughes et al. (1979) proposed another upwind FEM scheme based on a special quadrature rule applied to the advection term. Soon it was realized that, like the finite difference counterparts, the finite element upwind procedures tend to produce overdiffusive solution in 2D and 3D as well as in transient situations (Brooks and Hughes, 1982).

In the FEM, the false diffusion can be reduced by a Petrov-Galerkin formulation with the streamline upwind scheme (SUPG) proposed by Brooks and Hughes (1982), which may be viewed as a modification to the classical Galerkin finite element method. The physical idea of SUPG is to increase control over the advective-derivative term by adding an artificial diffusion term in the weighting function which acts only in the streamline direction (Hughes, 1987). Rice and Schnipke (1985) noted that the SUPG of Brooks and Hughes (1982) can exhibit small non-physical spatial oscillations in the solution field of a transported scalar. They proposed a monotone streamline upwind (MSU) finite element method that presents a streamline approximation to the convection terms, rather than to modify the weighting function. They claim that this method is more stable than SUPG. The extension of the MSU finite element method of Rice and Schnipke (1985) to quadratic finite element has been proposed by Hill and Baskharone (1993), which does not exhibit any non-physical spatial oscillations, nor suffer from the traditional problem of excessive numerical diffusion. Shemirani and Jambunathan (1992) found that the methods of SUPG and MSU, however, generally violate the conservation laws, resulting in global imbalance of transported quantities. They proposed a Conservation Monotone Streamline Upwind (CMSU) formulation using simplex elements. The method is shown to accurately model the advection phenomena with significantly smaller numerical diffusion than the existing methods and results are free of all spatial oscillations.

Baliga and Patankar (1980) proposed a control volume based finite element method (CVFEM) using the flow-oriented, upwind type interpolation that significantly reduces false diffusion. However, it encountered negative coefficient difficulties in the discretization equations which can become quite serious when obtuse-angled triangular elements, or tetrahedral elements with a solid angle exceeding $\pi/2$ steradian, are used in problems that involve high Peclet numbers (Saabas, 1991, Masson et al., 1994). A mass-weighted, skewed upwinding procedure (MWUS) was proposed by Schneider and Raw (1986), which is based on CVFEM with a quadrilateral element. They claimed

that the potential for the development of spatial oscillations in the domain does not exist. The MWUS was also implemented by Saabas (1991) using both three-node triangular and four-node tetrahedral elements in two- and three-dimensions, respectively, and a co-located equal-order primitive variable formulation. Other applications of MWUS with CVFEM are also found in Afshar (1992) on a quadrilateral element, and Masson et al. (1994) on a triangular element. Similar attempts has been used based on a staggered control volume scheme (Rida, 1993) and will be extended in the present work.

2.2 Pressure-Velocity Coupling

In incompressible flow problems, another difficulty lies in the calculation of the unknown pressure field, which can be related to the fact that only pressure gradients appear in the momentum conservation equations. The pressure field is indirectly derived from the incompressibility constraint, i.e. continuity equation. Because of this, if velocities and pressure are stored at the same location, when the central differencing scheme is applied to both the continuity equation and the pressure gradient terms in the momentum equations, it has been shown to produce nonphysical oscillations in the pressure field, or checkerboard pressure field (Patankar, 1980).

2.2.0 Vorticity-Stream function

Early work based on the vorticity-stream function formulation (Gosman et al., 1969) which satisfies the incompressibility constraint identically, avoids the necessity of computing the pressure. This formulation was adopted by Elkaim et al. (1993), McKenty et al. (1993) and Meng et al. (1992) using the control volume finite element method on unstructured triangular grid for the simulation of the turbulent reacting flows. However, difficulties for applying boundary conditions on vorticity and extension to three dimensions is not immediate. Due to these difficulties, the primitive

variable formulation is preferable. The differences between the vorticity-stream function and primitive variable formulation are discussed by Roache (1976).

To eliminate the checkerboard pressure problem when using the primitive variable formulation, several methods based on the different storage locations for velocities and pressure have been developed.

2.2.1 Staggered Grid Method

The checkerboard pressure field can be prevented by using a staggered grid arrangement as first proposed by Harlow and Welch (1965) in their marker and cell (MAC) method. Since it has been widely used by Patankar and Spalding (1972) in their SIMPLE (semi-implicit method for pressure-linked equation), and its variants SIMPLER (Patankar, 1980), SIMPLEST (Spalding, 1980), and SIMPLEC (Van Doormaal and Raithby, 1984). Essentially, the method consists in storing pressure at the main grid nodes in the discretized calculation domain, and staggering the velocity components relative to these nodes (Fig. 2.1(a)). In the resulting momentum equation, pressure appears at adjacent, rather than alternate nodes, and the discretized continuity equation can use the velocity components at sides directly, and so that no interpolation is needed.

The staggered grid method has been widely used in the solution of complex flow problems in regular orthogonal grid, curvilinear orthogonal and non-orthogonal grids with considerable success (Maliska and Raithby, 1984, Karki and Patankar, 1988, Shyy and Vu, 1991). However, it was found that this approach fails when the grid undergo bends that exceeds 90° (Shyy and Vu, 1991). The difficulties with staggered grid approach led to the development of co-located schemes using the primitive variables formulation. However, most of these methods need special procedures to treat the decoupling of the pressure and velocity field.

Extension of the MAC method to triangular elements can be found in the complementary volume method of Nicolaides (1989, 1990) and a similar method

named the dual variable method of Hall et al. (1991). The resulting arrangements are shown in Figure 2.1(b), where pressure is stored at the circumcenters, and the velocity components u_i directed along the dual mesh edges which is perpendicular to its edges. The complementary control volumes or covolumes are formed by joining the circumcenters of all triangulations. Using these methods, the pressure gradients in the momentum equations can be discretized directly as in the MAC method. However, to avoid the reentrant problems when constructing the polygonal control volumes, these methods are restricted to the use of equilateral triangles and acute triangles (Hall et al., 1991).

2.2.2 Equal-Order, Cell-Centered Method

The first equal-order, co-located FVM is the cell-centered method. In the arrangement shown in Figure 2.1(c) and 2.1(d), all the dependent variables (u,v,p) are stored at the cell center. The control volume based on the rectangular grid (Fig. 2.1(c)) has been widely used in the co-located finite volume method computations, by Rhie and Chow (1983), Reggio and Camarero (1986), Peric et al. (1988), Miller and Schmidt (1988), Majumdar (1988), Kobayashi and Pereira (1991) and Smith et al. (1993), etc.. The key feature in cell-centered method for incompressible flow is the appropriate evaluation of cell-face velocity and pressure, or the treatment of pressure-velocity coupling. The special procedure has been classified as Pressure Weighted Interpolation (Rhie and Chow, 1983, Miller and Schmidt, 1988) and Momentum Interpolation (Majumdar, 1988) by Smith et al. (1993).

Rhie and Chow (1983) introduced a method of determining the convective velocities at cell faces which are obtained by interpolations between grid nodes. The pressure gradient term is excluded from averaging, and treated directly by a pressure difference of the node pressures. Different from the above method, Reggio and Camarero (1986) proposed an opposed differencing scheme in which the velocity gradients are obtained by upwind differencing and pressure gradients by downwind

differencing. These procedures ensure strong velocity-pressure coupling, and thus eliminate the pressure wiggles. However, Majumder (1988) found that the results based on Rhie and Chow's method is under-relaxation factor dependent, and proposed a new momentum interpolation method in an iterative solution that is independent of the under-relaxation parameter used. Thiart (1990) proposed a similar procedure based on the momentum interpolation method.

2.2.3 Equal-Order, Vertex-Based Method

The second equal-order, co-located method commonly used in FVM, FEM and CVFEM is the vertex-based method. In this method, the same control volumes for both the velocity and pressure in the control volume method, or, in the case of finite elements, the same shape functions are used. It includes the bilinear velocity/bilinear pressure element and the linear velocity/linear pressure element, as shown in Fig. 2.1(e) and Fig. 2.1(f), respectively. The 4-node quadrilateral element (Fig. 2.1(e)) has been implemented by Rice and Schnipke (1986) using the FEM, by Schneider and Raw (1987) and Afshar (1992) using CVFEM. The triangular element (Fig. 2.1(f)) has been used by Prakash and Patankar (1985), and Sabbas (1991) and Masson et al. (1994) using CVFEM. The procedures for dealing with the pressure-velocity coupling can be classified as: the method of Prakash and Patankar (1985), the method of Schneider and Raw (1987), and the method of Rice and Schnipke (1986).

In the method of Prakash and Patankar (1985), the continuity equation is integrated over an element to obtain the discretization equation for pressure. The velocity field used in the integration of continuity equation is not the nodal velocity field but a different velocity field, derived from the discretized momentum equation at an element vertex. This new velocities can be expressed as the pseudo-velocities plus the pressure coefficients multiplied by pressure gradient. The pressure gradient is uniform by assuming the pressure varies linearly over an element. The quantities, such as pseudo-velocities and pressure coefficients at any other points in the element

are obtained by assuming a linear variation of these quantities over the element. Because the new velocity field is driven by the pressure difference between adjacent grid points, its substitution into the continuity equation yields a pressure algebraic equation that eliminates spurious oscillations.

In the method of Schneider and Raw (1987), the convected variables and pressure at the control volume faces or integration points, are expressed in terms of the nodal values using a local discrete analog to the governing differential equation at the control volume face in order to close the algebraic representation of the conservation equations. For the velocity at the integration points, a one-dimensional N-S equation was considered by using an upwind differencing for convection modelling and central differencing for pressure gradient and diffusion terms. The resulting integration point velocity serves the tight coupling with the node velocities and node pressures. The integration point velocities are then substituted into the momentum equation and used to derive a Poisson equation for pressure. The authors claim that the method permits accurate convection modelling and preclusion of pressure-velocity decoupling. Recently, Schneider and Karimian (1992) extended this method for solving both incompressible and compressible flows.

In the method of Rice and Schnipke (1986), the closure relation between velocities and pressure is obtained from the discretized momentum equation, where the velocities at each grid point are expressed as the pseudo-velocities plus the pressure gradient term. These relations are then substituted into the integrated continuity equation and used to form the pressure algebraic equation. They showed that the resulting pressure equation does not exhibit spurious pressure modes.

The equal-order vertex-based method simplifies the book-keeping of the different control volumes used in the staggered grid approach. This method assumes a continuous approximation of pressure in each element. Alternatively, when piecewise constant pressure is assumed in each element, constitutes the unequal-order vertex-based schemes in the FEM.

2.2.4 Unequal-Order, P1/P0 Element

The unequal-order elements include a bilinear-velocity/constant pressure element (Q1/Q0) and a linear-velocity/constant pressure (P1/P0) element, as shown in Fig. 2.1(g) and Fig. 2.1(h), respectively. The 4-node quadrilateral element (Fig. 2.1(g)) has been used by Benim and Zinser (1986) with SIMPLE-like segregated finite element method, by Mukhopadhyay et al. (1993) with an explicit transient CVFEM. The 3-node triangular element (Fig.2.1(h)) has been implemented by FIDAP (1991) using the penalty function method and SIMPLE-like segregated method. However, as discussed by Benim and Zinser (1986), this type of element may give checkerboard pressure oscillation. In the method of Mukhopadhyay et al. (1993), the cell-face velocity and pressure corrections are derived from an explicit discretized momentum equations. These relations are then used in the derivation of the pressure equation which has a strong diagonal dominance ensuring the correct pressure-velocity coupling. The P1/P0 element (Fig. 2.1(h)) is used in the present work. To avoid the checkerboard pressure field, we suggested that the momentum interpolation can be used for evaluating cell-face velocity and pressure based on the control volume method, this is the fundamental approach of the present study in the treatment of the pressure-velocity coupling. The interest of piecewise constant pressure approximation over a continuous approximation of pressure is probably a better approximation of mass conservation, and the possibility of an easy elimination of the pressure, thus reducing the number of equations (Thomasset, 1982).

2.2.5 Unequal-Order, P1 Nonconforming/P0 Element

From the numerical computation point of view, it is difficult to impose boundary conditions for dependent variables at the corner points of the calculation domain when using elements in Figures 2.1 (e), (f), (g) and (h). This is further compounded when computing the normal direction at these points is required for the

turbulent flow computations. This difficulty can be easily overcome by an arrangement such as the P1 nonconforming/P0 element of Crouzeix-Raviart (1973), in which velocities are stored at midpoint of sides, and pressure is assumed piecewise constant over an element, as shown in Fig. 2.1(j). This method has been implemented by Thomasset (1982) for practical computations in the finite element methodology. The application of this type element using the finite volume TVD schemes for solving the Euler shock problem may be found in Ware and Berzins (1992). The 4-node quadrilateral grid in which velocities are stored at midpoint of sides and pressure constant at center point has been used by Maliska and Raithby (1984), as shown in Fig. 2.1(i), where the momentum equations for cartesian velocities (u,v) at sides are solved over the staggered control volume, then it is used only to compute the contravariant velocity components that enter into the mass conservation constraint. Using this method, the checkerboard pattern of pressure can be avoided.

While the checkerboard-type pressure problem can be overcome by the most of the aforementioned methods, no numerical method can be regarded as the best for all the fluid flow problems. Most of the existing numerical methods have at least one or more of the following limitations:

- Difficulty in application to the complex geometries.
- No explicit physical interpretation.
- Difficulty to impose the pressure boundary condition.
- Extension to 3 dimensional flows is not immediate.

Finite element methods have geometric flexibility and ease of extension to high order schemes, but do not lend themselves to an explicit physical interpretation. The CVFEM combines the intrinsic geometric flexibility of FEM together with the direct physical invocation of a conservation principle on the control volumes. The unequal-order scheme of Baliga and Patankar (1983) and the equal-order scheme of Prakash

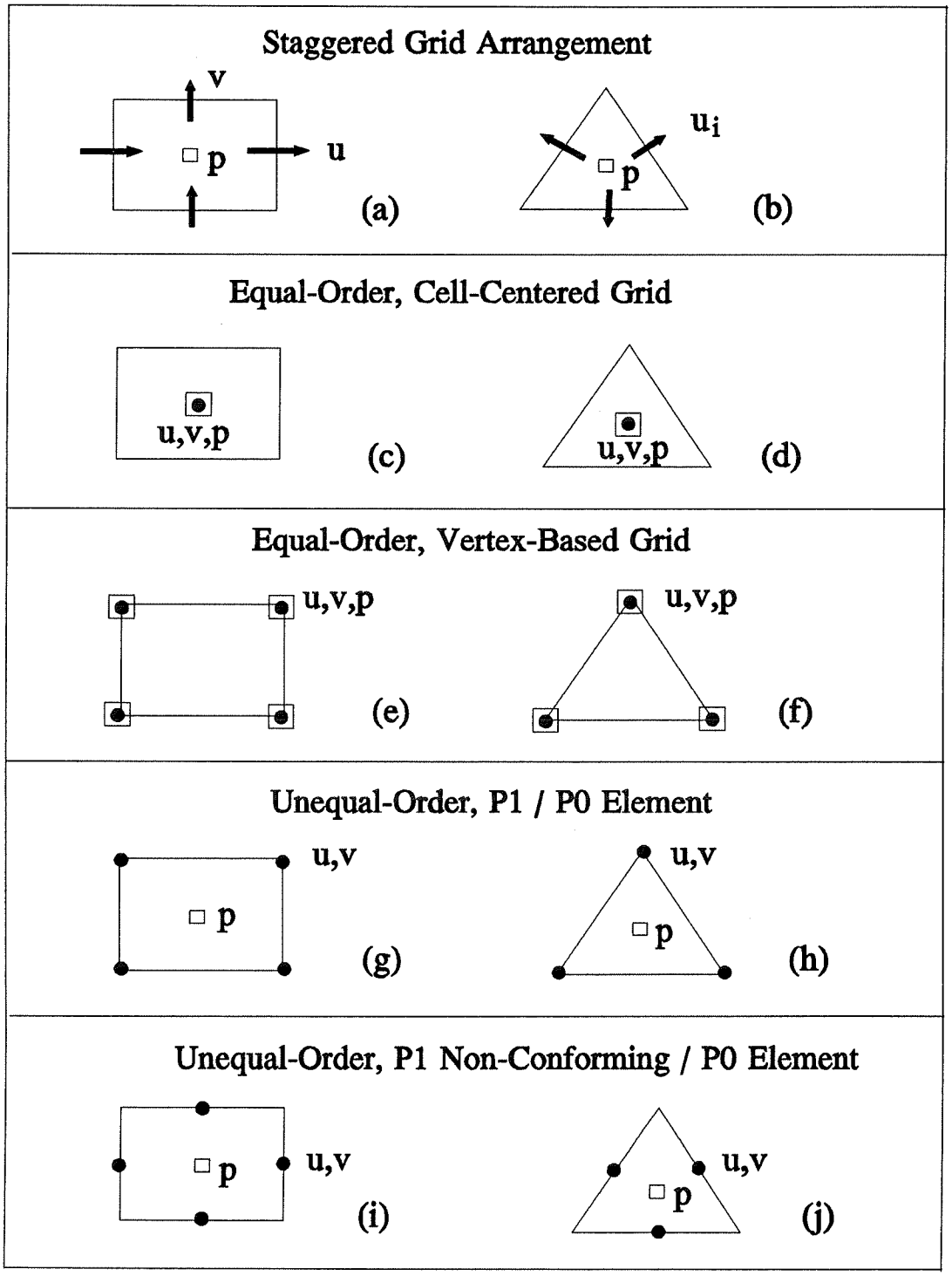

Figure 2.1: The storage locations used in the first-order scheme with the primitive variable formulation

and Patankar (1985), respectively are typical of this class of schemes. In the method of Baliga and Patankar (1983), the pressure is computed at fewer grid points than that of the velocity, but the pressure boundary condition must be provided. In the method of Prakash and Patankar (1985), the velocity and the pressure are computed at the same grid points, but it still needs to specify the boundary condition for pressure. Both the methods of Baliga and Patankar (1983) and Prakash and Patankar (1985) used the same form interpolation function, i.e. the flow-oriented upwind function without consideration of the source term in the transport equations. In an attempt to improve his previous equal-order method, Prakash (1986) proposed a second method, where a new flow-oriented, upwind type shape function includes the effects of the source terms in the streamwise direction in the transport equations. The same interpolation function is used to derive algebraic formulations to both the continuity and the momentum equations. Hookey and Baliga (1988) modified the interpolation function of Prakash (1986), to include source term effects in both directions parallel and normal to the mean flow within each element. The pressure correction equation involves up to 25 neighbouring nodes in two dimensional problems (Hookey, 1989). This makes extension to three dimensional flows difficult.

Staggering has proved to be a very effective method to avoid the pressure checkerboard patterns, but in the case of finite volume it has only been used for structured grid. This work proposed an extension to unstructured grid of the CVFEM scheme. The theoretical basis is equivalent to the P1 non-conforming/P0 element and P1/P0 element of the finite element method.

2.3 Solution Algorithm

For primitive variable formulations, once the required convection-diffusion formulation is chosen, the essence of the method lies in the treatment of the coupling between the momentum and continuity equation. Two methods of handling this are the

artificial compressibility method (Chorin, 1976) and the penalty function method (Reddy, 1982). The artificial compressibility method is based on the addition of an artificial time derivative of pressure to the continuity equation. This results in a pressure distribution such that a divergence-free velocity field is ensured. It is noted that the added term must vanishes for time-accurate solutions. Turkel (1987) extended this concept by adding the pressure time derivative to the momentum equations and can be considered as a preconditioning method to accelerate the convergence to a steady state for both incompressible and compressible flows. In FEM, the penalty function method reduces problems of conditional (or constrained) extremum to problems without constraints by the introduction of a penalty on the infringement of constraints (Reddy, 1982). In the application to incompressible flows, one replaces the incompressibility constraint by a relation between the velocity and pressure, thus eliminating the pressure terms in the momentum equations. Comparing the artificial compressibility method and the penalty function method, Shih et al. (1989) pointed out that these two methods are exactly the same. Both methods need to reconstruct the continuity equation by adding the extra pressure term, then eliminate the pressure in the momentum equations. The choice of free parameters is very important for application of these two methods.

2.3.1 Segregated Solution Algorithm

An alternative to artificial compressibility and penalty methods is the use of fully coupled solution algorithms in conjunction with direct Gaussian elimination type solution for the numerical solution of the incompressible flow equations. This method of solution requires less CPU time compared to most other methods for problems of moderate size. However, as the number of unknown is increased, the cost becomes too expensive, both in terms of storage and CPU time. Thus, these serious limitations have led to the development of alternative algorithms based on segregated forms of solution.

A number of segregated solution methods currently employed originate from

the SIMPLE procedure of Patankar and Spalding (1972). This method solves the pressure and velocity algebraic equations separately, one at a time. Because of slow convergence and the need of heavy under-relaxation of the SIMPLE procedure, some enhancements have been developed.

Patankar (1980,1981) introduced the SIMPLER (SIMPLE-revised) method, in which a pressure correction equation is used for obtaining only the velocity corrections, while a separate pressure equation is solved for the evaluation of pressure. This method brings a significant saving of computation time compared to the SIMPLE method. Another variant is the SIMPLEC (SIMPLE-Consistent approximation) procedure proposed by Van Doormaal and Raithby (1984), using a consistent approximation for the treatment of the velocity correction fields. It avoids the inconsistency of the SIMPLE procedure. The pressure correction equation does not use under-relaxation. They showed that this is less expensive than SIMPLER for the problems solved. The SIMPLEST procedure was developed by Spalding (1980), who recommended an explicit treatment of convection and implicit treatment of diffusion in the momentum equation. Another enhancement of SIMPLE is called PISO (Pressure Implicit with Splitting of Operators), proposed by Issa (1985). It is a non-iterative method for handling the pressure-velocity coupling of the implicitly discretised fluid flow equations, which is essentially the same as the SIMPLER procedure for incompressible flows.

2.4 Turbulence Modeling: Two-Equation Models

Based on the pioneering work of Prandtl's mixing length theory and Kolmogorov's and Prandtl's one-equation models, the turbulence models in use today employ two differential equations for the turbulent length and time scales, and constitute the first complete turbulence models. Variations of these two-equation models are of interest for practical applications and under further development. These

include the High-Reynolds number standard k-ϵ model of Launder and Spalding (1974), the Near-wall and Low Reynolds number k-ϵ models (Patel et al., 1985), the k-ω model of Wilcox (1988), the k-τ model of Speziale et al. (1992), and the recently developed Renormalization Group (RNG) k-ϵ model of Yakhot and Orszag (1986), as well as a Multiple-Scale turbulence model of Duncan et al. (1993).

2.4.1 Standard k-ϵ Model

In the standard k-ϵ model of Launder and Spalding (1974), the turbulence kinetic energy k and its dissipation rate ϵ are calculated from transport equations in the fully turbulent flow region, and the Reynolds-stress tensor is represented by an eddy viscosity model constructed from k, ϵ and mean flow field. The turbulent eddy viscosity can be determined from the transport equation of k and ϵ, defined as:

$$\mu_t = C_\mu \rho \frac{k^2}{\epsilon} \tag{2.1}$$

For wall bounded flows, wall functions are adopted to blend the fully turbulent region with the near wall region, because of the predominance of viscous effect in that region. Used in conjunction with wall functions, the k-ϵ model is reasonably well behaved, and has been applied to the solution of many practical problems with a moderate amount of success. Because this model cannot be integrated directly to a solid wall, particularly in problems where wall transport properties are important, the development of various Low-Reynolds-number near-wall corrections have been proposed and will be reviewed.

2.4.2 Low-Reynolds-Number Near-Wall k-ϵ Models

The low-Reynolds-number models avoid the use of wall functions, and instead, propose a method for determining the various turbulence parameters all the way to the surface itself. The eddy viscosity is defined as:

$$\mu_t = C_\mu f_\mu \rho \frac{k^2}{\tilde{\epsilon}} \tag{2.2}$$

where f_μ is a damping function. In some versions, $\tilde{\epsilon}$ is equal to the actual dissipation ϵ, while in others it is $\tilde{\epsilon} = \epsilon - D$, where D depends on the version considered and is non-zero only in the viscosity affected region. The various Low-Reynolds number versions of the k-ϵ model differ in the form of the damping functions, in the values of the closure coefficients and in the surface boundary condition imposed on $\tilde{\epsilon}$. Details are given by Patel et al. (1985) and Wilcox (1993b).

The Low-Reynolds number k-ϵ models have the undesirable feature of requiring very high numerical resolution near the wall, and perform poorly in adverse-pressure-gradient boundary layers. Furthermore, the damping functions in these models were developed for attached boundary layers and are not always well behaved in separated flows (Rodi, 1991). In attempts to improve such situations, the two-layer model is adopted. It uses the one-equation model of Norris and Reynolds (1975) near the walls, because this model performs well in adverse-pressure-gradient boundary layers (Rodi and Scheuerer, 1986). For flow over a backward-facing step, the two-layer model predicted the reattachment length with much better agreement with the experiments of Driver and Seegmiller (1985), and it also produces a small second corner eddy which is absent in the calculation with standard k-ϵ model.

2.4.3 k-ω and k-τ Models

The k-ϵ model is the most widely used two-equation model, while k-ω and k-τ models are recently developed additions. The major difference between these models lies in the application of wall boundary conditions for the length scale variable and the source terms introduced in the turbulent variable transport equations.

The k-ω model of Wilcox (1988) is a two-equation model based on a transport equation for the turbulent time scale, where the turbulent kinetic energy k and

turbulent time scale ω are solved. The turbulent viscosity for this model is:

$$\mu_t = \gamma^* \frac{\rho k}{\omega} \tag{2.3}$$

where γ^* is the model constant, and ω is defined by $\omega = \epsilon/(\beta \cdot k)$.

With no viscous damping of the model's closure coefficients and without resorting to wall functions, the model equations can be integrated to the solid boundary. Hence, the k-ω model is more computational robust than the k-ϵ model for the integration of turbulent flows through the viscous sublayer. Furthermore, it has been designed to predict the proper wake strength in equilibrium adverse pressure gradient boundary layer flows. However, when this model is applied to free shear layers, a strong dependency of the results on the freestream value of ω has been found (Menter, 1992). Wilcox (1993a) proposed a modified version that eliminates the model's freestream boundary condition sensitivity and without destroying its accuracy for boundary layers in adverse pressure gradient and for transitional boundary layers. He shows that the k-ω model is superior over all other turbulence models for wall-bounded flows.

Instead of solving the turbulent length scale transport equation, a modeled transport equation for the turbulent time scale $\tau = 1/\omega$ is solved in k-τ model of Speziale et al. (1992). The eddy viscosity for k-τ model is:

$$\mu_t = C_\mu \rho k \tau \tag{2.4}$$

The advantage of this model is in the wall behaviour of τ. In the low Reynolds number form, at a solid wall, the dissipation rate ϵ can have a finite value at the wall, while, the turbulent kinetic energy is zero. Then the value of ω ($\omega = \epsilon/(\beta \cdot k)$) at the wall is infinity and the value of τ ($\tau = k/\epsilon$) at the wall is zero. This behaviour gives the k-τ model advantages over both the k-ϵ and k-ω models at low Reynolds numbers, because the equations are integrated directly to the wall and these boundary conditions

greatly affect the numerical behaviour of the solution.

2.4.4 RNG k-ϵ Model

The Renormalization Group (RNG) k-ϵ model is derived from statistical principles (Yakhot and Orszag, 1986). It is based on Gaussian statistics where an expansion is made about an equilibrium state by using the correspondence principle. In the high Reynolds number limit, the RNG model is identical to the standard k-ϵ model of Launder and Spalding (1974). The major difference between the RNG k-ϵ model and the standard k-ϵ model lies in the near wall treatment. The RNG k-ϵ model can be integrated directly to a solid wall without the need for wall damping functions. The constants of the RNG k-ϵ model are calculated explicitly by the theory, while, in the standard k-ϵ model, the constants are obtained from benchmark experiments for equilibrium turbulent boundary layers and isotropic turbulence, and are given in Table 2.1, respectively. Beyond having the attractive feature of no undetermined constants, the RNG k-ϵ model of Yakhot and Orszag (1986) automatically bridges the eddy viscosity to the molecular viscosity as a solid boundary is approached, thus eliminating the need for the use of empirical wall function or Van Driest damping. However, in the RNG k-ϵ model of Yakhot and Orszag (1986), the constant $C_{\epsilon 1} = 1.063$ is dangerously close to one, which constitutes a singular point of the ϵ-transport equation (Speziale and Thangam, 1992). To overcome this shortcoming, the new version of RNG k-ϵ model was recently adopted by Speziale and Thangam (1992) for the calculation of turbulent separated flows. The constants of this model are also given in Table 2.1.

Table 2.1: Comparison of model constants of k-ϵ, RNG and new version of RNG

	C_μ	$C_{\epsilon 1}$	$C_{\epsilon 2}$	σ_k	σ_ϵ
k-ϵ	0.09	1.44	1.92	1.0	1.3
RNG	0.085	1.063	1.72	0.7179	0.7179
RNG*	0.085	$C_{\epsilon 1}^*$	1.68	0.7179	0.7179

$$C_{\epsilon 1}^* = 1.42 - \eta(1-\eta/\eta_0)/(1+\beta\eta^3) \qquad (2.5)$$

It was shown by Speziale and Thangam (1992) that when this model is extended to include an anisotropic eddy viscosity, the predicted mean reattachment point is almost identical to the experimental data. The RNG k-ϵ model has been successfully implemented by a commercial finite volume program FLUENT (1993), where turbulent flow results shown based on the RNG k-ϵ model are much better than those of the k-ϵ model.

2.4.5 A Multiple-Scale Turbulence Model k_p-ϵ_p-k_t-ϵ_t

A multiple-scale turbulence model has been derived by Duncan et al. (1993). This model splits the energy spectrum into a high wave number regime and a low wave number regime, which correspond respectively to a region where the turbulent kinetic energy is produced by interaction with the mean flow and a region where the turbulent energy is transferred from the production region. Thus two sets of k_p-ϵ_p-k_t-ϵ_t equations are established, where k_p is the kinetic energy contained within the production region and ϵ_p is the rate at which energy is passed from the low wave number range into the high wave number range, k_t is the kinetic energy contained in the smaller eddies and ϵ_t is taken to be equivalent to the dissipation rate at the high wave number end of the spectrum. The eddy viscosity for this model is defined as:

$$\nu_t = C_\mu \frac{(k_t + k_p)^2}{\epsilon_p} \tag{2.6}$$

where the coefficients are determined by examining the decaying and homogeneous turbulence. This model has been applied to boundary-free turbulent shear flows with good agreement with data. Until now, there are no reports on wall bounded flows applications of this model.

2.4.6 Turbulence Near-Wall Functions

The wall function is derived by considering that the flow in the near wall region can be represented by a Couette flow approximation based on the logarithmic form of the law of the wall. The standard form of the near-wall model is the two-layer law of Launder and Spalding (1974), given by:

$$\frac{u}{u_\tau} = \begin{cases} y^+, & (y^+ < 11.63) \\ \frac{1}{\kappa}\ln(Ey^+), & (y^+ \geq 11.63) \end{cases} \tag{2.7}$$

where E is a wall roughness parameter, and κ is the von Karman constant. u_τ is the friction velocity and y^+ is the dimensionless normal distance from the wall. The wall function is applied at the first point located within the inner region of the turbulent boundary layer.

A new way of treating the wall functions was proposed by Chieng and Launder (1980) and latter by Amano (1984). In the two-layer model of Chieng and Launder (1980), the near-wall cell is treated as viscous sublayer up to a distance from the wall and fully turbulent beyond this, the first computational point lies outside the viscous

sublayer. In this model, the mean generation rate and mean dissipation rate of the k equation in the numerical cell adjacent to the wall is evaluated, while, the value of ϵ in the near-wall cell is approximated under local equilibrium condition. In the two-layer model of Amano (1984), the treatment of the ϵ equation in the near-wall cell takes into consideration the fact that the value of ϵ near the wall is an order of magnitude larger than that in the fully turbulent core and reaches its maximum at the wall. Each term in the ϵ equation is evaluated in accordance with the k equation rather than approximated under local equilibrium conditions. However, it was found that both linear and logarithmic profiles deviate from the experimental data in the buffer layer.

In order to improve the accuracy, another wall function method is proposed in which the velocity profile based on the Reichardt law, is defined as:

$$\frac{u}{u_\tau} = \frac{1}{\kappa}\ln(1+0.4y^+)+7.8\left[1-\exp(-\frac{y^+}{11})-\frac{y^+}{11}\exp(-0.33y^+)\right] \qquad (2.8)$$

Reichardt's law closely matches the experimentally observed velocity profile across the viscous sublayer ($y^+ < 5$), the transitional sublayer ($5 < y^+ < 30$) and the fully turbulent layer beyond ($y^+ > 30$). This method has been used by Autret et al. (1987) and a commercial finite element program FIDAP (1991).

A three-layer model was implemented by Thangam and Speziale (1992), in which all three layers, the viscous sublayer, the transitional sublayer and fully turbulent layer are considered. The law of the wall is then given by:

$$\frac{u}{u_\tau} = \begin{cases} y^+, & (y^+ \le 5) \\ -3.05+5\ln y^+, & (5<y^+<30) \\ 5.5+2.5\ln y^+, & (y^+ \ge 30) \end{cases} \qquad (2.9)$$

It was shown by Thangam and Speziale (1992) that the three layer law of the

wall, with standard k-ϵ model predicts a reattachment point longer than that of the two-layer law of the wall for flows over a turbulent backward facing step. However, the three-layer law of the wall boundary condition does not affect the turbulence stress profile.

The three-layer near wall model of Amano (1984) is comprised of a viscous sublayer, a buffer layer, and an overlap layer in the near-wall cell. In the application of the three-layer model, the first computational point lies outside the buffer layer and assumes the near-wall cell is large enough. He showed that the three-layer model gives better predictions than the two-layer model, but the latter requires less computational time. Details of the treatment of the three-layer model are given in Amano (1984).

2.4.7 Turbulence Modelling from a Numerical Viewpoint

The turbulence models previously described can be implemented by any well established numerical method, such as finite differences, finite volume, finite element, as well as control volume based finite element methods. Most of the early works on turbulence modelling uses the finite-difference and/or finite volume method based on hybrid central/upwinding differencing scheme, such as Chieng and Launder (1980).

Rhie and Chow (1983) applied the finite volume collocated method to solve the turbulent flows over airfoils with and without trailing edge separation. The k-ϵ model with wall functions was utilized to describe the turbulent flow processes. Their work used a general curvilinear coordinate system based on the TEACH code with SIMPLE method, thus eliminating the geometric limitation of TEACH code written for cartesian or cylindrical coordinates. They show that without separation, the k-ϵ turbulent model predicted values in reasonably good agreement with the experimental data; with separation, the k-ϵ model predicted poor results.

Zhu and Rodi (1992) have used the finite volume method with standard k-ϵ model to simulate the axisymmetric confined jets in a diffuser. It uses an equal-order, cell-centered grid with all the dependent variables stored at the geometric centre of the

control volumes. They solved the discretized equations based on a curvilinear coordinate system to treat the complex geometries. Three discretization schemes were used to approximate the convection terms, i.e. hybrid central/upwind differencing, QUICK and SOUCUP (Combined Second-Order Upwind, Central differencing and first-order upwind schemes). They showed that the high-order discretization of the turbulence equations plays a crucial role in accurately simulating turbulent flows.

Morgan et al. (1977) demonstrated the use of a mixing length and a two-equation turbulence model with the finite element method. They solved the coaxial jet flow using the Prandtl's mixing length model and fully developed pipe and channel flows using the k-l two-equation model. The solution domain considered does not extend to the wall but terminates inside the fully turbulent region. The near wall boundary condition is treated by the wall function method. Latter, they extended the method by using the k-ϵ model (Morgan et al., 1979) and solved the same flow problems, the results compared favourably with other numerical method predictions.

Benim and Zinser (1985) used a segregated solution algorithm with SUPG finite element method to solve pipe flows and confined jet flows. The turbulence is solved by the k-ϵ two-equation turbulence model. Instead of using the near wall first point of the boundary element to estimate the wall shear stress, the near wall second point in the boundary element is considered. The velocity components as well as the turbulent quantities k and ϵ are interpolated by bilinear function, a constant pressure is assumed on a quadrilateral element.

Comini and Del. Giudice (1985) demonstrated the use of the SIMPLER algorithm of Patankar (1980) coupled with the k-ϵ model with wall functions. The 8-node isoparametric elements are used for all variables. They solved a fully developed channel flow and a backward-facing step flow.

Autret et al. (1987) reported on the solution of turbulent flows by a Galerkin finite element method. They solve the turbulent flow over a backward-facing step using the k-ϵ model. The wall region is treated through the Reichardt's law. They show how

the numerical reattachment length is underpredicted, and an appropriate choice of C_μ can gives qualitatively better results.

Benim (1990) reported the solution of steady confined turbulent swirling flow by a SUPG finite element method. The momentum and continuity equation are solved using a segregated algorithm. Both the k-ϵ model and the algebraic stress model (ASM) are considered. He showed that the ASM leads to more accurate results for swirling flows compared to the k-ϵ model.

Manouzi and Fortin (1991) developed a transmission finite element method to model the boundary layer flow. The method is based on a domain decomposition into subdomains near a solid boundary. This boundary element has both linear and logarithmic variation for the vertical direction and a quadratic variation in the horizontal direction. It was found that the latter provides a more accurate representation of the logarithmic-linear velocity profile to the boundary of the flow domain. They calculated the poiseuille flow and flow over a backward-facing step.

Elkaim et al. (1992) developed a numerical procedure to solve turbulent flow with the k-ϵ model based on a control volume finite element method. They treated the pressure-velocity coupling by the vorticity-streamfunction formulation. Both the law of wall and Low-Reynolds number formulations are implemented to take into account the wall effects. They found the latter to perform better in recirculation regions.

Zuercher and Rozon (1993) demonstrated the turbulence modelling using the commercial control volume finite element method code Aerovisc/TASCflow. Two-layer and k-ϵ turbulence models with and without an additional dissipation rate equation source term modification were considered. In the application of two-layer turbulence model, the computation domain is divided into two regions: away from walls and near walls. They used the combination of the standard k-ϵ model away from the wall and a one-equation model in the near wall region. They found that two-layer model provided improved predictive capability compared to the wall function approach. For the turnaround duct test case, flow separation was predicted using the

two-layer model, whereas it was not using the k-ϵ turbulence model and a log-law wall function method.

2.5 Combustion: The Conserved Scalar Approach

Chemical reactions usually involve many species and proceed through a large number of finite rate reaction steps. Essentially, these reaction processes can be described by conservation equations for the mean value of each species, which in turn leads to computation of the mean reaction rates of each species. These reaction rates are inevitably highly nonlinear functions of the temperature and the concentration of species, as well as theirs corresponding second-moment correlations. However, knowledge of these quantities is insufficient to obtain reaction rates, which makes it very difficult to simulate the combustion process. A simplification of the above difficulty is the use of the conserved scalar approach (Bilger, 1980). Considering the turbulent nonpremixed flame with two streams of reactants, where turbulent mixing is important and the chemical reactions are assumed sufficiently "fast" for all reactions to go to equilibrium as soon as the reactants are mixed. Then the calculation of the mean reaction rates in the conservation equations of species is no longer required as all species may be determined simply in terms of strictly conserved scalar variables. Following Bilger (1980), the reaction takes place in an irreversible, single step as follows:

$$1\,kg\ Fuel + s\,kg\ Oxidant \rightharpoonup (s+1)\,kg\ Products \tag{2.10}$$

where the reaction rate obeys:

$$\dot{w}_F = \dot{w}_O/s = -\dot{w}_P/(s+1) \tag{2.11}$$

and the linear relationships for the conserved scalar variables as:

$$\begin{cases} \beta_{FO} = Y_F - Y_O/s \\ \beta_{FP} = Y_F + Y_P/(s+1) \\ \beta_{OP} = Y_o + sY_P/(s+1) \end{cases} \tag{2.12}$$

Here, Y_F, Y_O, and Y_P represent the mass fractions of fuel, oxidant and products, respectively, and s is the stoichiometric ratio of oxidant required to burn 1 kg fuel. β_{FO}, β_{FP} and β_{OP} are the conserved scalars of the mixture fractions.

The preferred choice of conserved scalar is the mixture fraction, others may be formed using the sensible enthalpy. The conserved scalar approach is suited only when there are two uniform reactant feeds, then linear relationships among all the conserved scalars exist (Bilger,1980). It is not only useful in one-step reaction, but it can also be extended to two-step reactions (Nikjooy et al., 1988) and multi-step reactions such as the chemical equilibrium model of Gordon and McBride (1971). Based on the conserved scalar approach, the combustion models can be classified as: the fast chemistry reaction model, probability density function of conserved scalars, chemical equilibrium model, laminar flamelet model, or the finite rate chemistry with a two-variable modification, such as eddy-break-up model (Spalding, 1971b) and eddy dissipation combustion model (Magnussen and Hjertager,1976).

2.5.1 Fast Chemistry Reaction Model

The fast chemistry reaction model assumes that the reaction is so fast that fuel and oxidant do not co-exist anywhere, except within an infinitely thin flame sheet (both the fuel and the oxidant will be zero when the mixture is stoichiometric). According to the above assumption, Williams (1965) concluded that a linear combination of species conservation equations for fuel and oxidant, yields an equation whose form is identical to the conservation equation of chemically inert species without source terms. In this model, only one conservation equation of mixture fraction is solved. Recent applications of this model by different numerical methodologies are made by Kim

(1987) with finite element method, by Elkaim et al. (1993) with CVFEM and vorticity streamfunction formulation, by Liu et al. (1993) with finite volume multigrid method. The advantage of this model is that it allows the solution to converge easily because the governing equation of the mixture fraction has no source term. While this model assumes that fuel and oxidant cannot co-exist, some available experimental results are contrary to this assumption and indicate that the fuel and the oxidant may exist at the same location but at different times. Modifications to account for this co-presence of the reactants, were made by Spalding (1971a), Lockwood and Naguib (1975) and Bilger (1975).

2.5.2 Probability Density Function Model

Consideration of the concentration fluctuations, or unmixedness and intermittency, has led to the development of the probability density function (PDF) model. The PDF of conserved scalars by the mean and the variance (e.g. mixture fraction f and concentration fluctuation variable g) can be specified from three types of assumed forms, double delta PDF of Spalding (1971a), beta PDF of Jones (1979) and clipped Gaussian PDF of Lockwood and Naguib (1975). By comparing various PDF models for the hydrogen-air round jet diffusion, Jones (1979) concluded that while the double delta PDF gives rise to unrealistic results, the clipped Gaussian and Beta PDF provide good agreement with little difference. Recently, a comparative study of the delta and beta PDF models were made by Kim and Chung (1989) with finite element method, by McKenty et al. (1993) with control volume finite element method. Good agreement being obtained with experimental data for the conserved scalar field and for the mean composition. When more accurate forms of the PDF are required, the direct calculation of PDF is needed (Pope, 1976, O'Brien, 1980).

2.5.3 Chemical Equilibrium Model

For reversible reaction, the fast chemistry assumption implies that the forward

and back reaction rates are fast compared with the turbulent mixing processes, thus the composition of the mixture at a given point at any particular instant will be the same as that reaches if the mixture were isolated and allowed to come to chemical equilibrium (Bilger, 1980). Bilger suggested that for many species and multiple reactions, the chemical equilibrium constants of molecular species can be calculated from the elemental composition and enthalpy defined by a conserved scalar approach. The most reliable method for the calculation of the equilibrium state of a gas is based on the minimising of the Gibbs free energy, which is described by Gordon and McBride (1971). This has lead to a well tested and reliable computer program that has been used by Liew et al. (1981), Jones and Whitelaw (1982) for different reaction problems. Another discussion of the minimization of free energy technique can be found in Heywood (1986). In case of methane/air mixtures, Jones (1979) showed that in their chemical equilibrium results, in the fuel lean regions, negligible quantities of CO are present; in the fuel rich region, appreciable CO concentration exists.

2.5.4 Flamelet Model

In the laminar flamelet concept the turbulent diffusion flame is considered as an ensemble of thin laminar diffusion flamelets. The model is applicable if the length scales of the turbulent eddies are much larger than the reaction zone thickness of the flamelets (Rogg et al., 1986). The laminar flamelet concept can be used to determine the composition and temperature as a function of the conserved scalar (such as mixture fraction). The flamelet can be specified from the reaction mechanism provided by either experimental measurement or numerical prediction.

Liew et al. (1981) established their flamelet model on the experimental data of Mitchell et al. (1980). They supposed that the microscopic element in the model describing local mixture state and burning, has the structure of an undisturbed laminar diffusion flame. This provides unique relationships for all thermochemical variables in terms of the conserved scalar (or mixture fraction) alone. These relationships are

then averaged, for the turbulent flame using an assumed PDF of the conserved scalar. By comparing the results between the flamelet model and the chemical equilibrium model of Gordon and McBride (1971), they showed that their flamelet model yields substantial improvements in the prediction of mean CO concentration in the fuel rich regime of an open turbulent methane/air diffusion flame. The specification of the flamelet model using numerical prediction may be found in Liew et al. (1984). They proposed a simple method for the incorporation of detailed non-equilibrium hydrocarbon chemistry into a representative flow field model. The microscopic element in the turbulent ensemble is taken to be a stretched laminar flamelet, drawn from a library of such flamelets in which the extent of local stretching is characterized by Damkohler number. The application of the flamelet model, were also shown by Rogg et al. (1986) to partially premixed diffusion flamelets with detailed chemistry, by Askari-Sardhai et al. (1985) to propane/air reaction, by Cant et al. (1990) to premixed turbulent flame, respectively. Recently, McKenty (1992) established a micro-flame model for methane/air flames based on the experimental data of Mitchell et al. (1980). The model relates the species mass fraction of the combustion products to the mean mixture fraction. It is shown that this model gives better predictions of CO and H_2 mass fraction than the chemical equilibrium model for fuel rich mixtures.

2.5.5 Eddy Dissipation Combustion Model

Extension of the conserved scalar approach to the case of finite rate chemistry is carried out by considering an additional variable which is affected by the chemical kinetics. The eddy-break-up (EBU) model of Spalding (1971b) combines the effects of mixing and kinetics through the use of the eddy break-up rate and the kinetic rate of reaction in a laminar premixed flame. Magnussen and Hjertager (1976) extended the idea of the EBU model, and proposed the eddy dissipation concept (EDC) for both turbulent diffusion and premixed flames. Based on EBU or EDC model, a single step, irreversible fast reaction described by two differential equations, one for the mixture

fraction, another for mass fraction of fuel are solved. This approach is semi-empirical and not soundly based in theory (Bilger, 1980). It is however widely used in the combustion community due to its simplicity and flexibility in applications to 3D complex geometries (Bai and Fuchs, 1993). Jessee et al. (1993) presented a finite volume method for the solution of turbulent reacting flows using a finite chemical kinetics model based on the eddy dissipation concept. Extension of the EBU model to a two-step global reaction of hydrocarbon fuel described by Westbrook and Dryer (1981) is carried out by Nikjooy et al. (1988) using the finite volume method, where the three equations for unburnt fuel, carbon monoxide (CO) and mixture mass fraction are solved, two of these equations have a non-zero EBU source terms. Application of the EDC model to a four-step reduced reaction mechanism of hydrocarbon fuel suggested by Hautman et al. (1981) are made by Bai and Fuchs (1993), with the use of the finite difference together with a multi-grid method and a local grid refinement technique. Other applications of EDC model by using the different numerical methods, were also found in Benim (1989) with FEM, by Mckenty (1992) with CVFEM and a vorticity-streamfunction formulation.

2.5.6 Other Methods

Much work is presently underway in predicting turbulent flows through direct numerical simulations (McMurty and Givi, 1989), PDF modelling (Chen et al., 1989) and finite chemical kinetics embedded in the flow calculations (Vos, 1987).

Direct numerical simulation refers to the numerical solution of the exact aerothermodynamical equations of the unsteady turbulent reacting flow field (McMurty and Givi, 1989). No turbulence modelling is required because of the turbulence is obtained as the direct solution of the unsteady equation. However, the large disparity in time and length scales and limited computer capacity, makes this method impractical for most practical applications.

PDF modelling on turbulent nonpremixed methane jet flames was demonstrated

by Chen et al. (1989) using the Monte Carlo simulation. The chemical reaction models are considered as a five-scalar, four-step reduced mechanism and a four-scalar constrained equilibrium model, respectively. They make use of the PDF submodel to handle five scalars, while turbulence velocity field is described by a second-order moment closure. Hsu et al. (1993) developed a PDF approach for compressible turbulent reacting flows for the use with a CFD flow solver. The PDF of the species mass fraction and enthalpy are obtained by solving a PDF evolution equation using a Monte-Carlo scheme. Their scheme is the combined finite-volume Monte-Carlo procedure. However, the PDF approach has only been used in some simple applications due to its complexity.

Vos (1987) showed the numerical solution of turbulent reacting flows using finite chemical kinetics with the finite volume method. He proposed a two-step, pseudo-time-splitting algorithm for the solution of mass fraction equations. This technique is also implemented by Coelho and Pereira (1992) for predicting methane/air laminar diffusion flame with a finite rate chemical kinetics combustion model using a local grid refinement technique. In the first step, convection and diffusion of all species in the standard governing equations are solved by the Gauss-Seidel line by line iterative procedure. In the second step, chemical reactions are taken into account for all mass fractions simultaneously by integrating the stiff ordinary-differential equations with chemical source term using a general chemical kinetics code package CHEMKIN (Kee et al., 1980). Similar procedures are adopted by Jessee et al. (1993) for the finite chemical kinetics calculation using the eddy dissipation concept, but the reaction time is controlled by the local turbulence rather than by the local residence time (Coelho and Pereira, 1992) for the given control volume. In order to predict the CO and NO, they make use of the simplified thermal NO_x reaction mechanism of Miller and Bowman (1989). Radhakrishnan and Pratt (1988) proposed a fast algorithm for the calculation of chemical kinetics equations by using exponentially-fitted integration algorithms namely CREK1D.

2.6 Radiation Modelling

Radiation is the dominant mechanism of energy transfer to the walls of large scale combustion chambers. The difficulties associated with radiation modelling are the multi-dimensional nature of the phenomena, the integro-differential nature of radiative transfer equation, and the coupling between the radiative transfer equation and energy conservation equation (Chiu, 1990). Unlike the flow field, which can be solved directly by a spatial integration algorithm, for radiation, both spatial integration and angular integration have to be carried out. There are several radiation models, such as Zonal (Hottel and Sarofim, 1967), Monte-Carlo (Howell, 1968), Flux (Gosman and Lockwood, 1973) methods, etc.. The excellent reviews of various radiation models on combustion system are given by Viskanta and Menguc (1987), and by Howell (1988).

In this section, several well established radiation models are discussed with emphasis on their application to irregular shaped complex geometries and coupling to the flow equations. The problems posed by the application to practical furnaces are presented.

2.6.1 Zonal Method

The Zonal method is based on the view factor and mean beam length concepts. Essentially geometric in its approach, the domain is divided into a number of surface and volume zones about which radiation balance and total energy balance are formulated. Each zone is considered to be uniform in temperature and radiation properties. The heat release and the flow patterns are specified in advance. Geometrical exchange factors (exchange areas) between each zone pair are supposed to be known a priori.

The advantage of this method is that it can approach an exact solution for the radiative fluxes as the number of zones is increased, and even for a relatively coarse zoning, it can give good results.

The major difficulty of applying this method is the tedious evaluation of the direct exchange areas. Attempts to improve the zonal method were made by Larsen and Howell (1985) with an exchange factor method, by Naraghi et al. (1988) with a continuous exchange factor method in participating media, by Saltiel and Naraghi (1991) with an exchange factor method in nonhomogeneous media, respectively. Considering the anisotropically scattering media, Yuen et al. (1992) developed a Generalized Zonal method. However, there is a difficulty in matching the required grid sizes for radiation and fluid flow field (Howell, 1988) and the calculation of the exchange areas remains very difficult for complex geometries (Viskanta and Mengüç, 1987).

2.6.2 Monte Carlo Method

The Monte Carlo method is based on a statistical approach. The exchange factors are automatically calculated as the randomly chosen energy releases are tracked through the domain for their lifetimes. This method can in principle be programmed to include an exact simulation of all important physical processes (Howell, 1988). Applications may be found in Taniguchi (1969), Steward and Cannon (1971), Gupta et al. (1983), Burns et al. (1992) and Gorner and Dietz (1993), which illustrate its geometry flexibility and ability to handle difficult problems.

The drawbacks of this method is that it requires long computation time to obtain good results due to the method's statistical approach. Another difficulty is the grid size incompatibility, in which the computational element size required for statistical accuracy in the Monte Carlo solution may not be compatible with the grid size necessary for numerical solution of the energy equation, even given sufficiently fast and cheap computation capability (Howell, 1988).

2.6.3 Flux Methods

In the flux methods the angular variation of the radiant intensity in space is

assumed to be of a certain functional form. The integro-differential radiative transfer equation then reduce to a set of partial differential equations. The various flux methods are classified as Flux Model, Spherical Harmonics (P-N) method, Discrete Ordinates (S_N) method according to the different functions (or weighting coefficients) used.

Because this class of methods is essentially a field method, they can easily be incorporated into existing flow and reaction solvers.

Flux Models

The flux model includes the 2-Flux model (Siddall and Selcuk, 1974), 4-Flux model (Lockwood and Spalding, 1971) and 6-Flux model (Patankar and Spalding, 1974) in 1-, 2- and 3-dimensional heat transfer problems, respectively. In this model, the space is divided into 2, 4 and 6 directions along each coordinate direction, and the intensity is assumed uniform in each direction. DeMarco and Lockwood (1975) developed a new flux model, in which a six-term Taylor's series expansion is used to represent the directional dependency of intensity and resulting in 6 flux partial differential equations. The result is shown to be better than that of the 6-Flux model. The application of the various Flux models in combustion chambers may be found in Khalil (1982).

The flux models provide a very economical tool for predicting radiative heat transfer in rectangular shaped enclosures (Benim, 1988). However, due to the lack of coupling between the radiant fluxes, the accuracy with this method is limited. Also, these methods are generally not compatible with arbitrary shaped geometries, and their application to complex geometries is not straightforward (Benim, 1988). Improvement of the accuracy of the flux model, has led to the development of the P-N and S_N methods, which has a tight coupling between the radiant fluxes.

Spherical Harmonics (P-N) Method

The Spherical Harmonics (P-N) method assumes that the angular distribution

of radiant intensity in a medium can be approximated by a finite series of spherical harmonics. The intensity is expanded in an orthogonal series of products of a position dependent coefficient and a normalized spherical harmonic function. The order of the approximation N is the truncation of the series. In principle, as N increases to infinity, the solution approaches the exact solution of the radiative transfer equation.

A general description of P-N method is given in the book by Davison (1957). It has been widely used in various problems with good accuracy (Ratzel and Howell, 1983, Mengüç and Viskanta, 1985, Modest and Sikka, 1991). Usually, the P-3 method is appropriate for the application to engineering problems with good accuracy and moderate computational time.

The disadvantage of applying the P-N method lies in its inflexibility. Deriving and using of the expansions of order N greater than 3 becomes very difficult (Howell, 1988). For example, for N equal to 5, the derivations are more complex and costs as compared to the P-3 method with negligible improvement in accuracy (Mengüç and Viskanta, 1985).

Discrete Ordinates Method

The discrete ordinates method (S_N) (Chandrasekhar, 1960) assumes that the angular distribution of intensity about a location can be expressed by a discrete set of intensities which span the entire solid angle of 4π. The angular integral of intensity is discretized by numerical quadrature. The discrete ordinates equations are obtained by evaluation of the radiative transfer equation in these specified directions.

The S_N method has been widely used in the thermal radiation community: by Fiveland (1984, 1988), Truelove (1974, 1988), Kim and Lee (1988), Jamaluddin and Smith (1988,1992), Chai et al. (1993 b,c,d) for simple geometries, by Sanchez and Smith (1992), Chai et al. (1993 a,c) for complex geometries. The accuracy of the S_N method depends on the selection of discrete directions and associate weights, the choice of quadrature scheme may be found in Carlson and Lathrop (1968), Fiveland

(1984,1991) and Wakil and Sacadura (1992). The use of the S_4 method is found to be slightly more accurate than P-3 method (Fiveland, 1984). Extension of the S_N method with the finite element formulation is shown by Fiveland et al. (1993).

For problems where scattering dominates, this method works very well, but errors may arise if it is applied to absorption dominated problems due to the "ray effect" (Lathrop, 1968). Discussions on "ray effect" occurring on the application of the S_N method are given by Chai et al. (1993d). They concluded that the ray effect arises by the inability of the discretized intensity distribution to fully represent the actual continuous intensity distribution, it is independent of the spatial discretization. By increasing the number of ordinate directions, the ray effect can be reduced, but cannot be eliminated (Fiveland, 1984). Similar to the false diffusion concept in fluid flow, they introduced a new concept "false scattering" for radiation which appears in the application of the S_N method, and is a consequence of spatial discretization and is independent of the angular discretization. It happens when a beam is not aligned with the grid line in the multi-dimensional computations.

2.6.4 Discrete Transfer Method

The discrete transfer method was proposed by Shah (1979), and Lockwood and Shah (1981). Firstly, the surface of the enclosure is divided into subsurfaces, and the volume of the medium is divided into cells (or Zones); secondly, taking each subsurface as a hemisphere, the emitted radiation is subdivided into beams, where each beam is assumed to have positive and negative propagation direction (Fluxes); finally, the beams are drawn hemispherically from each subsurface in prescribed directions (similar to Monte Carlo method, in random direction). The solution proceeds along individual rays of intensity, one at a time, instead of solving for all the intensities in the field. It can be classified as the ray tracing method. A survey of the state-of-the-art of ray tracing procedure are given by Glassner (1989). This method can be considered as a combination of the Zonal method, Flux Model and Monte Carlo technique. It

retains their advantages while avoiding their shortcomings.

Because the number of beams is specified in advance, it can be more economic than the Monte Carlo solution which needs a lot of random beams to obtain good results. It is flexible and able to handle complex geometries. In application to absorption media, finer discretization can yield any desired degree of precision, and even reproduce the exact solutions (Lockwood and Shah, 1981). For gas flames, where the scattering is zero, the method can provide excellent results as evidenced by the work of Abbas et al. (1984, 1986), Fiveland and Wessel (1986), Carvalho et al. (1987,1988, 1990), Meng et al. (1992). Extension of this method to cylindrical enclosures for the isotropic scattering medium were made by Carvalho et al. (1991). Application of this method to complex geometries are given by Murthy and Choudhury (1992), Meng et al. (1993). When scattering is considered, a simple average is used in the discrete transfer computations, unlike the S_N method which use a more accurate numerical quadrature. This will reduce the accuracy when this method is applied to solve anisotropic scattering problem.

Discrete transfer method may also suffer from the ray effect, as shown by Viskanta and Menguc (1987), Carvalho (1991) and Meng et al. (1993), but the false scattering is not found. This is due to the ray tracing approach, where the intensity is solved along the "upwind" ray propagation direction.

2.6.5 Other Methods

The radiative transfer equation can be solved by other methods, as the finite element method (FEM) (Razzaque et al., 1983,1984, Fiveland et al., 1993) and finite volume method (FVM) (Raithby and Chiu, 1991), as well as boundary element method (BEM) (Bialecki, 1991).

The advantage of using FEM is that it offers the possibility of high accuracy, and can be used with the same grid as for the flow and energy conservation equation. Furthermore, it can be applied to complex geometries. However, this method is still

limited when using very coarse grid, due to the high computational cost (Howell, 1988). Tan (1989) used the product-integration method to solve radiation problems, significantly reducing the solution time of FEM.

The FVM can give good accuracy on coarse grid. The intensity at the integration points are determined from the solution of the radiative transfer equation using the skewed upwinding procedure (Raithby, 1976b). It satisfies the global conservation constraints for intensity and heat flux, hence prevents the occurrence of the "ray effect" encountered in the S_N method (Chiu, 1990).

Using BEM, the integration is over the boundary, no volume integrals are present in BEM, thus it requires fewer calculations (Bialecki, 1991). However, because the ray-tracing method is used in BEM computations, it may suffer from the disadvantages of the discrete transfer method when scattering has to be considered.

2.6.6 Radiation Models for Complex Geometries

Most of the radiation models have the ability to deal with irregular and complex geometries. The Monte-Carlo method (Burns et al., 1992, Gorner and Dietz, 1993) is very flexible and can provide high accuracy if a sufficient number of random rays is chosen. However, at the cost of computation efficiency. The Zonal method (Hottel and Sarofim, 1967) and its extension, the Exchange Factor method (Naraghi et al., 1988) can be computationally efficient but have the problems of computing the exchange factors in very complex geometries. Saltiel and Naraghi (1990) developed a new discrete exchange factor method, where the exchange factors are calculated from point to point. It is flexible because unstructured triangular meshes are used. Lisienko et al. (1992) presented a Zone-Node method for radiating gas in complex geometries, with two set of grids, a fine curvilinear orthogonal grid for the computation of the flow field and a coarse grid for the computation of radiation. Haidekker (1991) demonstrated the radiation solution in complex 3D geometries using the zonal, the imaginary plane and the discrete transfer method. Both the blocking technique and the

curvilinear coordinate system are used to deal with the irregular shaped enclosures, where the computation meshes are based on unstructured rectangular meshes.

Chai et al. (1993e) presented a procedure to model radiation in irregular geometries using the discrete ordinates method. They dealt with the irregular boundary using the blocking or ladder-like approximation, such as used in past finite difference procedure based on structured cartesian grids. The finer the mesh, the more realistic the representation of the real boundary. However, the memory is used inefficiently when the blocking technique is used. Chiu (1990) developed a finite volume method based on the discrete ordinates approximations of RTE. For simple domain considered, the irregular shaped boundary is treated by dividing the azimuthal angle in accordance with the orientations of the bounding surfaces; for complex geometries, the special treatment of intensity is considered when the angular grid with solid angles straddling over a boundary surface.

Unlike the discrete ordinates method, the discrete transfer method can make perfect angular discretization to match the real boundary. This is because the method is based on a ray tracing approach, the ray directions are specified in advance on each emitting surface arbitrarily. Applications of the discrete transfer method for complex geometries are shown by Murthy and Choudhury (1992) on a non-orthogonal rectangular grid, by Meng et al. (1993) on unstructured triangular grids.

2.6.7 Emissivity Models

The above approximation methods assume that the radiative transfer equation is in a form applicable to homogeneous and gray media. For the nongray medium, the spectral effect of the radiation has to be considered, and the radiative transfer equation should be integrated over the entire wavelength spectrum. Naturally, this will make the computation times prohibitive. Under some situations this is not necessary, for example, in natural gas or oil fired combustors, only three species contribute significantly to the radiation in the infrared region. These species are the products of

the combustion, i.e. carbon dioxide, water vapour and hot soot particles within the flame produced by the thermal decomposition of fuel lean situations (Khalil, 1982). The gases radiate in several bands, while the soot emits continuously over a wide range of wavelength. It is only necessary to represent the spectral effects by several bands for each species instead of using whole wavelength in real gases of combustors.

The simple model of accounting for the spectral effect is Hottel's "emittance charts" and the "sum of gray gases" methods (Hottel and Sarofim, 1967), which were borrowed from the atmospheric physics, and named "narrow band models" (Goody, 1964). In Hottel's method, the determination of the coefficients is based on a trial and error graphical fitting technique of Hottel and Sarofim (1967). For CO_2-H_2O mixture, the emissivity could be fitted by a "one-clear plus two-gray gas" by Truelove (1974). When more than two-term fits are considered, Hottel's fitting method tends to be rather time consuming. Taylor and Foster (1974) proposed a least-squares technique for determining the coefficients. For CO_2-H_2O mixtures the emissivity is fitted by a "one-clear plus three-gray gas" model, in the temperature range from 1200 to 2400 K. Good accuracy is obtained for a large range of path length. The application of "mixed grey and clear gas" formulation to the real furnace gas may be found in Abbas et al. (1984, 1986), Carvalho et al. (1987,1988,1990).

A more useful approach to modelling the spectral properties of the gases is the wide-band models of Edwards (1968), in which the band emittance of these gases is considered as a function of total and partial pressure, path length and temperature. This method makes the band properties of the gas mixture relatively easy to calculate, but the computation time is longer than the mixture of gray gas model of Hottel and Cohen (1958). Docherty and Fairweather (1988) incorporated the wide band model into the computation of the nonhomogeneous combustion products by the discrete transfer method, they showed a good agreement with the narrow band model results for both spectral and total radiative intensities.

2.6.8 Radiation Modelling in Real Scale Furnaces

Early reports on the modelling of the flow, combustion and heat transfer in real scale industrial furnaces are mainly based on the flux models. Gosman and Lockwood (1973) have studied the flow, heat transfer and chemical reaction processes in a gaseous-fired cylindrical furnace. The flow field was solved by the vorticity-stream function combined with two-equation k-ϵ turbulence model using the finite difference method. The chemical reaction is considered as a single-step fast chemistry reaction model. Heat transfer is determined by solving the specific enthalpy equation coupled with radiation. The radiation model is considered as a four flux model. Encouraging agreement is obtained between the predicted and measured distribution of temperature and radiant heat transfer along the furnace wall. However, because the effect of the "unmixedness" phenomena was neglected in the combustion computations, the flow field is unsatisfactory. Considering the unmixedness, Gosman et al. (1978) used a beta PDF model for the prediction of various gas-fired cylindrical furnaces, where the radiation transfer is calculated with a new flux model of Lockwood and Shah (1978). A general procedure for the computation of 3D flow with combustion and heat transfer has been described by Patankar and Spalding (1974), where the six flux radiation model is considered. Latter, this procedure was applied to the case of the experimental rectangular furnace of the International Flame Research Foundation (IFRF), Holland by Pai et al. (1978). Farouk and Sidawi (1993) developed a 3D computation model for the simulation of the turbulent reactive flow of the natural gas fired industrial furnace. The turbulent flow is simulated by a k-ϵ-g model, and the combustion model is based on the local instantaneous equilibrium where the combustion process is assumed to be micro-mixing limited. A gray six-flux model is used in the prediction of radiation transfer.

Recently, the discrete transfer method has become popular in the prediction of the large-scale combustion furnaces. Abbas et al. (1984) demonstrated the predictions of the flow, combustion and heat transfer within a refinery process heater, where the

radiation transfer is handled by the discrete transfer method with the mixed gray and clear gas emissivity model. In the consideration of the computational economy, the whole computation domain is divided into two zones with the burner region and the main combustion chamber region. The radiation calculations were performed simultaneously on a coarse grid where the radiation source for each flow cell is calculated on a volumetric basis. A similar procedure was implemented by Abbas and Lockwood (1986) for the prediction of power station boilers. Fiveland and Wessel (1986) developed a numerical furnace model (FURMO) for 3D pulverized-fuel fired furnace. They used the discrete transfer method in the solution of the radiation transfer, where the absorption and scattering coefficients in the radiative transport equations for particle-gas mixture are considered. The scattering coefficients are computed using Mie theory (Van De Hulst, 1957) by estimating the amount of each particle type in the computational cell, and the absorption coefficient for gas mixture is calculated using the wide-band model of Edwards (1967). Carvalho et al. (1987, 1988, 1990) and Coelho and Carvalho (1993) have demonstrated the simulation of 3D flow, reaction and heat transfer in industrial glass furnaces and boilers. Most of their computations are based on the domain decomposition method. The governing equations are solved by finite-difference/finite volume method, and a staggered grid is used for velocity components. They made use of the discrete transfer radiation model along with the Hottel's mixed gray gas model. The different techniques in the application of the discrete transfer method to the large-scale furnaces are shown. These techniques involve: update of the radiation variables less frequently than the others, usually every 10 iterations for the radiation calculations (Carvalho et al., 1987, 1990); using coarse grid for radiation calculations (Carvalho et al., 1990, Coelho and Carvalho, 1993); less rays per each boundary cell, usually 4 and 8 rays (Carvalho et al., 1988). Fairweather et al. (1992) reported the prediction of the structure and thermal radiation received around a turbulent reacting jet discharging into a cross-flow. Both flamelet and soot formation and consumption are derived from a global reaction scheme for hydrocarbon

combustion. In their computation, the radiation received external to a flame was computed from converged flow field calculations through the use of a 3D adaption of the discrete transfer method coupled to a narrow band model of radiative transfer.

The application of the discrete ordinates method to the boiler is reported by Jessee et al. (1993). The use of the Monte-Carlo method with the approximated flow and heat release to industrial furnaces may be found in Gorner and Dietz (1993).

Most of the aforementioned methods are based on finite difference/finite volume method, which suffer from the difficulty in dealing with the complex geometries. The typical example is that the irregular-shaped wall is treated by stepwise approximation (Carvalho et al., 1987). This difficulty can be overcome by using the finite element method or the control volume finite element method.

Benim (1989) introduced a finite element solution of a turbulent diffusion flame in furnace. The combustion rates are estimated using the eddy dissipation concept model. The moment method (Benim, 1988) is used which allows the derivation of an approximation local field equation for the radiation intensity, and it can be directly used in irregular grids. The procedure is then applied to the simulation of flame 29 of the M-2 trials performed in the IFRF, with good agreement with experimental data and with finite difference predictions. Engelman and Jamnia (1991) introduced a numerical procedure for the simulation of the effects of gray-diffuse surface radiation on the temperature field of fluid flows using FIDAP. The radiation is solved by using the view factor methods with non-participating medium. They showed the coupling between the energy equation and the radiation heat transfer exchange relationship in their finite element method. For considering the participating medium, Jamnia (1992) incorporated the P-1 approximation model in the FIDAP code. By testing different cases, he showed that the advantage of this method lies in its simplicity of incorporating in a general purpose code. Meng et al. (1992) presented a control volume finite element method for the simulation of the turbulent reacting flow in furnaces. The flow is solved by the vorticity streamfunction formulation and the k-ϵ

two-equation model. The chemical reaction is considered as the fast chemistry. The radiation heat transfer is solved by a discrete transfer method on an unstructured triangular grid. The heat flux to the furnace wall is good agreement with the experiment data of the M-2 trials, flame 29 of the IFRF.

2.7 Choice of Overall Numerical Model

Criteria for choosing a model and a numerical scheme lie in its conceptual simplicity, economy of computation, ability to handle complex geometries and possibility of extension to three dimensional flow problems. Based on the previous review, the choice for the basic components of the overall numerical model is as follows:

Fluid Flow: Control Volume Finite Element Method

- Primitive variable (u,v,p)
- Staggered grid arrangement
- Unstructured mesh
- Segregated solution algorithm

Turbulence: Two-Equation Model

- k-ϵ model and wall functions

Combustion: Diffusion Flames Models

- Fast chemistry reaction model
- Delta and Beta PDF model
- Eddy dissipation model
- Chemical equilibrium model
- Flamelet model

Radiation: Discrete Transfer method

- Mixed gray and clear gas model

The proposed numerical method namely an unequal-order, Staggered Control-Volume Finite-Element Method (SCVFEM) for fluid flow and heat transfer has been developed. The method use primitive variables on a three-node triangular element. Pressure is stored at the centroid of each triangular element, while velocity components and other scalar variables are located at the midpoint of sides or at vertices of each element. Depending on the location of the variables, this leads to two different schemes: Face-centered scheme when variables are stored at the midpoint of each side; and Vertex-centered scheme when variables are stored at vertices.

The classical technique of staggering of variables used in structured grids is extended to an unstructured mesh by using two control volumes. The control volume for the continuity equation is the triangular element itself. The control volumes for the momentum equations and the other scalar transport equations depend on the scheme used. For the Face-centered, the co-volumes are constructed by joining the centroid and vertices encompassing the common side of two neighbouring elements; while, for the Vertex-centered, the polygonal control volume surrounding each node is constructed by joining the centroid of elements to the midpoints of the corresponding sides. The discretized control volume for any conservation equations is ensured to be conservative in the whole calculation domain. The integration of the general conservation equation is carried out on these discretized control volumes. The resulting algebraic equations for pressure, velocity components as well as other scalar variables have the conservative properties. A segregated solution algorithm is used.

Chapter 3

Mathematical and Physical Models

3.1 Introduction

In this chapter, the Favre-averaged equations governing the mass, momentum, turbulent quantities, and energy are presented for turbulent reacting flows. The equations are given in 2D cartesian and axisymmetric forms for variable density flows as encountered in combustors and furnaces. Among these, the turbulence is characterized by two-equation k-ϵ model based on eddy viscosity concept, with the wall function method near the solid wall. The fast chemistry, finite reaction rate, chemical equilibrium and micro-flame models are used for turbulent diffusion flames. The influence of turbulence fluctuation on combustion is introduced by using the assumed delta and beta probability density functions. Radiation is considered through the discrete transfer method incorporated in the source term of the energy equation. The spectral property of real furnace gases is provided by the mixed grey and clear gas model, where only water vapour and carbon dioxide are presumed to contribute significantly to the gaseous radiation.

3.2 Mean Flow Equations

The Favre-averaged transport equations of mass and momentum may be written as:

Continuity Equation:

$$\frac{\partial}{\partial x}(r\rho u) + \frac{\partial}{\partial y}(r\rho v) = 0 \tag{3.1}$$

x-Momentum Equation:

$$\begin{aligned}\frac{\partial}{\partial t}(r\rho u) + \frac{\partial}{\partial x}(r\rho u \cdot u) + \frac{\partial}{\partial y}(r\rho v \cdot u) &= \frac{\partial}{\partial x}\left(r\mu_{eff}\frac{\partial u}{\partial x}\right) + \frac{\partial}{\partial y}\left(r\mu_{eff}\frac{\partial u}{\partial y}\right) \\ &+ \frac{\partial}{\partial x}\left(r\mu_{eff}\frac{\partial u}{\partial x}\right) + \frac{\partial}{\partial y}\left(r\mu_{eff}\frac{\partial v}{\partial x}\right) \\ &- r\frac{\partial P}{\partial x} - \frac{2}{3}\frac{\partial}{\partial x}\left[r\mu_{eff}\left(\frac{\partial u}{\partial x}+\frac{1}{r}\frac{\partial (rv)}{\partial y}\right)\right]\end{aligned} \tag{3.2}$$

y-Momentum Equation:

$$\begin{aligned}\frac{\partial}{\partial t}(r\rho v) + \frac{\partial}{\partial x}(r\rho u \cdot v) + \frac{\partial}{\partial y}(r\rho v \cdot v) &= \frac{\partial}{\partial x}\left(r\mu_{eff}\frac{\partial v}{\partial x}\right) + \frac{\partial}{\partial y}\left(r\mu_{eff}\frac{\partial v}{\partial y}\right) \\ &+ \frac{\partial}{\partial x}\left(r\mu_{eff}\frac{\partial u}{\partial y}\right) + \frac{\partial}{\partial y}\left(r\mu_{eff}\frac{\partial v}{\partial y}\right) \\ &- r\frac{\partial P}{\partial y} - (2\mu_{eff}\frac{v}{r})\alpha_{axi} + \rho w^2 \alpha_{axi} \\ &- \frac{2}{3}\frac{\partial}{\partial y}\left[r\mu_{eff}\left(\frac{\partial u}{\partial x}+\frac{1}{r}\frac{\partial (rv)}{\partial y}\right)\right]\end{aligned} \tag{3.3}$$

The above equations are valid for both cartesian and cylindrical coordinates with r=1 and α_{axi}=0 or r=y and α_{axi}=1 for cartesian or cylindrical coordinates respectively. When considering swirling flows in axisymmetric burners, the transport equation of tangential velocity is given as follows:

θ- Momentum Equation:

$$\frac{\partial}{\partial t}(r\rho w) + \frac{\partial}{\partial x}(r\rho u w) + \frac{\partial}{\partial y}(r\rho v w) = \frac{\partial}{\partial x}\left(r\mu_{eff}\frac{\partial w}{\partial x}\right) + \frac{\partial}{\partial y}\left(r\mu_{eff}\frac{\partial w}{\partial y}\right) - \left(\frac{\mu_{eff}}{r} + \rho v + \frac{\partial \mu_{eff}}{\partial y}\right) w \tag{3.4}$$

where, in the above equations, u, v and w represent the velocity components in the x, y and θ coordinates, respectively. P is the pressure, ρ is the density, and μ_{eff} is the effective viscosity.

3.3 Turbulence Model

In the present study, the standard two-equation k-ϵ turbulence model (Launder and Spalding, 1974) with wall function is implemented. The governing equations for the turbulent kinetic energy and its dissipation rate are given by:

Turbulent Kinetic Energy Equation:

$$\frac{\partial}{\partial t}(r\rho k) + \frac{\partial}{\partial x}(r\rho u k) + \frac{\partial}{\partial y}(r\rho v k) = \frac{\partial}{\partial x}\left(r\frac{\mu_{eff}}{\sigma_k}\frac{\partial k}{\partial x}\right) + \frac{\partial}{\partial y}\left(r\frac{\mu_{eff}}{\sigma_k}\frac{\partial k}{\partial y}\right) + r(G_k - \rho\epsilon) \tag{3.5}$$

Turbulent Energy Dissipation Rate Equation:

$$\frac{\partial}{\partial t}(r\rho\epsilon) + \frac{\partial}{\partial x}(r\rho u\epsilon) + \frac{\partial}{\partial y}(r\rho v\epsilon) = \frac{\partial}{\partial x}\left(r\frac{\mu_{eff}}{\sigma_\epsilon}\frac{\partial \epsilon}{\partial x}\right) + \frac{\partial}{\partial y}\left(r\frac{\mu_{eff}}{\sigma_\epsilon}\frac{\partial \epsilon}{\partial y}\right) + \frac{r\epsilon}{k}(C_1 G_k - C_2\rho\epsilon) \tag{3.6}$$

where G_k is the turbulent generation term:

$$G_k = \mu_t \left[2\left(\left(\frac{\partial u}{\partial x}\right)^2 + \left(\frac{\partial v}{\partial y}\right)^2 + \left(\frac{v}{r}\right)^2 \alpha_{axi}\right) + \left(\frac{\partial w}{\partial x}\right)^2 + \left(r\frac{\partial}{\partial y}\left(\frac{w}{r}\right)\right)^2 + \left(\frac{\partial u}{\partial y} + \frac{\partial v}{\partial x}\right)^2 \right]$$
$$- \frac{2}{3}\left[\rho k + \mu_t\left(\frac{\partial u}{\partial x} + \frac{1}{r}\frac{\partial (rv)}{\partial y}\right)\right]\left(\frac{\partial u}{\partial x} + \frac{1}{r}\frac{\partial (rv)}{\partial y}\right) \qquad (3.7)$$
$$- \frac{\mu_t}{\rho^2 \sigma_t}\left(\frac{\partial \rho}{\partial x}\frac{\partial P}{\partial x} + \frac{\partial \rho}{\partial y}\frac{\partial P}{\partial y}\right)$$

It can be seen that terms involving $\partial\rho/\partial x, \partial\rho/\partial y$ in G_k are inserted to account for variable density effects. These terms come from the pressure-velocity correlation in the Favre-averaged equations for k and ϵ (Kim and Chung, 1989) and are identically zero for constant density flows.

The turbulent eddy viscosity for the k-ϵ model is defined as:

$$\mu_t = C_\mu \rho \frac{k^2}{\epsilon} \qquad (3.8)$$

giving for the effective viscosity:

$$\mu_{eff} = \mu + \mu_t \qquad (3.9)$$

The model constants recommended by Launder and Spalding (1974) are:

σ_k	σ_ϵ	C_1	C_2	C_μ
1.0	1.3	1.44	1.92	0.09

This model is valid only in fully turbulent flow regions. Close to the solid walls, the local Reynolds number of the turbulence becomes small, and the viscous effects dominate turbulent ones. Two methods, either the wall function method or the

low-Reynolds number modelling method can be used in that region. In the present study, only the wall function method is considered.

3.3.1 Wall Function Methods

In the wall function method it is assumed that the shear stress is uniform up to a distance y within the near-wall region. For the first grid point next to the wall (see Fig. 3.1), one defines a friction velocity u_τ as:

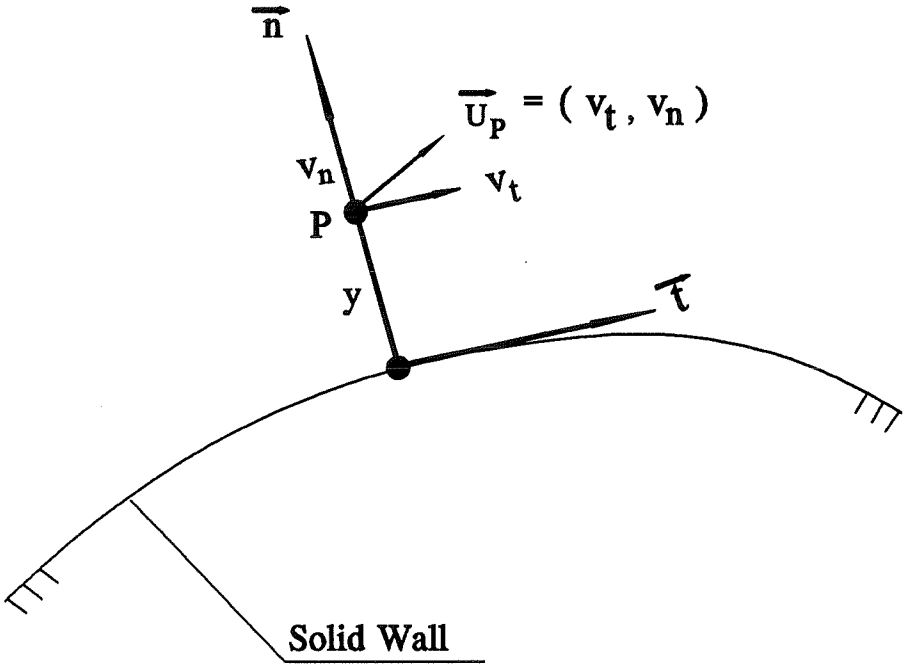

Figure 3.1: Grid point near the solid wall

$$u_\tau = \sqrt{\frac{|\tau_w|}{\rho}} \tag{3.10}$$

where τ_w is the wall shear stress. In the two-layer law of the wall, the wall shear stress can be defined by:

$$\tau_w = \begin{cases} \dfrac{\mu}{y} v_t & (y^+ < 11.63) \\ \dfrac{\rho u_\tau}{\frac{1}{\kappa}\ln(Ey^+)} v_t & (y^+ \geq 11.63) \end{cases} \tag{3.11}$$

where v_t is the velocity component parallel to the wall, E and κ are the roughness parameter (E=9.0 for a smooth wall) and the Von Karman constant (κ = 0.42) , respectively. y^+ is the dimensionless distance in the normal direction from point P to the wall, which is defined as:

$$y^+ = \frac{\rho\, y\, u_\tau}{\mu} \tag{3.12}$$

When considering convective heat transfer, the near-wall heat flux is determined by (Chung, 1993):

$$\dot{q}_w = \begin{cases} \dfrac{\mu c_p (T - T_w)}{Pr\, y} & (y^+ < 11.63) \\ \dfrac{\rho c_p (T - T_w) u_\tau}{Pr_t \left[\frac{1}{\kappa}\ln(Ey^+) + \frac{P(Pr)}{Pr_t}\right]} & (y^+ \geq 11.63) \end{cases} \tag{3.13}$$

where the function $P(Pr)$ is given by Jayatilleke (1969) of the form:

$$\frac{P(Pr)}{Pr_t} = 9.24 \left[\left(\frac{Pr}{Pr_t}\right)^{\frac{3}{4}} - 1\right]\left[1 + 0.28\exp\left(-0.007\frac{Pr}{Pr_t}\right)\right] \tag{3.14}$$

here, Pr is the molecular Prandtl number of gas, Pr_t is the turbulent Prandtl number, $\dot{q}_w$ is specified as a Neumann type boundary condition in the energy equation.

Once τ_w (or u_τ) is found, the near-wall point values for k and ε are then determined from:

$$k_p = \frac{u_\tau^2}{\sqrt{C_\mu}} \tag{3.15}$$

$$\epsilon_p = \frac{|u_\tau|^3}{\kappa y_P} \tag{3.16}$$

The key point in the application of the two-layer wall function method is the determination of the wall shear stress at the log law region ($y^+ \geq 11.63$). Two methods are implemented in the calculation of wall shear stress, one is the classical approximation method, which is based on the balance of generation and dissipation of energy in the near wall region (Launder and Spalding, 1974); another is the direct iteration method, in which the friction velocity based on the near wall velocity log law profile is directly solved by using a quasi-newton iteration (Garon, 1994).

Classical Approximation Method

In the classical approximation method of Launder and Spalding (1974), it is assumed that the convection and diffusion term in the streamwise direction are neglected in the near-wall region. Then the equation for the turbulent kinetic energy Eq. (3.5) yields that production and dissipation term are in local equilibrium, i.e. $G_k = \rho\epsilon$. Based on this assumption, the following relation is established from Eq. (3.7):

$$\mu_t \left(\frac{dv_t}{dy} \right)^2 = \rho \epsilon \tag{3.17}$$

Since it is assumed that the shear stress is uniform over the near wall region, then we have:

$$\tau_w = \mu_t \left(\frac{\partial v_t}{\partial y} \right) \tag{3.18}$$

Multiplying Eq.(3.17) with μ_t , substituting $\epsilon = C_\mu \rho k^2 / \mu_t$ in the right-hand side, and using the definition of τ_w in Eq.(3.18), it yields:

$$\tau_w = \rho k C_\mu^{\frac{1}{2}} \tag{3.19}$$

Then the corresponding friction velocity is given by:

$$u_\tau = C_\mu^{\frac{1}{4}} k^{\frac{1}{2}} \tag{3.20}$$

This relation avoids problems with singularities at the reattachment point where the wall shear stress vanishes (Speziale and Thangam, 1992). Substituting Eq. (3.20) into Eq. (3.11), yields an expression for the wall shear stress as a function of k and v_t ,

$$\tau_w = \begin{cases} \dfrac{\mu}{y} v_t & (y^+ < 11.63) \\ \dfrac{\rho C_\mu^{\frac{1}{4}} k^{\frac{1}{2}}}{\frac{1}{\kappa}\ln(Ey^+)} v_t & (y^+ \geq 11.63) \end{cases} \tag{3.21}$$

with y^+ as a function of k ,

$$y^+ = \frac{\rho\, y\, C_\mu^{\frac{1}{4}} k^{\frac{1}{2}}}{\mu} \tag{3.22}$$

Direct Iteration Method

Since the logarithmic law relation for the velocity profile holds in the near-wall region, from Eqs. (3.10) and (3.11), we have:

$$\frac{|v_t|}{u_\tau} = \frac{1}{\kappa}\ln(Ey^+) \tag{3.23}$$

Substituting Eq. (3.12) into Eq. (3.23) for y^+ , gives:

$$|v_t| - \frac{u_\tau}{\kappa}\ln(\frac{Ey\rho}{\mu}u_\tau) = 0 \tag{3.24}$$

The determination of the friction velocity in Eq. (3.24) is based on two steps. Firstly, assuming that the near-wall point lies in the viscous sublayer, the linear relation is used for determining the shear stress, giving:

$$\tau_w = \mu \frac{v_t}{y} \tag{3.25}$$

and the friction velocity is expressed as:

$$u_\tau = \sqrt{\frac{|\tau_w|}{\rho}} = \sqrt{\frac{\mu |v_t|}{\rho y}} \tag{3.26}$$

together with the expression y^+ in Eq. (3.12).

Secondly, if $y^+<11.63$, then the relation Eqs. (3.25)-(3.26) are applied. If $y^+\geq 11.63$, the log law relation Eq. (3.24) is used directly for evaluating the friction velocity using the quasi-newton iteration. From the value of u_τ , the near-wall shear stress can be determined from Eq. (3.10), and the near-wall point k and ε are then determined from Eqs. (3.15)-(3.16).

3.3.2 Velocity Boundary Condition on Arbitrary Wall

The boundary condition for velocities are imposed by using the slip boundary condition. Firstly, we assume that the wall is impermeable, and that there is equality between the stress tensor in the flow and the wall shear stress computed from the law of the wall. For the 2D cartesian coordinates, this is expressed by the following relation on an arbitrary wall, as shown in Figure 3.2:

$$\mu_{eff} \frac{\partial}{\partial n} (\vec{U}_P \cdot \vec{t}) = \tau_w \, sgn(-\vec{U}_P \cdot \vec{t}) \tag{3.27}$$

where, the left hand side of (3.27) represents the stress tensor in the flow, and the right hand side is the wall shear stress computed from the wall function relation.

Secondly, the shear stress is equal to zero in the normal direction to the flow near the wall. The velocity vector $\vec{U}_P$ is decomposed into its tangential and normal

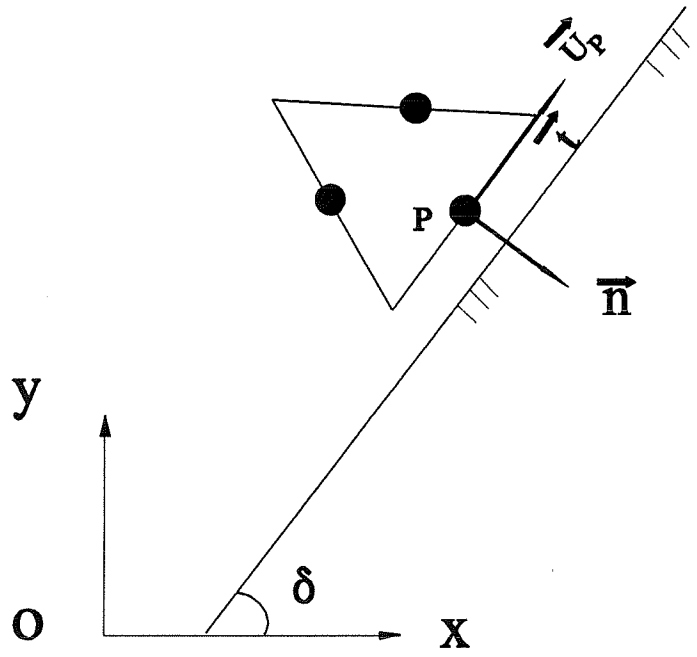

Figure 3.2: Implementing the wall functions for an arbitrary wall

components v_t and v_n , and the following geometric relations are derived for an arbitrary boundary as:

$$\begin{cases} \dfrac{\partial v_t}{\partial n} = \left(\dfrac{\partial u}{\partial n}\right)\cos\delta + \left(\dfrac{\partial v}{\partial n}\right)\sin\delta \\ v_n = u\sin\delta - v\cos\delta \end{cases} \tag{3.28}$$

Substituting Eq. (3.27) into (3.28), together with the no-slip condition $\vec{U}_p \cdot \vec{n} = 0$, then the following boundary conditions for cartesian velocities u and v are established, which are taken as Neumann and Dirichlet type boundary conditions for wall velocities:

- Horizontally predominant wall $(0 \le |\delta| \le \frac{\pi}{4})$:

$$\begin{cases} \left(\dfrac{\partial u}{\partial n}\right)_P = \dfrac{1}{\cos\delta}\left(\dfrac{\tau_w}{\mu_{eff}}\, sgn(-\vec{U}_P \cdot \vec{t})\right) - \tan\delta \left(\dfrac{\partial v}{\partial n}\right)_P \\ v_P = u_P \tan\delta \end{cases} \tag{3.29}$$

- Vertically predominant wall $(\frac{\pi}{4} < |\delta| \le \frac{\pi}{2})$:

$$\begin{cases} u_P = v_P \cot\delta \\ \left(\dfrac{\partial v}{\partial n}\right)_P = \dfrac{1}{\sin\delta}\left(\dfrac{\tau_w}{\mu_{eff}}\, sgn(-\vec{U}_P \cdot \vec{t})\right) - \cot\delta \left(\dfrac{\partial u}{\partial n}\right)_P \end{cases} \tag{3.30}$$

where, in the case of a horizontally predominant wall, the wall shear stress generated by u velocity is greater than that of by v velocity, the boundary condition for u velocity is considered as Neumann type, then its corresponding v velocity is determined from the geometric constraint relation as the Dirichlet type boundary condition. In the case of a vertically predominant wall, the conclusion is vice versa.

For axisymmetric cylindrical coordinates with swirl, we have:

$$\begin{cases} \vec{U}_P \cdot \vec{n} = 0 \\ \mu_{eff} \dfrac{\partial}{\partial n}(\vec{U}_P \cdot \vec{t}_1) = \tau_w\, sgn(-\vec{U}_P \cdot \vec{t}_1) \\ \mu_{eff} \dfrac{\partial}{\partial n}(\vec{U}_P \cdot \vec{t}_2) = 0 \end{cases} \tag{3.31}$$

where $\vec{t}$ and $\vec{n}$ are the tangential and normal directions of the wall, respectively.

The unit vector $\vec{t}_1$ is the velocity vector direction (including the swirl

component), and the unit vector $\vec{t}_2$ is perpendicular to both the direction $\vec{t}_1$ and the normal direction of the wall $\vec{n}$, defined as (Figure 3.3):

$$\begin{cases} \vec{t}_1 = \dfrac{\vec{U}_P}{\|\vec{U}_P\|} \\ \vec{t}_2 = \vec{n}\times\vec{t}_1 \end{cases} \tag{3.32}$$

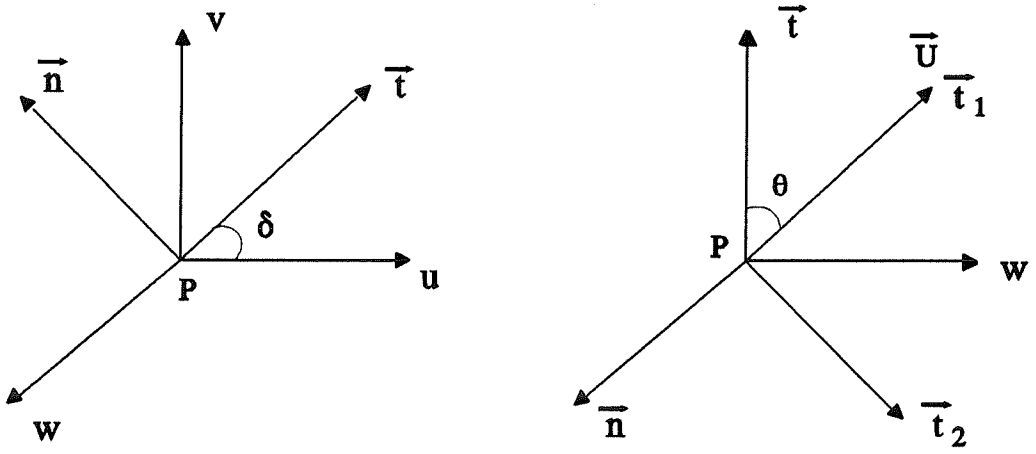

Figure 3.3: Velocities at an arbitrary wall

In Figure 3.3, θ is defined as the angle between the wall tangential direction and the velocity vector direction. When the three velocities u, v and w are considered, from Eq. (3.31), we can derive the following boundary conditions for velocities:

- Horizontally predominant wall $(0 \leq |\delta| \leq \frac{\pi}{4})$:

$$\begin{cases} \left(\dfrac{\partial u}{\partial n}\right)_P = \dfrac{\cos\theta}{\cos\delta}\left(\dfrac{\tau_w}{\mu_{eff}}\, sgn(-\vec{U}_P\cdot\vec{t}_1)\right) - \tan\delta\left(\dfrac{\partial v}{\partial n}\right)_P \\ v_P = u_P \tan\delta \\ \left(\dfrac{\partial w}{\partial n}\right)_P = \sin\theta\left(\dfrac{\tau_w}{\mu_{eff}}\, sgn(-\vec{U}_P\cdot\vec{t}_1)\right) - \cos\delta\,\dfrac{w_P}{r_P} \end{cases} \tag{3.33}$$

- Vertically predominant wall $(\frac{\pi}{4} < |\delta| \leq \frac{\pi}{2})$:

$$\begin{cases} u_P = v_P \cot\delta \\ \left(\dfrac{\partial v}{\partial n}\right)_P = \dfrac{\cos\theta}{\sin\delta}\left(\dfrac{\tau_w}{\mu_{eff}}\, sgn(-\vec{U}_P\cdot\vec{t}_1)\right) - \cot\delta\left(\dfrac{\partial u}{\partial n}\right)_P \\ \left(\dfrac{\partial w}{\partial n}\right)_P = \sin\theta\left(\dfrac{\tau_w}{\mu_{eff}}\, sgn(-\vec{U}_P\cdot\vec{t}_1)\right) - \cos\delta\,\dfrac{w_P}{r_P} \end{cases} \tag{3.34}$$

The Eqs. (3.33) and (3.34) reduce to the 2D case when the swirl is null.

Following Autret et al. (1987) and Chung (1993), in the context of finite elements, the wall function method can be implemented by assuming a constant shear stress up to a distance y_p within the near wall region of the flow. The wall function relations and the wall velocity relations can be applied at these boundary nodes, as shown in Fig. 3.4 for both Face-centered and Vertex-centered schemes.

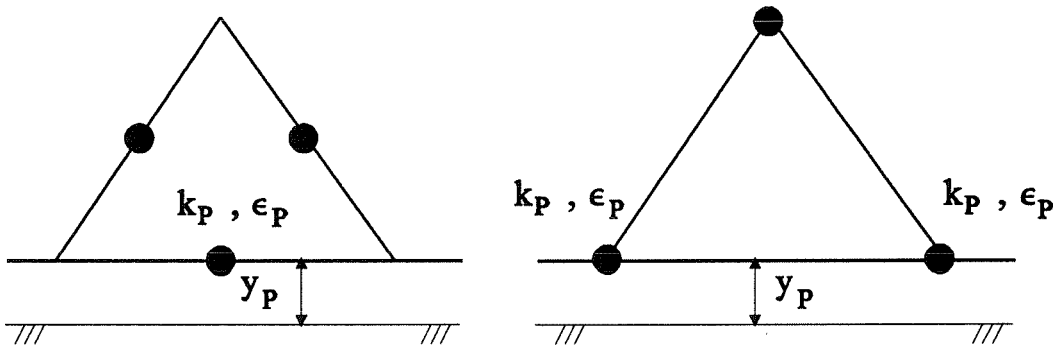

Face-centered scheme Vertex-centered scheme

Figure 3.4: Boundary nodes in the near-wall region

3.4 Turbulent Reacting Flow with Variable Density

In diffusion flames, the reaction rate is assumed sufficiently fast, then the reaction time is negligibly short in comparison to the mixing time. The whole reaction process is controlled by the mixing. In this situation, the instantaneous molecular species may be determined directly by strictly conserved scalar variables.

In this section, several combustion models for turbulent diffusion flames are summarized, these involve the fast chemistry reaction model, probability density function model, eddy dissipation concept model, equilibrium model and micro-flame models.

3.4.1 Fast Chemistry Reaction Model

The fast chemistry reaction model assumes that: the fuel and oxygen cannot exist at the same place at any time; reaction is infinitely fast, single step, and irreversible; the equilibrium is attained; and all the exchange coefficients are equal. The fuel and oxygen always combine in a stoichiometric ratio s to produce (s+1) of products, i.e.

$$1\,kg\,Fuel + s\,kg\,Oxygen \rightarrow (s+1)\,kg\,Products$$

The conserved scalar mixture fraction f is defined as:

$$f = \frac{\xi - \xi_A}{\xi_F - \xi_A} \tag{3.35}$$

and

$$\xi = m_{fu} - m_{ox}/s \tag{3.36}$$

where the subscripts A and F denote the air and the fuel stream conditions at inlet, and m_{fu} and m_{ox} are mass fraction of the fuel and oxygen, respectively.

The conservation equation for the mixture fraction f is (Khalil, 1982):

$$\frac{\partial}{\partial t}(r\rho f) + \frac{\partial}{\partial x}(r\rho u f) + \frac{\partial}{\partial y}(r\rho v f) = \frac{\partial}{\partial x}\left(r\frac{\mu_{eff}}{\sigma_f}\frac{\partial f}{\partial x}\right) + \frac{\partial}{\partial y}\left(r\frac{\mu_{eff}}{\sigma_f}\frac{\partial f}{\partial y}\right) \tag{3.37}$$

where σ_f is the effective schmidt number of the mixture fraction f, taken from 0.6 to 0.9.

This model assumes that a diffusion flame is divided into two regions:

Region 1 : the oxidant and the products co-exist, $0 < f < f_{st}$

$$\begin{cases} m_{fu} = 0 \\ m_{ox} = m_{ox,A}\left(1-\dfrac{f}{f_{st}}\right) \le m_{ox,A} \end{cases} \tag{3.38a}$$

Region 2 : the fuel and the products co-exist, $f_{st} < f < 1$

$$\begin{cases} m_{fu} = m_{fu,F}\left(\dfrac{f-f_{st}}{1-f_{st}}\right) \\ m_{ox} = 0 \end{cases} \tag{3.38b}$$

where f_{st} is the stoichiometric value of the mixture fraction, defined as:

$$f_{st} = \left(1+S\frac{m_{fu,F}}{m_{ox,A}}\right)^{-1} \tag{3.39}$$

The energy conservation equation for enthalpy can be expressed as:

$$\frac{\partial}{\partial t}(r\rho h)+\frac{\partial}{\partial x}(r\rho u\cdot h)+\frac{\partial}{\partial y}(r\rho v\cdot h) = \frac{\partial}{\partial x}\left(r\frac{\mu_{eff}}{\sigma_h}\frac{\partial h}{\partial x}\right)+\frac{\partial}{\partial y}\left(r\frac{\mu_{eff}}{\sigma_h}\frac{\partial h}{\partial y}\right)+S_h \tag{3.40}$$

where, S_h is the radiation source or sink, written as the divergence of the radiative flux, which can be obtained from the solution of the radiative transfer equation.

In Eq. (3.40), the enthalpy h is defined as:

$$h = c_{p,mix}T + H_{fu}m_{fu} \tag{3.41}$$

where the mixture specific heat is calculated from each of the gases present in the mixture as:

$$c_{p,mix} = \sum_{j=1}^{5} m_j \cdot c_{pj} \tag{3.42}$$

The specific heats for each species are assumed to vary linearly with the temperature as:

$$c_{pj} = a_j + b_j \cdot T \tag{3.43}$$

where the values of a_j's and b_j's are taken from Khalil et al. (1975).

Furthermore, for adiabatic flame, the enthalpy can also be expressed as the conserved scalar, the linear relation between the enthalpy and mixture fraction can be expressed as (Bilger,1980):

$$h = (h_F - h_A)f + h_A \tag{3.44}$$

where h_F and h_A are the values of enthalpy at fuel and air inlet, respectively.

The temperature can be determined from thermodynamics relation Eq. (3.41) as:

$$T = \frac{h - H_{fu}m_{fu}}{c_{P,mix}} \tag{3.45}$$

The density of the mixture can be defined by the equation of state:

$$\rho = \frac{W_{mix} P}{\bar{R} T} \tag{3.46}$$

where R is the universal gas constant, P is the pressure, and W_{mix} is the molecular weight of the mixture, defined as:

$$W_{mix} = \left[\sum_j \frac{m_j}{W_j} \right]^{-1} \tag{3.47}$$

This model is simple and easy of application. However, the concentration fluctuation is not taken into account in this model, because it assumes that the fuel and oxygen cannot co-exist at the same place at any time. The consideration of the concentration fluctuation, requires the development of the probability density function model.

3.4.2 Probability Density Function Model

The following assumptions are made for the simplified probability density function (PDF) model (Khalil, 1982): the fuel and oxygen may co-exist at the same place but at different times; the reaction is infinitely fast, single step, irreversible; the equilibrium is attained; all the exchange coefficients are equal. Based on a conserved scalar approach, the simplified PDF approach requires a two-parameter form of the PDF in terms of the mean f and its variance g which are determined from the solution of their respective conservation equation. The conservation equation for g is defined as (Khalil, 1982):

$$\frac{\partial}{\partial t}(r\rho g)+\frac{\partial}{\partial x}(r\rho u g)+\frac{\partial}{\partial y}(r\rho v g) = \frac{\partial}{\partial x}\left(r\frac{\mu_{eff}}{\sigma_g}\frac{\partial g}{\partial x}\right)+\frac{\partial}{\partial y}\left(r\frac{\mu_{eff}}{\sigma_g}\frac{\partial g}{\partial y}\right) + rC_{g_1}\mu_t\left[\left(\frac{\partial f}{\partial x}\right)^2+\left(\frac{\partial f}{\partial y}\right)^2\right]-rC_{g_2}\rho\frac{\epsilon}{k}g \tag{3.48}$$

where σ_g is the schmidt number of g, C_{g1} and C_{g2} are model constants, are given by 2.8 and 2.0, respectively. Compared with the mixture fraction Eq.(3.37), Eq.(3.48) has a non-zero source term, which represents the generation and dissipation of the variable g.

The density-weighted mean value $\phi(f)$ of any scalar variables can be evaluated by using scalar function with a probability density function $P(f)$:

$$\tilde{\phi} = \int_0^1 \phi(f)P(f)df \tag{3.49}$$

Two types of the assumed probability density function, delta and beta PDFs are considered below.

Delta PDF

The shape of the double delta PDF of Spalding (1971a), is established by assuming the rectangular wave variation of f with time, this model can be divided into four regions:

Region 1 : ($0 < f < 1$)

$$\begin{cases} P(f) = \frac{1}{2}[\delta(f_+) + \delta(f_-)] \\ f_+ = f + g^{\frac{1}{2}} \\ f_- = f - g^{\frac{1}{2}} \end{cases} \tag{3.50a}$$

Region 2 : ($f < 0.5,\ f-g^{\frac{1}{2}} < 0$)

$$\begin{cases} P(f) = a_2\delta(0) + a_3\delta(f_+) \\ a_2 = g/(f(f+g/f)) \\ a_3 = f(f+g/f) \end{cases} \tag{3.50b}$$

Region 3 : ($f > 0.5,\ f+g^{\frac{1}{2}} > 1$)

$$\begin{cases} P(f) = a_2\delta(f_-) + a_3\delta(1) \\ a_2 = (1-f)/(1-f+g/(1-f)) \\ a_3 = g/((1-f)^2+g) \end{cases} \tag{3.50c}$$

Region 4: where large oscillations of f are imposed,

$$\begin{cases} P(f) = (1-f)\delta(0) + f\delta(1) \\ g_{\max} = (1-f)f \end{cases} \tag{3.50d}$$

Beta PDF

The beta PDF can be defined as (Jones, 1979):

$$p(f) = \frac{f^{a-1}(1-f)^{b-1}}{\int_0^1 f^{a-1}(1-f)^{b-1}df} \tag{3.51a}$$

with

$$a = f\left(\frac{f(1-f)}{g}-1\right) \tag{3.51b}$$

$$b = (1-f)\left(\frac{f(1-f)}{g}-1\right) \tag{3.51c}$$

where the fluctuation g must satisfy the following conditions, $0 \le g \le g_{max}$. This constraint results in that $a \ge 0$ and $b \ge 0$ in the use of beta PDF.

3.4.3 Chemical Equilibrium Model

By relating the thermochemical state of the mixture to the mixture fraction, it is assumed that the reaction rate is sufficiently fast so that the chemical equilibrium state may be reached. The mixture composition and temperature are determined from f by calculation of chemical equilibrium for the initial reactant concentrations. In order to reduce computational effort only those species predominately present in the products are considered. Follow McKenty (1992), the chemical reaction for methane/air can be simplified as:

$$\begin{aligned}&\varepsilon\varphi CH_4+\nu_{O_2}O_2+\nu_{N_2}N_2 \rightleftharpoons \nu_1 CH_4+\nu_2 CO_2\\&+\nu_3 CO+\nu_4 H_2O+\nu_5 H_2+\nu_6 O_2+\nu_7 N_2+\nu_8 NO\end{aligned} \tag{3.52}$$

where φ is the equivalence ratio, ε is the molar ratio of fuel/air and ν_i are the coefficient of products.

The above equation can be solved by using the minimization of free energy technique by Heywood (1986). The element mass balance constraints are:

$$\sum_{j=1}^{n} a_{ij} \nu_j - b_i^* = 0 \qquad for\ i = 1,2,...,l \tag{3.53}$$

where the stoichiometric coefficient a_{ij} are the number of kilomoles of element i per kilomole of species j, b_i^* is the number of kilomoles of element i per kilogram of mixture, and ν_j is the number of kilomoles of species j per kilogram of mixture. The equilibrium condition can be given for species as:

$$\mu_j^o + RT\ln\left(\frac{\nu_j}{\nu}\right) + RT\ln\left(\frac{P}{P_o}\right) + \sum_{i=1}^{l} \lambda_i a_{ij} = 0 \quad for\ j = 1,...,n \tag{3.54}$$

where $\nu = \sum_{j=1}^{n} \nu_j$, and μ_j^o is the chemical potential in the standard state and P is the mixture pressure, λ_i are lagrangian multipliers.

Eqs. (3.53) and (3.54) permit the determination of equilibrium compositions for a given temperature T and pressure P, these nonlinear systems of equations are solved by Newton-Raphson method. Detailed description of this model may be found in McKenty (1992).

3.4.4 Micro-Flame Model

Because the chemical equilibrium model over-estimates CO levels in regions where the mixture is very rich or where the turbulence is very high, a laminar micro-flame model was developed by Mckenty (1992).

For laminar flames it is assumed that the reaction rate is a function of initial reactant concentrations and of temperature. The thermochemical state may be expressed as a function of mixture fraction from experimental data in laminar flames. For turbulent flames, it is further supposed that each calculation point constitutes a

laminar micro-flame, the turbulence influences this laminar micro-flame through the effect of the mixture fraction fluctuation g. Then the thermochemical state of the mixture can be expressed as a function of the mean mixture fraction f. This model is used for the prediction of CO and H_2 mass fraction in methane/air diffusion flames, details of this model may be found in McKenty (1992).

3.4.5 Eddy Dissipation Combustion Model

The eddy dissipation combustion model was proposed by Magnussen and Hjertager (1976) based on the EBU model of Spalding (1971b). In this model, the reaction rate of the fuel is controlled by the turbulent mixing rate ϵ/k, and the reactant with the minimum concentration in the mixture. The use of this model requires to solve at least two differential equations, one for the mixture fraction f, another for the mass fraction of fuel m_{fu}. The conservation equation of fuel can be given by:

$$\frac{\partial}{\partial t}(r\rho m_{fu})+\frac{\partial}{\partial x}(r\rho u\cdot m_{fu})+\frac{\partial}{\partial y}(r\rho v\cdot m_{fu}) = \frac{\partial}{\partial x}\left(r\frac{\mu_{eff}}{\sigma_{fu}}\frac{\partial m_{fu}}{\partial x}\right)+\frac{\partial}{\partial y}\left(r\frac{\mu_{eff}}{\sigma_{fu}}\frac{\partial m_{fu}}{\partial y}\right) - \frac{m_{fu,b}}{m_{fu}+m_{fu,b}}rA\rho\frac{\epsilon}{k}\cdot\min\left(m_{fu}, \frac{m_{O_2}}{s}\right) \tag{3.55}$$

where m_{O_2} and $m_{fu,b}$ are the mass fractions of oxygen and fuel burnt, respectively. A is the model constant taken to be 4.0 (Hjertager and Magnussen, 1982).

3.5 Radiative Transfer Equation

The radiative transfer equation (RTE) can be expressed as (Lockwood and Shah, 1981):

$$\frac{dI}{ds} = -(k_a+k_s)I + k_a\frac{E_g}{\pi} + \frac{k_s}{4\pi}\int_{4\pi} p(\vec{\Omega},\vec{\Omega}')I(\vec{\Omega}')d\Omega' \qquad (3.56)$$

where I is the radiation intensity in the direction $\vec{\Omega}$, s is the distance along that direction. k_a and k_s are the gas absorption and scattering coefficients, E_g is the gas blackbody emissive power σT^4, and $p(\vec{\Omega},\vec{\Omega}')$ is the probability that incident radiation in the direction $\vec{\Omega}'$ will be scattered into the increment of solid angle $d\Omega$ about $\vec{\Omega}$ (Figure 3.5). The above equation expresses the change of the intensity in the specified direction $\vec{\Omega}$, in terms of absorption and out-scattering, the emission and the in-scattering by the three terms of the right-hand-side, respectively.

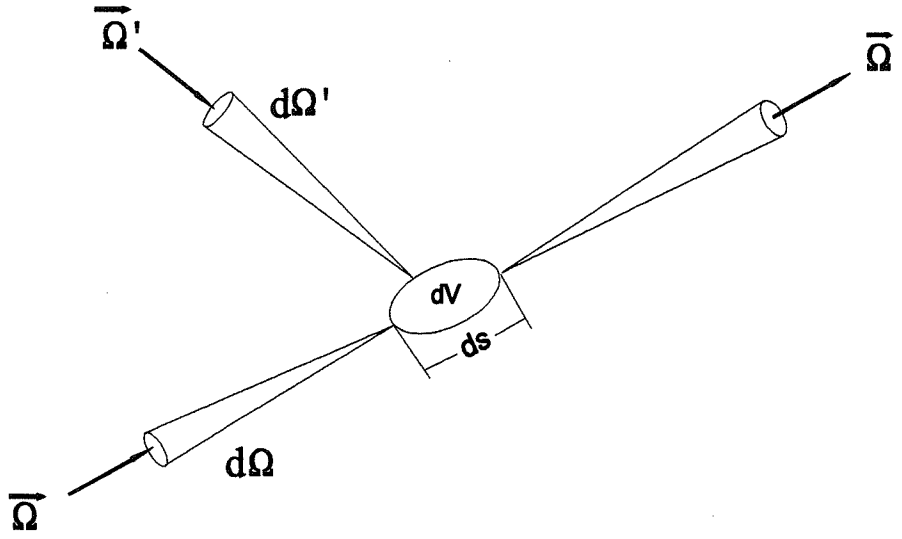

Figure 3.5: A monochromatic pencil of radiation across an element volume along the path of propagation

To solve Eq.(3.56) using the discrete transfer method (Lockwood and Shah,

1981), we define an extinction coefficient $k_e = k_a + k_s$, an elemental optical depth $ds^* = k_e ds$ and a modified emissive power E^* :

$$E^* = \frac{1}{k_e}\left(k_a E_g + \frac{k_s}{4}\int_{4\pi} p(\vec{\Omega},\vec{\Omega}')I(\vec{\Omega}')d\Omega' \right) \tag{3.57}$$

Then Eq. (3.56) may then be re-written as:

$$\frac{dI}{ds^*} = -I + \frac{E^*}{\pi} \tag{3.58}$$

For a ray travelling through the domain, this equation describes the change of the ray's intensity when passing through an absorbing, emitting and scattering medium. The discrete transfer method is based on solving Eq. (3.58) for a number of discrete representative rays (or beams) that travel through the considered domain, details will be given in Chapter 4 for the solution procedure of radiation.

3.6 Summary of the Transport Equations

The general form of the transport equation can be expressed as:

$$\frac{\partial}{\partial t}(r\rho\phi) + \frac{\partial}{\partial x}(r\rho u\phi) + \frac{\partial}{\partial y}(r\rho v\phi) = \frac{\partial}{\partial x}\left(r\Gamma_\phi \frac{\partial \phi}{\partial x}\right) + \frac{\partial}{\partial y}\left(r\Gamma_\phi \frac{\partial \phi}{\partial y}\right) + S_\phi \tag{3.59}$$

The above equation can be used for unsteady, turbulent, variable density, cartesian or axisymmetric flows, and can be reduced to laminar flow or constant density flows as well as steady flows. The meaning of variable ϕ, and coefficients Γ_ϕ, and S_ϕ are given in Table 3.1. For the control volume method, the general form of the transport equation (3.59) can be written in the vectorial conservation form as:

$$\frac{\partial}{\partial t}(r\rho\phi)+\nabla\cdot\vec{J} = S_\phi \tag{3.60}$$

with the continuity equation:

$$\nabla\cdot(r\rho\vec{v}) = 0 \tag{3.61}$$

where ϕ is a general scalar dependent variable, ρ is the density, S_ϕ is the volumetric generation rate or source term, $\vec{J}$ is the combined convection and diffusion flux of the scalar ϕ,

$$\vec{J} = r(\rho\vec{v}\phi - \Gamma\nabla\phi) \tag{3.62}$$

where $\vec{v}$ is velocity vector, r is the radius with r=1 for 2D cartesian coordinates. Γ is the diffusion coefficient (see Table 3.1). In Eq. (3.60), when the diffusion of ϕ is not governed by Fick's Law, the diffusion terms that do not fit the gradient expression Eq. (3.62) are included in the source term S_ϕ which is listed in Table 3.1. For examples, when flow is turbulent, time-averaging or Favre-averaging forms of the governing equations are used, then Eqs.(3.60)-(3.62) are interpreted as the time-mean or mass-mean values of the relevant variables, and Γ may stand for the turbulent viscosity.

Table 3.1: Values of ϕ, Γ and S_ϕ in the general transport equations.

	ϕ	Γ	S_ϕ
Mass	1	μ_{eff}	0
x-Momentum	u	μ_{eff}	$\frac{\partial}{\partial x}\left(r\mu_{eff}\frac{\partial u}{\partial x}\right)+\frac{\partial}{\partial y}\left(r\mu_{eff}\frac{\partial v}{\partial x}\right) - r\frac{\partial P}{\partial x}-\frac{2}{3}\frac{\partial}{\partial x}(r\mu_t\nabla\cdot\vec{v})$
y-Momentum	v	μ_{eff}	$\frac{\partial}{\partial x}\left(r\mu_{eff}\frac{\partial u}{\partial y}\right)+\frac{\partial}{\partial y}\left(r\mu_{eff}\frac{\partial v}{\partial y}\right)-r\frac{\partial P}{\partial y} -(2\mu_{eff}\frac{v}{r})\alpha_{axi}-\frac{2}{3}\frac{\partial}{\partial y}(r\mu_t\nabla\cdot\vec{v})$
Kinetic energy	k	$\frac{\mu_{eff}}{\sigma_k}$	$r(G_k - \rho\epsilon)$
Dissipation rate	ϵ	$\frac{\mu_{eff}}{\sigma_\epsilon}$	$\frac{r\epsilon}{k}(C_1G_k - C_2\rho\epsilon)$
Mixture fraction	f	$\frac{\mu_{eff}}{\sigma_f}$	0
Fuel	m_{fu}	$\frac{\mu_{eff}}{\sigma_{m_{fu}}}$	$-\frac{m_{fu,b}}{m_{fu}+m_{fu,b}}r\rho A\frac{\epsilon}{k}\min\left(m_{fu},\frac{m_{o2}}{s}\right)$
Fluctuation	g	$\frac{\mu_{eff}}{\sigma_g}$	$rC_{g1}\mu_t\left[\left(\frac{\partial f}{\partial x}\right)^2+\left(\frac{\partial f}{\partial y}\right)^2\right]-rC_{g2}\rho\frac{\epsilon}{k}g$
Enthalpy	h	$\frac{\mu_{eff}}{\sigma_h}$	rS_h

Chapter 4

Numerical Method

4.1 Overview

For the solution of the advection-diffusion equations encountered in the fluid flow and combustion problems, in this work a staggered control-volume finite element method (SCVFEM) is proposed and developed for steady/unsteady, 2-D cartesian and axisymmetric geometries. The method uses the primitive variables (u,v,p) based on a triangular element. There is one degree of freedom for pressure and three for velocities yielding an unequal order scheme and since the pressure and velocities are not stored at the same location, the scheme is staggered. Depending on the location of velocities, there are two related SCVFEM schemes; Face-centered scheme when velocities are stored at the midpoint of the sides, Vertex-centered scheme when the velocities are stored at the vertices. The other properties, such as the turbulent kinetic energy k and its dissipation rate ϵ, turbulent eddy viscosity μ_t , mixture fraction f and its variance g, mass fraction of fuel m_{fu} , enthalpy h, temperature T and density ρ, as well as the source term S, etc. follow the storage location of velocities. The following main points characterise the proposed SCVFEM:

- Combined form of the flow-oriented upwind function and mass weighted upwind function based on the local Peclet number.
- Treatment of the pressure-velocity coupling by using a control volume mesh for the velocity field and its dual mesh for the pressure field.
- Pressure gradient field which appears in the momentum equations is obtained by using a linear reconstruction of the pressure field.

- A segregated solution algorithm similar to SIMPLE method is used.

4.2 The Discretized Equations

The control volumes associated with a typical node i, internal or on a boundary are shown in Figure 4.1 and 4.4, respectively. When applying the conservation principle to this control volume, Eq.(3.60) can be written as follows:

$$\int_{iaoci} \frac{\partial}{\partial t}(r\rho\phi)dV + \int_a^o \vec{J}\cdot\vec{n}ds + \int_o^c \vec{J}\cdot\vec{n}ds - \int_{iaoci} SdV$$

$$+[\ \textit{Similar contributions of other elements associated with node } i\ ] \qquad (4.1)$$

$$+[\ \textit{boundary condition, if applicable}\ ] = 0$$

The contribution to the node i from one element as shown in Fig. 4.2, consists of a transient term, a convection-diffusion term and a source term.

Transient Term

The integration of the transient term of Eq. (4.1) can be expressed as:

$$\int_{iaoci} \frac{\partial}{\partial t}(r\rho\phi)dV = \frac{A_e}{3} r_1 \rho_1^n \left(\frac{\phi_1^{n+1} - \phi_1^n}{\Delta t} \right) \qquad (4.2)$$

where A_e is the area of the triangular element; ϕ_1^{n+1} and ϕ_1^n are the value of ϕ_1 at the time levels n+1 and n, respectively. $\Delta t = t^{n+1} - t^n$ is the time step, ρ_1^n is the

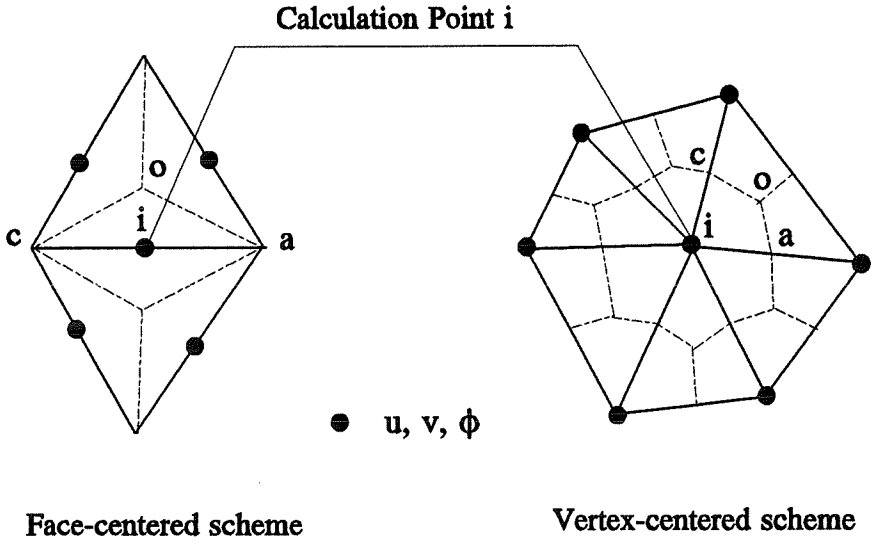

Figure 4.1: Calculation point i of internal element contributions

density at the time n and at the variable location 1.

Convection-Diffusion Term

The integration of the convection-diffusion flux for dependent variable ϕ, uses hybrid interpolation. It is based on the flow-oriented upwind function of Baliga and Patankar (1980) and the skewed mass-weighted upwind function of Schneider and Raw (1986), where the switch between these two interpolation functions depends on the local element Peclet number.

Following Baliga and Patankar (1980), the locally exact interpolation function is obtained from the 2D cartesian, steady, convection-diffusion equation without source term expressed as:

Consider a new coordinate system (X,Y) (Figure 4.2), whose origin is located

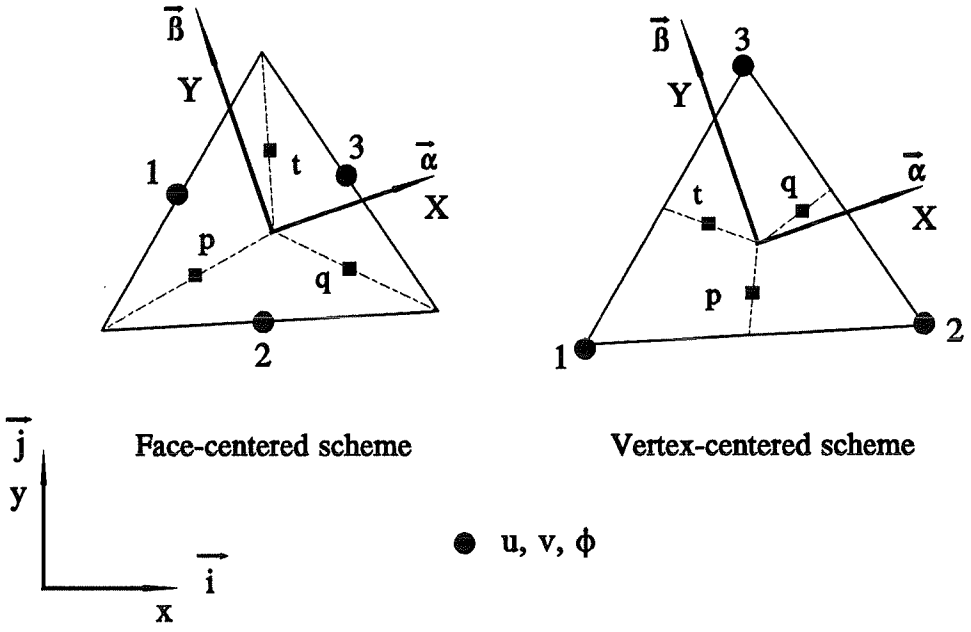

Figure 4.2: The local flow-oriented coordinates (X,Y) of an element

$$\rho\frac{\partial}{\partial x}(u\phi)+\rho\frac{\partial}{\partial y}(v\phi) = \Gamma\left(\frac{\partial^2\phi}{\partial x^2}+\frac{\partial^2\phi}{\partial y^2}\right) \tag{4.3}$$

at the centroid, where the X axis is aligned with the element-average velocity vector $\vec{v}_{av}$:

$$\vec{v}_{av} = \frac{u_1+u_2+u_3}{3}\vec{i}+\frac{v_1+v_2+v_3}{3}\vec{j} \tag{4.4}$$

where $\vec{i}$, $\vec{j}$ denote unit vectors in global (x,y) coordinates, respectively.

Let U and V be the corresponding velocity components in the (X,Y) coordinates, then,

$$U_{av} = \|\vec{v}_{av}\|, \quad V_{av}=0$$
$$\vec{v}_{av}=U_{av}\vec{\alpha} \tag{4.5}$$

where $\vec{\alpha},\vec{\beta}$ denote unit vector in local (X,Y) coordinates, respectively.

Based on (X,Y) coordinates, Eq. (4.3) can be rewritten as:

$$\rho U_{av}\frac{\partial\phi}{\partial X} = \Gamma\left(\frac{\partial^2\phi}{\partial X^2}+\frac{\partial^2\phi}{\partial Y^2}\right) \tag{4.6}$$

The exact solution of Eq. (4.6) in the local flow coordinates (X,Y) is given as follows:

$$\begin{cases} \phi = AZ+BY+C \\ Z = \dfrac{\Gamma}{\rho U_{av}}\left\{ \exp\left[\dfrac{\rho U_{av}}{\Gamma}(X-X_{max})\right]-1 \right\} \end{cases} \tag{4.7}$$

where X_{max} is the maximum value of the X coordinates of three vertices of an element, and A, B, C are the coefficients, can be uniquely determined in terms of (X,Y) coordinates of three nodes 1, 2, 3 and the corresponding values of ϕ.

In each element, the convection-diffusion flux $\vec{J}$ can be expressed as:

$$\vec{J} = J_X\vec{\alpha} + J_Y\vec{\beta} \tag{4.8a}$$

where

$$\begin{cases} J_X = r(\rho U\phi - \Gamma\dfrac{\partial\phi}{\partial X}) \\ J_Y = r(\rho V\phi - \Gamma\dfrac{\partial\phi}{\partial Y}) \end{cases} \tag{4.8b}$$

Based on the exponential interpolation function Eq. (4.7), the convection-

diffusion flux in Eq. (4.8b) can be expressed as:

$$\begin{cases} J_X = r(\rho(U - U_{av})AZ + \rho U(BY + C) - \Gamma A) \\ J_Y = r(\rho V AZ + \rho V(BY + C) - \Gamma B) \end{cases} \tag{4.9}$$

The other interpolation function is based on the skewed mass-weighted upwind scheme (MWUS) of Schneider and Raw (1986) developed for a rectangular mesh with a vertex scheme. The extension of MWUS to a triangular mesh with both Face-centered and Vertex-centered scheme of SCVFEM are considered in the present study, as shown in Fig. 4.3. The procedure for computing the value of ϕ_p is as follows:

If $\dot{m}_p > 0$ then

$$\begin{cases} \phi_p = f\phi_t + (1-f)\phi_1 \\ f = \min\left[\max\left(\frac{\dot{m}_t}{\dot{m}_p}, 0\right), 1\right] \end{cases} \tag{4.10a}$$

If $\dot{m}_p < 0$ then

$$\begin{cases} \phi_p = f\phi_q + (1-f)\phi_2 \\ f = \min\left[\max\left(\frac{\dot{m}_q}{\dot{m}_p}, 0\right), 1\right] \end{cases} \tag{4.10b}$$

where $\dot{m}_p = [r\rho(\vec{v}\cdot\vec{n})]_p S_{ao}$ is the mass flow rate through the integration face p, and $\dot{m}_q$, $\dot{m}_t$ are the mass flow rates across the integration face q and t, with a similar expression to $\dot{m}_p$. Combining the expressions of Eq. (4.10a) and Eq. (4.10b), together with similar expressions for faces q and t, the values ϕ_p, ϕ_q and ϕ_t at integration points p,q and t can be expressed as:

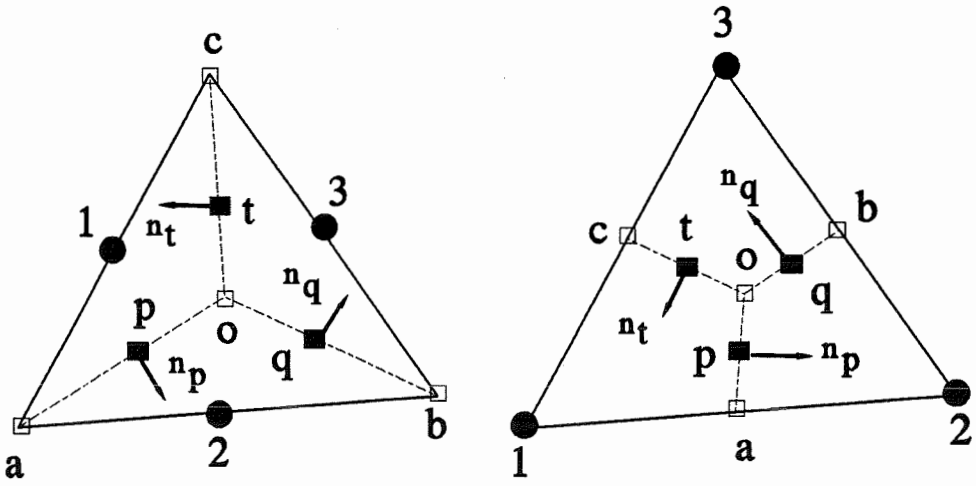

Face-centered scheme

Vertex-centered scheme

- ● u, v, ϕ
- ■ Integration Points p, q and t
- □ Endpoints of sub-control volume a,b,c and o

Figure 4.3: Integration paths for the two schemes of SCVFEM

$$\begin{cases} \phi_p = a_1\phi_t + b_1\phi_1 + c_1\phi_2 + d_1\phi_q \\ \phi_q = a_2\phi_p + b_2\phi_2 + c_2\phi_3 + d_2\phi_t \\ \phi_t = a_3\phi_q + b_3\phi_3 + c_3\phi_1 + d_3\phi_p \end{cases} \tag{4.11}$$

The simultaneous solutions for ϕ_p, ϕ_q, ϕ_t in terms of the nodal values ϕ_1, ϕ_2, ϕ_3 can be determined by inverting a 3 x 3 matrix of element interpolation coefficients, which is directly used in the calculation of the convection fluxes at the integration faces. To calculate the diffusion terms $\partial\phi/\partial X$, $\partial\phi/\partial Y$, a linear interpolation function with respect to (X,Y) coordinates is assumed:

$$\phi = \xi X + \gamma Y + \delta \tag{4.12}$$

where the coefficients ξ, γ ,δ are uniquely determined from the values of ϕ at the

point 1,2,3 and its corresponding locations. Then the diffusion term can be expressed as follows:

$$\frac{\partial \phi}{\partial X}=\xi, \quad \frac{\partial \phi}{\partial Y}=\gamma \tag{4.13}$$

The integration of the convection-diffusion flux in Eq. (4.1) can be approximated by using the midpoint rule as:

$$\begin{aligned} \int_a^o \vec{J}\cdot\vec{n}ds &= \int_a^o (J_X n_X + J_Y n_Y)ds \\ &= [(J_X)_p (n_X)_p + (J_Y)_p (n_Y)_p] s_{ao} \end{aligned} \tag{4.14a}$$

$$\begin{aligned} \int_o^c \vec{J}\cdot\vec{n}ds &= \int_o^c (J_X n_X + J_Y n_Y)ds \\ &= [(J_X)_t (n_X)_t + (J_Y)_t (n_Y)_t] s_{oc} \end{aligned} \tag{4.14b}$$

where $(n_X)_p, (n_Y)_p$ and $(n_X)_t, (n_Y)_t$ are the components of normals in the counter clockwise direction of the integration faces $\overline{ao}$ and $\overline{oc}$, respectively. The dependent variable ϕ and its derivatives $\partial\phi/\partial X, \partial\phi/\partial Y$ appearing in the convection-diffusion flux J_X and J_Y are determined from the above hybrid interpolation function, other variables such as density and viscosity are assumed to vary linearly over an element.

In the calculation of the coefficients of the convection-diffusion flux, the switch between the exponential interpolation function and the skewed mass-weighted upwinding function is determined according to the Peclet number of an element, i.e., when Pe $\leq$ Pe_{max}, the exponential function is used, while, when Pe $>$ Pe_{max}, the skewed mass-weighted upwind function is used. The maximum Peclet number of an element is defined as:

$$Pe_{max} = \max\left[\frac{\rho U_{av}}{\Gamma}(X_{max}-X_i)\right] \tag{4.15}$$

where X_i is the X coordinate at variable locations. The specification of the Pe_{max} follows the exponential difference scheme (Spalding, 1972) and Power-Low scheme of Pantakar (1981). In the present work, the values $Pe_{max} = 10$ for laminar flow and $Pe_{max} = 2$ for turbulent flow are recommended to the above hybrid schemes. However, for turbulent swirling flow and turbulent reacting flows, only the mass-weighted upwind scheme is used.

Source Term

The integration of the source terms can be approximated as:

$$\int_{iaoci} SdV = \frac{A_e}{3}(S_C+S_P\phi_1) \tag{4.16}$$

where the linearization of the source terms in the transport equations, S_C and S_P are determined by making use of the always-positive variables rule of Patankar (1980).

The total element contributions to the conservation equation for the control volume associated with internal node i are obtained by adding the above expressions for the transient, convection-diffusion and source terms as:

$$\int_{iaoci}\frac{\partial}{\partial t}(r\rho\phi)dV+\int_a^o \vec{J}\cdot\vec{n}ds+\int_o^c \vec{J}\cdot\vec{n}ds-\int_{iaoci} SdV$$
$$=C_1\phi_1^{n+1} + C_2\phi_2^{n+1} + C_3\phi_3^{n+1} + C_1^o\phi_1^n + B_1 \tag{4.17}$$

The above expression gives a fully implicit formulation, which avoids the stability restrictions on the time step.

4.2.1 Boundary Conditions

For a node located at the boundary of the calculation domain, the control volume arrangements for both schemes are shown in Figure 4.4.

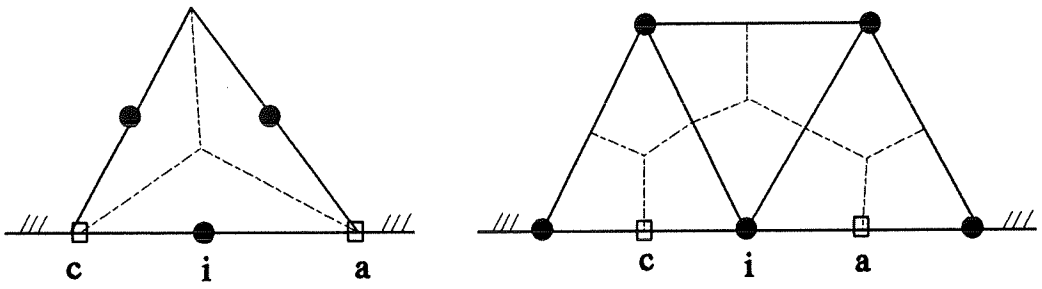

Face-centered scheme Vertex-centered scheme

● u, v and ϕ

□ Endpoints of control co-volume

Figure 4.4: The calculation point i located at the boundary

The boundary flux can be approximated by the integration of the convection-diffusion flux over the boundary side $\overline{ca}$ as:

$$[\ \textit{Flux out of the control volume side } \overline{ca}\ ] = \int_c^a (\vec{J}\cdot\vec{n})\,ds \tag{4.18}$$

Three types of the boundary conditions are considered.

Type 1: Specified Boundary Condition (Dirichlet B.C.)

$$\phi_i = \phi_{specified} \tag{4.19}$$

Type 2: Specified Flux Boundary Condition (Neumann B.C.)

$$\left(\Gamma\frac{\partial\phi}{\partial n}\right) = q_1+q_2\phi \tag{4.20}$$

where q_1, q_2 are specified by the user, depending on the equation to be solved. Eq.(4.20) is valid for the whole side $\overline{cia}$, and it is assumed that ϕ prevail at point i. Then the integration of Eq.(4.18) becomes:

$$\begin{aligned}\int_c^a \vec{J}\cdot\vec{n}ds &= [r\rho(\vec{v}\cdot\vec{n})\phi - r(q_1+q_2\phi)]_{ca}s_{ca} \\ &= r_i[(\dot{m}-q_2)\phi-q_1]_{ca}s_{ca}\end{aligned} \tag{4.21}$$

where $\dot{m}$ is the mass flow rate over the boundary surface $\overline{ca}$. ϕ can be approximated by linear interpolation function or by using the dependent variable value at point i.

Type 3: Outflow Boundary Condition

Usually, the distribution of ϕ is not known at the outflow boundary, hence, the uniform flow boundary condition is assumed and the diffusion flux of ϕ is considered to be negligible relative to the convective flux, i.e.

$$\vec{J}_{outflow} = r\rho\vec{v}\,\phi \tag{4.22}$$

Then the treatment of outflow boundary condition can be considered as Neumann type boundary condition which is similar to Type 2.

4.2.2 Final Form of the Discretized Equations

Expressions similar to Eq.(4.17) can be derived for the contributions of all elements associated with the control volume around an internal or a boundary node i. After substituting these expressions into Eq.(4.1), the final form of the discretized algebraic equations can be expressed as:

$$a_i\phi_i^{n+1} = \sum_{nb} a_{nb}\phi_{nb}^{n+1} + a_i^0\phi_i^n + b_i \qquad (4.23)$$

where, the summation is taken over all the neighbours of the node i. For Face-centered scheme, the number of neighbours of the node i is always equal to 4, while for Vertex-centered scheme, the number of neighbours of node i vary.

4.3 Treatment of Pressure-Velocity Coupling

In order to couple the continuity and momentum equations, a pressure-velocity closure is required for deriving the algebraic pressure equation. In the present study, this is established by using the momentum integration over the co-volume, as shown in Figure 4.5.

Consider the 2D cartesian or axisymmetric, unsteady, incompressible momentum equation in its vectorial conservative form:

$$\frac{\partial}{\partial t}(r\rho\vec{v}) + \nabla\cdot(r\rho\vec{v}\otimes\vec{v} - r\mu_{eff}\nabla\vec{v}) = -r\nabla P + \vec{S} \qquad (4.24)$$

where $\vec{v}$ is the velocity vector, ρ is the density of the fluid and μ_{eff} is the effective viscosity. The symbols ∇ and $\otimes$ denote the gradient/divergence and outer product operators. P is the pressure, and r is the radius.

Integrating Eq.(4.24) over the co-volume Ω_c (see Figure 4.5) around the point

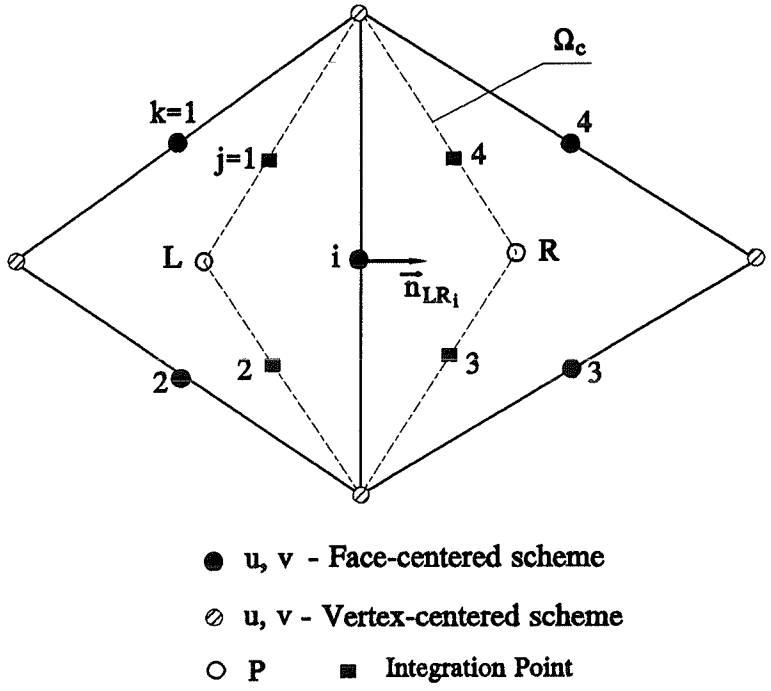

Figure 4.5: Co-Volume used for deriving the Pressure-Velocity Closure

i, we have:

$$\int_{\Omega_c} \frac{\partial}{\partial t}(r\rho\vec{v})dV + \oint_{\partial\Omega_c}(r\rho\vec{v}\otimes\vec{v} - r\mu_{eff}\nabla\vec{v})\cdot\vec{n}ds = -\int_{\Omega_c} r\nabla P dV + \int_{\Omega_c}\vec{S}dV \quad (4.25)$$

It should be noted that when dealing with the pressure-velocity coupling the velocity components are used at midpoints of each side of a triangle. Fig. 4.5 shows the calculation point i and its neighbouring points k = 1,2,3,4. However, due to the fact that velocities are stored at vertices in the Vertex-centered scheme (the shadowed circles at vertices of the triangle, as shown in Fig.4.5), the velocities are obtained at k=1,2,3,4 locations by a linear interpolation. Let j =1,2,3,4 be the integration midpoints of the integration faces, and L and R represent the left and right centroids of each element which share the common side i. Pressure is assumed constant over each element and is stored at the centroid of the element.

In the following, we will deal with the integration of Eq. (4.25) by considering separately the transient term, the convection-diffusion term, the pressure gradient term and the source terms as was done for Eq. (4.1).

Transient Term

The integration of the transient term can be expressed as:

$$\int_{\Omega_c} \frac{\partial}{\partial t}(r\rho\vec{v})dV = \frac{1}{3}(A_L+A_R) r_i \rho_i^n \left(\frac{\vec{v}_i^{n+1}-\vec{v}_i^n}{\Delta t} \right) \tag{4.26}$$

where A_L and A_R are the area of elements L and R, respectively.

Convection-Diffusion Term

For convection-diffusion flux in Eq. (4.25), the midpoint approximation is used to calculate the integral. It can be expressed as:

$$\oint_{\partial\Omega_c} (r\rho\vec{v}\otimes\vec{v} - r\mu_{eff}\nabla\vec{v})\cdot\vec{n}ds = \sum_{j=1}^{4} [r\rho(\vec{v}\cdot\vec{n})^n\vec{v}^{n+1} - r\mu_{eff}(\vec{n}\cdot\nabla\vec{v})^{n+1}]_j S_j \tag{4.27}$$

Eq. (4.27) can be treated as the general discretized equation, where $\phi = \vec{v}$ by using hybrid interpolation.

Pressure Gradient Term

The key point of the pressure-velocity closure is the treatment of the pressure gradient term in the above equation. The pressure gradients in Eq. (4.25) can be integrated by parts as:

$$\int_{\Omega_c} r\nabla P dV = \int_{\Omega_c} \nabla(Pr) dV - \int_{\Omega_c} P\nabla r dV \tag{4.28}$$

where the first term of right hand side of Eq. (4.28) can be calculated by using Gauss's theorem along the integration path j =1 to 4:

$$\int_{\Omega_c} \nabla(Pr) dV = \oint_{\partial\Omega_c} rP\vec{n} ds = \sum_{j=1}^{4} r_j P_j \vec{n}_j s_j \tag{4.29}$$

Since the pressure is assumed constant over each element, the use of geometric condition gives (Appendix A),

$$\int_{\Omega_c} r\nabla P dV = (P_R - P_L)\vec{n}_{LRi} r_i s_i = \Delta P_i \vec{n}_{LRi} r_i s_i \tag{4.30}$$

where $\vec{n}_{LRi}$ constitutes the normal of the side s_i directed from the triangle L to the triangle R, as shown in Figure 4.5.

Source Term

The source term in Eq. (4.25) is treated as follows:

$$\int_{\Omega_c} \vec{S} dV = \frac{A_L + A_R}{3}(\vec{S}_c + \vec{S}_p \phi_i) \tag{4.31}$$

By summing all the contributions of transient, convection-diffusion, pressure, and source terms, and the boundary conditions for velocity $\vec{v}$, the final form of the discretized momentum equation can be expressed as:

$$a_i \vec{v}_i^{\,n+1} + \sum_{k=1}^{4} a_k \vec{v}_k^{\,n+1} = a_i^0 \vec{v}_i^{\,n} - \Delta P_i r_i s_i \vec{n}_{LRi} + \vec{d}_i \qquad (4.32)$$

This is the relation of the Pressure-Velocity closure, it will be used in the derivation of the pressure algebraic equation.

4.4 Pressure Equation and Pressure Gradient

The control volume for the continuity equation is the triangular element itself, where the pressure is stored at the centroid of the element, as shown in Figure 4.6.

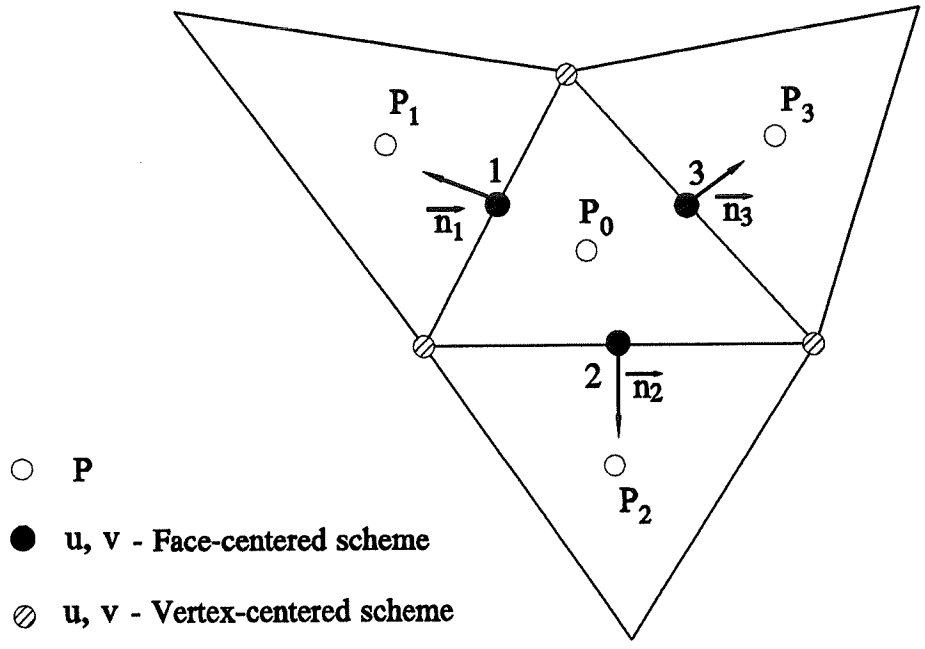

Figure 4.6: The node cluster involved in the discretized pressure equation

By integrating the continuity equation (3.61) over the control volume of P_0,

using the midpoint approximation, we have:

$$\sum_{i=1}^{3} \rho_i r_i \vec{v}_i^{n+1} \cdot \vec{n}_i s_i = 0 \tag{4.33}$$

where s_i is the length of the side i of the triangle P_0, the integration points 1, 2 and 3 are the midpoints of each side, and $\vec{n}_i$ is the outward normal of the integration side of the element P_0, as shown in Figure 4.6.

For the Face-centered scheme, the velocities at points 1,2,3 can be used directly, because the velocities are stored at the midpoint of sides. However, in Vertex-centered, linear interpolation for the velocities at sides is used since the velocities are stored at vertices of the element. The pressure-velocity closure relation (Eq. (4.32)) applies to both schemes and is used to derive the pressure discretized algebraic equation by substituting into the integrated continuity equation. For convenience, both sides of Eq.(4.32) are divided by coefficient a_i, giving:

$$\vec{v}_i^{n+1} = \vec{v}_i^{*} - \Delta P_i \vec{\alpha}_i \tag{4.34a}$$

with

$$\begin{cases} \vec{v}_i^{*} = \dfrac{-\sum_{k=1}^{4} a_k \vec{v}_k^{n} + a_i^{0} \vec{v}_i^{n} + \vec{d}_i}{a_i} \\ \vec{\alpha}_i = r_i \dfrac{s_i}{a_i} \vec{n}_{LRi} \end{cases} \tag{4.34b}$$

Substituting Eq.(4.34) into Eq.(4.33), we can obtain the following relation:

$$\sum_{i=1}^{3} \rho_i r_i (\vec{v}_i^* - \vec{\alpha}_i \Delta P_i) \cdot \vec{n}_i s_i = 0 \tag{4.35}$$

where, $\vec{n}_i$ is the outward normal of the integration sides i directed from P_0 to P_i (Figure 4.6). $\vec{\alpha}_i$ is a vector normal to the side i directed from the element "L" to the element "R", it has the same direction as the vector $\vec{n}_{LRi}$ in Figure 4.5. The difference between $\vec{n}_i$ and $\vec{\alpha}_i$ is that: for a given face direction, $\vec{n}_i$ is always the outward normal of this face, while $\vec{\alpha}_i$ may be inward or outward normals, which depends on the definition of the co-volume. The pressure difference then can be written as:

$$\begin{cases} \vec{\alpha}_i \cdot \vec{n}_i > 0 \\ \Delta P_i = P_R - P_L = P_i - P_0 \end{cases} \tag{4.36a}$$

or

$$\begin{cases} \vec{\alpha}_i \cdot \vec{n}_i < 0 \\ \Delta P_i = P_R - P_L = -(P_i - P_0) \end{cases} \tag{4.36b}$$

Substituting Eq.(4.36) into Eq.(4.35), the final form of pressure equation can be expressed as follows:

$$c_0 P_0 + \sum_{i=1}^{3} c_i P_i = \epsilon \tag{4.37a}$$

with:

$$c_i = \rho_i r_i^2 \frac{s_i^2}{a_i} \tag{4.37b}$$

$$c_0 = -\sum_{i=1}^{3} c_i \tag{4.37c}$$

and

$$\epsilon = -\sum_{i=1}^{3} \rho_i r_i s_i (\vec{v}_i^{\,*} \cdot \vec{n}_i) \tag{4.37d}$$

It should be noted that in Eq. (4.32) the pressure field cannot correct both velocity components (u,v) but only the normal velocity component. This is because that velocities (u,v) at the co-volume face are contacted with only two pressure points. Then the pressure difference caused by these two pressures depends on the face orientation. Hence, the pressure gradient ($\partial p/\partial x, \partial p/\partial y$) cannot be determined uniquely based on these two pressures. To overcome this problem, a pressure reconstruction method is used to obtain the pressure gradient field by using the complete pressure field.

Assuming that the pressure varies linearly over the triangle $P_1P_2P_3$, as shown in Fig. 4.7, we have,

$$P = ax + by + c \tag{4.38}$$

where the coefficients a, b, and c can be determined from the values of pressure at point P_1, P_2, P_3 as well as their corresponding locations, and P_1, P_2, P_3 are the neighbours of the triangle P_0.

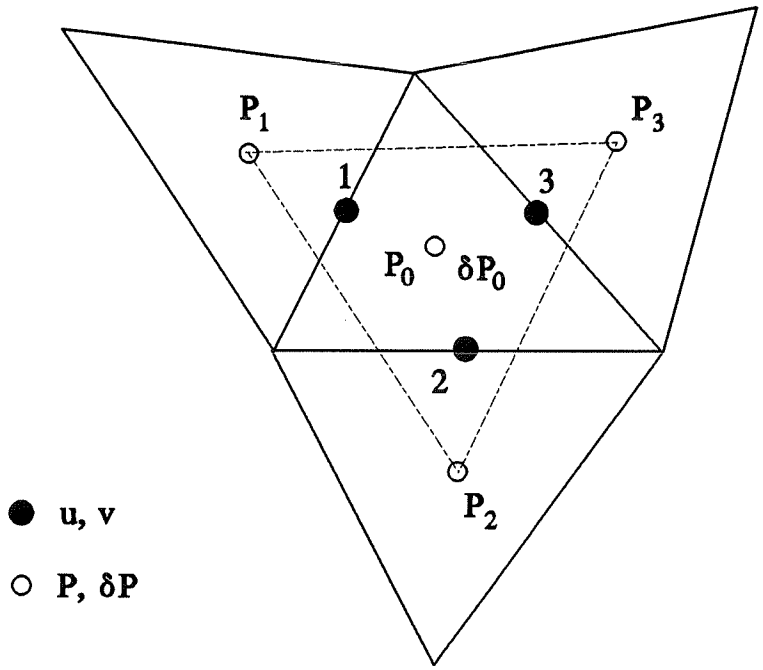

Figure 4.7: Pressure reconstruction used for obtaining the pressure gradient in triangle element P_0

The pressure gradients in the element P_0 can be expressed as:

$$\left(\frac{\partial P}{\partial x}\right)_0 = a, \qquad \left(\frac{\partial P}{\partial y}\right)_0 = b \tag{4.39}$$

These relations are then used in the solution of the momentum equations as source terms, where the pressure gradients should be directly integrated by volume, instead of faces. A Neumann type boundary condition for pressure along the normal direction is used to determine the pressure gradient at boundary elements, as shown in Figure 4.8, where $P_2 = P_0$.

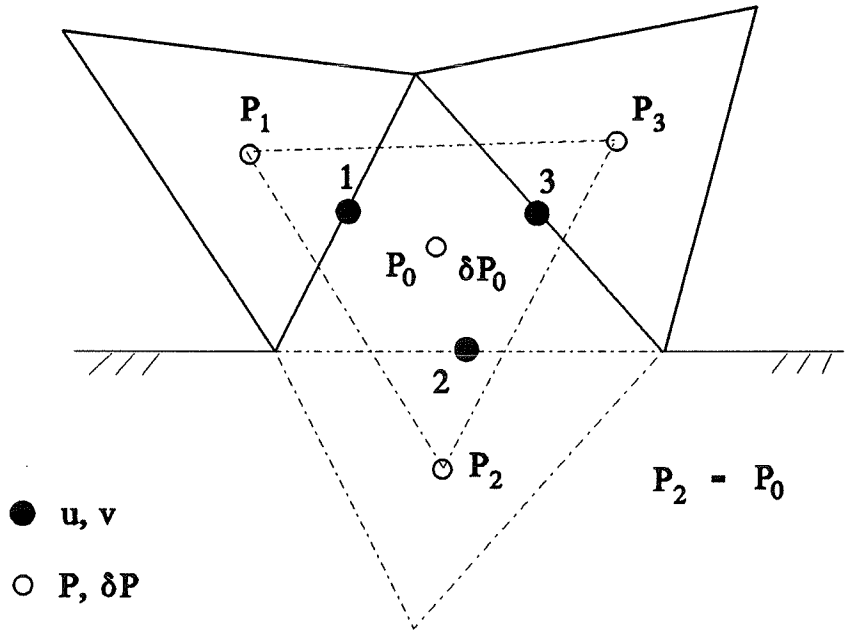

Figure 4.8: The pressure gradient at the boundary element

4.5 Solution of the System

The discretized transport equation for each variable can be written in a matrix system as follows:

$$A\vec{x} = \vec{b} \tag{4.40}$$

where A is a sparse matrix, x and b are vectors. The solution method uses a LU factorization with a skyline storage scheme, where only the nonzero length of a column or row is stored for each equation. Details may be found in Page et al. (1989).

For the steady case, the transient term is dropped from the discretized general form of the transport equation (4.23) as:

$$a_i^{\phi}\phi_i = \sum_{nb} a_{nb}^{\phi}\phi_{nb} + b_i^{\phi} \tag{4.41}$$

To make the solution stable, usually, the under-relaxation factor method suggested by Patankar (1980) is used. In the present work, the E-factor formulation of Van Doormaal and Raithby (1984) is implemented to improve the convergence. Then Eq.(4.41) becomes:

$$a_i^{\phi}\left(1+\frac{1}{E}\right)\phi_i = \sum_{nb} a_{nb}^{\phi}\phi_{nb} + b_i^{\phi} + \frac{a_i^{\phi}}{E}\phi_i^0 \tag{4.42}$$

where ϕ_i^0 is the value of ϕ_i from the previous iteration. The value of E range from 0.5 to 10 in the computation process.

4.6 Radiation Heat Transfer

The purpose of the present discrete transfer method is to couple the proposed unstructured grid solver for reacting flows with radiation calculations. This extension not only retains the original discrete transfer method's features (Lockwood and Shah, 1981), but also offers others advantages, such as grid concentration, adaptivity and even moving grids.

4.6.1 Solution Procedure

Consider a 2D infinite arbitrary enclosure containing a participating medium, as shown in Figure 4.9.

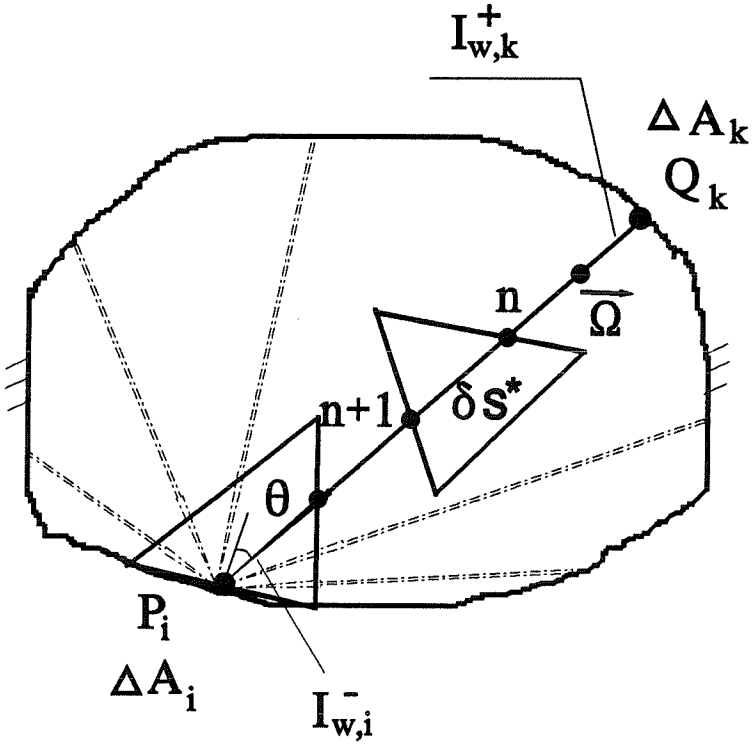

Figure 4.9: Typical rays in participating medium of an irregular-shaped domain

The surfaces (or walls) of the enclosure are divided into number of subsurfaces, and the volume of the medium is divided into discrete non-overlapping triangular elements. The hemisphere which encompasses each surface element is arbitrarily divided into N (= Nθ x Nϕ) equal segments from each of which a ray is issued. The directions of the rays (or beams) are specified by the polar angle θ and azimuthal angle ϕ, and their intensity leaving from each surface, $I^{+}_{w,i}$ is assumed to be uniform on each subsurface. The temperature of each of the elements and subsurfaces as well as the values of the intensity $I^{+}_{w,i}$, are assumed to be known, either from a previous iteration values or from an initial guess. For a gray surface, the iteration procedure to update the new set of intensities is described. The new value of $I^{+}_{w,i}$ leaving one surface ΔA_i is calculated from:

$$I^{+}_{w,i} = \frac{q^{+}_{w,i}}{\pi} = (1-\varepsilon_w)\frac{q^{-}_{w,i}}{\pi} + \varepsilon_w \frac{E_w}{\pi} \tag{4.43}$$

where ε_w is the surface emissivity, E_w is the surface emissive power σT_w^4, $q^{+}_{w,i}$ and $q^{-}_{w,i}$ are the heat fluxes leaving from and arriving at the subsurfaces ΔA_i.

The heat flux, $q^{-}_{w,i}$ is obtained from the integration of $I^{-}_{w,i}$ about the entire hemisphere on the center point P_i of ΔA_i (Chan, 1987),

$$q^{-}_{w,i} = \int_{\phi=0}^{2\pi}\int_{\theta=0}^{\frac{\pi}{2}} I^{-}_{w,i} \cos\theta_i \, d\Omega_i = \sum_{i=1}^{N} I^{-}_{w,i} \cos\theta_i \, \Delta\Omega_i \tag{4.44}$$

where $I^{-}_{w,i}$ is the incident intensity at P_i of a ray within a solid angle $\Delta\Omega_i$, originating from point Q_k on the k subsurface.

The intensities $I^{-}_{w,i}$ and $I^{+}_{w,k}$ are obtained by integrating Eq. (3.58) along the direction of $\vec{\Omega}$, and E^*, the modified emissive power defined by Eq. (3.57), is assumed uniform in each element, from which the following recurrence relation is established:

$$I_{n+1} = \frac{E^*}{\pi}(1-e^{-\delta s^*}) + I_n e^{-\delta s^*} \tag{4.45}$$

where, the subscripts n and n+1 designate integration points along the ray separated by distance δs. I_n and I_{n+1} are the values of intensity entering and leaving a triangular element respectively, and δs^* is the optical length within the volume (see Figure 4.9).

The whole calculation of intensity as well as the radiation sink or source are based on the following steps:

i) calculate the successive integration locations n+1, n ... by a ray Ω_i from point P_i to the opposing wall Q_k.

ii) the relation Eq.(4.45) is applied along the ray from Q_k to P_i to obtain $I^-_{w,i}$ from the value of $I^+_{w,k}$ which is computed by Eq.(4.43). Therefore, $q^-_{w,i}$ can be evaluated by summing over all the rays arriving at the hemisphere about P_i. A new set of values $I^+_{w,i}$, is calculated by Eq.(4.43) for all enclosure subsurfaces. The solution procedure is iterated until the desirable accuracy is achieved.

iii) calculate the radiation sink or source term $(\nabla\cdot\vec{q}_r)$ for the energy conservation equation. The net amount of energy emitted by the n^{th} element by the ray from a subsurface area of ΔA_i can be expressed as:

$$S_{n,i} = (I_{n+1}-I_n)\cos\theta_i \Delta\Omega_i \Delta A_i \tag{4.46}$$

By shooting out all the rays hemispherically in a set of prescribed directions and in N solid angles from each of the subsurface, and summing up over all the rays M, which contribute to the n^{th} element, the rate of total net loss of radiative energy from this element volume ΔV_n is given by Chan (1987):

$$\int_{\Delta V_n} \nabla\cdot\vec{q}_r dV = \int_{\Delta A_n} \vec{q}_r\cdot d\vec{A} = \sum_{i=1}^{M} S_{n,i} \tag{4.47}$$

This term is used in the solution of the energy transport equation to couple the radiative heat transfer with the energy conservation equation.

4.6.2 Ray Tracing

Cartesian Enclosures

The difference between triangular and rectangular elements lies in the treatment of geometric aspects. For a structured rectangular mesh, the linear interpolation between the emitted ray and the element sides can be easily calculated. This can be done by increasing (or decreasing) the index of grid line i or j along the ray's

propagation direction, the intersection point can then be determined. Details for the treatment of rectangular meshes may be found in Shah (1979).

For an unstructured triangular element, the intersection between the emitted ray and the element sides can be classified in two cases in the present methodology. Case 1 is the usual case, where the ray intersects one side (ab or bc) of an element abc, as shown in Figure 4.10. This depends on whether the angle between the ray direction PQ and the wall side ca is smaller than the angle between bP and wall side ca. The intersection point n can be calculated simply by the linear interpolation between ray PQ and side ab (or bc).

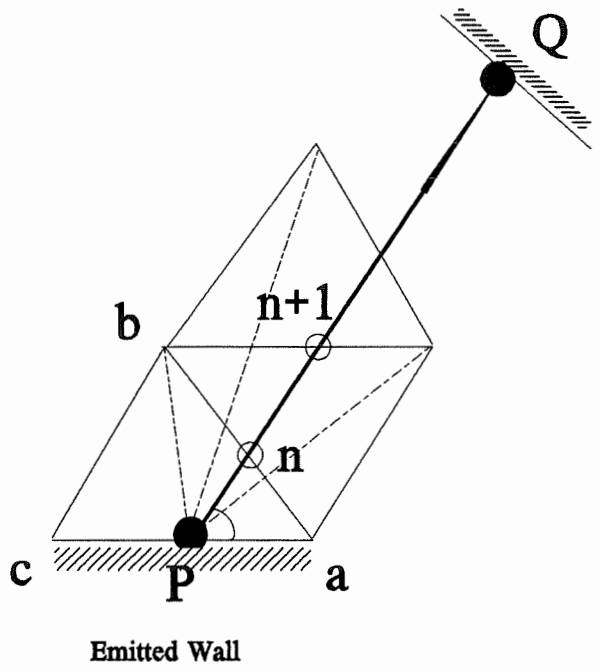

Figure 4.10: Geometric calculation in case of the ray intersects with one side of a triangle

Case 2 occurs when the emitted ray passes through vertex b, as shown in Figure 4.11 and 4.12 (In this case, the ray cannot cross the vertex a, because ca is the emitted wall). Around point b, all the neighbouring triangular elements are considered,

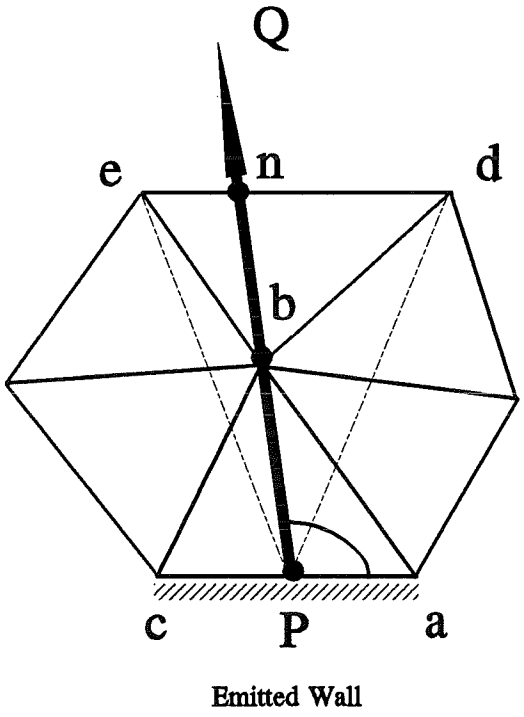

Figure 4.11: Geometric calculation in case of the ray passes through a vertex of a triangle

except for element abc, because the ray has visited this element. For each neighbouring element, the side which does not include vertex b (example: side ed) is used to determine the interpolation point n. This can be done by assessing whether the angle between ray PQ and wall side ca is included inside angles ePa and dPa (Figure 4.11). Special treatment is necessary when ray PQ overlaps with side bd (Figure 4.12). In this case, the average extinction coefficient and emissive power in elements 1 and 2 is used in the calculation of intensity in Eq.(4.45). The interpolation point n is same as the point d.

Once the interpolation point n is found, a similar procedure can be used to determine the point n+1, ..., until the ray impinges a wall cell. In the meantime, we calculate the distance the ray travels in each element along its path.

The present method is not restricted to triangular elements with acute angles. It can be applied to obtuse triangles as well.

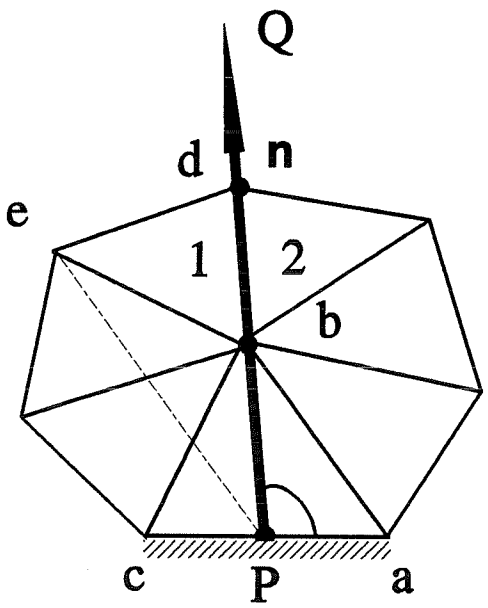

Figure 4.12: Geometric calculation in case of the ray overlaps with side

In the application of this method, the different grid density is used for the unstructured mesh. In the case where a high gradient of radiant energy exists of the domain, the fine grid is adopted. In other regions where the radiant energy is not notable, a coarse grid can be used. Using variable grid density for different regions of the solution domain, can save computing time, while maintaining high accuracy.

The different solution strategy is adopted to solve turbulent reacting flow coupled with radiation. For the aerodynamic and reaction solver, a fine grid is necessary to describe the flow and species. If the radiation solver uses the same grid as fluid flow solver, it requires long computing time, especially when the radiation properties are temperature dependent. Based on the same set of the computation grid as the flow solver, the radiation variables are updated less frequently than that of the flow and the chemical reactions, usually, per 5 or 10 iterations are preferred.

Cylindrical Enclosures

Although in cylindrical enclosure, the geometry of the domain is quite different from the cartesian coordinate, the radiative transfer equation used is exactly the same as the cartesian ones. In a 2D axisymmetric cylindrical enclosure, we are mainly interested in the radiation heat transfer in the representative plane (Figure 4.13). In order to implement the discrete transfer method, even in 2D case, the ray-tracing procedure used here is same as that of the 3D cylindrical enclosure, i.e. the representative directions have to be originated from the whole enclosure (or the whole wall surface), as shown in Figure 4.13.

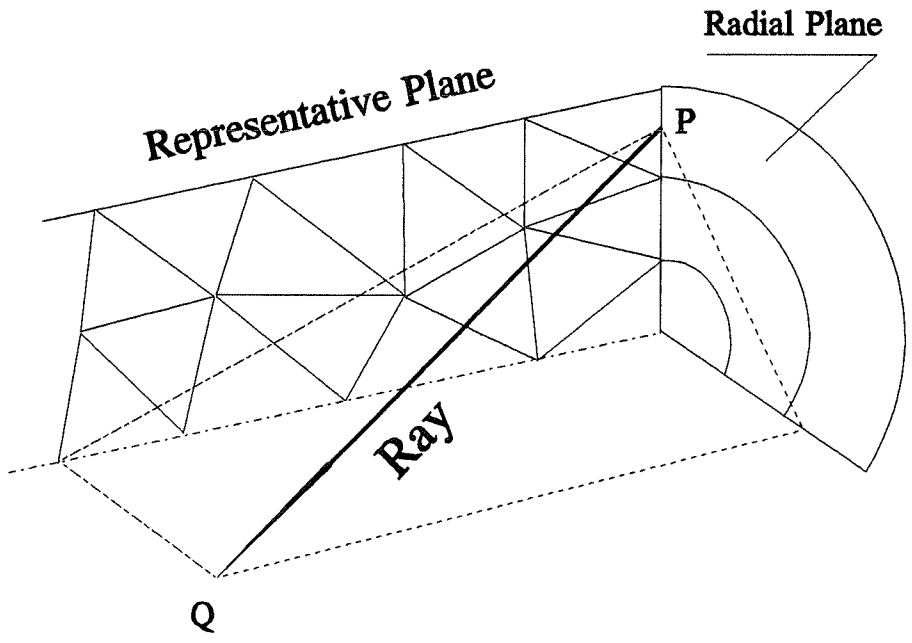

Figure 4.13 Projection of the ray-tracing direction in one quadrant of a cylindrical enclosure

4.6.3 Treatment of In-Scattering

Unlike the discrete ordinates method (Fiveland, 1984), angular integrals of the

intensity in the in-scattering term are discretized by numerical quadrature. In the present discrete transfer method, the in-scattering term, like the emissive power, is presumed constant over a triangular element. According to Chan (1987), Eq.(3.57) is discretized as:

$$E^* = \frac{1}{k_e}\left(k_a E_g + \frac{k_s}{4}\sum_{4\pi} p(\vec{\Omega}_{P_iQ_k}, \vec{\Omega}'_{P_iQ_m})\, I(\vec{\Omega}'_{P_iQ_m})_{avg}\, \Delta\Omega'_{P_iQ_m}\right) \qquad (4.48)$$

where $I(\vec{\Omega}'_{P_iQ_m})_{avg}$ is a value averaged over the element. The arithmetic mean of its values entering and leaving an element in the $\vec{\Omega}'$ direction will be taken for computing purpose, as shown in Figure 4.14. However, mathematically, the accuracy of angular integral of the intensity which is based on the arithmetic mean is less than that of which the numerical quadrature. This leads to the accuracy of the discrete transfer results for considering the in-scattering term is less than that of the discrete ordinates method.

It should be noted that in the consideration of the in-scattering term, the number of rays must be large enough to avoid the "ray effect", especially in the case where the intensity may be zero at one specified direction in an element in the application of ray-tracing procedure (Chai, 1993), this phenomena may be referred to the "statistical error", due to the method's statistical based approach.

4.7 Solution Algorithm of the SCVFEM

The overall solution algorithm of SCVFEM is based on the following steps:

1. Guess a velocity field and all the other variables.

2. Calculate coefficients in the momentum equations based on the Co-Volume integration and then obtain $\vec{v}_i$ from Eq.(4.34a) and Eq.(4.34b) by substituting the values of neighbour velocities. This step suits for both Face-centered and Vertex-

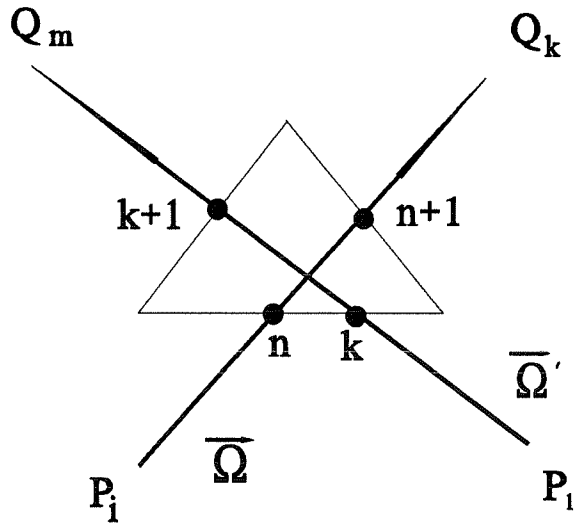

Figure 4.14: The treatment of in-scattering

centered schemes.

3. Solve the pressure Eq. (4.37a)-(4.37d), then obtain the pressure field.

4. Using the pressure reconstruction method, obtain the pressure gradient field Eq.(4.39).

5. Solve the momentum equations over the Co-Volume (Face-centered scheme), or Polygonal control volume (Vertex-centered scheme) to obtain the velocity field, where the source terms of the momentum equations include the pressure gradient field.

6. Solve the turbulent equations k and ϵ, update μ_t and wall boundary conditions for turbulent flows.

7. Solve the mixture fraction f, mass fraction of fuel, and other combustion models for obtaining the concentration of chemical species.

8. Solve the radiative transfer equation to obtain the radiation source and heat flux at wall.

9. Solve the enthalpy equation if radiation exists.

10. Compute the temperature and density field for reacting flows.

11. Return to Step 2 with all renewed values, repeat until the solution converge.

The above solution algorithm has a little difference with well known solution methods, such as SIMPLE algorithm.

In the above solution algorithm, the variable E-factor and the variable under-relaxation parameters for dependent variables are used. This strategy makes the numerical solution converged faster than that of only use constant under-relaxation parameters. Also, the inner-loops for flow variable (u,v,p), turbulent variables (k,ϵ) and other transport equations are also tested.

4.8 Features of the proposed SCVFEM

The present SCVFEM has certain features in both the accuracy and the treatment of the boundary conditions. Firstly, for both Face-centered and Vertex-centered schemes, there is no need to impose the boundary condition for pressure. Secondly, for Face-centered scheme, it is easy to impose the boundary condition for velocities, transport variables and radiation intensity at each boundary face, it also avoids the difficulty to impose the boundary condition at the discontinuous corner point of the computation domain with Vertex-based schemes. Finally, with the equivalent number of unknowns and the same accuracy required, the CPU time of Face-centered scheme is less than that of Vertex-centered scheme, this will be illustrated in Chapter 5.

Due to the element used in the present SCVFEM with Face-centered scheme is same as the well known finite element P1 non-conforming/P0 element (Crouzeix and Raviant, 1973, Figure 2.1(j)), and it is also very close to that of the complementary volume method (Nicolaides, 1989, Figure 2.1 (b)), then it is necessary to illustrate the differences among these methods.

In the P1 non-conforming/P0 finite element method, the discretised momentum equations for velocity components (u,v) are derived by using the variational method. The incompressibility constraint is taken into account in the 2D case by the construction of a zero divergence basis (Thomasset, 1982), then the pressure is eliminated, the penalty method is used to solve the discretised equations.

In the complementary volume method, contrast to the more usual approach using two velocity components (u,v) and one control volume (like SCVFEM does), its unusual characteristics are the use of only one velocity component, -normal to each edge of the triangulation, and two complementary control volumes, one is the polygonal control volumes consistent of joining the circumcenters of the triangles surrounding nodes of the triangulation; another is the triangular element as its control volume. These two complementary control volumes are used to discretise the momentum equation and incompressibility constraints in transformed div-curl systems of the momentum equations in 2D problems. The tangential velocity components which is used for the approximation of the convective terms are constructed from the normal velocity fields.

Chapter 5

Computational Results

The proposed scheme has been implemented and a number of test cases carried out to validate the code and the scheme. In particular the two nodal arrangements, face and vertex centered were compared for accuracy and cost. Similarly the two methods for implementing the wall function were also compared. The different combustion models are tested for turbulent reacting flow with variable density.

Finally, the SCVFEM is applied to the practical combustion problems, where the radiation heat transfer is considered. The results are compared with other numerical method and the experimental data.

5.1 Driven Cavity Flow

5.1.1 Problem Description

The steady, 2D-cartesian, laminar recirculating flow of an incompressible Newtonian fluid contained in a square enclosure where the fluid motion is driven by a sliding lid as shown in Fig. 5.1 is considered. Results obtained with the SCVFEM proposed in this thesis using both Face-centered and Vertex-centered schemes on unstructured grid, will be presented for Reynolds numbers of 100, 400 and 1000. The results are compared with the benchmark predictions of Ghia et al. (1982).

The following tests are examined:

A. The same number of elements for Reynolds number of 100.

B. An equivalent number of unknowns for Reynolds number of 100.

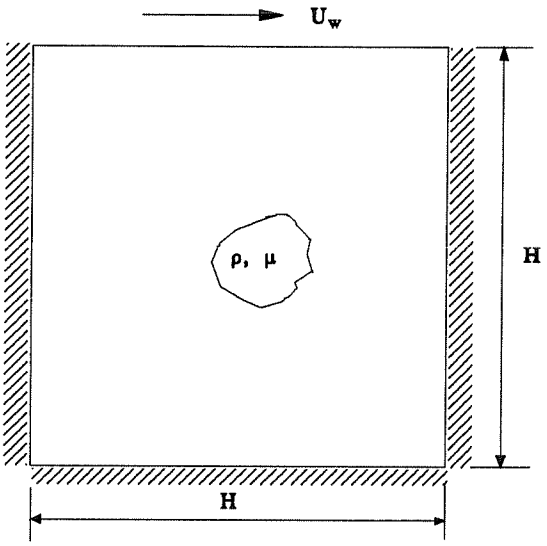

Figure 5.1: Geometry of a square driven cavity

C. The capability of the two schemes for high Reynolds number flows.

In the above tests, the boundary conditions for the u,v velocities at solid walls are equal to zero, and at the top wall u = 1 m/s, v = 0. The relaxation E-factors, $E^u = E^v = 4$ for Re = 100, $E^u = E^v = 2$ for Re = 400 and 1000 are used. The under-relaxation parameters of u, v and p are taken as 0.5. The maximum element Peclet number $Pe_{max} = 10$ is used as the limit between the exponential function and the upwind function.

5.1.2 Comparison of the Face-centered - Vertex-centered schemes

A. The same number of elements for Reynolds number of 100

Figure 5.2 shows the unstructured mesh containing 832 elements. The predicted velocity field is given in Fig. 5.3 for Reynolds number of 100.

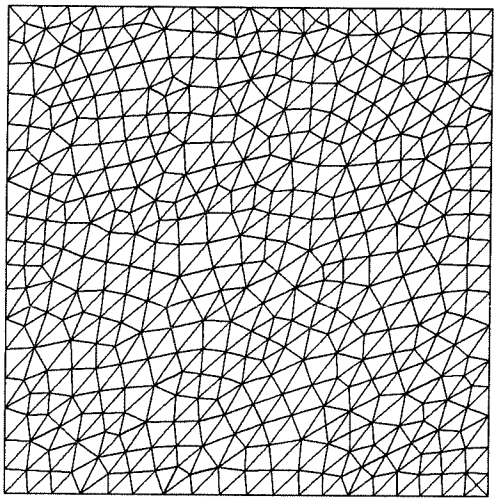

Figure 5.2: The computational mesh of a square driven cavity (832 elements)

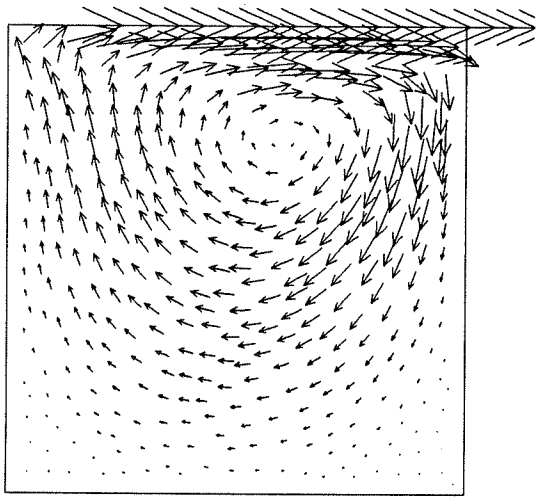

Figure 5.3: The predicted velocity field of a square driven cavity at Re=100

The u-velocity profile at the vertical centerline and the v-velocity profile at the horizontal centerline are shown in Fig. 5.4 (a) and (c), respectively. Table 5.1 gives

the number of iterations and the CPU times needed for both schemes to get the converged solutions.

Table 5.1: Comparison of the number of iterations and CPU times needed for both schemes on the same number of elements (832) for Reynolds number of 100

Scheme	Face-Centered	Vertex-Centered
iterations	530	215
Residual	10^{-7}	10^{-7}
CPU (s)	310.5	153.2

Using 5000 elements, for both schemes, the u- and v-velocity profiles at the vertical centerline and the horizontal centerline are in good agreement with the results of Ghia et al. (1982) at Re = 100, as shown in Fig. 5.4 (b) and (d).

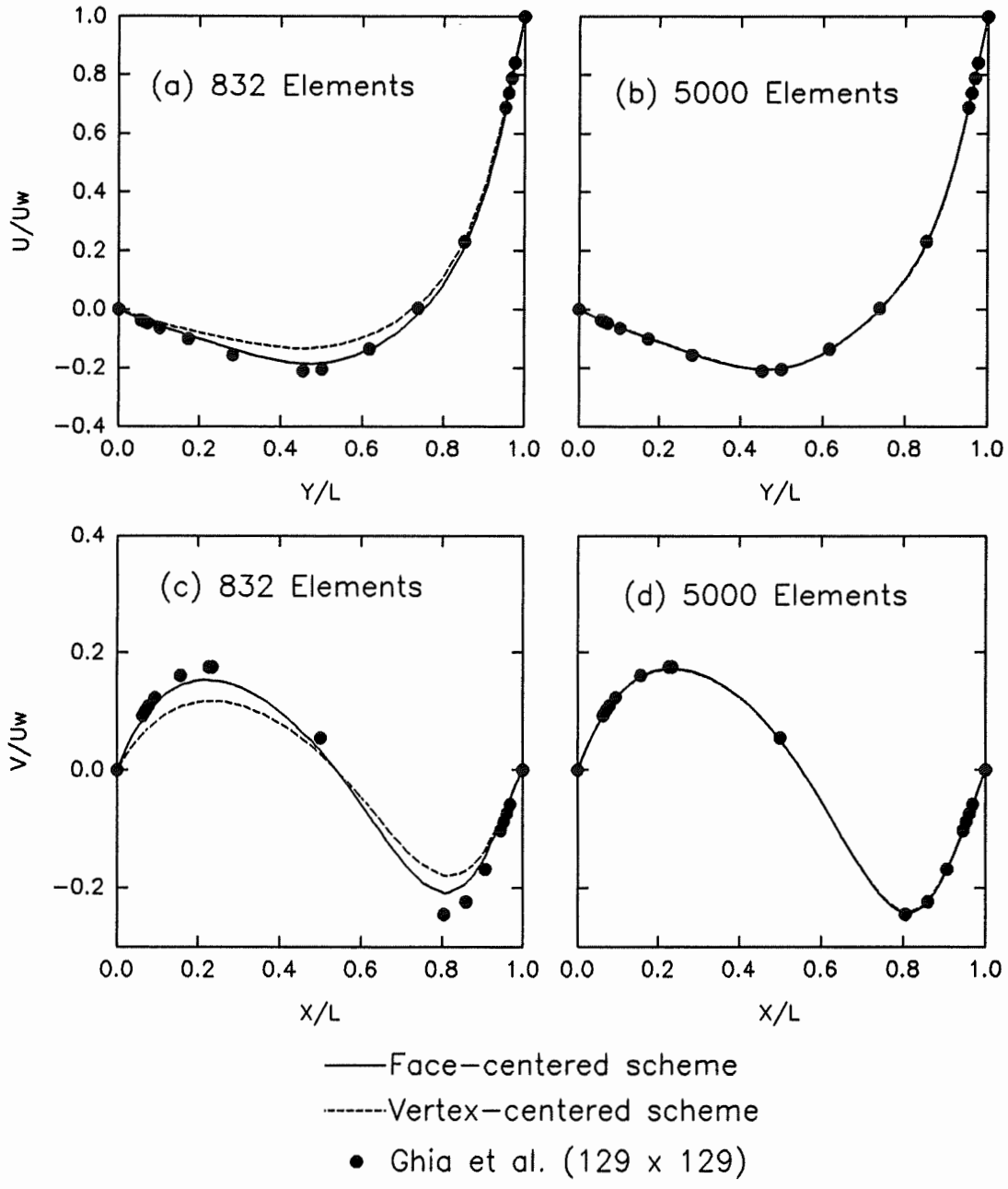

Figure 5.4: Comparison of the u-velocity at the vertical centreline and the v-velocity at the horizontal centreline of the cavity for Re=100 with the same number of elements for two schemes of the SCVFEM

B. An equivalent number of unknowns for Reynolds number of 100

Because for a given grid, the number of unknowns is different for Face-centered and Vertex-centered schemes, they should be compared on the basis of the number of degrees of freedom rather than number of elements. Two different grids, for Face-centered scheme 19x19 nodes, which contains 1008 degrees of freedom (sides), and for Vertex-centered scheme 31x31 nodes, which involves 961 degrees of freedom (vertices) are considered. The convergence history of the u-velocity for both schemes are shown in Fig. 5.5. The u-velocity profile at the vertical centerline and the v-velocity profile at the horizontal centerline are plotted and compared in Fig. 5.6. The comparison of the CPU times and the number of iterations are shown in Table 5.2 for both schemes.

Table 5.2: Comparison of the number of iterations and CPU times needed for both schemes on the equivalent number of degrees of freedom for Reynolds number of 100

Scheme	Face-Centered	Vertex-Centered
iterations	535	405
Residual	10^{-7}	10^{-7}
CPU (s)	220.9	611.0
Degree of freedom	1008	961

C. Effect of Reynolds number

The effect of Reynolds number on the two schemes is investigated. The computation meshes used for Re = 400 are 31x31 and 51x51 nodes, and for Re = 1000 47x47 and 81x81 nodes. Fig. 5.7 (a),(c),(b) and (d) show the results for the u-velocity profile at the vertical centerline and for the v-velocity profile at the horizontal centerline, respectively. We can see that for sufficiently fine grids there is little or no difference between these two schemes. The difference between the present predictions

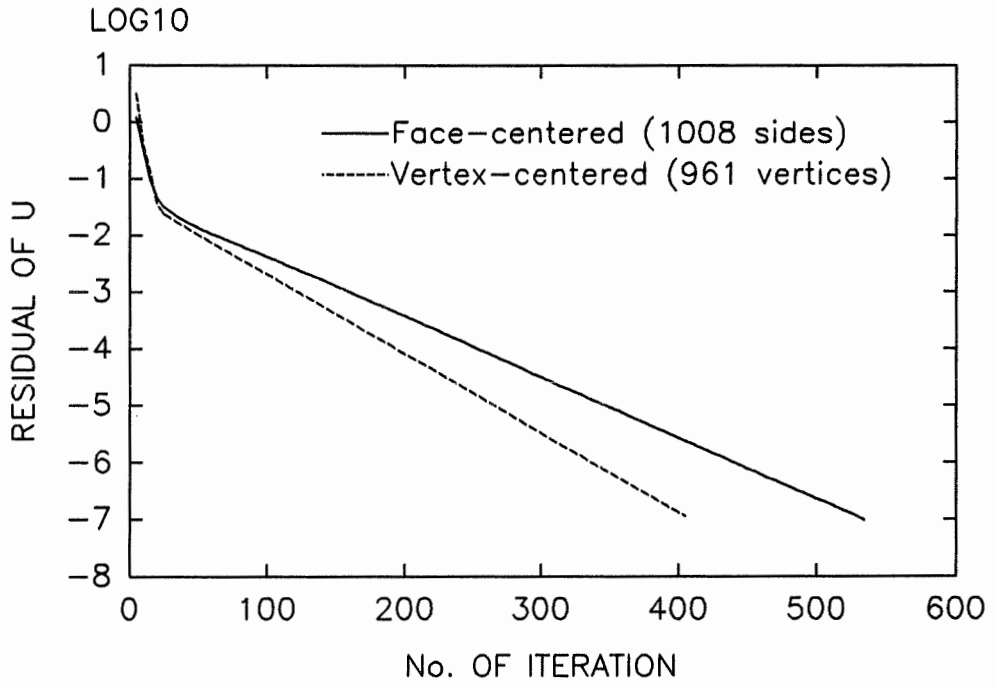

Figure 5.5: The convergence rate of the u-velocity for both Face-centered and Vertex-centered schemes

and the results of Ghia et al. (1982) is probably due to the upwind interpolation function (Rida,1993) and insufficient numerical resolution, the grid used in Ghia et al. is 129x129 nodes. The comparison of the CPU times and the number of iterations are shown in Table 5.3 for both schemes at Reynolds number of 400 and 1000.

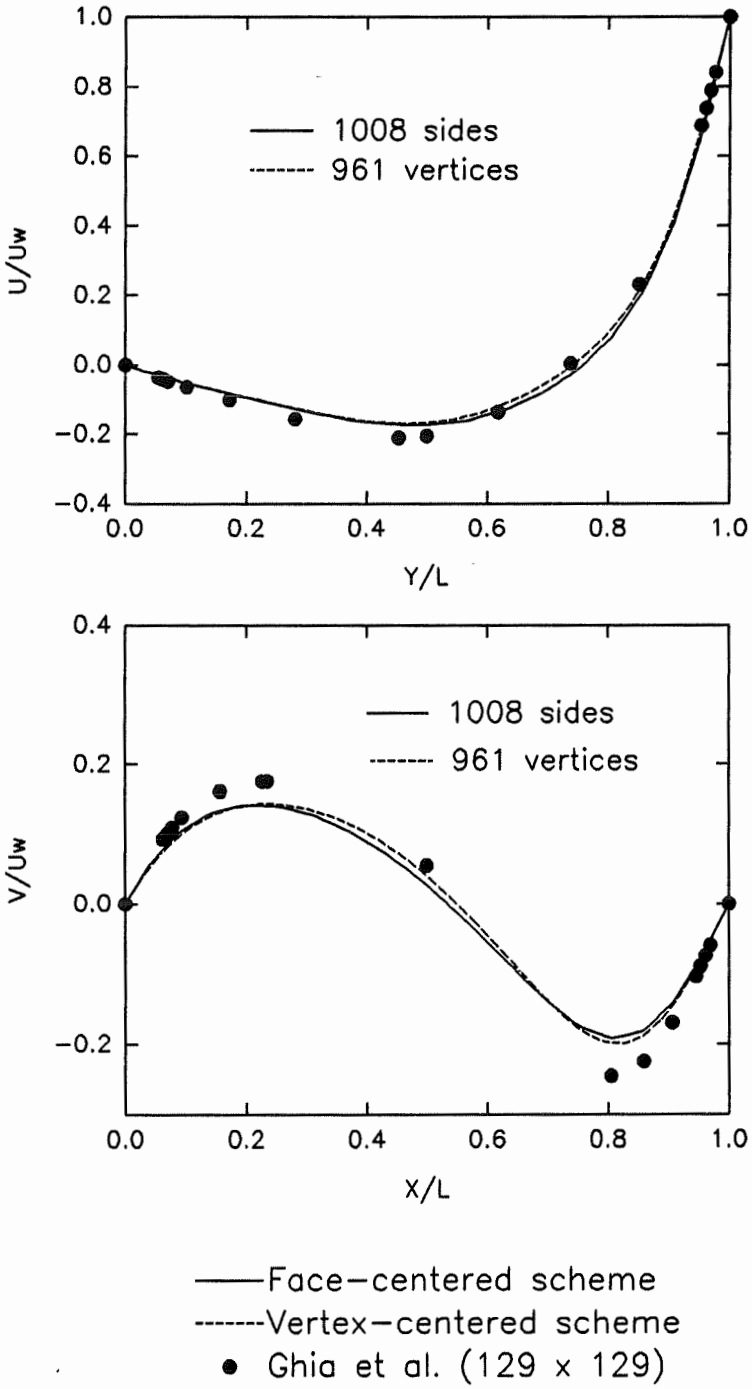

Figure 5.6: Comparison of the u-velocity at the vertical centreline and the v-velocity at the horizontal centreline of the cavity for Re=100 with an equivalent number of unknowns for two schemes of the SCVFEM

Table 5.3: Comparison of the number of iterations and CPU times needed for both schemes on Reynolds number of 400 and 1000, respectively

Reynolds Number	400		
Scheme	Face-C.	Face-C.	Vertex-C.
Grid (nodes)	31x31	51x51	51x51
Iterations	1080	714	473
Residual	10^{-6}	10^{-6}	10^{-6}
CPU (s)	1.217×10^{3}	3.58×10^{3}	1.483×10^{3}
Degree of freedom	2760	7600	2601
Reynolds Number	1000		
Scheme	Face-C.	Face-C.	Vertex-C.
Grid (nodes)	47x47	81x81	81x81
Iterations	2500	4400	5000
Residual	10^{-6}	10^{-6}	10^{-6}
CPU (s)	0.9204×10^{4}	12.047×10^{4}	5.77×10^{4}
Degree of freedom	6440	19360	6561

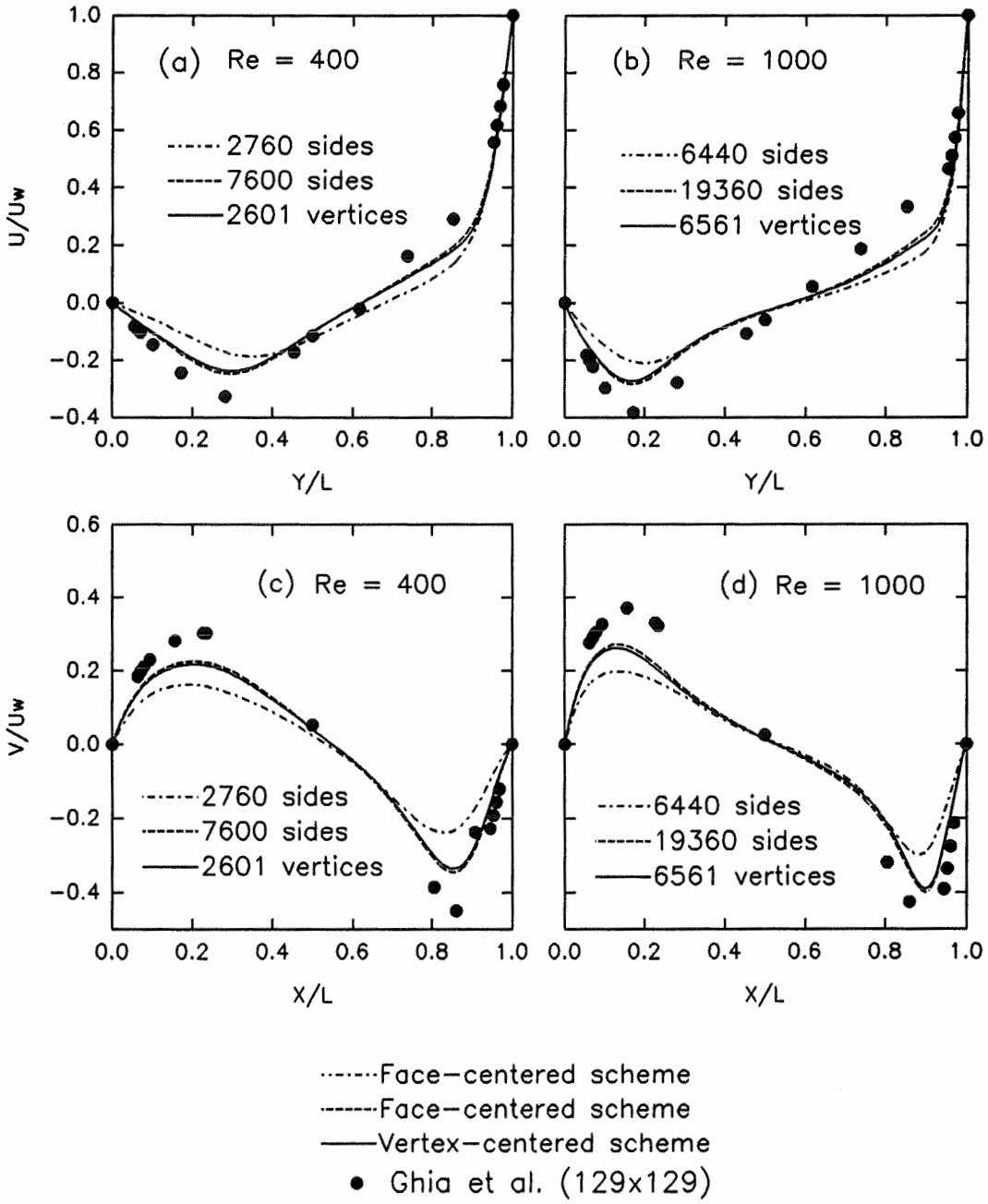

Figure 5.7: Comparison of the u-velocity at the vertical centreline and the v-velocity at the horizontal centreline of the cavity for Re=400 and Re=1000 for two schemes of the SCVFEM

5.2 Flow Over an Obstacle

5.2.1 Problem Description

The steady, two-dimensional, laminar flow of an incompressible fluid over an obstacle mounted in a closed channel is considered to examine the accuracy and the capability of the two SCVFEM schemes for predicting the recirculation length under inflow and outflow boundary conditions. The experimental configuration of Carvalho et al. (1987) is used in this test, as shown in Figure 5.8. The Reynolds number based on the obstacle height and the average inlet velocity is equal to 145.

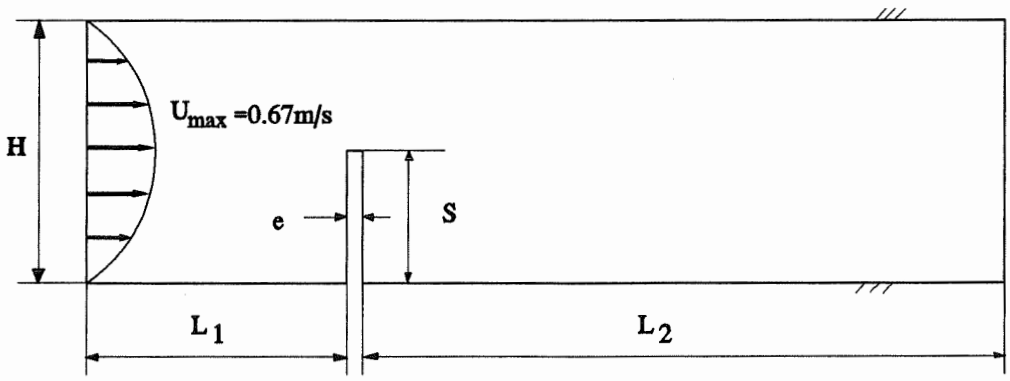

H = 0.010 m S = 0.005 m e = 0.001 m L_1 = 0.030 m L_2 = 0.120 m

Figure 5.8: Geometry of the flow over an obstacle

The unsteady state formulation is used for obtaining the steady state solution. For the Face-centered scheme, a non-uniform Mesh A contains 3728 elements (5711 sides as unknowns) is considered, as shown in Figure 5.9. While, for Vertex-centered scheme, three sets of computational meshes are used, Mesh A contains 1984 nodes

(3728 elements) as unknowns; Mesh B involves 3202 nodes (6128 elements), and Mesh C contains 4355 nodes (8386 elements) are used.

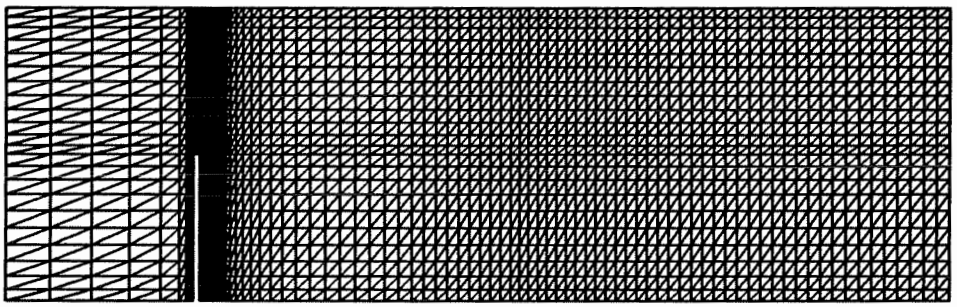

Figure 5.9: The computational mesh of the flow over an obstacle

5.2.2 Results

The predicted velocity field is shown in Figure 5.10.

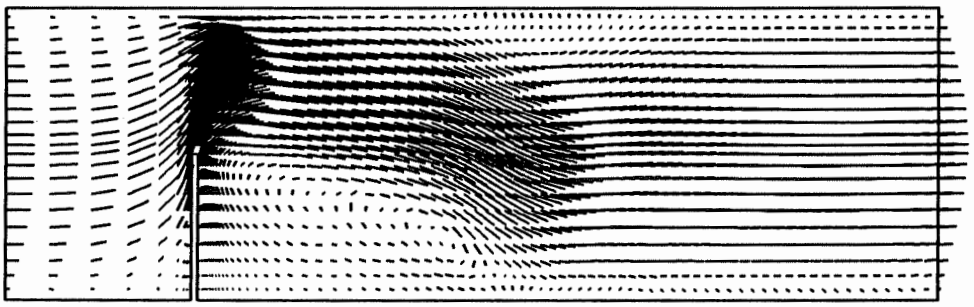

Figure 5.10: The predicted velocity field of the flow over an obstacle

Figures 5.11 and 5.12 show the distribution of the u-velocity profile at four stations downstream from the obstacle: x/S = 2.4, 4.4, 11, 24 for the different meshes

using the two schemes. From these results, we found that the accuracy of the Face-centered scheme with Mesh A (with 5711 sides) is comparable with that of the Vertex-centered scheme with the fine Mesh C (4355 Nodes), and both results are in good agreement with the experimental data. Table 5.4 gives the predicted recirculation length obtained with each mesh for both the Face-centered and Vertex-centered schemes.

Table 5.4: The predicted recirculation length of the flow over an obstacle by using two schemes of the SCVFEM.

Mesh	Unknowns	Scheme	Recirculation Length
Mesh A	5711 Sides	Face-centered	10.28 m
Mesh A	1984 Nodes	Vertex-centered	12.40 m
Mesh B	3202 Nodes	Vertex-centered	10.77 m
Mesh C	4355 Nodes	Vertex-centered	10.57 m
Experiment			9.0 - 11.0 m

From this test, we can see that both Face-centered scheme and Vertex-centered scheme predict the recirculation flows under inflow and outflow boundary conditions. From Table 5.4, it is seen that the recirculation length predicted by the Face-centered scheme with Mesh A and for Vertex-centered scheme with Mesh B and C are close to the experimental reattachment point obtained by Carvalho et al. (1987) in the regions ($9 < x/S < 11$).

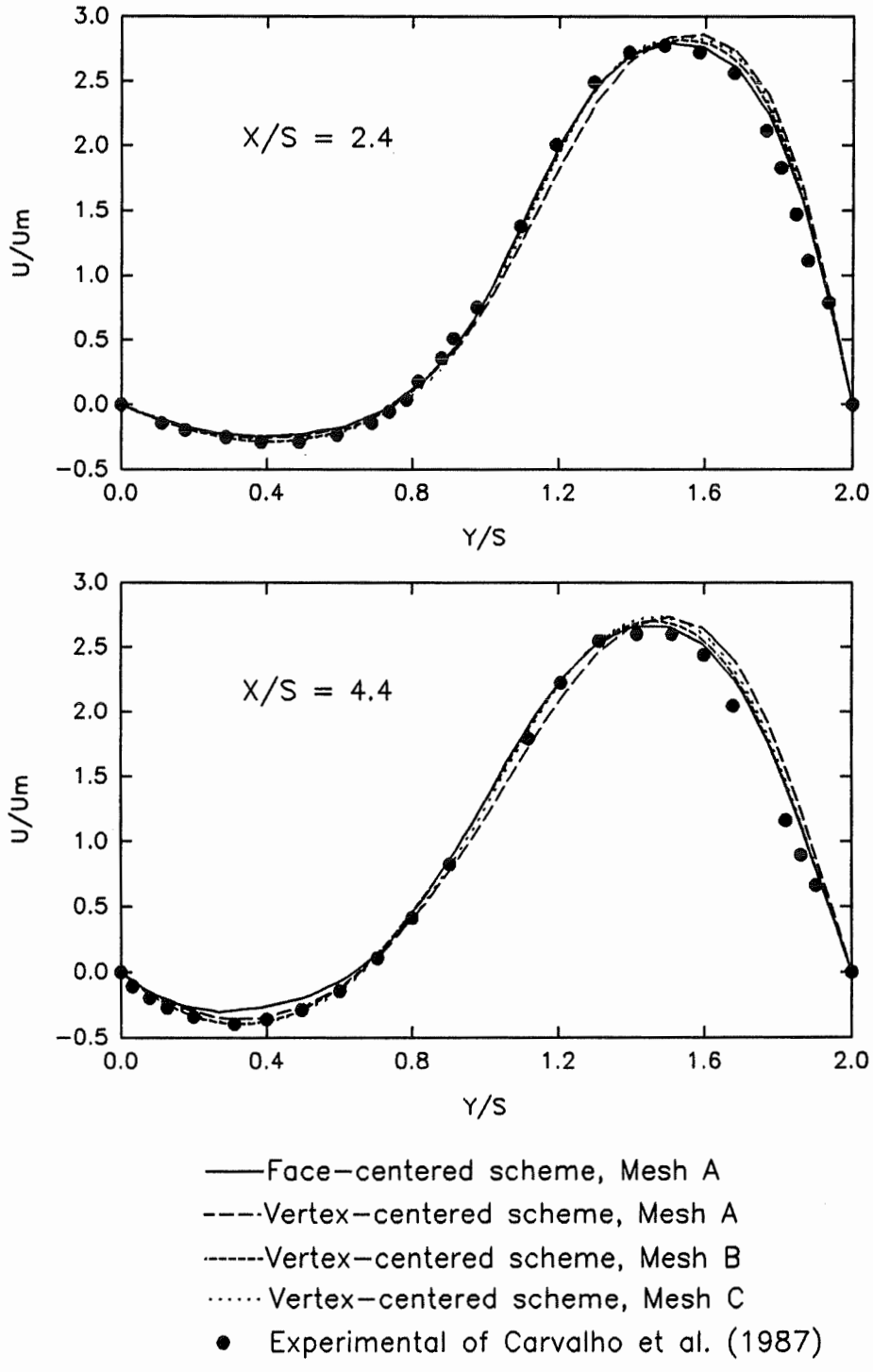

Figure 5.11: Comparison of predicted and measured u-velocity profiles at sections x/S = 2.4 and 4.4

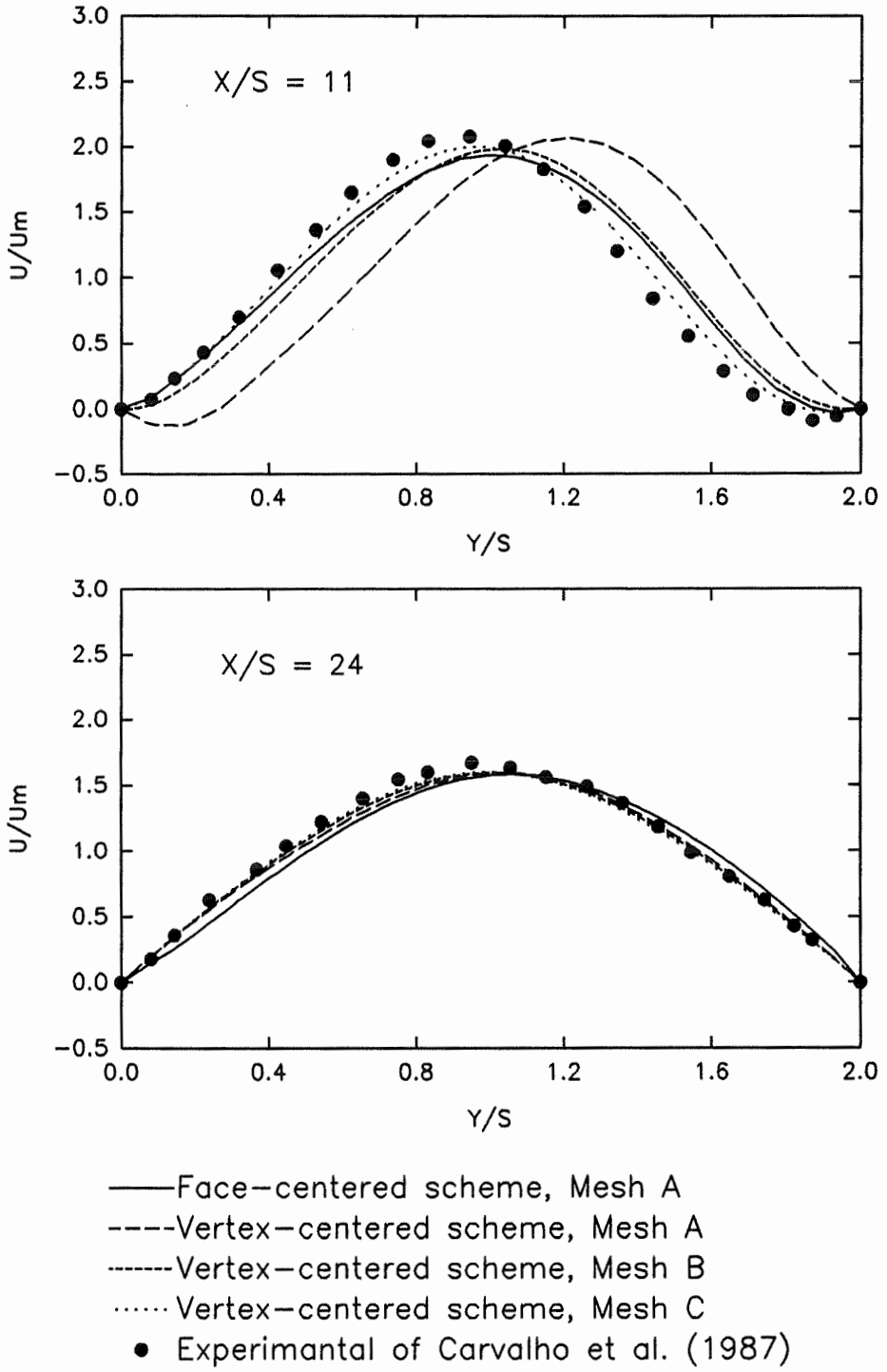

Figure 5.12: Comparison of predicted and measured u-velocity profiles at sections x/S = 11 and 24

5.3 Turbulent Channel Flow

5.3.1 Problem Description

To validate the proposed wall function method and to show its independence with respect to wall orientation, turbulent channel flows at 0° and 30° angles are considered as given in Figures 5.13 (a) and (b). The Reynolds number based on the channel height and inlet velocity is 11,400.

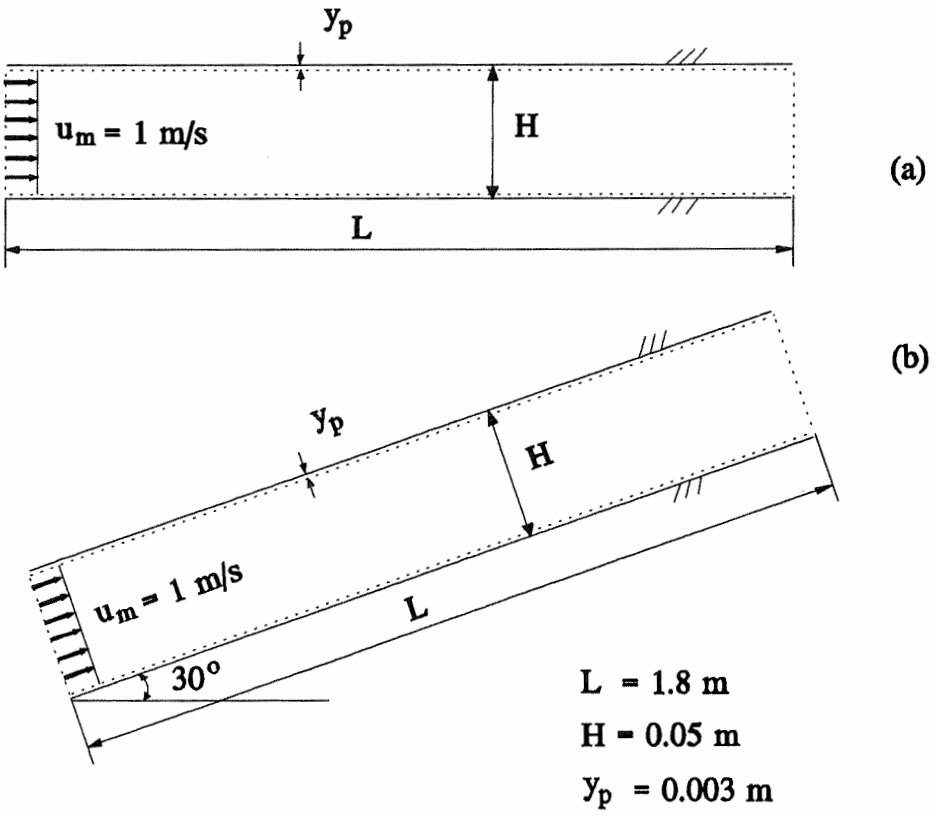

Figure 5.13: A schematic of the turbulent channel flows

The computational mesh contains 4274 elements (2250 nodes), as shown in Figure 5.14.

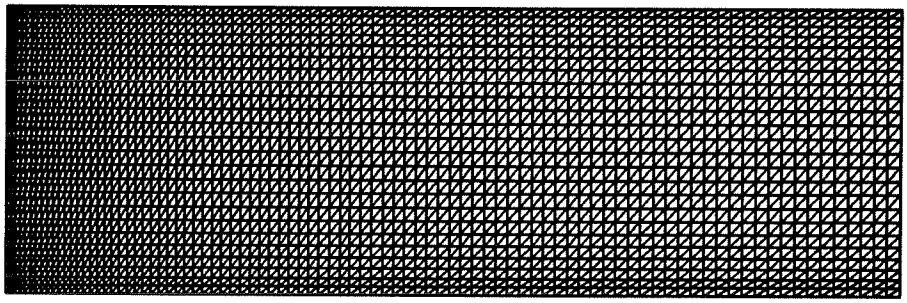

Figure 5.14: The computational mesh of the turbulent channel flows

For this test the Face-centered scheme using the steady state formulation is used. The relaxation E-factor for all the dependent variables are taken as 1, the under-relaxation parameters for u, v, p, k and ϵ are equal to 0.3. A uniform inlet velocity of 1m/s, and the inlet turbulent kinetic energy and its dissipation rate are determined from:

$$k = \lambda \cdot u^2 \qquad \epsilon = \frac{C_\mu k^{\frac{3}{2}}}{a \cdot H} \tag{5.1}$$

with λ=0.003, a=0.03.

The convergence criterion of a dependent variable ϕ is determined from the summation of the discretized transport equation over all the control volumes with respect to the inlet total flux of ϕ ,

$$Residu_\phi = \frac{\sum \left(a_i \phi_i^{n+1} + \sum_{k=1}^{nb} a_k \phi_k^{n+1} - a_i^0 \phi_i^n - b_i \right)_{domain}}{\sum (\rho \vec{v} \cdot \vec{n} \phi A)_{inlet}} \tag{5.2}$$

where, the computation is stopped after the residuals of all the dependent variables are less than 10^{-3}.

5.3.2 Results

The fully developed velocity profiles at the channel exit are plotted for both the 0° and 30° angles cases in Figure 5.15 which shows they are identical.

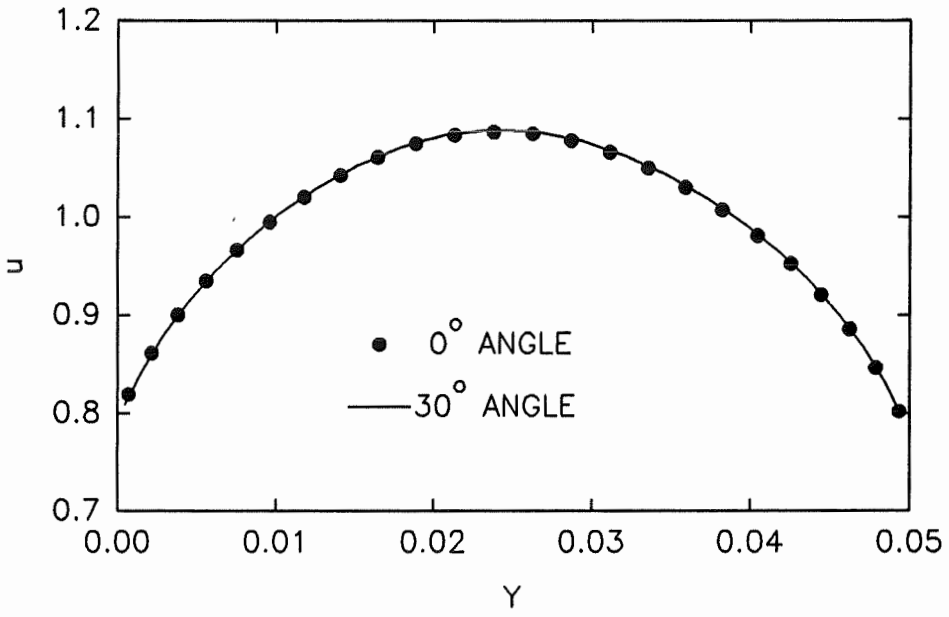

Figure 5.15: The developed velocity profiles at the exit of the channel flows with 0° and 30° angles

5.4 Turbulent Flow Over a Backward Facing Step

5.4.1 Problem Description

The steady, 2D turbulent flow over a backward facing step is considered to validate the present turbulent model and the wall function methods. This is a flow which separates and reattaches enclosing a recirculating region. Accurate experimental data for this problem is available from Westphal et al. (1984), and numerical predictions with k-ϵ two-equation model are available in the work of Autret et al. (1987). The Reynolds number based on the step height and the inlet velocity is 42000. This test problem is to assess the accuracy of the proposed SCVFEM to solve a complex turbulent flow problem. The geometrical configuration of the flow and boundary parameters are depicted in Figure 5.16.

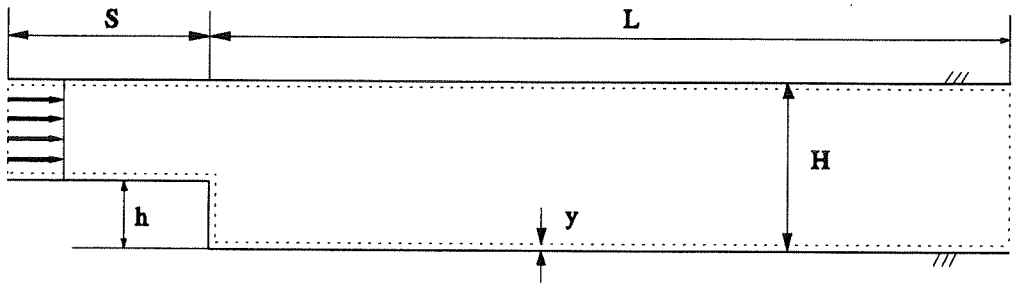

Figure 5.16: The geometrical configuration of the turbulent flow over a backward facing step

In this problem, two sets of tests are conducted. One is to compare the two numerical schemes, i.e. the Face-centered scheme and Vertex-centered scheme, where the 3-layer wall function of Speziale and Thangam (1992) with the classical

approximation method is used. Another set of tests is the implementation of the 2-layer wall function by using two different methods; the classical approximation method of Launder and Spalding (1974) and the direct iteration method of Garon (1994) described in Chapter 3.

At the inlet a flat velocity profile with a value of unity is prescribed and boundary conditions for the turbulent parameters in Eq. (5.1) are $\lambda = 0.003$, $a = 0.03$. Following Autret et al. (1987), the downstream channel length L is taken 20 step heights downstream from the step corner. The unsteady state formulation is used for obtaining the steady state solution using a computational mesh of 10826 elements (or 5580 nodes). In the test of the implementation of the 2-layer wall function methods, the downstream channel length L is extended to 30 step heights downstream of the step corner, to ensure that the local error for all of the quantities was of the same order as the interior values (Thangam and Speziale, 1992). Calculations are based on the steady state formulation, in which the E-factor varies from 1 to 5. Furthermore, the variable under-relaxation parameters for u, v, p vary from 0.3 to 0.6, for k, ϵ are taken from 0.6 to 0.8, and for turbulent viscosity μ_t is from 0.3 to 0.6. Three set of grids are considered, they are: Mesh A with 3640 elements (or 1921 nodes), as shown in Figure 5.17, Mesh B with 7144 elements (or 3713 nodes), and Mesh C with 16034 elements (or 8217 nodes). The maximum residues of all dependent variables in the calculation domain are less than 1×10^{-4} for converged solutions.

5.4.2 Results

Figures 5.18 and 5.19 show the predicted velocity field and turbulent kinetic energy field, respectively. The distributions of u-velocity and turbulent kinetic energy k are compared with the experimental data of Westphal et al. (1984) at stations downstream from the step, located at x/H = 4, 8, 12 and 20.

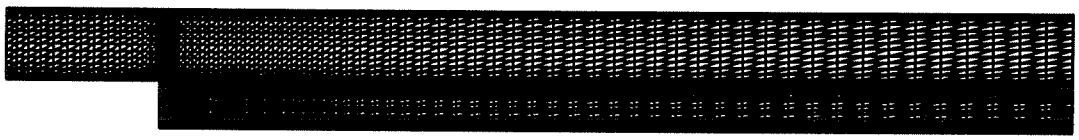

Figure 5.17: The computational mesh of the turbulent flow over a backward facing step

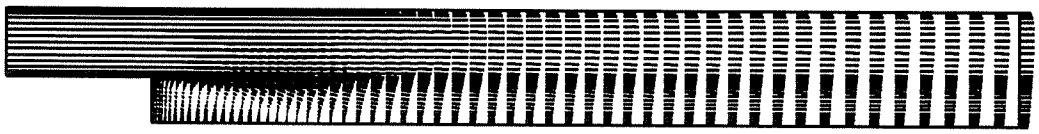

Figure 5.18: The predicted velocity field of the turbulent flow over a backward facing step

A. Comparison between classical approximation method and direct iteration method

To compare the results obtained with the classical approximation method and the direct iteration method in the implementation of the 2-layer wall function, three

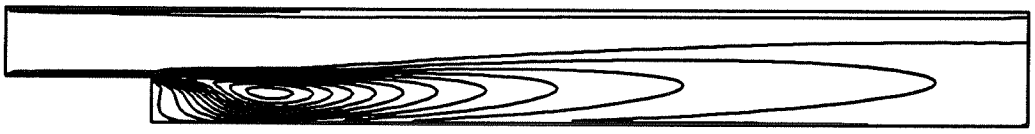

Figure 5.19: The predicted turbulent kinetic energy field of the turbulent flow over a backward facing step

sets of the computational grids, Mesh A, B and C are used in the calculation with the Face-centered scheme. Table 5.5 gives the predicted reattachment length and CPU times. As the mesh becomes finer, the predicted reattachment length increases for both the classical approximation method and the direct iteration method, although underpredict the reattachment length, measured by Westphal et al. (1984) at about 7.33. Furthermore, it is also found that the predicted reattachment length by the classical approximation method is longer than that obtained by the direct iteration method. The profiles of u-velocity and turbulent kinetic energy k with Mesh C are plotted in Figure 5.20 and Figure 5.21. From Fig. 5.20, we found that at section x/H=20, the velocity profiles obtained by the direct iteration method is much better than that of by the classical approximation method. The reason may be that the wall shear stress obtained by the direct iteration method is more realistic than that of the classical approximation method in the fully developed turbulent flow regions.

Table 5.5: The predicted reattachment length of the turbulent flow over a backward facing step using Face-centered scheme

Mesh	Degree of freedom	Classical Approximation Method		Direct Iteration Method	
		Reattachment	CPU (s)	Reattachment	CPU (s)
A	5560 sides	5.45	3.1107×10^3	5.05	8.5271×10^3
B	10850 sides	5.76	1.9296×10^4	5.254	5.1828×10^4
C	24250 sides	6.13	1.6888×10^5	5.40	2.7425×10^5

B. Comparison between Face-centered scheme and Vertex-centered scheme

A comparison between results obtained from the Face-centered and Vertex-centered schemes and the 3-layer wall function of Speziale and Thangam (1992) with classical approximation method for the wall function was carried out. The predicted reattachment length obtained by Face-centered scheme is 6.01, while that from the Vertex-centered scheme is 5.935 with the same mesh of 5580 nodes. The predicted profiles of velocity and turbulent kinetic energy are also shown in Figure 5.22 and 5.23 for both schemes. From Fig. 5.22 and Fig. 5.23, it is found that the predicted velocity and turbulent kinetic energy by the Vertex-centered scheme are in better agreement with the experiment than those by the Face-centered scheme. One possible explanation is that in each boundary element, only one node is used to compute the wall shear stress in the Face-centered scheme. Thus the computed wall shear stress is approximately constant along the boundary side. In the Vertex-centered scheme, there are two boundary nodes along each boundary side, so that the computed wall shear stress varies linearly.

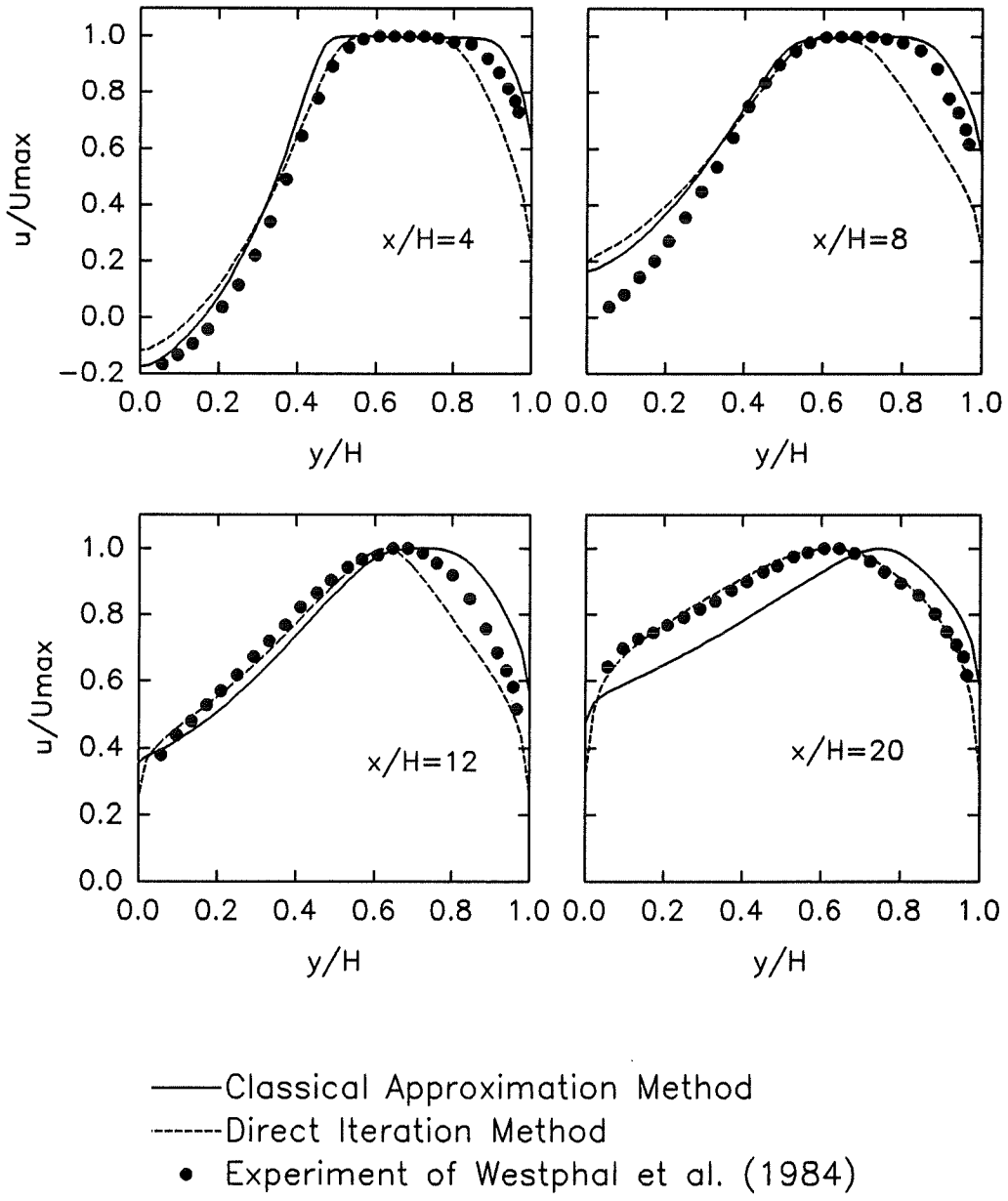

Figure 5.20: Comparison of numerical predictions of velocity with measurements of Westphal et al. at x/H=4,8,12 and 20 by using both Classical Approximation and Direct Iteration methods, respectively

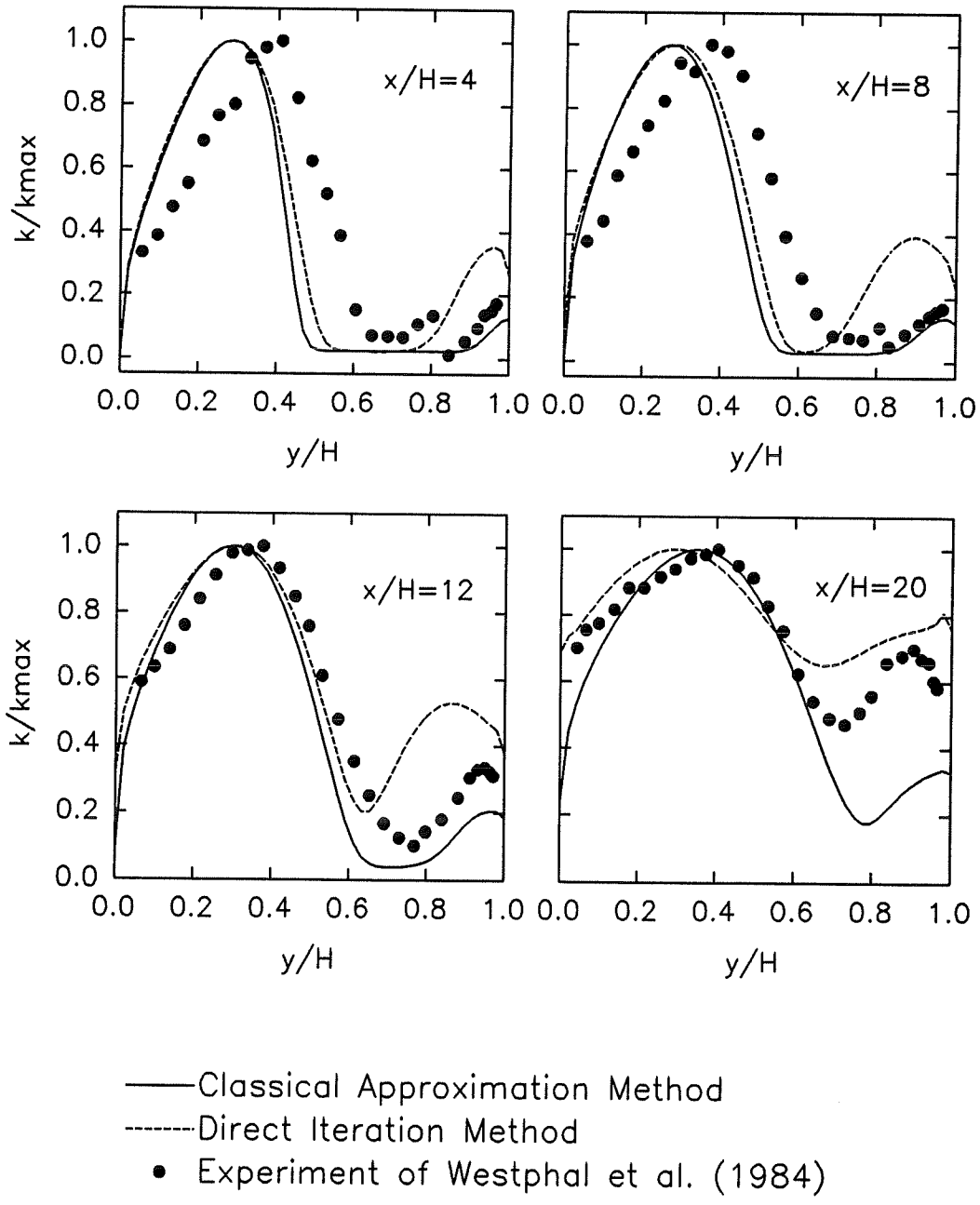

Figure 5.21: Comparison of numerical predictions of turbulent kinetic energy with measurements of Westphal et al. at x/H=4,8,12 and 20 by using both Classical Approximation and Direct Iteration methods, respectively

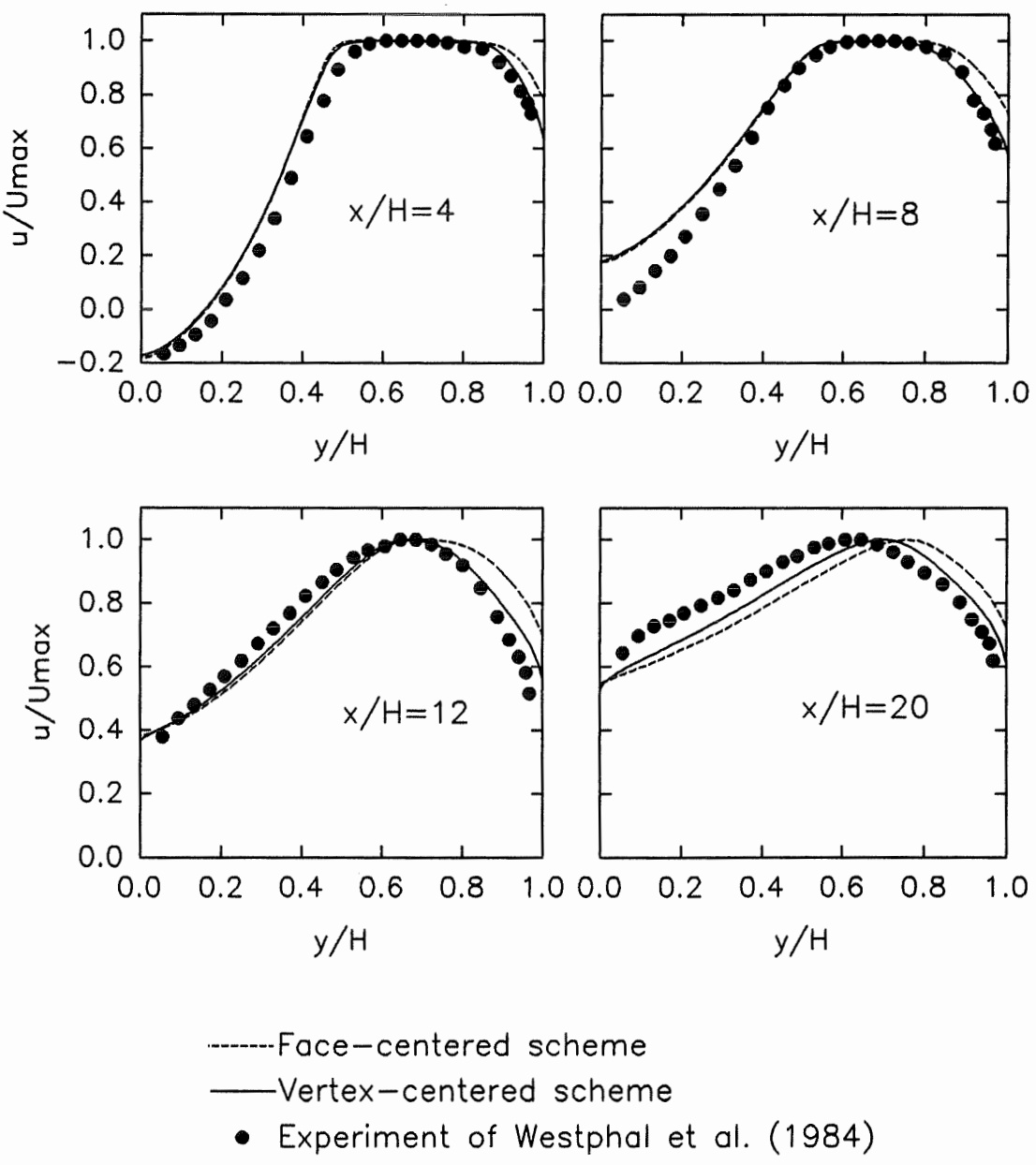

Figure 5.22: Comparison of numerical predictions of velocity with measurements of Westphal et al. at x/H = 4, 8, 12 and 20 by using both Face-centered and Vertex-centered schemes, respectively

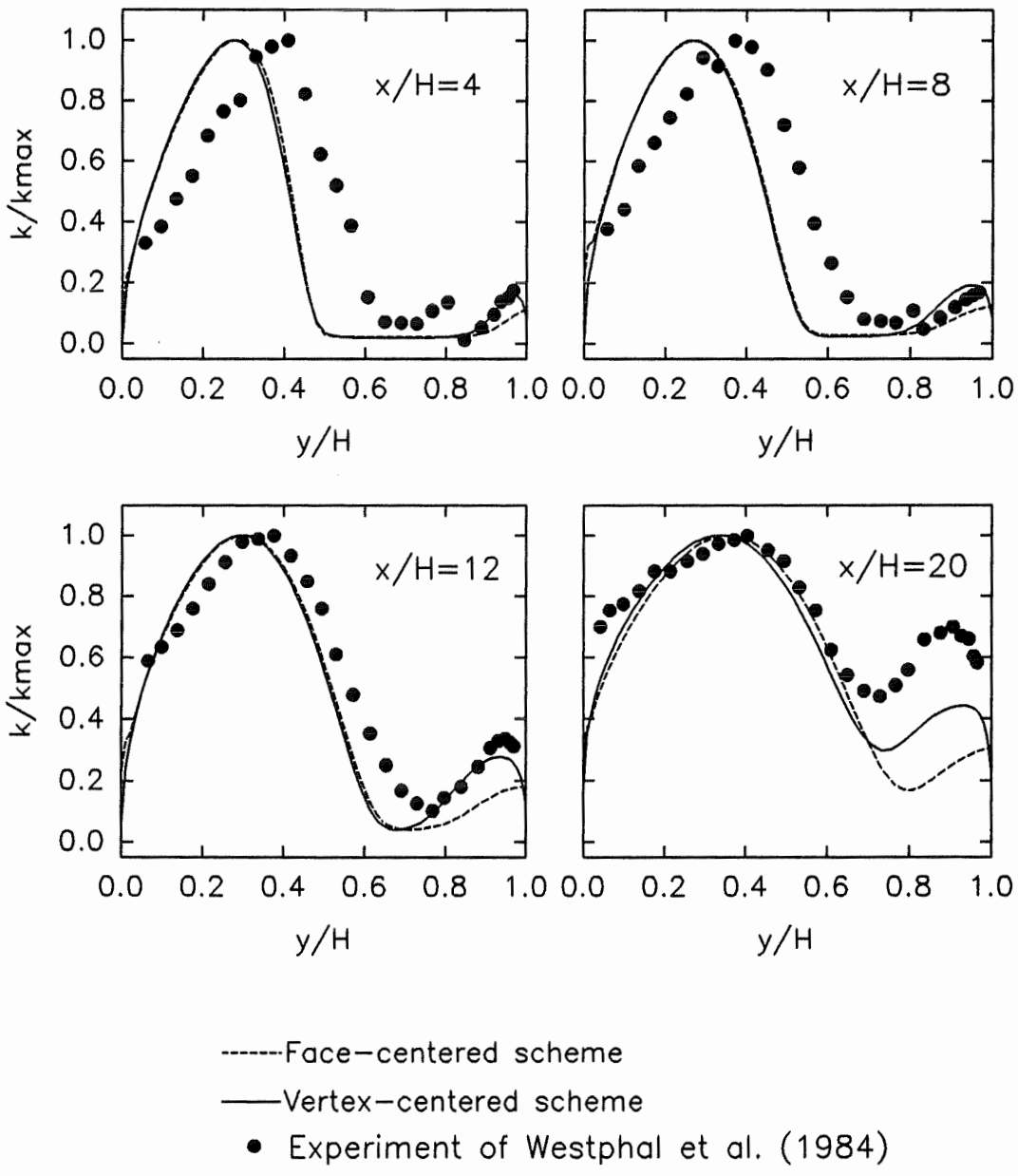

Figure 5.23: Comparison of numerical predictions of turbulent kinetic energy with measurements of Westphal et al. at x/H =4, 8, 12 and 20 by using both Face-centered and Vertex-centered schemes, respectively

5.5 Turbulent Flow Over a Pipe Expansion

5.5.1 Problem Description

The proposed SCVFEM is also applied to 2D axisymmetric turbulent flow in a sudden pipe expansion. The expansion ratio is 2.0 and the Reynolds number of 2 x 10^5 is based on the mean inlet velocity and outlet diameter. The schematic of flow and boundary parameters are given in Figure 5.24. Predictions of the velocity and turbulent kinetic energy based on both Face-centered and Vertex-centered schemes are compared with the experimental data. The experimental data for velocity and turbulent kinetic energy profiles at several streamwise locations are measured by Chaturvedi (1963). The numerical predictions of this problem using the finite element method has been given by Kim (1987).

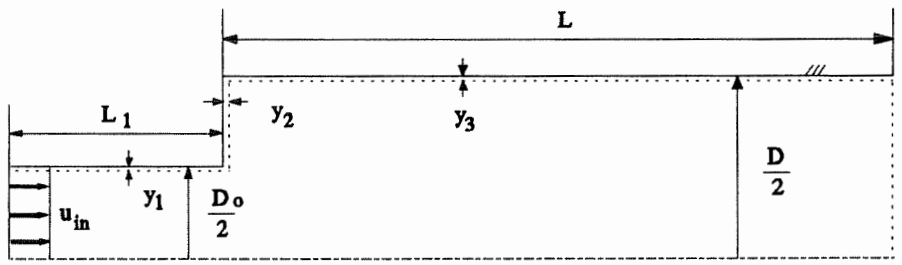

$D_o = 0.1$ m $D = 0.2$ m $L = 1.2$ m $L_1 = 2 D_o$

$y_1 = 0.002$ m $y_2 = 0.002$ m $y_3 = 0.004$ m $u_{in} = 31$ m/s

Figure 5.24: The flow parameters and the geometric dimensions of a pipe expansion

The uniform inlet velocity is 31m/s, the inlet turbulent parameters defined in

Eq. (5.1) are $\lambda = 0.005$, $a = 0.03$. The steady state formulation with the factor E = 2.0 for all the dependent variables is used, and the under-relaxation parameters for u, v, p, k, ϵ are 0.2, for the viscosity μ_t is 0.3. The computational mesh for both Face-centered and Vertex-centered schemes contains 2640 elements (4053 faces, 1414 vertices), as shown in Figure 5.25. The 2-Layer wall function with classical approximation method of Launder and Spalding (1974) is used in the computation. Solutions are converged at the maximum residues of all dependent variables are smaller than 10^{-3}.

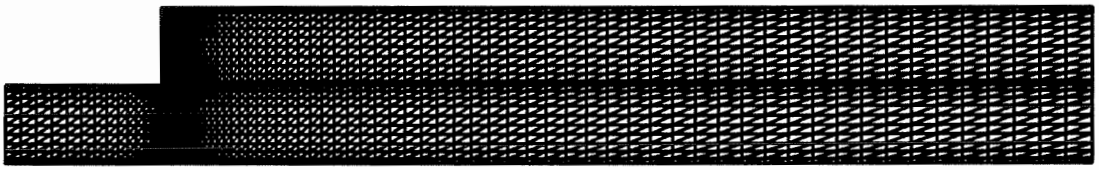

Figure 5.25: The computational mesh of the turbulent flow over a pipe expansion

5.5.2 Results

Figures 5.26 and 5.27 show the predicted velocity field and turbulent kinetic energy field, respectively.

Figures 5.28 and 5.29 show the predicted and measured axial velocity and turbulent kinetic energy profiles at four downstream locations: x/D_o = 1, 3, 6 and 8. From Fig. 5.28, we can see that the difference between the predicted and measured velocity profiles in the inlet region is small. At sections x/D_o = 1, 3 and 8 the velocity profiles compare very well with the experimental ones, while, at section x/D_o = 6, the difference increases near the axis. The reason for this difference is the underprediction

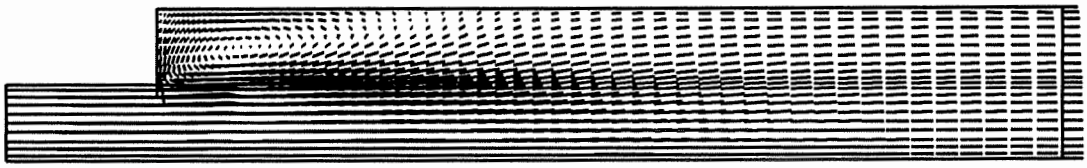

Figure 5.26: The predicted velocity field of the turbulent flow over a pipe expansion

Figure 5.27: The predicted turbulent kinetic energy field of the turbulent flow over a pipe expansion

of the turbulent kinetic energy near the centerline region for both Face-centered and Vertex-centered schemes, as shown in Fig. 5.29, which leads to an overprediction of the velocity. The reason is because the turbulent viscosity becomes smaller with the underprediction of the turbulent kinetic energy, leading to a large velocity.

The reattachment point found by Chaturvedi (1963) was $4.1D_o$, which is compared to the predicted reattachment point for Face-centered scheme of $3.82D_o$, and for Vertex-centered scheme of $3.75D_o$.

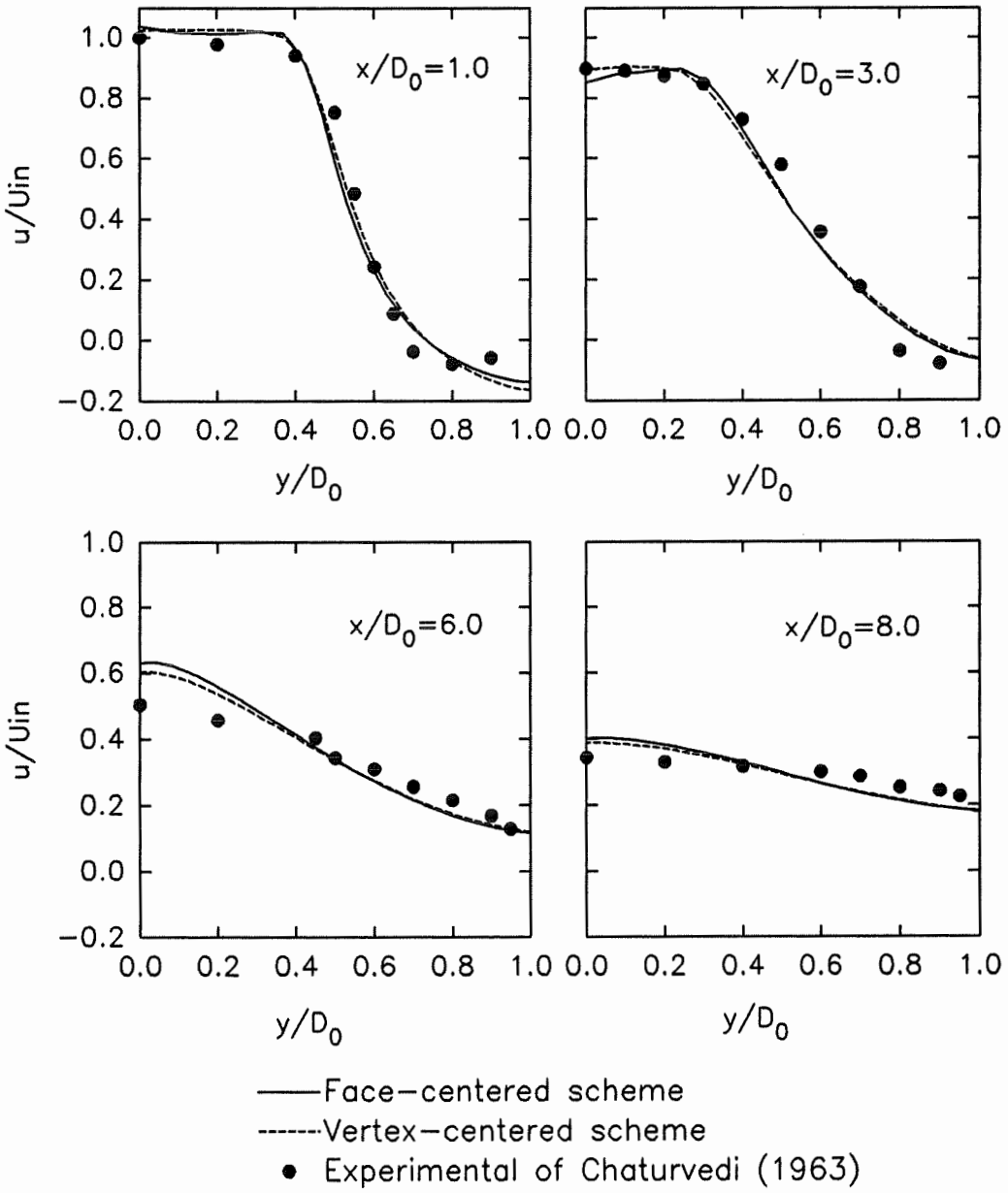

Figure 5.28: Comparison of predicted and measured axial velocity profiles at four downstream sections: x/D_o = 1, 3, 6 and 8

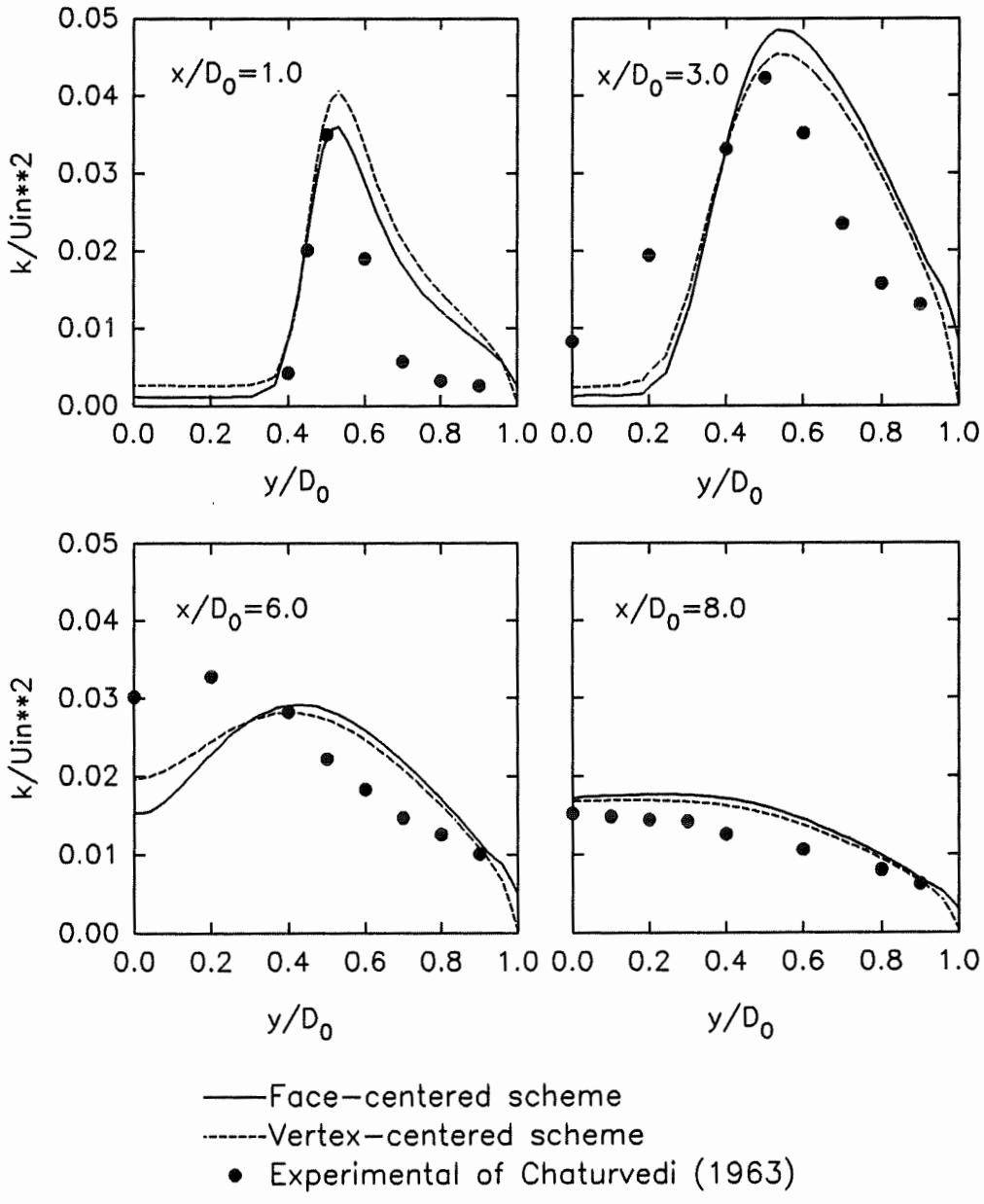

Figure 5.29: Comparison of predicted and measured turbulent kinetic energy profiles at four downstream locations: x/D_o = 1, 3, 6 and 8

5.6 Turbulent Flow In an Annular Turnaround Duct

5.6.1 Problem Description

Turbulent flow in a turnaround duct presents a severe test for separation. The occurrence of separation is dependent on the turning angle and the radius of curvature. As a benchmark test of turbulent flows involving strong separation, the steady flow in a 180° degree curved annular turnaround duct is selected. A schematic of the problem is given in Figure 5.30. Experimental studies of this flow have been conducted by Sharma and Ostermier (1987), the numerical predictions are given by FIDAP (1991).

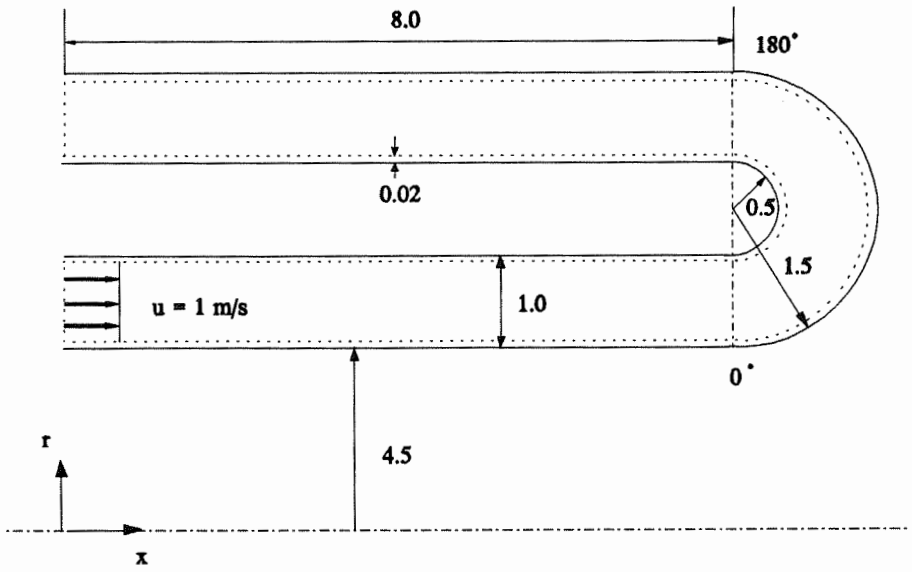

Figure 5.30: Problem schematic of turbulent flow in an annular turnaround duct

The computation mesh comprises of 2070 triangular elements as shown in Figure 5.31 with concentration towards the walls.

This is a 2D axisymmetric case, a flat velocity profile with a value of unity is

prescribed at the lower duct inlet. The Reynolds number based on duct width and inlet velocity is 100000. Flat profiles for the turbulent kinetic energy k = 0.001 and the turbulent dissipation rate ϵ = 0.0009 are also specified at the inlet, which correspond to a low turbulence intensity of 0.1%.

The unsteady state formulation with Face-centered scheme is used for obtaining the steady state solution. The under-relaxation factors for u,v are 0.2, for p is 0.12, for k and ϵ are 0.15, for turbulent viscosity is 0.2.

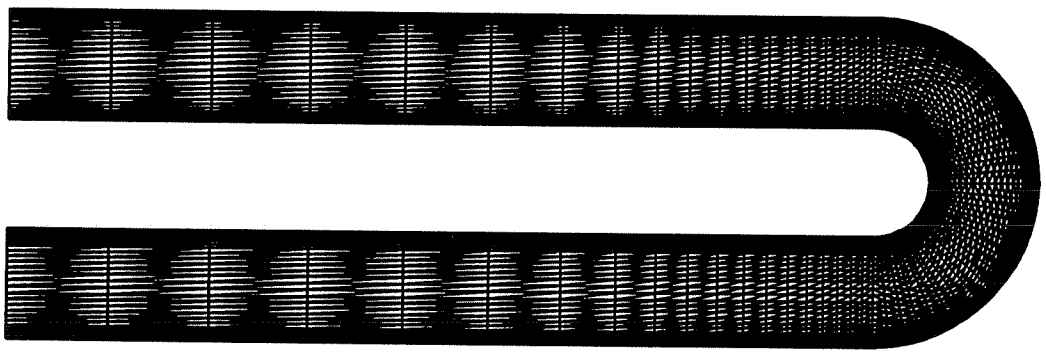

Figure 5.31: The computational mesh of an annular turnaround duct

5.6.2 Results

Figures 5.32, 5.33 and 5.34 depict the velocity, pressure and turbulent kinetic energy fields, respectively. The occurrence of separation and the consequent recirculation zone downstream of the bend is clearly discernible in the velocity vector fields. The tendency of the pressure distributions and the predicted separation features reasonably correspond to the FIDAP predictions. The u-velocity profiles at 0° and 180° degree locations are plotted in Figure 5.35, and compared with experimental data of Sharma and Ostermier (1987).

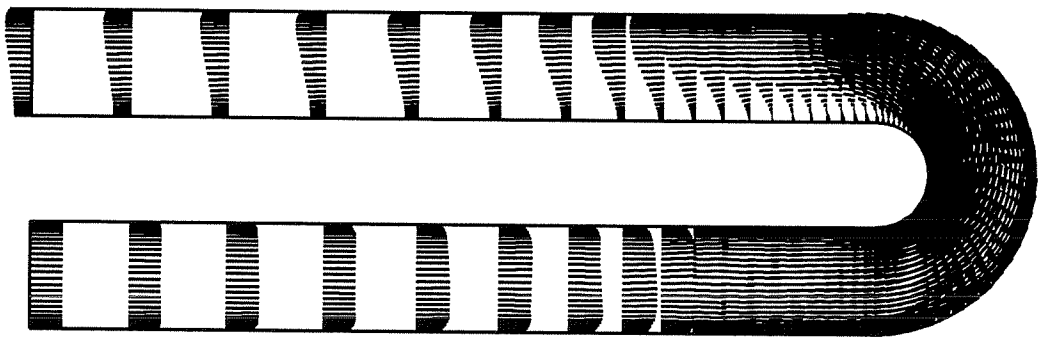

Figure 5.32: The predicted velocity field of turbulent flow in an annular turnaround duct

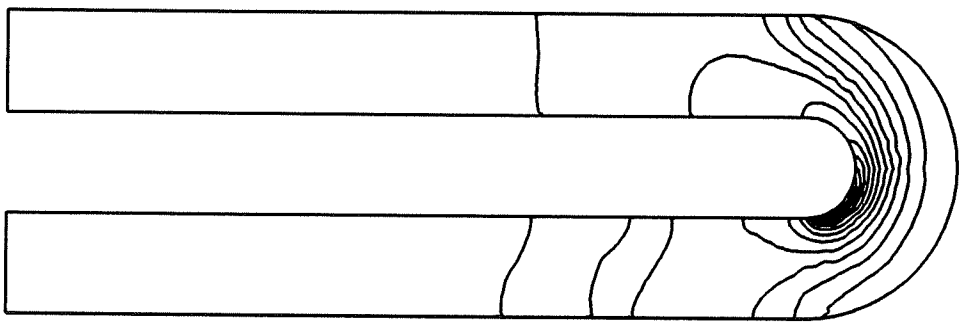

Figure 5.33: The predicted pressure field of turbulent flow in an annular turnaround duct

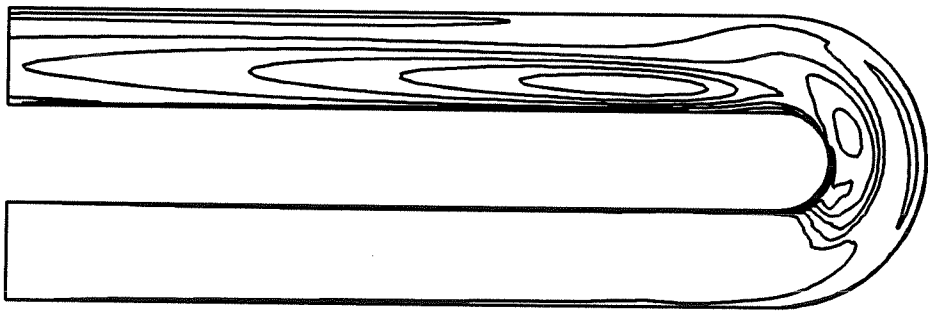

Figure 5.34: The predicted turbulent kinetic energy field of turbulent flow in an annular turnaround duct

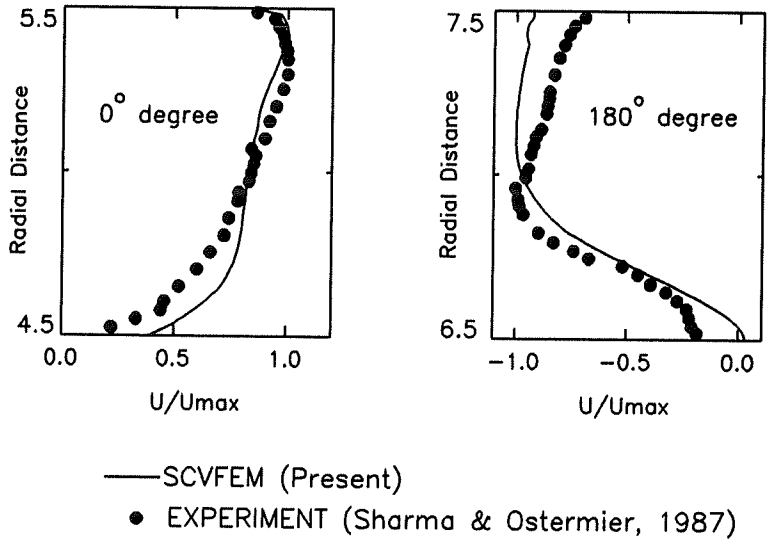

Figure 5.35: u-velocity profiles at 0° and 180° degree locations

5.7 Confined Axisymmetric Turbulent Diffusion Flame

5.7.1 Furnace of Lewis and Smoot (1981)

5.7.1.1 Problem Description

The geometry for this test is a cylindrical combustor with coaxial injectors, where the natural gas is injected by the primary tube and the air through the secondary annulus, as shown in Figure 5.36. The total pressure of the combustor is 94 KPa. In the fuel stream, the uniform inlet gas velocity is 21.3 m/s and the flow rate is 2.84 g/s, with the temperature 300 K. In the air stream, the uniform inlet air velocity is 34.3 m/s and the flow rate is 36.6 g/s, with the preheated temperature 589 K.

The available experimental measurements for natural gas combustion have been carried out by Lewis and Smoot (1981) together with the numerical predictions of Smith and Smoot (1981) using the chemical equilibrium combustion model with the finite difference method. Nikjooy et al. (1988) have used the fast chemistry reaction model and the finite-rate chemistry model with the finite volume method, and Elkaim et al. (1993) and Mckenty et al. (1993) with the fast chemistry, PDF, eddy dissipation, chemical equilibrium and micro-flame models with CVFEM.

In the present computations, both the classical approximation method of Launder and Spalding (1974) and the direct iteration method of Garon (1994) have been used, together with four combustion models, i.e. fast chemistry, eddy dissipation, chemical equilibrium and micro-flame models. Considering the concentration fluctuation of the flame, the beta and delta PDF models are also tested.

The computation mesh involves 3107 sides (2014 elements), as shown in Figure 5.37. In the computations, the Face-centered scheme is used for all the test cases. E varies from 1 to 2, and the under-relaxation parameters for the others dependent variables, such as u, v, p, k, ϵ, f, m_{fu}, h, T are taken from 0.2 to 0.5, that for the

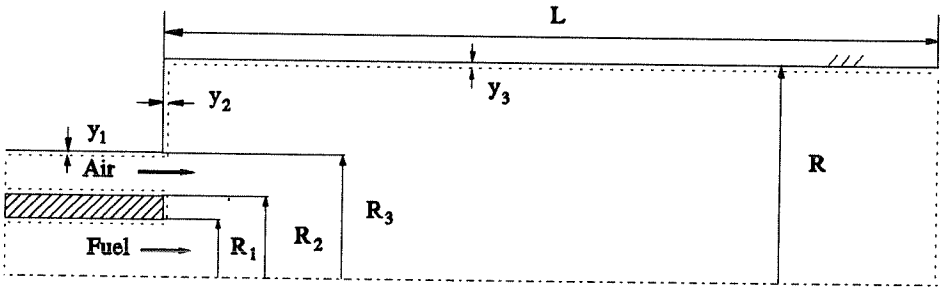

R_1 = 0.008 m R_2 = 0.0111 m R_3 = 0.0286 m R = 0.1016 m

y_1 = 0.001 m y_2 = 0.004 m y_3 = 0.008 m L = 1.524 m

Figure 5.36: Geometry of coaxial combustor of Lewis and Smoot (1981)

density is from 0.1 to 0.3 and that for the viscosity is from 0.2 to 0.4. The inlet turbulent parameters with λ=0.003, a=0.03 are used. The model constants are:

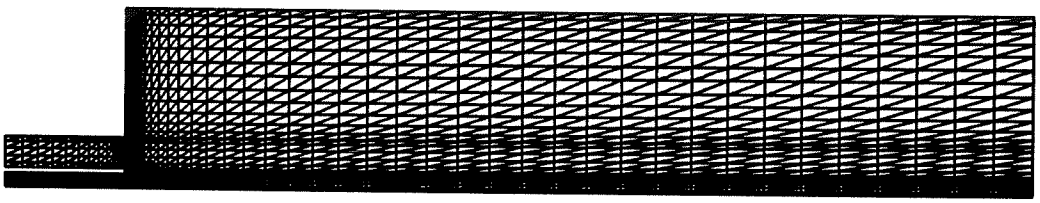

Figure 5.37: The computational mesh of furnace of Lewis and Smoot (1981)

C_μ	C_1	C_2	σ_k	σ_ϵ	σ_f	σ_{mfu}	σ_t	σ_g	A	C_{g1}	C_{g2}
0.09	1.44	1.92	1.0	1.3	0.6	0.6	0.7	0.6	4.0	2.8	2.0

5.7.1.2 Results

Figure 5.38 depicts the predicted velocity field using the fast chemistry reaction model, where the wall function is implemented by the direct iteration method. Figure 5.39 shows the contours of the mean mixture fraction based on fast chemistry, delta PDF and beta PDF, respectively. The PDF models exhibit a faster axial decay rate than does the non-PDF model. The delta PDF has the fast decay rate of the mean mixture fraction. The fast chemistry reaction model predicts a shorter recirculation length (1.5846D) than either the delta PDF (1.6633D) or the beta PDF (1.6403D). Figure 5.40 shows the contours of the mean temperature for these models. At the mixing region near the inlet, the temperature rises quickly at some distance downstream of the corner and the flame front is developed. The fast chemistry reaction model yields a narrow, high temperature flame front, the beta PDF produces a wide flame front, while the delta PDF creates a relatively narrow flame front.

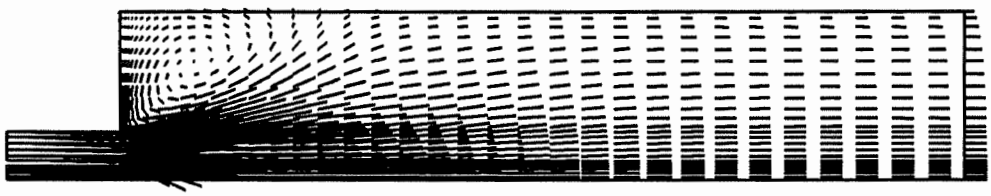

Figure 5.38: The predicted velocity field of furnace of Lewis and Smoot (1981) using the fast chemistry reaction model

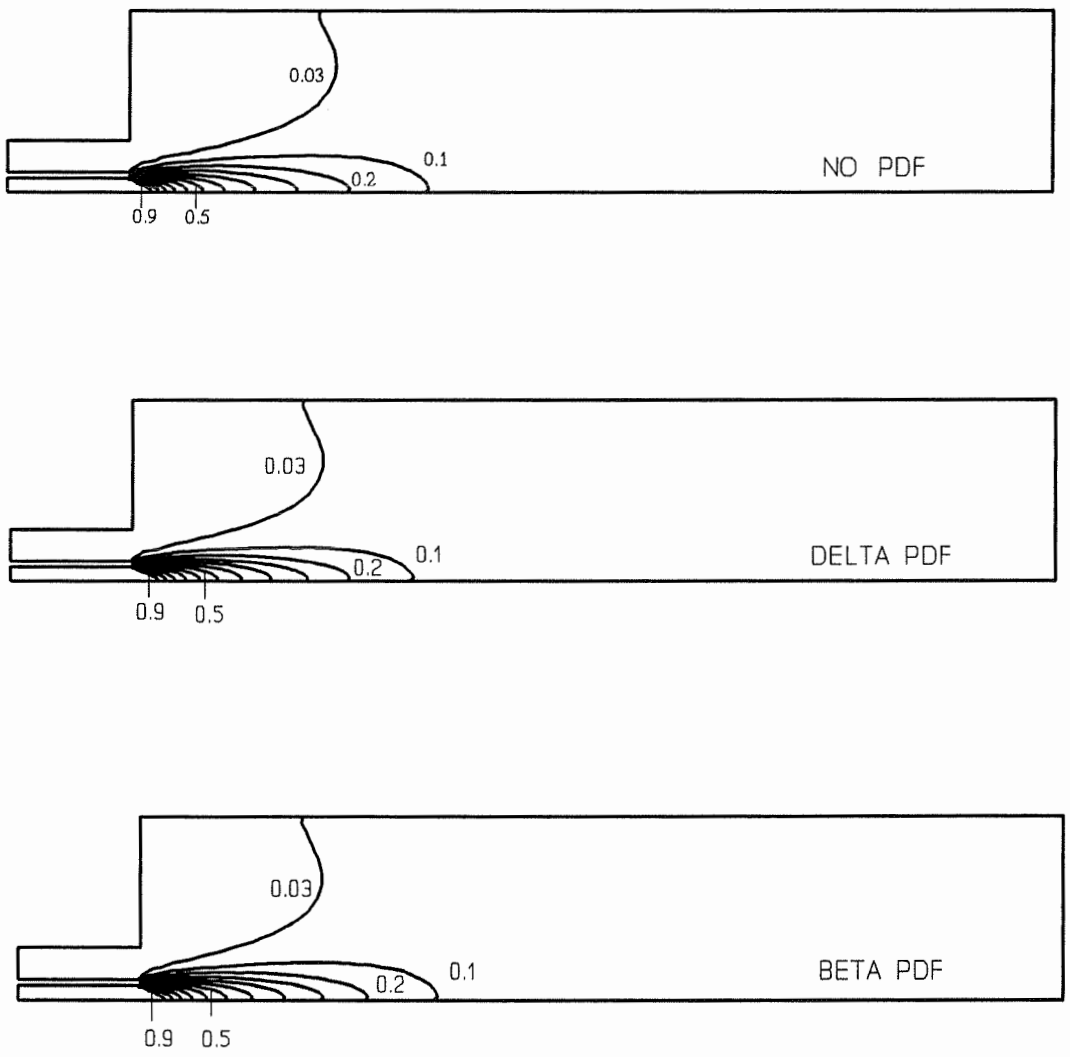

Figure 5.39: Contours of mixture fraction in a confined axisymmetric turbulent diffusion flame of Lewis and Smoot (1981) obtained by the fast chemistry, delta PDF and beta PDF models, respectively

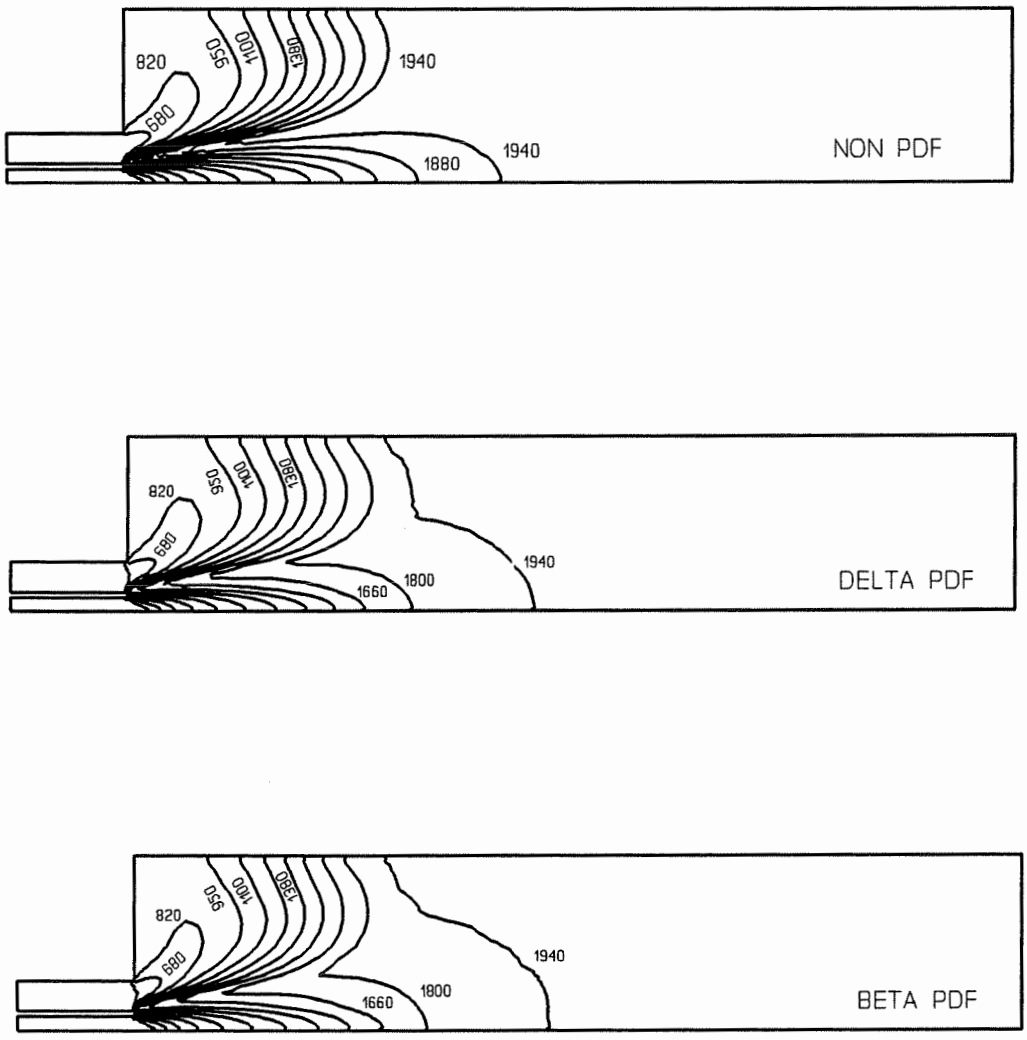

Figure 5.40: Contours of temperature in a confined axisymmetric turbulent diffusion flame of Lewis and Smoot (1981) obtained by the fast chemistry, delta PDF and beta PDF models, respectively

Because the predicted results show large differences between using the classical approximation method and the direct iteration method in the implementation of the 2-layer wall functions, comparison of the combustion results are presented for these two cases. Furthermore, the comparison between the present SCVFEM and other numerical method is also presented. Next, we will present the predicted results of mixture fraction and mass fraction of various species in several locations using the different combustion models.

A. Results based on the Classical Approximation Method

The predicted radial mixture fraction distributions for fast chemistry, chemical equilibrium, micro-flame and eddy-dissipation combustion models were computed using the classical approximation method in the implementation of the wall functions (Launder and Spalding,1974). These are shown at four sections x = 0.095 m, 0.175 m, 0.246 m and 0.327 m are plotted in Figure 5.41. In all cases, the mixture fraction is overpredicted in the mixing zone of the two jets. The disagreement can be attributed to the inadequate physical modelling of turbulence and the approximation of the wall functions. In the fully developed outlet region, the mixture fraction distributions for all the models become uniform, with a value of about 0.072. The predicted radial mass fraction distributions of CO_2, H_2O, CO and H_2 based on the above four combustion models at developed section x = 1.375 m are presented in Figure 5.42. It was noted that the chemical equilibrium model and the micro-flame model have the capability of predicting the chemical species of CO and H_2, which is not possible with the fast chemistry and eddy dissipation concept models in the present work. The micro-flame model gives the best results over all the models considered. For the concentration fluctuations, the delta and beta PDF models are considered. The predicted radial mixture fraction based on the PDF models in four sections at x = 0.095 m, 0.175 m, 0.246 m and 0.327 m are depicted in Figure 5.43. It can be seen that the fast chemistry reaction model predicts the fastest decay rate among the three models at the

mixing zone. However, neither model provides a satisfactory prediction near the centerline in the developing region. This apparent deviation may be mainly attributed to the turbulence model and wall functions.

B. Results based on the Direct Iteration Method

Using the direct iteration method in the implementation of the wall functions (Garon,1994), the predicted radial mixture fraction for fast chemistry, chemical equilibrium, micro-flame and eddy dissipation combustion models are plotted in Figure 5.44 at four sections x = 0.095 m, 0.175 m, 0.246 m and 0.327 m, respectively. It can be seen that the mixture fraction distributions for all sections are close to the experiments. Figure 5.45 shows the predicted radial mass fraction distributions of CO_2, H_2O, CO and H_2 using the above four combustion models at developed section x=1.375m. Figure 5.46 shows the predicted radial mixture fraction distribution at same four sections based on the PDF models. The results are also again close to the experiments at all four sections. From these results, we may conclude that the results based on the direct iteration method are much better than that of the classical approximation method. The reason may be referred to that the wall shear stress obtained by the direct iteration method is more realistic than that of the classical approximation method.

C. Comparison with Vorticity-Streamfunction Results

The SCVFEM predictions are also compared with the Vorticity-Streamfunction results of Mckenty (1992) using the fast chemistry reaction model. In the results of Mckenty (1992), the numerical solution is based on the control volume finite element method with the vorticity-streamfunction formulation on a mesh of 750 nodes. In the present predictions, two sets of computational grids, 2024 sides (720 nodes, 1301 elements) and 3107 sides (1094 nodes, 2014 elements) with the direct iteration method are considered, respectively. The mesh for the vorticity-streamfunction formulation

(750 nodes) is equivalent to that of the primitive variable formulation (720 nodes, 2024 sides). In Figure 5.47 the predicted radial profiles of the mixture fraction are compared with the measurements of Lewis and Smoot (1981). It can be seen that the results of the SCVFEM with 720 nodes are almost same as that of the Vortivcity-Streamfunction with 750 nodes. It was shown that when the grid becomes finer, the mixture fraction decay near the centerline decreases. All results are very close to experiments of Lewis and Smoot (1981).

D. Computational Efforts

Calculations were performed on a RISC 6000 model 520 work station, all the results are converged at the maximum residues for all the dependent variables less than 10^{-3}. For the coarse mesh with 2020 sides, the CPU time is 2.2817×10^4 seconds for the fast chemistry model. For the finer mesh with 3107 sides, the CPU times are 2.878×10^4 seconds for the fast chemistry model, 4.4936×10^4 seconds for the eddy dissipation model, 3.466×10^4 seconds for the chemical equilibrium model, 2.3849×10^4 seconds for the micro-flame model, 3.296×10^4 seconds for the delta PDF and 1.8417×10^5 seconds for the beta PDF models.

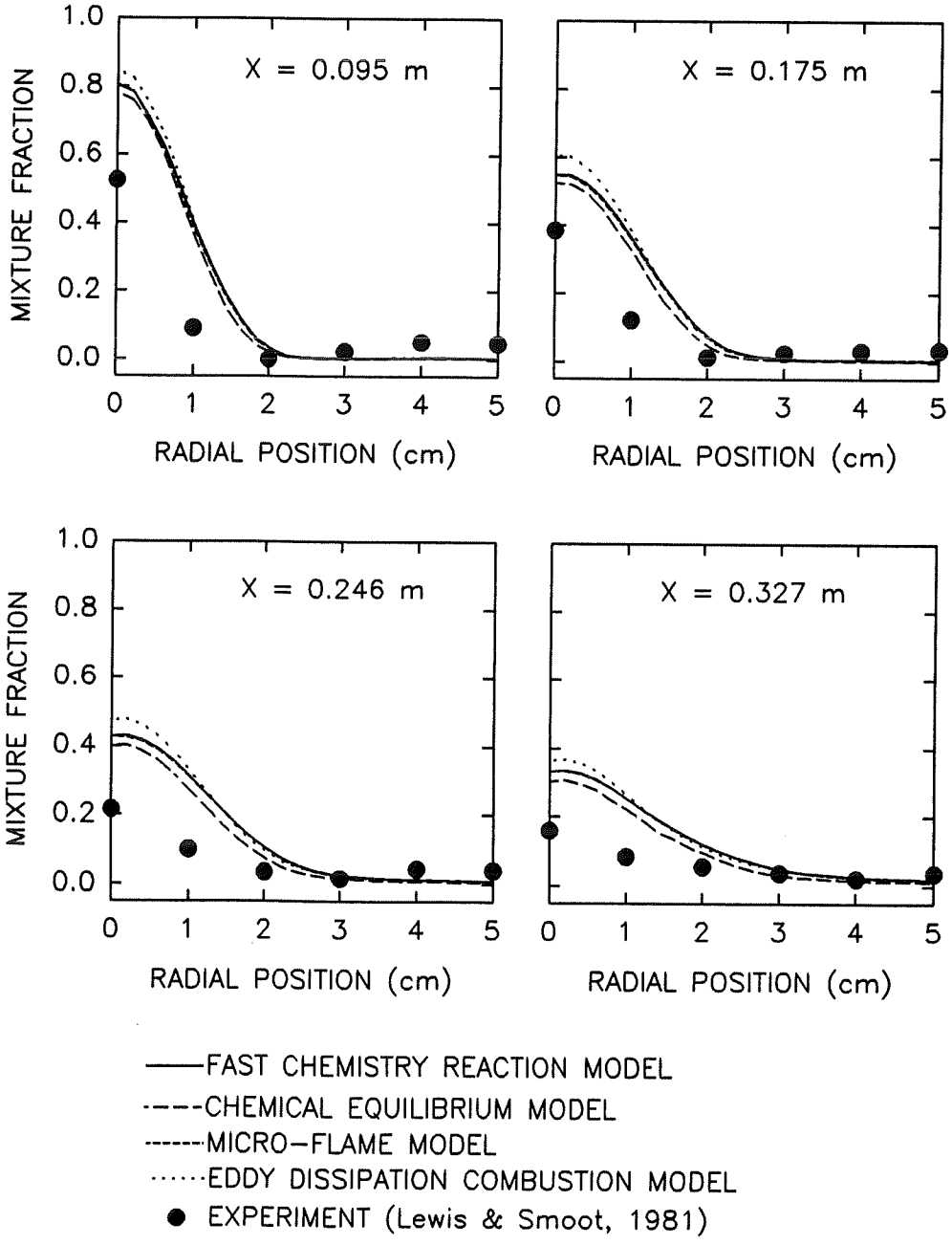

Figure 5.41: The predicted radial mixture fraction distribution at different axial stations based on four combustion models using the classical approximation method

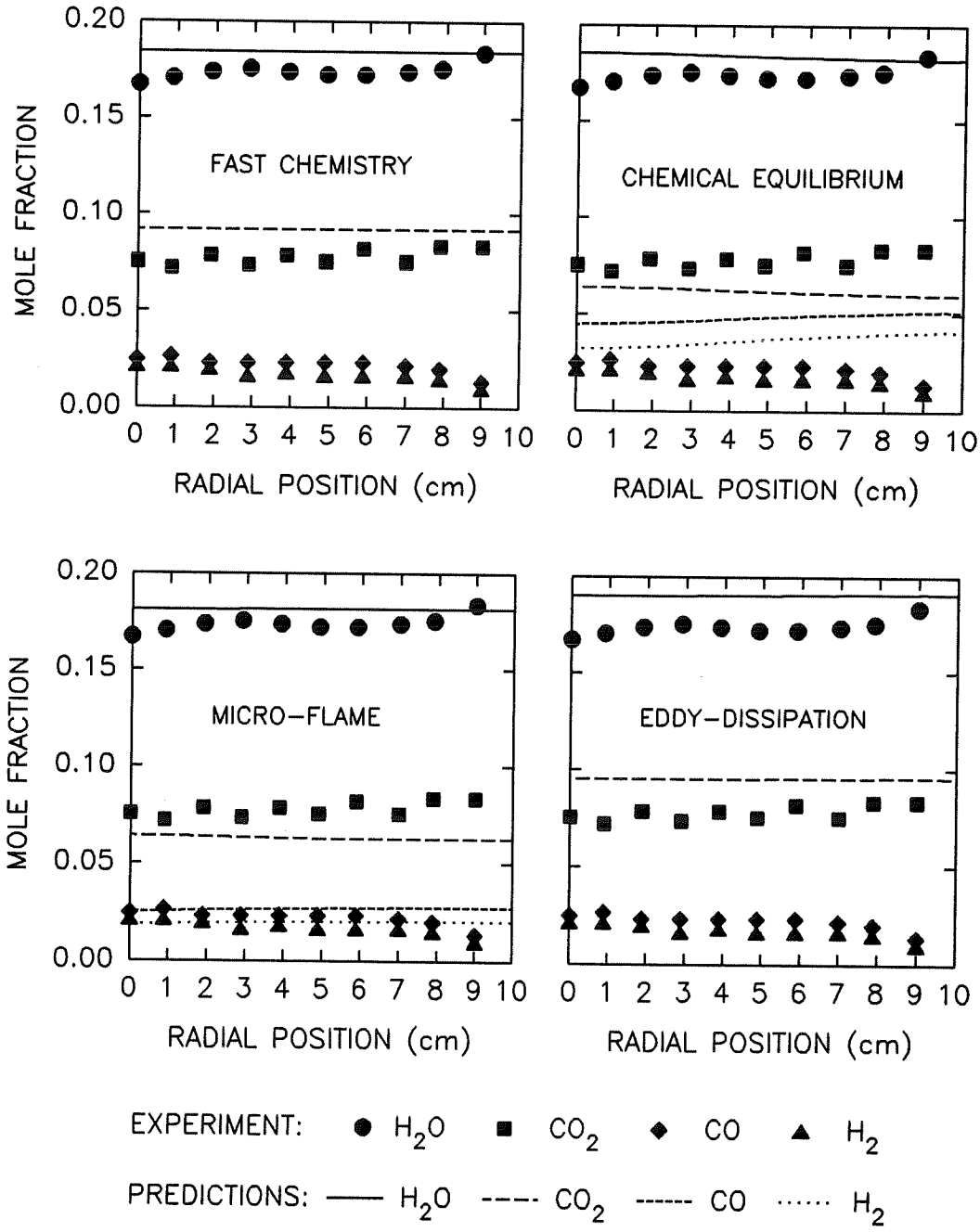

Figure 5.42: The predicted radial distribution of major species mole fraction at station 1.375m based on four combustion models using the classical approximation method

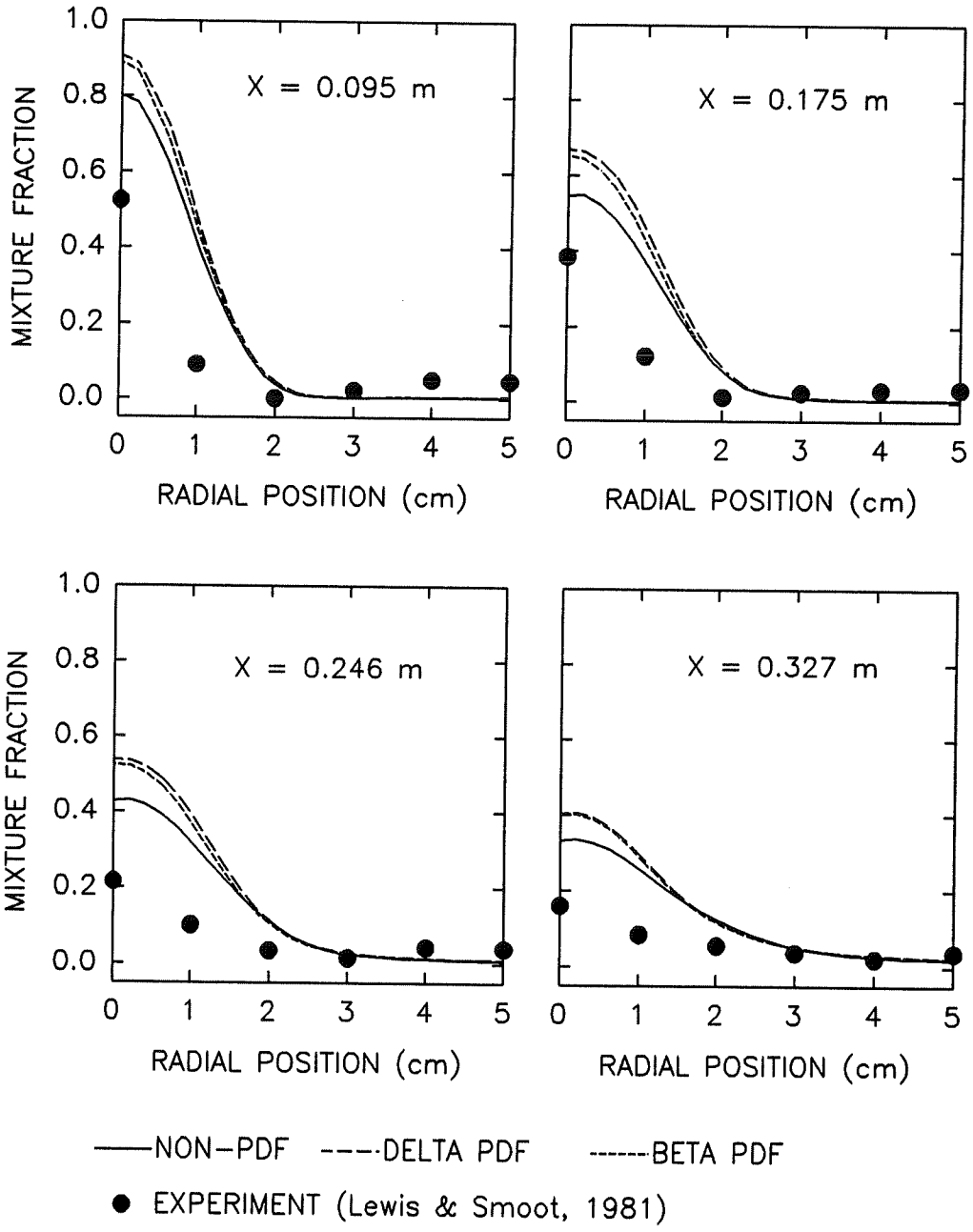

Figure 5.43: The predicted radial distributions of mixture fraction at different stations based on PDF models using the classical approximation method

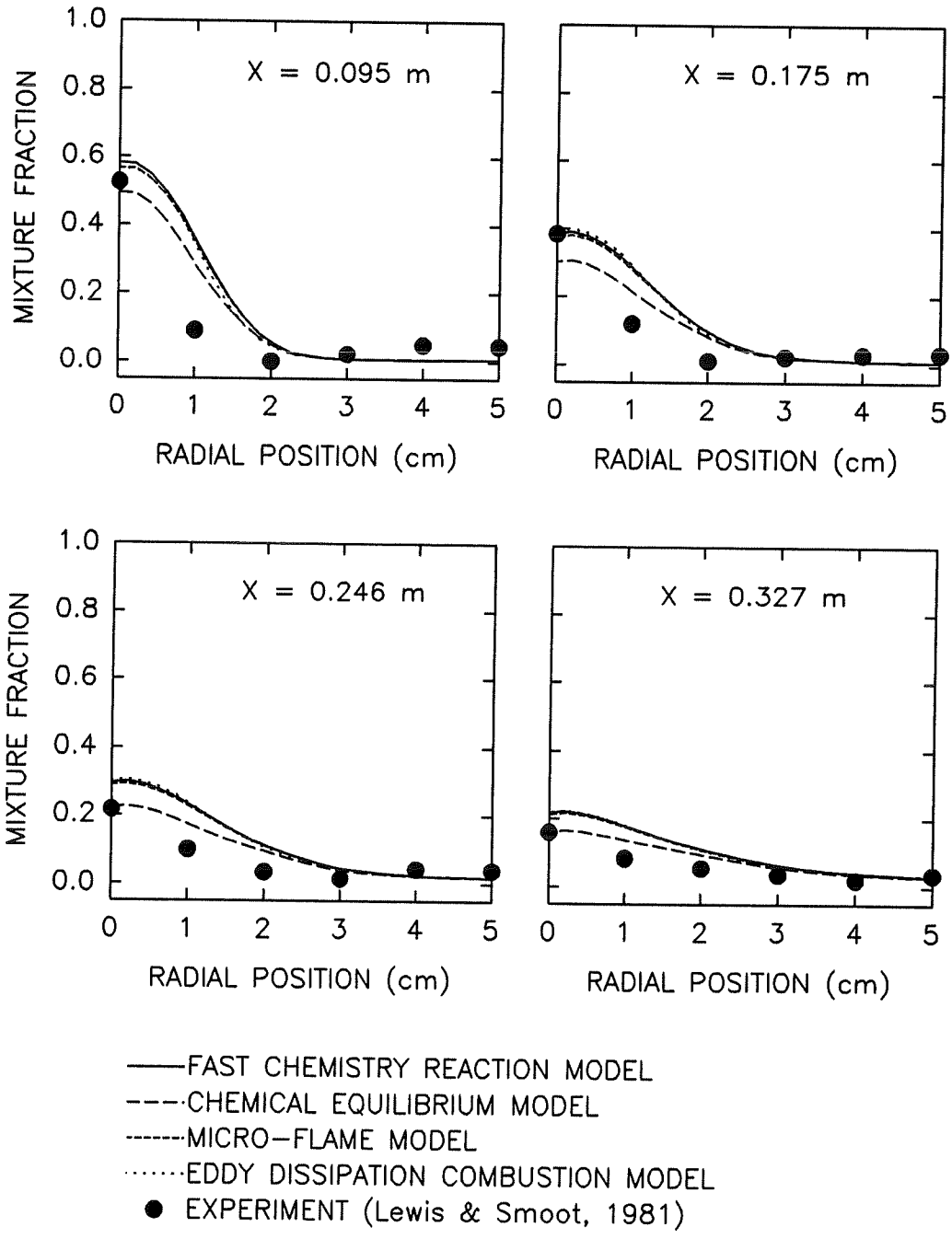

Figure 5.44: The predicted radial distribution of the mixture fraction at different stations based on four combustion models using the direct iteration method

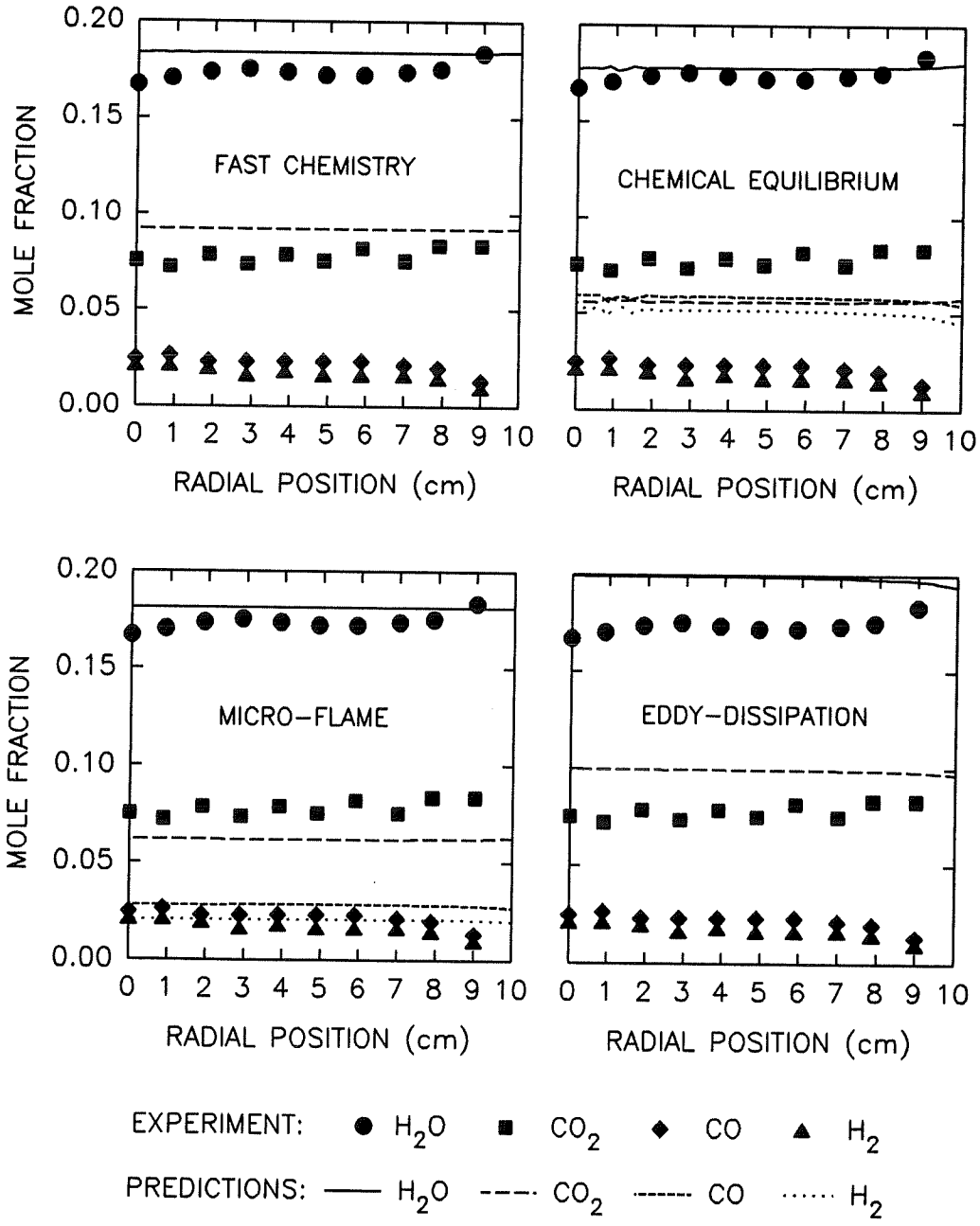

Figure 5.45: The predicted radial distributions of major species mole fraction at station 1.375m based on four combustion models using the direct iteration method

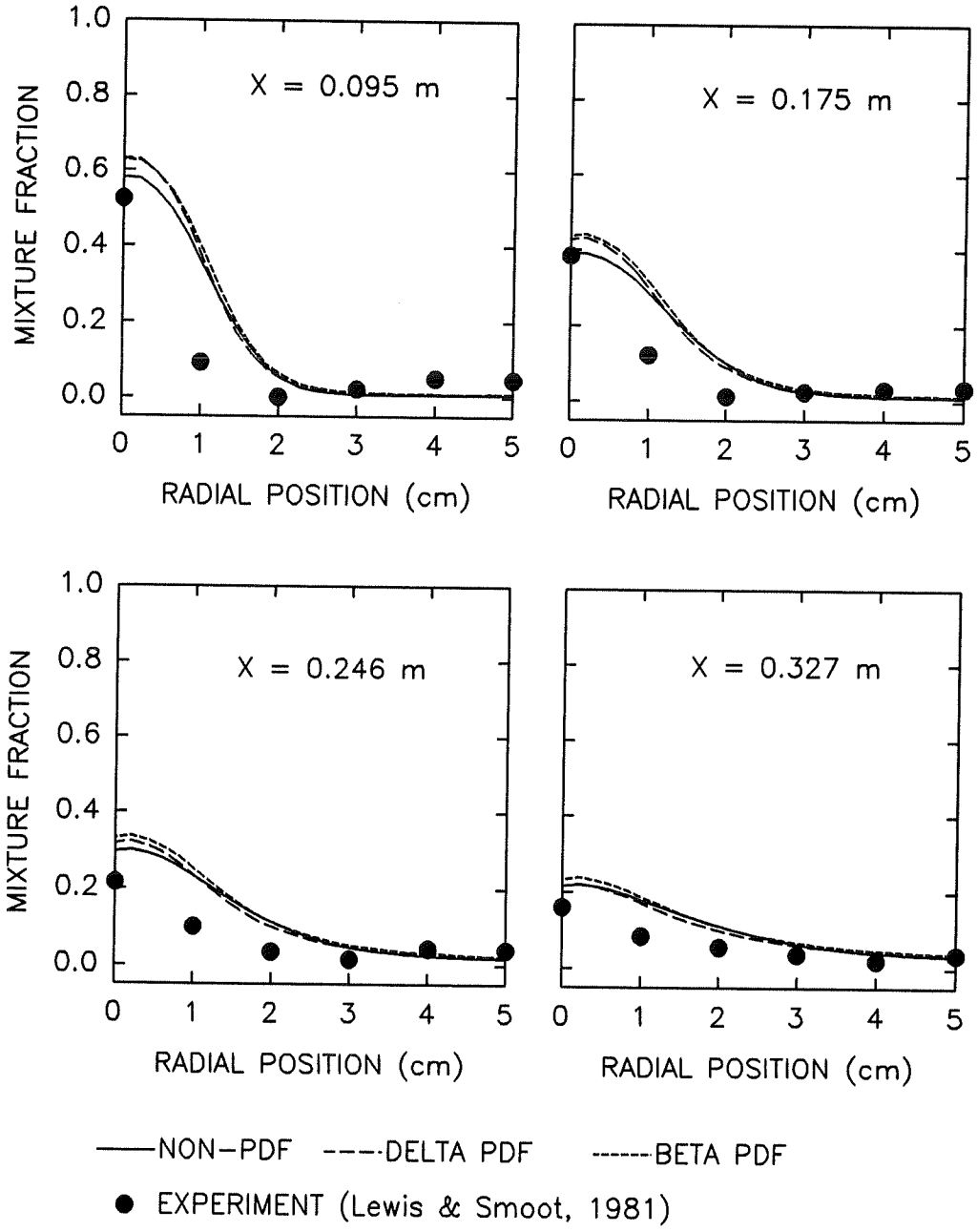

Figure 5.46: The predicted radial distributions of mixture fraction at four stations based on PDF models using the direct iteration method

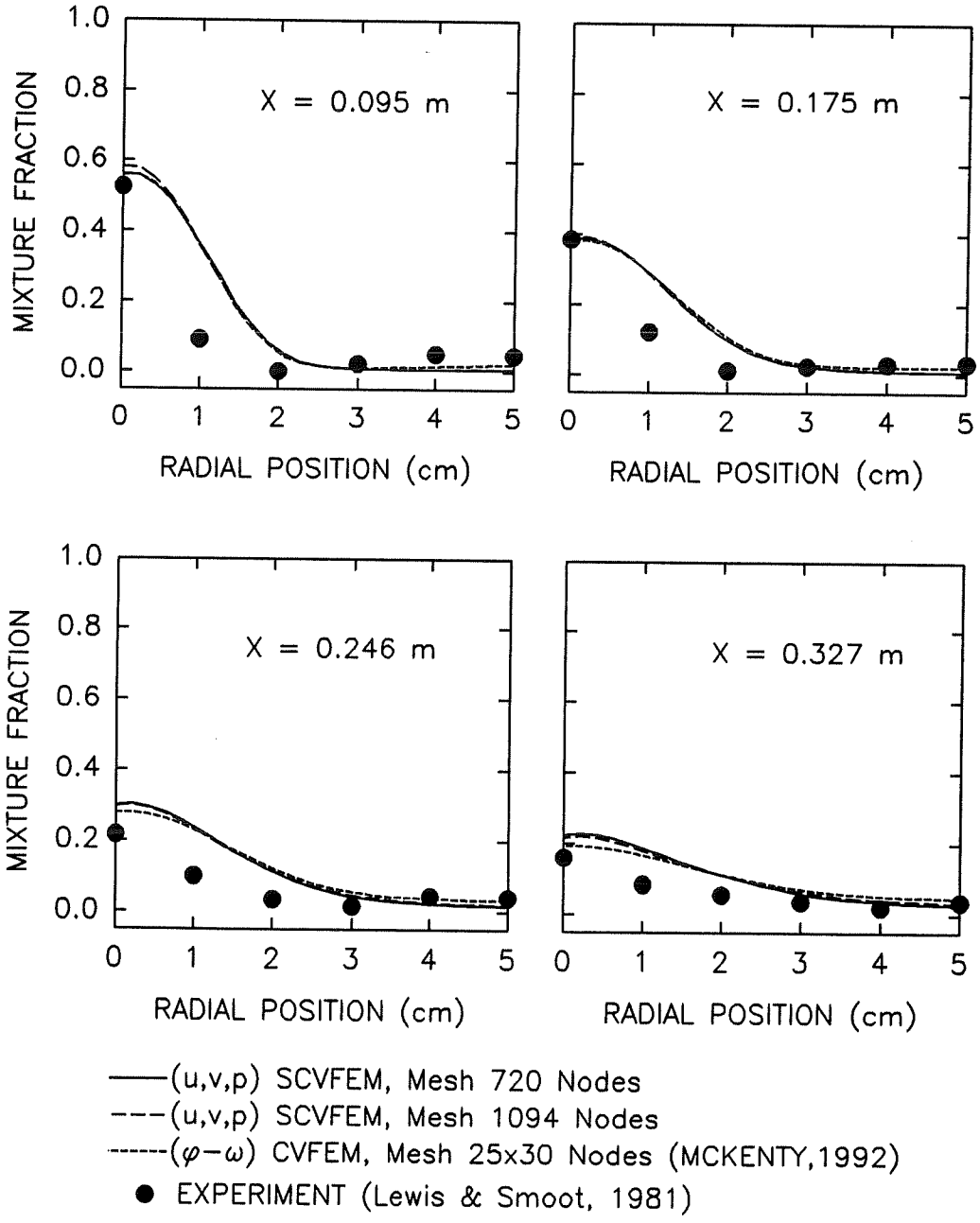

Figure 5.47: Comparison of the predicted radial mixture fraction profiles between the SCVFEM, φ-$\tilde{\omega}$ and experiments of Lewis and Smoot (1981)

5.7.2 Furnace of Lockwood et al. (1974)

5.7.2.1 Problem Description

A second simulation of turbulent reacting flows is that of Lockwood et al. (1974), which is different from the furnace of Lewis and Smoot (1981) both in dimension and inlet conditions. The flow geometry is shown in Figure 5.48.

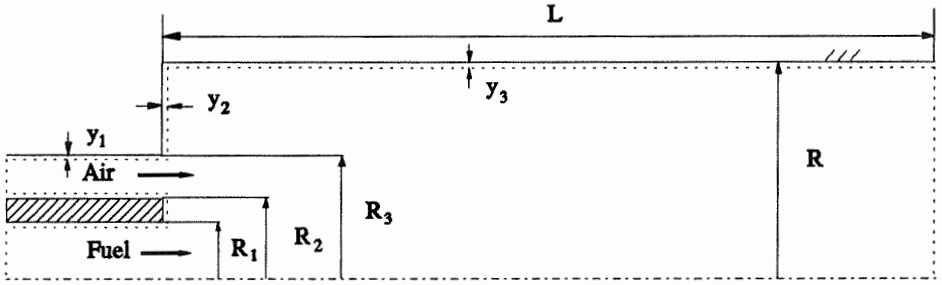

R_1 = 0.010 m R_2 = 0.022 m R_3 = 0.039 m R = 0.105 m

y_1 = 0.001 m y_2 = 0.004 m y_3 = 0.008 m L = 1.900 m

Figure 5.48: Geometry of coaxial combustor of Lockwood et al. (1974)

In these experiments, the fuel and air are entered as coaxial jets into a suddenly expanding chamber. In the present study, the fuel-air ratio of 0.0635, with Reynolds number equals to 16,030 is selected. The inlet fuel velocity is 21.57m/s, with the fuel temperature 344 K, the inlet air velocity is 13.46m/s with the air temperature 301 K. The fuel is the town gas, with a composition of 27% of CH_4, 8% of CO_2, 4% of N_2, 55% of H_2, 4% of CO, 2% of C_2H_6 and other. The calorific value of this mixture is 2.63 x 10^4 kJ/kg.

The computational mesh comprises 2028 sides (1306 elements), as shown in Figure 5.49. In this test, only the fast chemistry model with the Face-centered scheme is considered, because the predicted mixture fractions for each combustion model for first test shows a little difference. Both the classical approximation method and the direct iteration method are used for the calculation of wall functions. Others parameters, such as turbulent inlet conditions, boundary conditions, turbulent model constants and relaxation parameters are the same as for the test of Lewis and Smoot (1981).

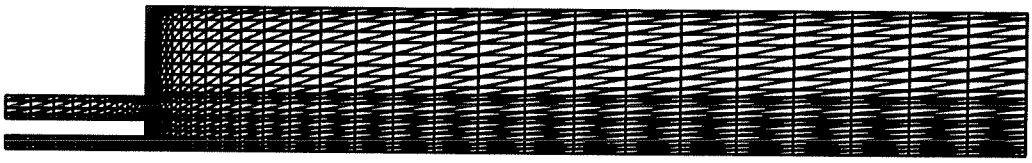

Figure 5.49: The computational mesh of the furnace of Lockwood et al. (1974)

5.7.2.2 Results

Figures 5.50, 5.51 and 5.52 show respectively the velocity, mixture fraction and temperature fields obtained with the classical approximation method and the direct iteration method. The predicted recirculation zone by the classical approximation method is 1.238D and 1.095D by the direct iteration method. The mixture fraction obtained by the direct iteration method exhibits a faster axial decay rate than that of the classical approximation method. As can be seen in Figure 5.52, the flame front obtained by the classical approximation method is longer than that of by the direct iteration method. In Figure 5.53, the predicted radial mixture fraction profiles are

compared with the measurements of Lockwood et al. (1974). It can be seen that the measurements exhibit a faster axial decay rate than do the predictions for all the cases. At all four stations, the direct iteration method predicts a faster decay rate than the classical approximation method. The predictions have the same qualitative trends as the experimental data. Calculations were performed on a RISC 6000 model 520, the CPU times spent by the classical approximation is 1.2699 x 10^4 seconds, and by the direct iteration method is 1.9625 x 10^4 seconds.

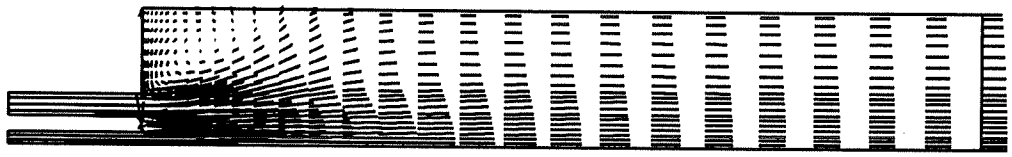

(a) Classical Approximation Method

(b) Direct Iteration Method

Figure 5.50: The predicted velocity field of the furnace of Lockwood et al. (1974)

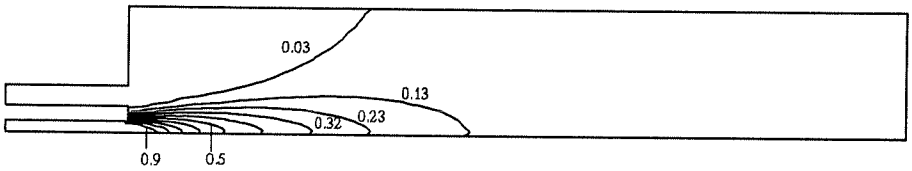

(a) Classical Approximation Method

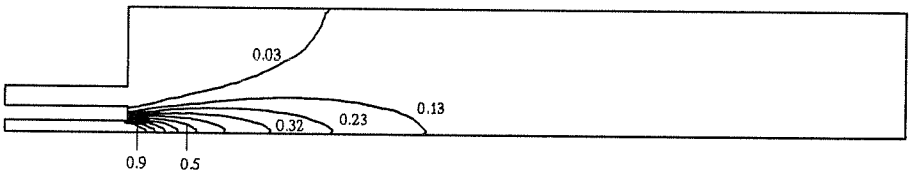

(b) Direct Iteration Method

Figure 5.51: The predicted mixture fraction field of furnace of Lockwood et al. (1974)

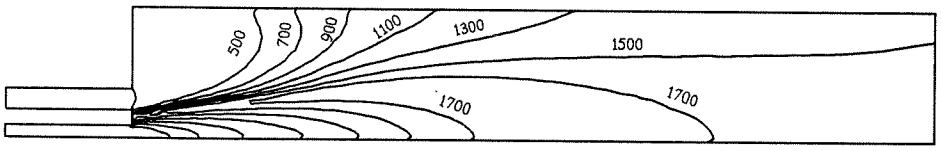

(a) Classical Approximation Method

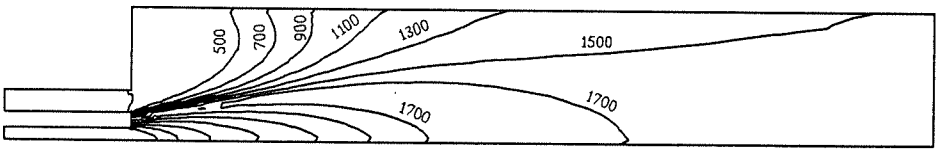

(b) Direct Iteration Method

Figure 5.52: The predicted temperature field of furnace of Lockwood et al. (1974)

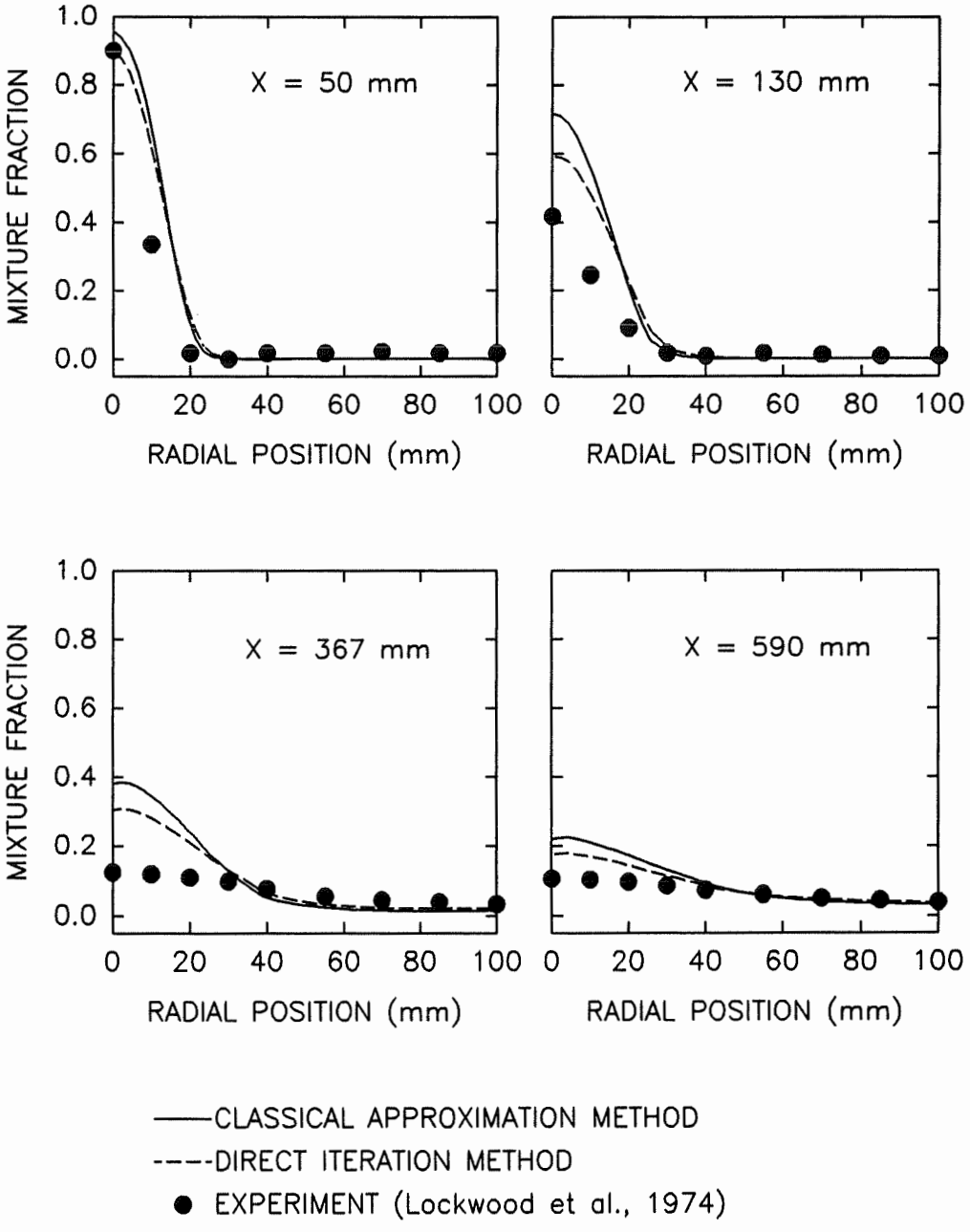

Figure 5.53: Comparison of predicted and experimental mixture fraction profile at different axial stations of furnace of Lockwood et al. (1974)

5.8 Results of Radiation

The discrete transfer method was implemented and applied to the 2D cartesian rectangular and triangular enclosures and axisymmetric cylinder furnaces using an unstructured triangular mesh. The following examples were chosen to compare the proposed procedure with exact solutions, original discrete transfer method (Lockwood and Shah, 1981) and other approximate methods. For cartesian coordinate, the tests involve:

- Absorbing/Emitting in a black rectangular enclosure
- Scattering in black rectangular enclosures
- Scattering in a gray triangular enclosure

For axisymmetric cylinder coordinate, the following tests are considered:

- Radiant heat transfer in idealized axisymmetric furnaces
- Radiant heat transfer in axisymmetric Delft furnace

5.8.1 Absorbing/Emitting in a Black Rectangular Enclosure

The discrete transfer method in the present methodology was applied to a rectangular enclosure with cold black walls and a purely absorbing/emitting medium maintained at an emissive power of unity, as shown in Figure 5.54. The surface heat transfer rate was computed for three optical conditions $k_gL=0.1$, 1.0, 10.0. Three sets of comparisons of the surface heat transfer rates are made. The first are the parametric analysis of the discrete transfer method for the absorbing medium ($k_gL=1.0$). The second set, are comparisons between the present discrete transfer method using triangular mesh solutions and the original discrete transfer method using a rectangular mesh (Lockwood and Shah, 1981). Finally, are comparisons between the present method and the exact solutions (Shah, 1979), as well as the S_4 discrete ordinates solutions (Fiveland, 1984).

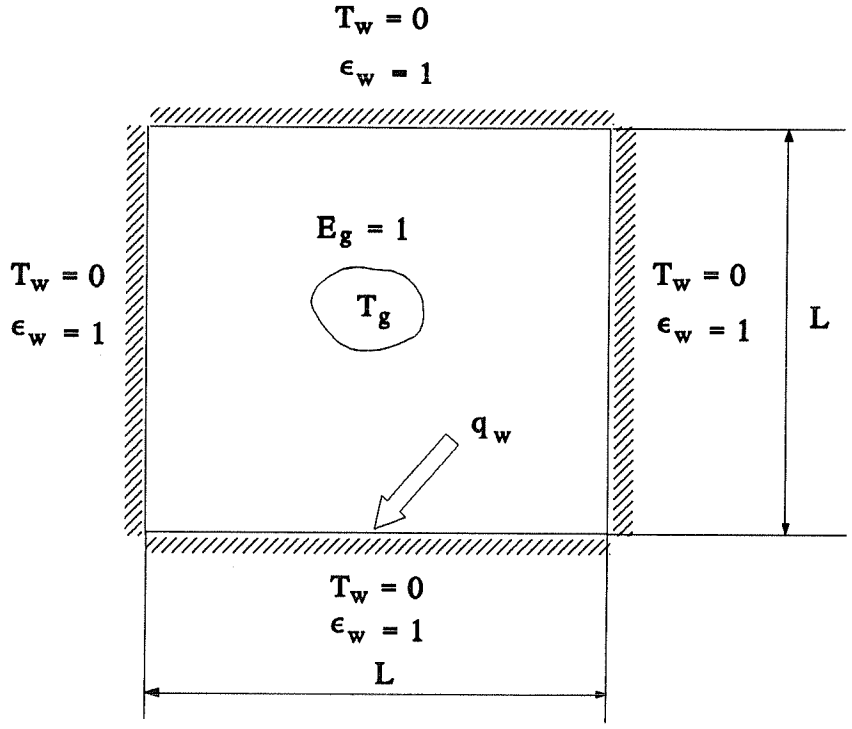

Figure 5.54: A schematic of rectangular geometry with absorb/emit medium

Parametric analysis of the discrete transfer method

The effect of the number of element and the number of rays on the solution was evaluated for the case of $k_gL = 1.0$. The comparison for 50, 98 and 200 elements and the exact solution (Shah, 1979) is shown in Fig. 5.55. For 50 elements, at least $N\theta$ x $N\phi = 4$ x 16 are needed. Whereas for 98 elements, $N\theta$ x $N\phi = 4$ x 8 are necessary to closely match the exact solution. For 200 elements and $N\theta$ x $N\phi = 4$ x 2, we do not obtain good results, however, when increasing to $N\theta$ x $N\phi = 4$ x 4, the results are in excellent agreement with the exact solution. This test shows that the number of the azimuthal angle $N\phi$ must at least be equal to 4, otherwise, we can not obtain good results, even for relatively fine grids (200 elements).

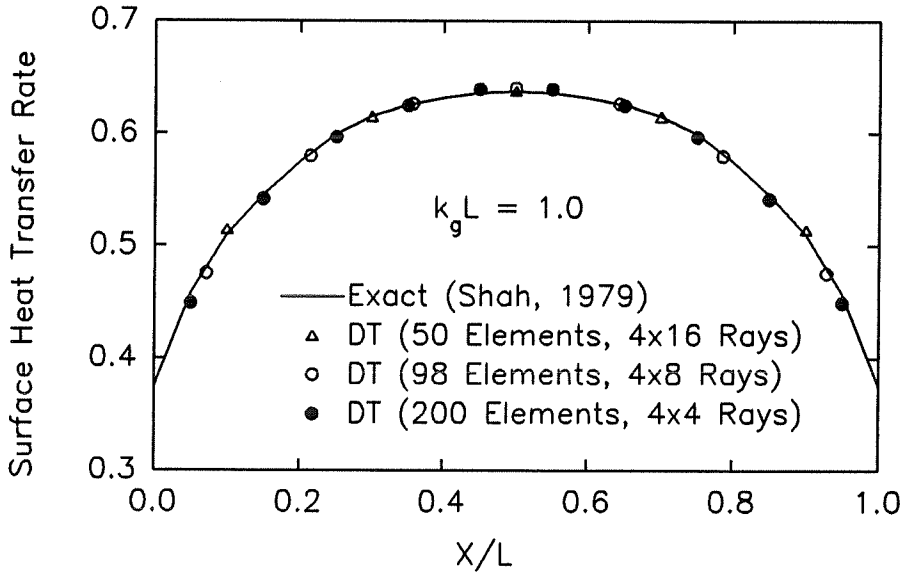

Figure 5.55: Minimum number of rays needed by the different meshes to closely approximate the exact solution for absorbing medium $k_gL = 1.0$

Comparison with original DT method

In this test case, we will compare the surface heat transfer rates of the original discrete transfer method (Lockwood and Shah, 1981) and the present discrete transfer method. The original discrete transfer method, using a 10 × 10 rectangular mesh and 64 rays per corresponding wall location, closely reproduced the exact solutions (Shah, 1979) for 3 optical thicknesses. For the comparison, 100 triangular elements and 64 rays for each corresponding wall location were used. Figure 5.56 shows the geometry and the unstructured triangular mesh. Fig. 5.57 and Fig. 5.58 are the comparisons between the present method solutions and the exact solutions. It is shown that the results very closely match the exact solutions. The CPU time with the present discrete transfer method was 0.95s on a IBM 3090 180 VF computer for an optical thickness equal to one. This problem was also solved on an 800 elements using 64 rays, the CPU time in this case was 9.25 seconds. For the pure absorbing/emitting medium, the discrete transfer method with rectangular mesh and with the triangular mesh gives excellent results.

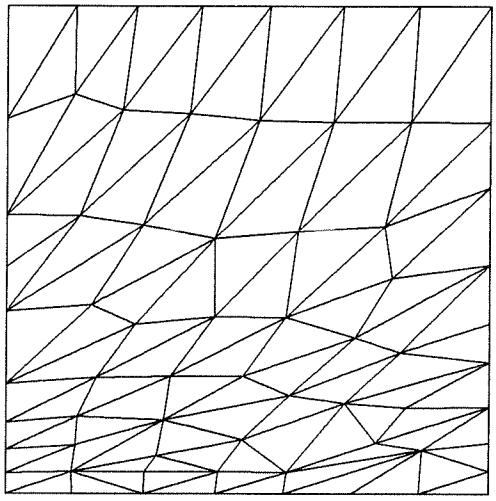

Figure 5.56: Unstructured triangular mesh for 2-D square enclosure

Comparison with other methods

Comparisons with the S_4 discrete ordinates method (Fiveland, 1984) are also shown in Figs. 5.57 and 5.58. For the absorbing/emitting media, it is clear that the present discrete transfer results provide excellent agreement with the exact solution and are better than those obtained with the S_4 discrete ordinates method.

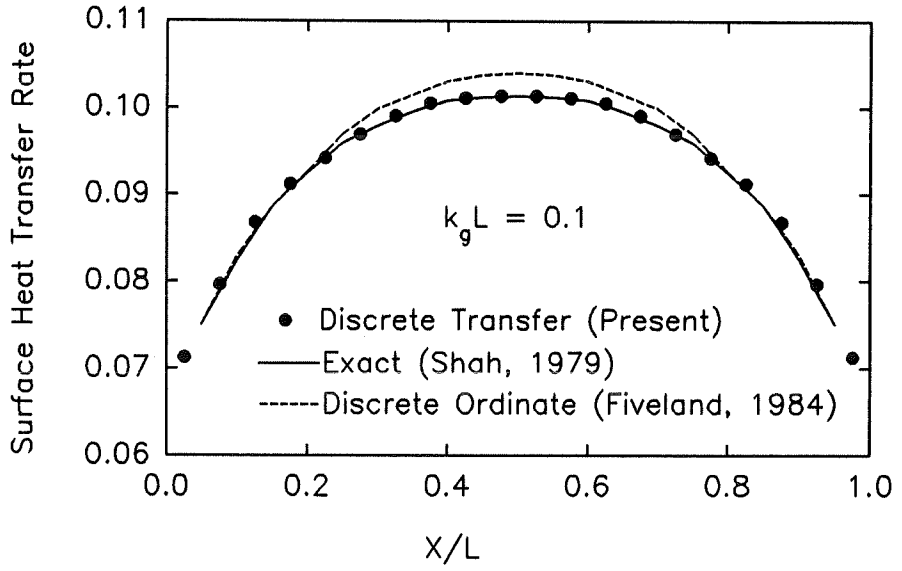

Figure 5.57: Surface heat transfer rate for a square enclosure with cold walls and absorbing medium for k_gL=0.1

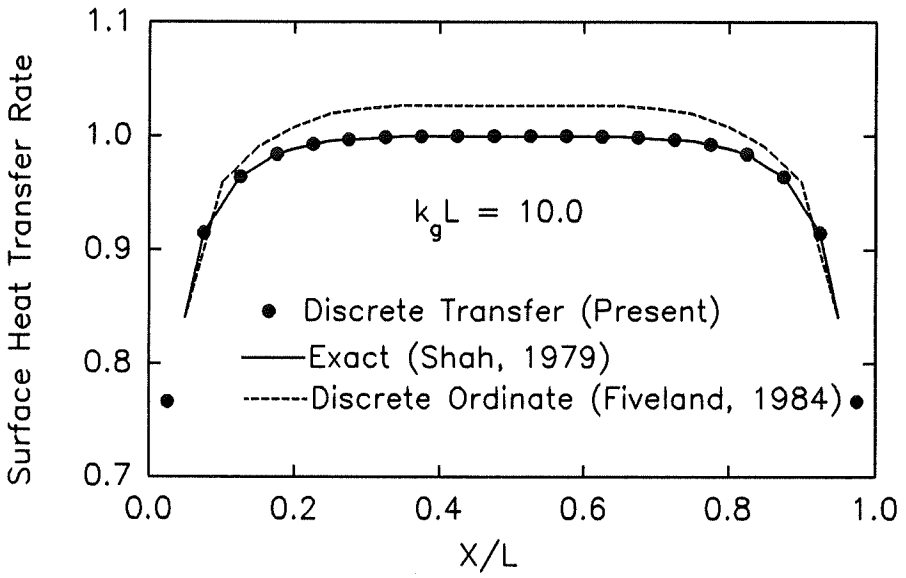

Figure 5.58: Surface heat transfer rate for a square enclosure with cold black walls and absorbing medium for k_gL = 10.0

5.8.2 Scattering in Black Rectangular Enclosures

This test is focused on isotropic radiative transfer in a square enclosure with black walls and a scattering cross section of unity shown in Fig. 5.59. The emissive power of one surface is set to unity, the others are set to zero.

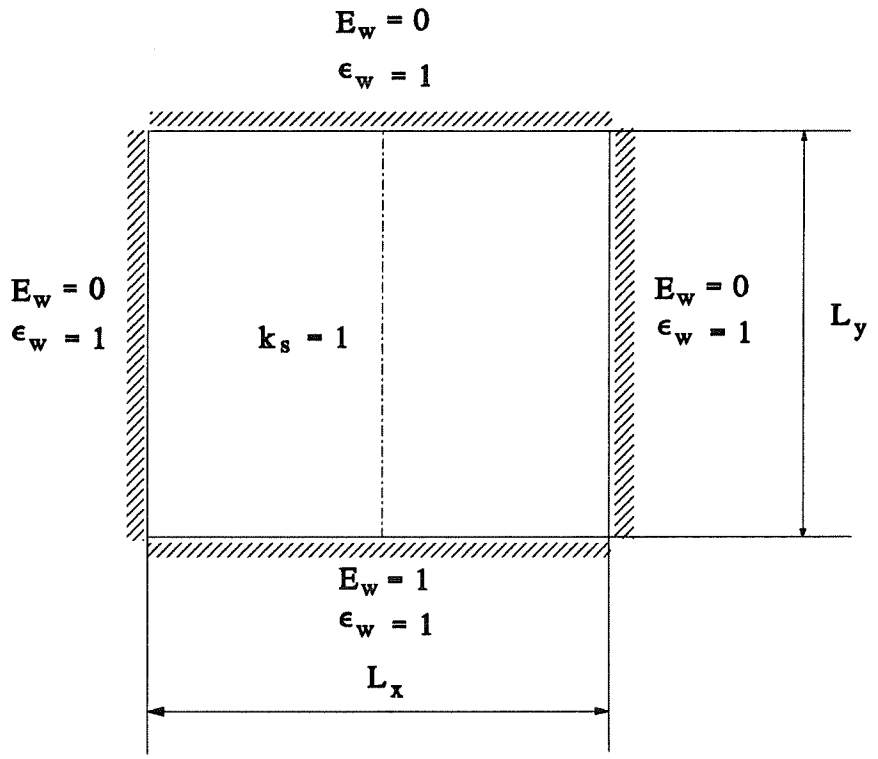

Figure 5.59: Geometry of a square enclosure with black walls and a scattering cross section of unity

Equal Aspect Ratio

The "ray effect" is the basic problem arised in the radiation computations. It appears in the angular discretization and it is independent of the spatial discretization. The reason can be referred to the inability of the discretized intensity distribution to fully represent the actual continuous intensity distribution. Care must be taken to avoid the "ray effect", as suggested by Viskanta and Mengüç (1987), the discrete transfer

method may be subject to this behaviour in both absorbing and scattering media. In scattering media, the "ray effect" tends to be more notorious (Carvalho, 1991). Then the number of elements has been increased to 800 and the number of rays per boundary surface to 64. Figure 5.60 shows the variation of the centerline incident radiant energy in a rectangular enclosure for an equal aspect ratio. The present discrete transfer solutions are compared with results from a Zonal analysis and the P_3 differential approximation (Ratzel and Howell, 1982), and with the S_4 discrete ordinates method (Fiveland, 1984). It can be seen from these results that the discrete transfer method using an unstructured triangular mesh compares well with these methods.

Unequal Aspect Ratio

For an enclosure with an high aspect ratio of $L_x/L_y = 5.0$ and $k_sL_y = 1.0$, the centerline incident radiant energy was obtained by using 200 elements and 64 rays per wall location. Figure 5.61 shows the comparison between the present discrete transfer solution, the discrete transfer using a rectangular mesh solution (Carvalho et al., 1991) and the results obtained by Modest (1975). The CPU time was 73 seconds on a IBM RISC 6000 Work Station. For the low aspect ratio case we chose $L_x/L_y = 0.1$ and $k_sL_y = 1.0$, i.e. the emitting wall is ten times smaller than side walls. Calculations were performed on a fine grid with 840 elements and 64 Rays. The results are compared with the discrete transfer solution on a rectangular mesh (Carvalho et al., 1991) and the results of Modest (1975), as shown in Figure 5.62. The results by the present discrete transfer with triangular mesh are lower than the results obtained by Modest. This is due to the aspect ratio of the geometry, as few rays emitted from the hot surface will reach the elements, called "ray effect". The same behaviour can be observed in the results of Carvalho et al. (1991).

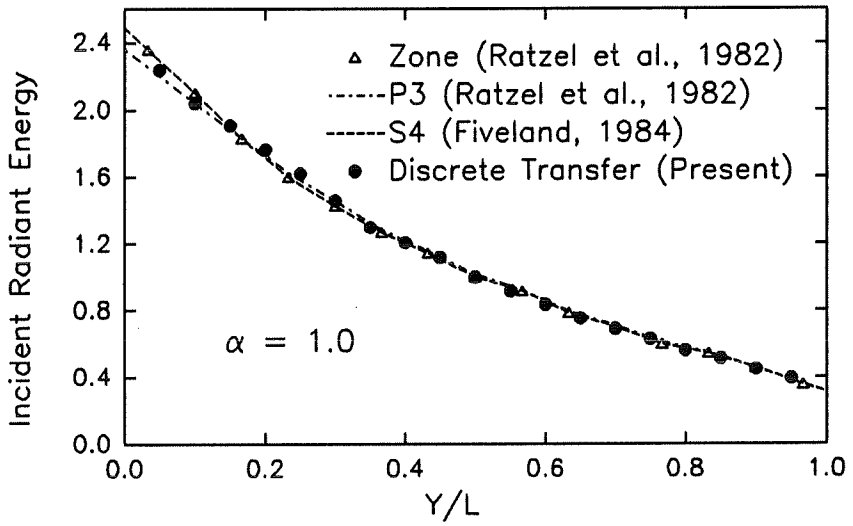

Figure 5.60: Centerline incident radiant energy for aspect ratio $L_x/L_y=1$ in a rectangular enclosure with a scattering medium $k_sL_y=1.0$

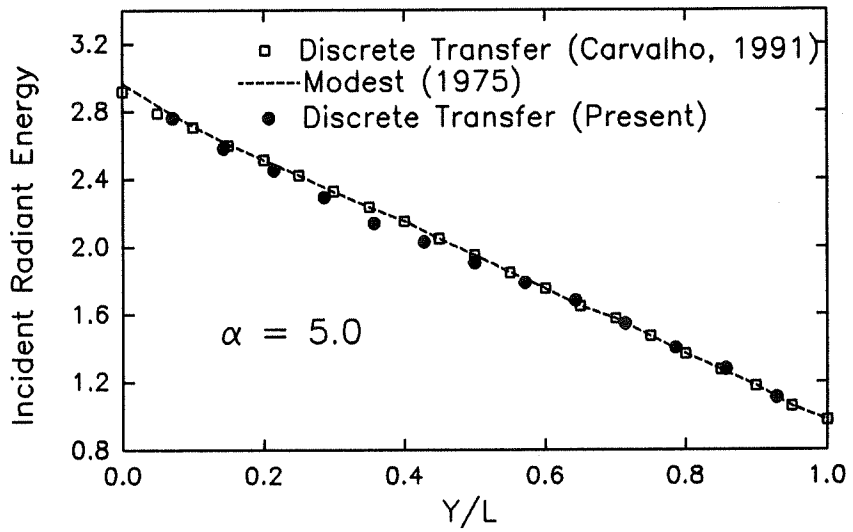

Figure 5.61: Centerline incident radiant energy for aspect ration $L_x/L_y=5$ in a rectangular enclosure with a scattering medium $k_sL_y=1.0$

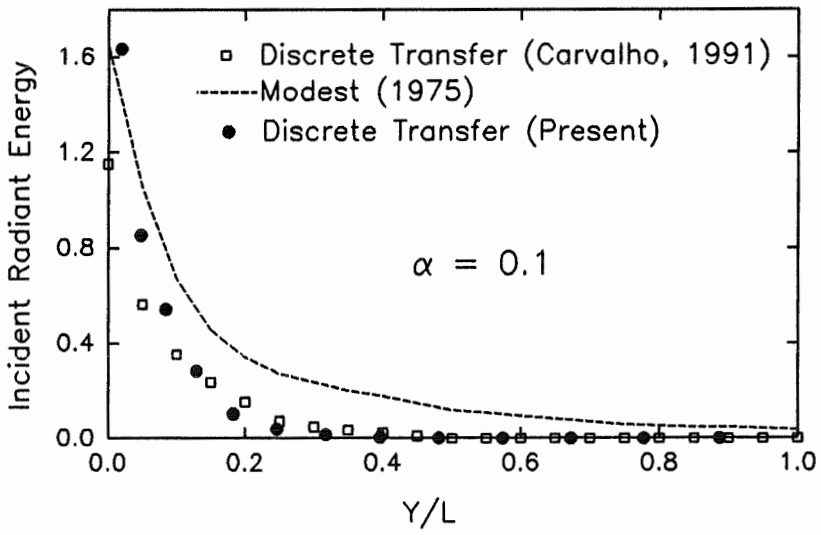

Figure 5.62: Centerline incident radiant energy for aspect ratio $L_x/L_y=0.1$ in a rectangular enclosure with a scattering medium $k_sL_y=1.0$

5.8.3 Pure Scattering in a Gray Triangular Enclosure

The calculation is performed on a complex geometry, a triangular enclosure with sharp edges with a hot obstruction shown in Figure 5.63, where the scattering coefficient are set to unity. The computational mesh, shown in Figure 5.64, includes 639 triangular elements. Near the hot obstruction and inside the sharp angles, the grid is refined. The isolines of emissive power are given in Figure 5.65. From this result, we can see that near the hot obstruction surface, a high gradient of emissive power exists and a fine grid is necessary to capture this behaviour. Inside the sharp angles where the emissive power is weak, a fine grid is also needed.

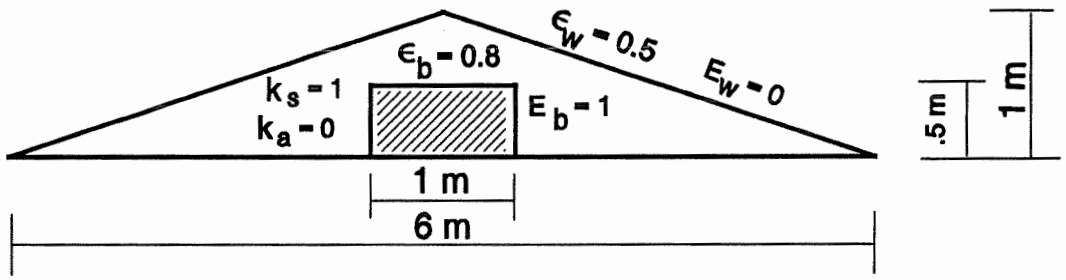

Figure 5.63: Geometry of the triangular enclosure with sharp edges contain hot obstruction

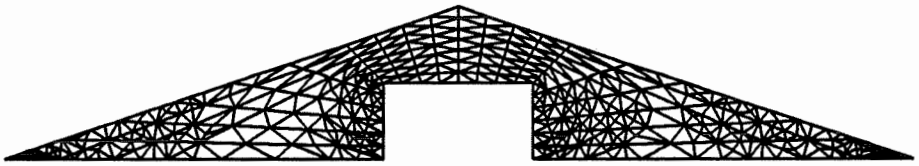

Figure 5.64: The computational mesh for triangular enclosure

Figure 5.65: Contour plot of emissive power for the triangular enclosure with sharp edges contain hot obstruction, E_w from wall to hot obstruction is 0 to 1, interval 0.05

5.8.4 Radiant Heat Transfer in Idealized Axisymmetric Furnaces

The geometry of a simplified cylindrical furnace is considered, as shown in Figure 5.66. This example is chosen to benchmark the discrete transfer model with unstructured mesh for an axisymmetric cylindrical coordinates. The gas (T_g) and wall (T_w) temperatures are assumed to be known.

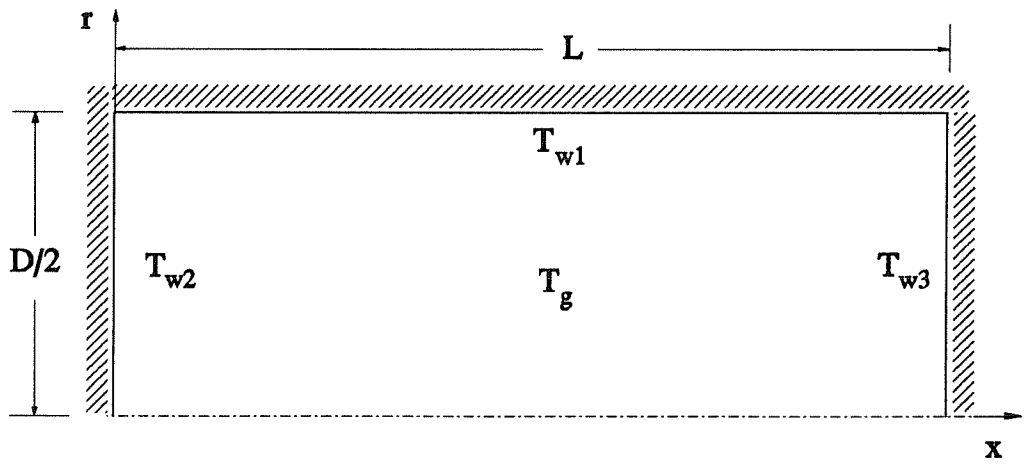

Figure 5.66: Geometry of cylindrical furnace

The incident (q_i) and net (q_w) radiant heat fluxes at walls are presented. They can be expressed as:

$$q_i = \int_{\phi=0}^{2\pi} \int_{\theta=0}^{\frac{\pi}{2}} I_{w,i}^{-} \cos\theta_i \, d\Omega_i = \sum_{i=1}^{N} I_{w,i}^{-} \cos\theta_i \Delta\Omega_i$$

$$q_w = q_i - q^+$$

where q^+ is the heat flux leaving from the wall.

This problem has been studied by Benim (1988) using the finite element method based on the moment method as radiation model. It is showed that the moment method predictions are comparable with the flux models. The zone method, being regarded as nearly exact solutions, is assumed to give the best solutions. Follows Benim (1988), three different cases are considered for this problem. The diameter is assumed to be the characteristic length for all cases.

Case 1

The dimensions of the furnace (Figure 5.66) are assumed to be:

$D = 1.69$ m, $L = 10.5$ m $(L/D = 6.2)$

The constant gas and wall temperatures are prescribed as:

$T_g = 1273$ K, $T_{w1} = T_{w2} = T_{w3} = 773$ K

The walls are assumed to be black, $\varepsilon_{w1} = \varepsilon_{w2} = \varepsilon_{w3} = 1.0$.

The optical depth is assumed to be $\tau_o = 0.423$. The computational mesh contains 836 triangular elements (470 nodes) is shown in Figure 5.67, near the wall, the grid is refined. In the computations, the number of rays for each surface is given by $N\theta \times N\phi = 2 \times 8$. Figure 5.68 shows the predicted net radiative heat flux along the furnace walls (side wall and cylinder bottom) using the DT method with unstructured grid. The results are compared with the zone method (Richter & Bauersfeld, 1974) and the moment method (Benim, 1988) predictions. The side wall heat flux is symmetric about the middle of furnace length (x/D = 3.1), and it is plotted up to this distance. The present procedure gives the better agreement with the zone method predictions, the maximum derivation of the present DT method from zone method results is about 2%, which is better than that of the moment method predictions with 6% error (Benim, 1988). The computer CPU time required for the present method is 68.1 seconds at IBM RISC 6000/model 520.

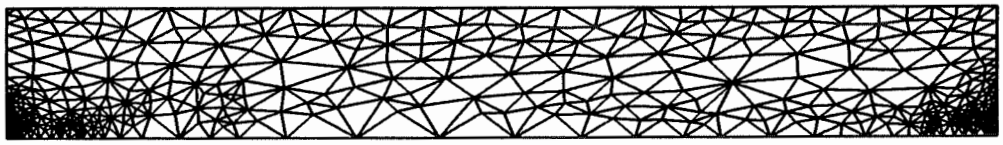

Figure 5.67: The computational mesh of furnace, Case 1

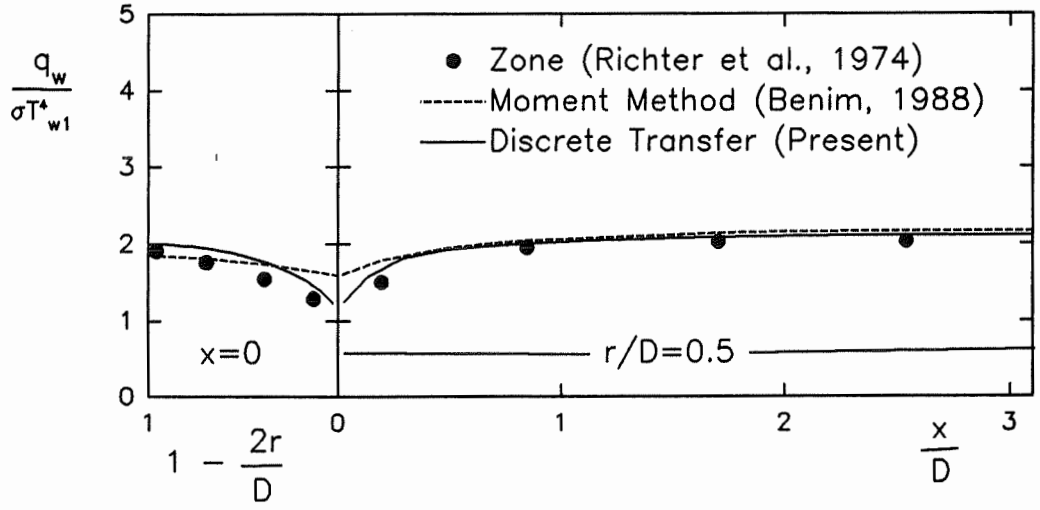

Figure 5.68: Net radiant heat flux variation along furnace walls, Case 1

Case 2

Different from Case 1, the dimensions of the furnace are changed to be

$D = 2.22$ m, $L = 6.25$ m $(L/D = 2.8)$

The wall temperatures and emissivities are prescribed as:

$T_{w1} = T_{w2} = T_{w3} = 300$ K, $\varepsilon_{w1} = \varepsilon_{w2} = \varepsilon_{w3} = 0.5$

The gas temperature is assumed to be constant in the radial direction, but varies

linearly with the axial distance according to T_g = -272 x + 2050 K.

The results are compared with the zone method (Lowes et al., 1973) and the moment method (Benim, 1988) predictions. Figure 5.69 shows the computational mesh involving 908 triangular elements (510 nodes), the grid is refined near the solid wall.

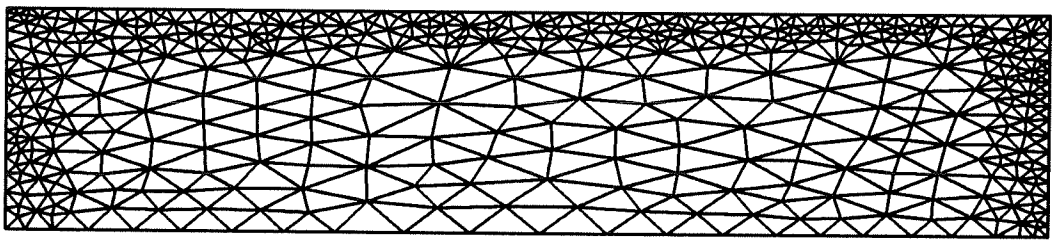

Figure 5.69: The computational mesh of furnace, Case 2 and Case 3

The variation of the incident heat flux along the side wall is presented in Figure 5.70 for three values of the optical depth, τ_o = 1.11, 0.444, 0.222, respectively. The agreement of the present results with the zone method predictions is excellent for all three values of the optical depth. The net radiant heat flux variation along the side wall is presented in Figure 5.71. Again, it is found that the present results agree very well with the zone method predictions for all three values of the optical depth. The present results for both the incident and net heat flux variations along the furnace wall are much better than that of the moment method predictions. The computer CPU time required is 883.90 seconds for τ_o = 1.11, 1031.14 seconds for τ_o = 0.444, and 1178.46 seconds for τ_o = 0.222, respectively at the IBM RISC 6000/model 520. It is found that when the optical depth becomes shorter, the computational time becomes longer.

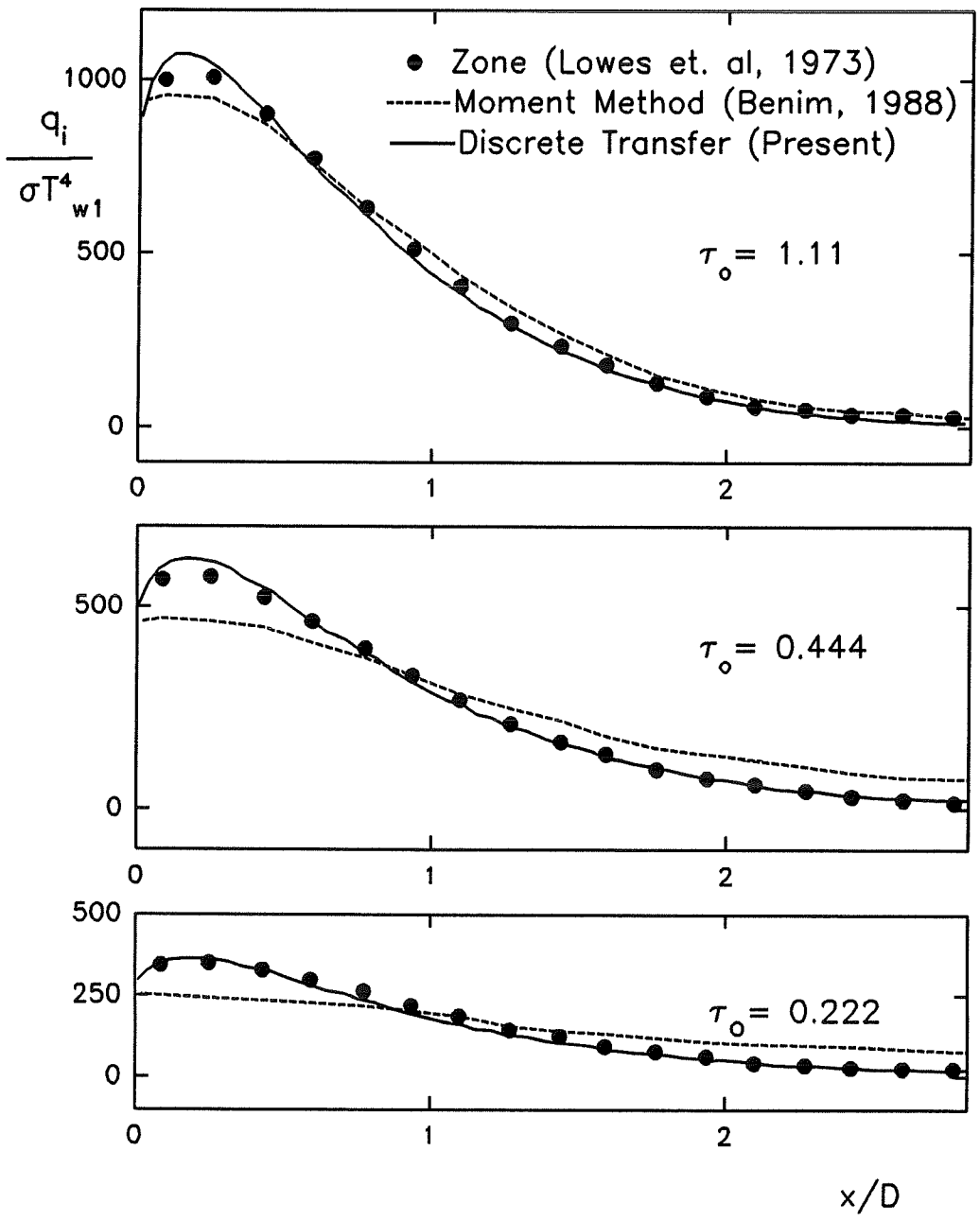

Figure 5.70: Incident heat flux variation along side wall, Case 2

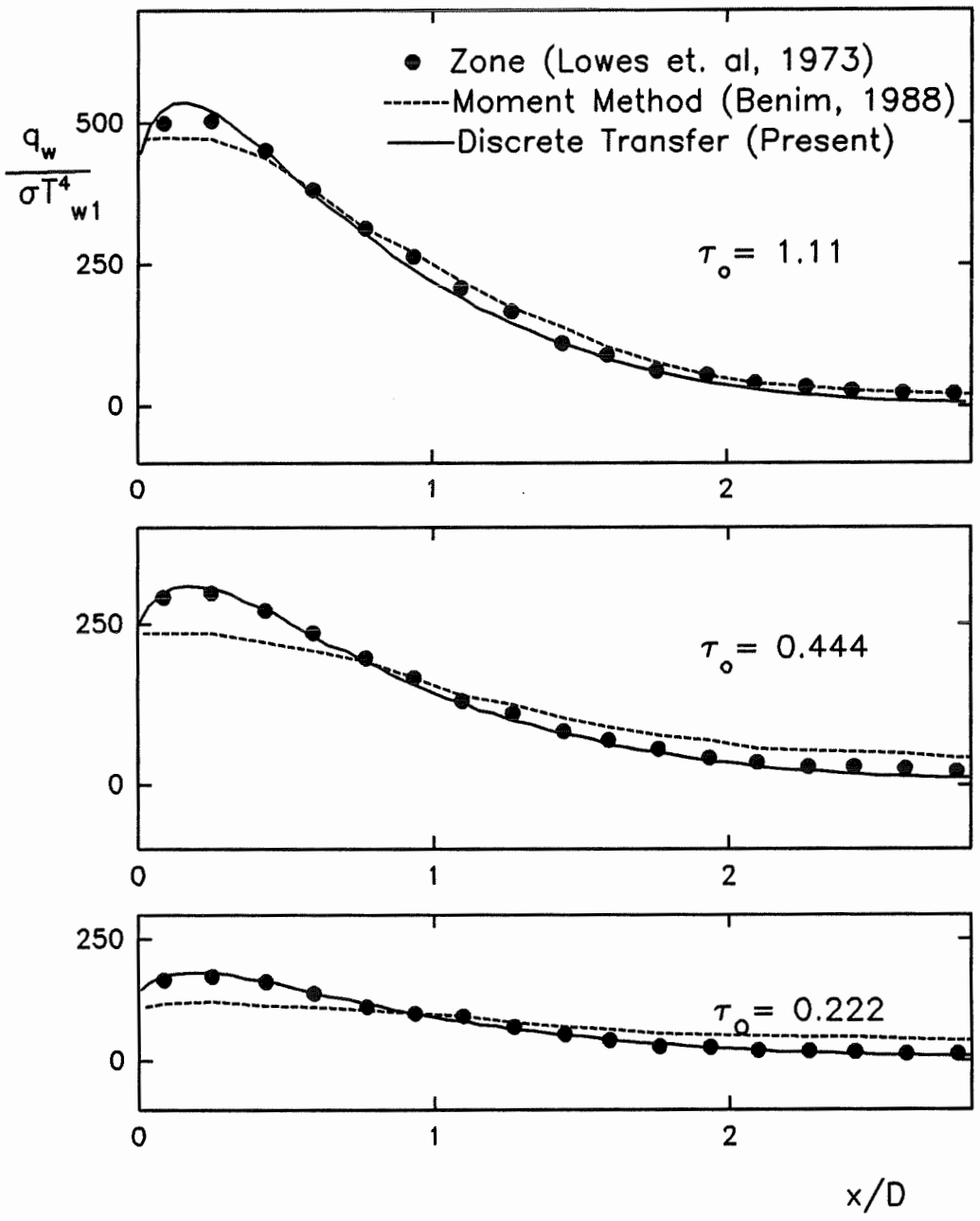

Figure 5.71: Net radiant heat flux variation along side wall, Case 2

Case 3

This case is almost same as Case 2, except the left wall temperature is changed to be: T_{w2} = 1300 K.

The results are compared with the zone method and moment method predictions of Michelfelder (1976) and Benim (1988). Figure 5.72 gives the incident heat flux along the side wall for τ_o = 0.444. The present prediction shows an excellent agreement with the zone methods results. The CPU time is 1031.47 seconds at the same computer as Case 1 and Case 2.

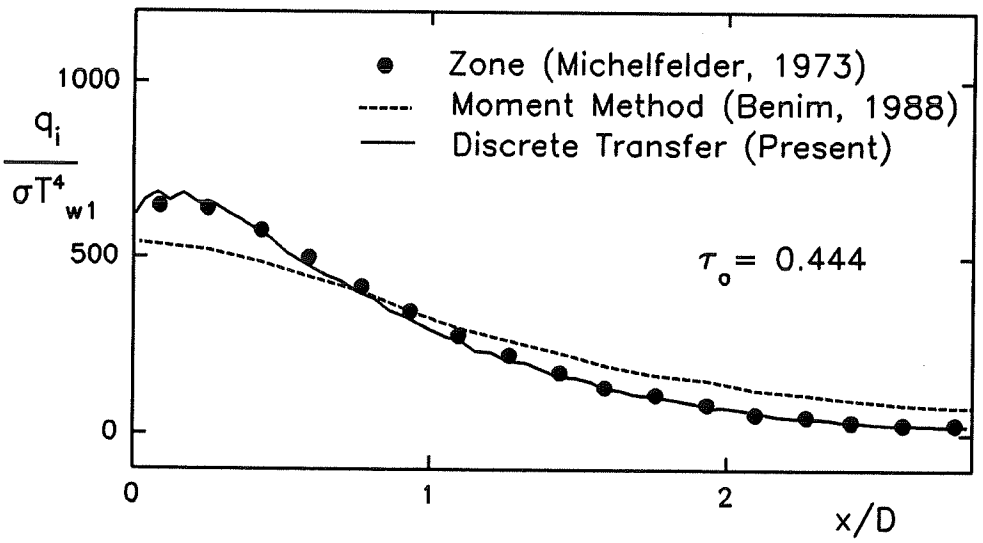

Figure 5.72: Incident heat flux variation along side wall, Case 3

5.8.5 Radiant Heat Transfer in Axisymmetric Delft Furnace

The discrete transfer predictions were compared with the experimental results obtained by Wu and Fricker (1971) in the cylindrical axisymmetric Delft furnace of the IFRF (Industrial Flame Research Foundation), and were also compared with the discrete ordinates method results using the S4 approximation of Jamaluddin and Smith (1988). The geometry and radiative properties of the medium and walls are shown in Figure 5.73, the measured temperatures inside the furnace with the rectangular mesh 3x17 are given by Jamaluddin and Smith (1988).

For comparison, a structured triangular mesh with 3x17x2, together with 16 rays per node is used in the present DT method computations.

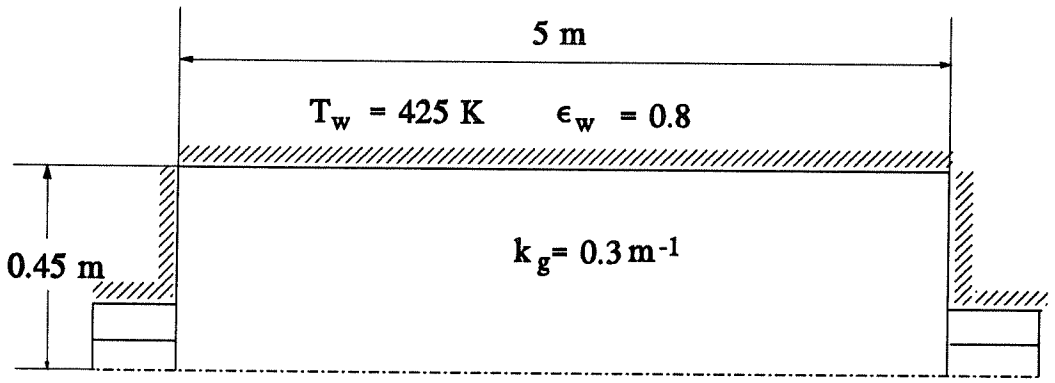

Figure 5.73: A schematic of Delft furnace

The comparison shown in Figure 5.74 clearly demonstrates that the Discrete Transfer results agree with the experimental and discrete ordinates S4 approximations. The CPU time required to obtain this result was 6.86 seconds in IBM 3090 180 VF computer.

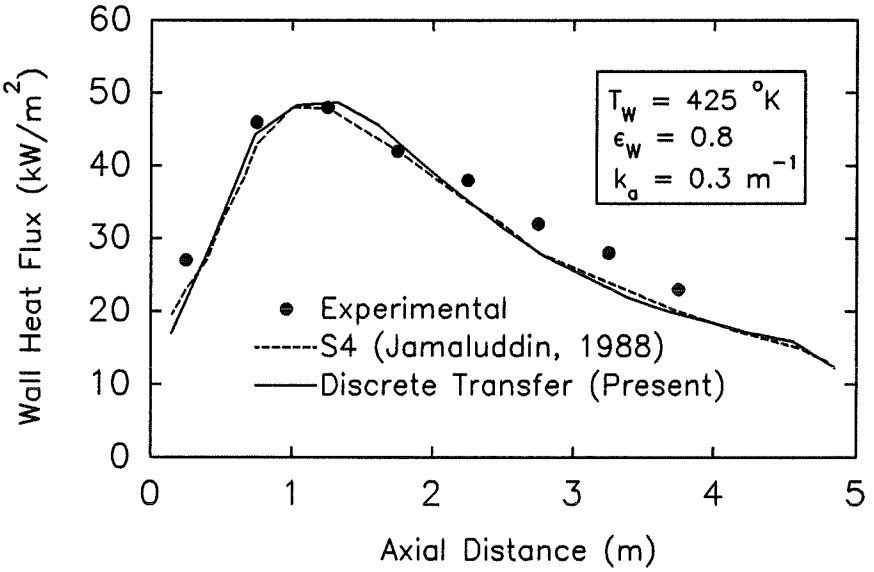

Figure 5.74: Wall heat flux distribution for the Delft furnace

5.8.6 Summary

The discrete transfer method was extended to an unstructured triangular mesh and applied to the prediction of radiative heat transfer for two-dimensional cartesian and axisymmetric enclosures containing an absorbing-emitting and isotropic scattering media. By comparison with the original discrete transfer method, exact solution and other numerical solutions, we have shown that for absorption dominant problems, the present discrete transfer method has given excellent solutions. For pure scattering problems, we obtain the same level of accuracy as other methods. The present method can be used for the computation of radiative heat transfer in gas combustion chambers with arbitrary geometries due to the computational economy and reasonable accuracy of this method.

5.9 Turbulent Diffusion Flame Coupled with Radiation

5.9.1 Problem Description

The present SCVFEM is assessed by investigating flame 29 of the M-2 trials performed at the International Flame Research Foundation (IFRF) (Michelfelder and Lowes, 1974). The furnace comprises a rectangular refractory chamber with 6.25m long and 2m x 2m in cross-section, and includes seventeen double-loop cooling-pipes used to provide thermal loading for system. Since the present mathematical model is axisymmetric, the furnace configuration is approximated by a cylinder having the same cross-sectional area as sketched in Figure 5.75.

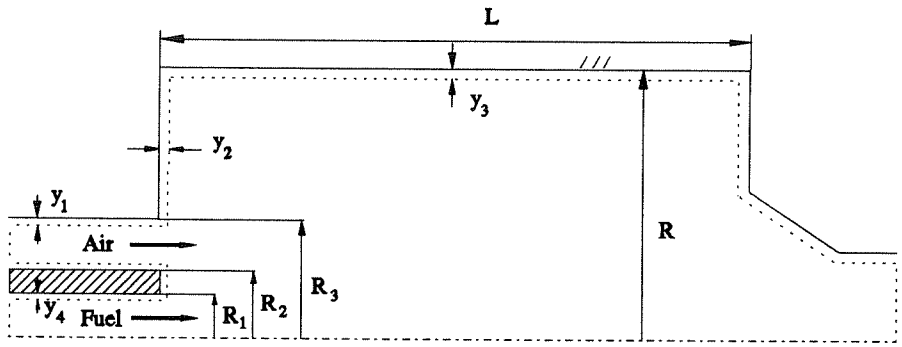

R_1 = 0.0163 m R_2 = 0.03 m R_3 = 0.088 m R = 1.08 m L = 6.25 m

y_1 = 0.001 m y_2 = 0.004 m y_3 = 0.008 m y_4 = 0.001 m

Figure 5.75: Geometry of experimental furnace M-2 trials flame-29 of Michelfeder and Lowes (1974)

The computation for this test is a non-swirling natural gas diffusion flame with axial fuel and coaxial air injection, the input thermal load is 3000 kW. The inlet mass flow rate of the natural gas through the central nozzle is 280 Kg/h, dry air with mass

flow rate of 3126 Kg/h and oxygen with mass flow rate of 170 Kg/h are injected through the coaxial nozzle. The IFRF M-2 trials were specifically conducted to provide detailed data for evaluating radiation models, detailed information about the experimental set-up can be found in Michelfelder and Lowes (1974). The numerical solution of this problem by the finite element method has been given by Benim (1989), by the control volume finite element method can be found in Meng et al. (1992).

5.9.2 Numerical Details

Figure 5.76 shows the computation mesh, which includes 2662 triangular elements (1419 nodes). The eddy-dissipation combustion model coupled with radiation is solved by using the discrete transfer method. The 2-layer wall function is implemented by the classical approximation method. An attempt to use the direct iteration method has failed for this test. The reason may be due to the inlet fuel velocity which is high (about 120 m/s). The equations for u, v, p, k, ϵ, f, m_{fu}, h are solved, in addition to the radiative transfer equation. Due to the highly non-linear property of these coupled equations, the combustion and radiation solutions are based on the converged turbulent flow and transport equations solutions as the initial fields. The E-factor is taken as 2 for all transport equations, and the variable under-relaxation parameters for all equations are taken from 0.3 to 0.7. The divisions of the solid angle $N\theta x N\phi = 1x4$ is used in the radiation computations. The inlet turbulent intensity is taken as 4.5% ($\lambda = 0.003$), and the inlet mixing length is given as 0.03 D. For the energy equation it is assumed that the heat transfer coefficients are known be experiments, where the cooling pipes-refractory wall combination of the furnace was replaced by an equivalent speckled wall with a temperature distribution based on measurements.

The following set of model constants are used,

C_μ	C_1	C_2	σ_k	σ_ϵ	σ_f	σ_{mfu}	σ_h	A
0.09	1.44	1.92	1.0	1.3	0.7	0.7	0.7	4.0

Since the standard turbulence model constants do not perform very well for round free jet, as recommended by Benim (1989), the model constants C_μ and C_2 are modified for the first half of the furnace as C_μ=0.075, C_2=1.89.

For CO_2-H_2O mixtures the emissivity is fitted by a one-clear three-gray gas model of Taylor and Foster (1974) in the temperature range 1200 - 2400 K. In this model, the total gas emittance is expressed as:

$$\epsilon_g = \sum_{n=1}^{4} (b_{1,n}+b_{2,n}\cdot T)\left[1-e^{-k_{g,n}(p_c+p_w)L}\right] \tag{5.3}$$

where the summation for n is over the gases of the assumed mixture, $b_{1,n}$ and $b_{2,n}$ are the weighting constants; p_w and p_c are the partial pressure of water vapour and carbon dioxide respectively, and L is a characteristic path length for a flow computational cell, taken as the square root of the sum of the squared sides of the element. Table 5.6 gives the values of the parameters under this model for a total pressure of 1 bar and p_w/p_c = 2 for gas combustion. The value of absorption coefficient k_g for the calculations is obtained from the "pseudogray" approximation (Abbas et al., 1984),

$$\epsilon_g = 1-e^{-k_g L} \tag{5.4}$$

In the computations, when the temperature is lower than 1200 K, the constant absorption coefficient k_g = 0.15 m^{-1} is assumed. The CPU time in IBM RISC/6000 model 520 is about 8.2 hours to obtain the converged solutions with residues for all

dependent variables less than 10^{-3}.

Table 5.6: Values of the coefficients $k_{g,n}$, $b_{1,n}$ and $b_{2,n}$ in the gas emissivity equations for a CO_2-H_2O mixture applicable to the temperature range 1200-2400 K.

n	$k_{g,n}$	$b_{1,n}$	$b_{2,n}$
1	0	0.346	0.0000473
2	0.69	0.266	0.0000719
3	7.4	0.252	-0.0000741
4	80.0	0.118	-0.0000452

5.9.3 Results

Figures 5.77 and 5.78 depict the predicted velocity field and temperature field, respectively.

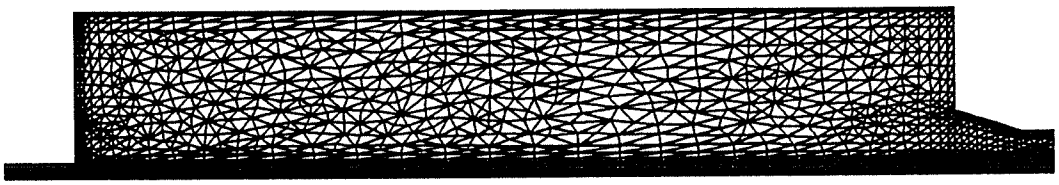

Figure 5.76: The computational mesh of M-2 trials flame-29

The predicted radial temperature profiles with and without radiation inside the furnace at four axial stations x = 0.555m, 1.295m, 2.775m and 5.735m are plotted

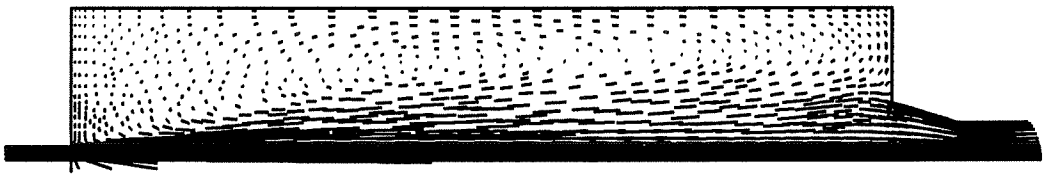

Figure 5.77: The velocity field of M-2 trials flame-29

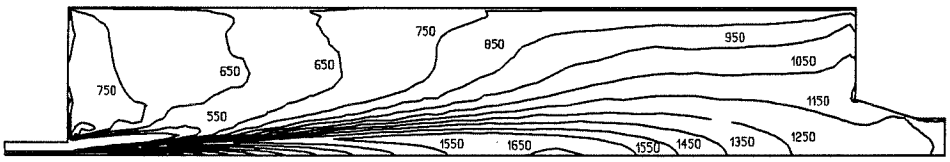

(a) WITHOUT RADIATION

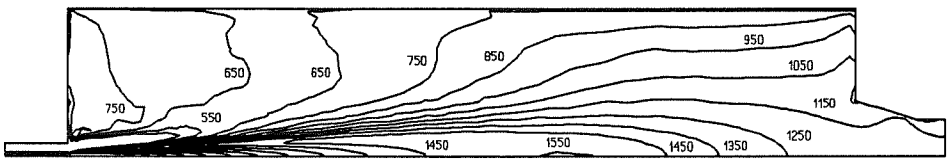

(b) WITH RADIATION

Figure 5.78: The temperature field of M-2 trials of flame-29 (deg. °C)

in Figure 5.79. The results with radiation are also compared with the finite element solution of Benim (1989), as shown in Figure 5.80. From Figure 5.79, in the mixing zone of the furnace (x=0.555m-1.295m), due to the fuel and oxygen is not fully

mixed, the temperature distributions at this region have shown a little difference between them with and without radiation. In the middle region of the furnace (x = 2.5-4.0m), the fuel and oxygen are fully mixed and burned, the mixture gas temperature is very high (up to the maximum temperature of 1550 °C at flame front, as shown in Fig. 5.78), then the radiation heat exchange between elements become very strong, the predicted maximum temperature with radiation is 110 °C less than that of without radiation in this region. From this temperature difference, we can see that the radiation is important for the large scale furnace calculations. Also, with radiation, the predicted temperature distribution becomes smooth in the flame zone. Outside the flame zone, due to a lower mixture gas temperature, the radiation becomes weaker, then the difference between with and without radiation is small. Near the exit of the furnace, the predicted temperature distribution with radiation is lower than that without radiation. The SCVFEM results are comparable with the finite element solutions of Benim (1989), as shown in Fig. 5.80, and they are agree well with experiments.

Axial temperature profile and axial concentrations of combustion products CO_2 and H_2O are also plotted in Figure 5.81 and 5.82, the results are compared with the experimental data.

The variation of the incident radiative heat flux along the furnace wall is shown in Figure 5.83. The result of the SCVFEM is comparable with the experiment and that of the finite element method (Benim, 1989).

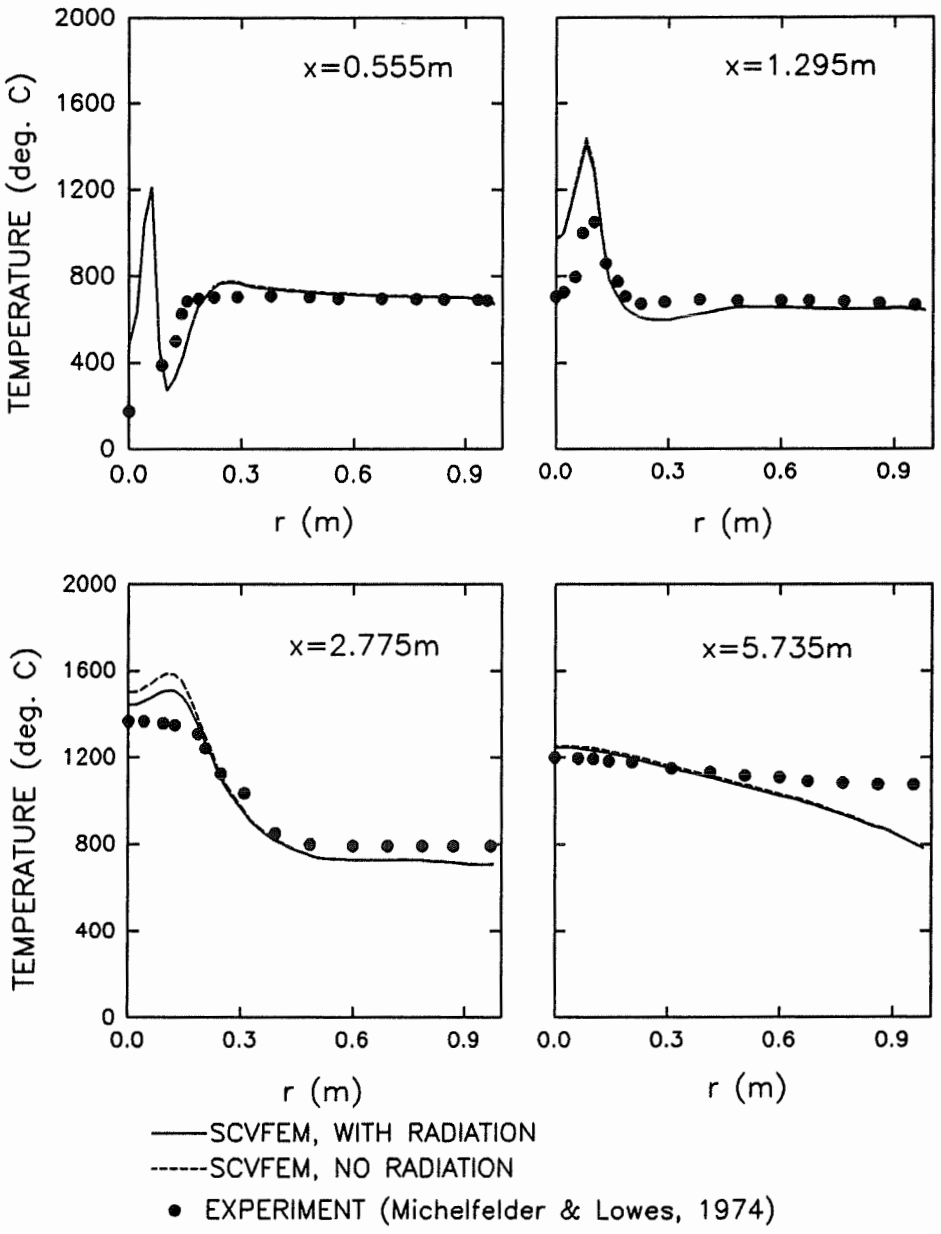

Figure 5.79: Comparison of the radial temperature profiles at four axial stations for turbulent reacting flows coupled with and without radiation using SCVFEM

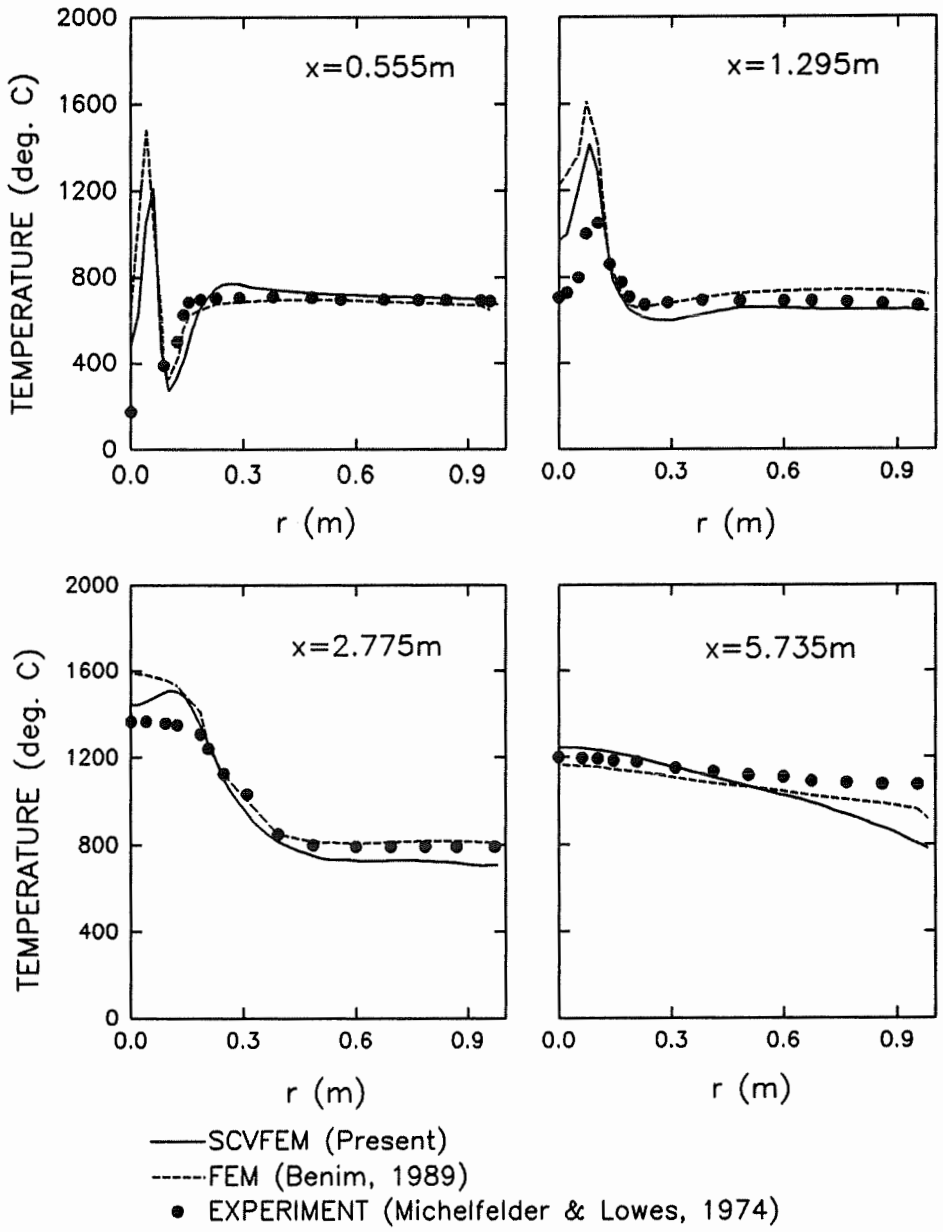

Figure 5.80: Comparison of the radial temperature profiles at four axial stations for turbulent reacting flows coupled with radiation between the SCVFEM and the finite element method predictions

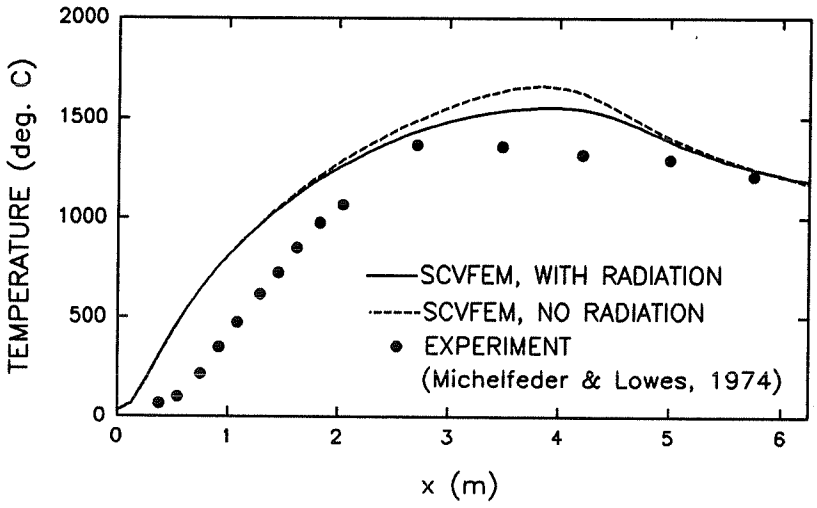

Figure 5.81: Comparison of the centerline axial temperature profiles between with and without radiation using the SCVFEM

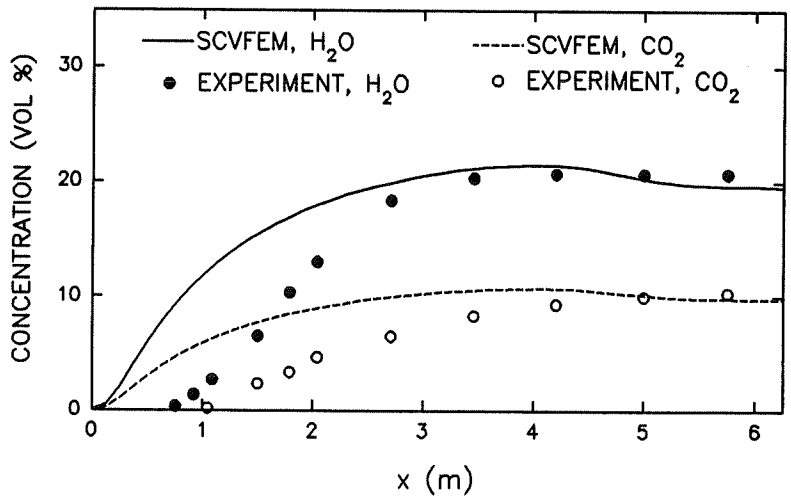

Figure 5.82: The centerline axial concentrations profiles of CO_2 and H_2O of M-2 trials flame-29

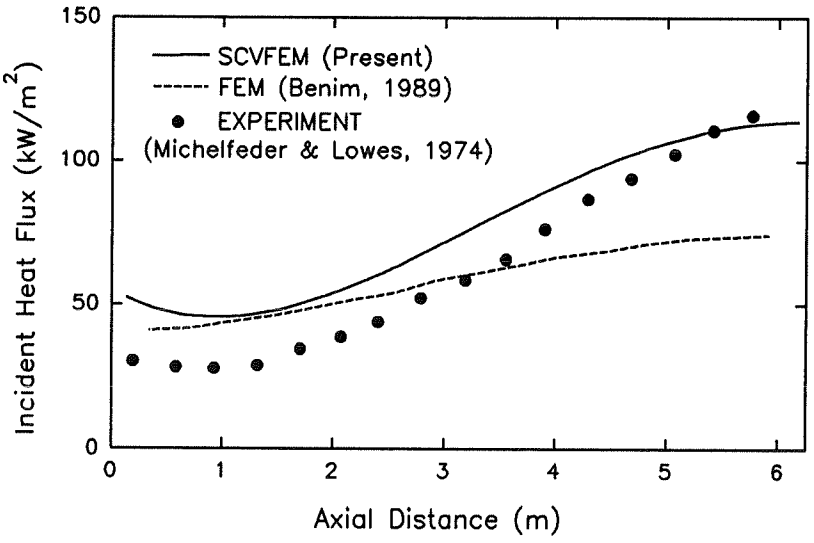

Figure 5.83: Comparison of the incident heat flux along the furnace wall between using the SCVFEM and the finite element method

Conclusions

The staggered control volume finite element method (SCVFEM) has been developed for the analysis of incompressible laminar and turbulent flows, turbulent reacting flows coupled with and without radiation, the following conclusions are drawn:

1. The present SCVFEM has been shown to predict successfully the various flow fields involving the complex physics in complex geometries.

2. The present algorithms share many useful features with successful finite difference, finite element and control volume finite element algorithms while retaining certain advantages of above algorithms such as the geometric flexibility, explicit physical interpretation, the imposition of natural boundary conditions and no necessity to impose the boundary condition for pressure.

3. The SCVFEM with Face-centered scheme has great features which is prior to most of the numerical methods with Vertex-centered scheme in the imposition of the boundary condition. With Face-centered scheme of SCVFEM, the imposition of the boundary condition for velocities, transport variables and radiation intensity at each boundary surface is straightforward, it avoids the difficulty with Vertex-centered scheme to impose the boundary conditions for above variables at the discontinuous corner point in the computational domain. Furthermore, with the equivalent number of unknowns and the same accuracy required, Face-centered scheme gives less CPU time than Vertex-centered scheme.

4. The sequential SCVFEM with the skewed, mass-weighted upwind interpolation function provides a robust approach for the computation of complex turbulent flows and turbulent reacting flows.

5. For turbulent flow over a backward facing step, the k-ϵ two equation model with wall function method is used. The implementation of the wall function is based on two methods, i.e. the classical approximation method and the direct iteration

method. The predicted recirculation length by using the classical approximation method is longer than that of by the direct iteration method. Both the classical approximation method and the direct iteration method underpredict the recirculation length by the error of 16% and 26%, respectively. At the fully developed flow region, the velocity profile obtained by the direct iteration method is very close to the experiments, it is better than that of by the classical approximation method. Also, the results obtained by Vertex-centered scheme is better than that of by Face-centered scheme.

6. The proposed SCVFEM with related combustion models has been successfully applied in the simulation of the 2D, confined axisymmetric turbulent diffusion flames, the agreement between experiments and predictions is reasonable. The predicted mixture fraction profiles by using the direct iteration method is very close to experiments, it is better than that of by using the classical approximation method. It seems that the direct iteration method is more diffusive than the classical approximation method.

7. The discrete transfer method was extended to an unstructured grid. From the benchmark tests, we found that for absorbing/emitting media, it gives excellent results; for pure scattering media, the results obtained by the discrete transfer method is comparable to other numerical methods.

8. The SCVFEM with combustion and radiation models are successfully applied to the prediction of practical furnace. For real furnace gas flame, the predicted temperature and radiant heat flux to the furnace wall agree well with experiments. From this tests, it is illustrated that the radiation heat transfer is very important for the large scale combustion furnace. Also, it is demonstrated that the classical approximation method is computational robust over the direct iteration method for the determination of wall functions in practical applications.

Recommendations

A few recommendations are intended as improvements and extensions of the present SCVFEM:

1. Because it is easy to impose the boundary condition for dependent variables with Face-centered scheme, extensions of the present SCVFEM with Face-centered scheme to second-order scheme and 3-Dimensional flows are straightforward. Also, the extension of the present incompressible SCVFEM to compressible flow is possible.

2. In order to use the present SCVFEM for the simulation of turbulent swirling flows, the additional improvements in the k-ϵ model (such as RNG k-ϵ model) or the use of more advanced an algebraic second-moment model (ASM) and a Reynolds-stress transport model (RSM) are necessary.

3. In order to predict the pollution products and more chemical species, the finite chemical kinetics combustion model should be considered for further study.

4. For gas combustion, the extension of the present discrete transfer method to 3-dimensional tetrahedral elements is straightforward. However, when considering an anisotropic scattering media, the discrete ordinates method is recommended.

5. For turbulent flows and turbulent reacting flows, an adaptive remeshing method will be considered in the future.

References

ABBAS, A.S., LOCKWOOD, F.C. and SALOOJA, A.P., 1984 "The Prediction of the Combustion and Heat Transfer Performance of a Refinery Heater," *Combustion and Flame*, Vol. 58, pp. 91-101.

ABBAS, A.S. and LOCKWOOD, F.C., 1986 "Prediction of Power Station Combustors," *Twenty-First Symp. (Int.) on Combustion*, pp. 285-292.

AFSHAR, M., 1992 *Investigation and Improvement of Some Recent FVM and CVFEM Practices for Two-Dimensional, Incompressible, Viscous Fluid Flow,* M.A.Sc. Thesis, McGill University, Montreal, Quebec, Canada.

AMANO, R.S., 1984 "Development of a Turbulence Near-Wall Model and Its Application to Separated and Reattached Flows," *Numerical Heat Transfer,* Vol. 7, pp. 59-75.

ASKARI-SARDHAI, A., LIEW, S.K., and MOSS, J.B., 1985 "Flamelet Modelling of Propane-Air Chemistry in Turbulent Non-Premixed Combustion," *Combust. Sci. and Tech.*, Vol. 44, pp. 89-95.

AUTRET, A. and GRANDOTTO, M. and DEKEYSER, I., 1987 "Finite Element Computation of a Turbulent Flow Over a Two-Dimensional Backward-Facing Step," *Int. J. Numer. Methods Fluids*, Vol. 7, pp. 89-102.

BAI, X.S. and FUCHS, L., 1993 "Calculation of Turbulent Combustion of Propane in Furnaces," *Int. J. for Numer. Methods in Fluids*, Vol. 17, pp. 221-239.

BAKER, A.J., 1983 *Computation of Fluid Flow By the Finite Element Method*, Hemisphere Publishing Corporation, Washington.

BALIGA, B.R. and PATANKAR, S.V., 1980 "A New Finite-Element Formulation for Convection-Diffusion Problems," *Numerical Heat Transfer*, Vol. 3, pp. 393-409.

BALIGA, B.R. and PATANKAR, S.V., 1983 "A Control Volume Finite-Element Method for Two-Dimensional Fluid Flow and Heat Transfer," *Numerical Heat Transfer*, Vol. 6, pp. 245-261.

BARTELDS, H., LOWES, T.M., MICHELFELDER, S., and PAI, B.R., 1973 "The Prediction of Heat Flux Distribution in Furnaces and Its Experimental Testing," *Comb. Instit. European Symposium*, Academic Press, London & New York, pp. 680-685.

BENIM, A.C. and ZINSER, W., 1985 "Investigation into the Finite Element Analysis of Confined Turbulent Flows Using a k-ϵ Model of Turbulence," *Comput. Meth. Appl. Mech. Eng.*, Vol. 51, pp. 507-523.

BENIM, A.C. and ZINSER, W., 1986 "A Segregated Formulation of Navier-Stokes Equations with Finite Elements," *Comput. Meth. Appl. Mech. Eng.*, Vol. 57, pp. 223-237.

BENIM, A.C., 1988 "A Finite Element Solution of Radiative Heat Transfer in Participating Media Utilizing the Moment Method," *Comput. Meth. Appl. Mech. Eng.*, Vol. 67, pp. 1-14.

BENIM, A.C., 1989 "Finite Element Solution of an Enclosed Turbulent Diffusion Flame," *Int. J. Numer. Meth. Fluids,* Vol. 9, pp. 289-303.

BENIM, A.C., 1990 "Finite Element Analysis of Confined Turbulent Swirling Flows," *Int. J. Numer. Meth. Fluids*, Vol. 11, pp. 697-717.

BIALECKI, R., 1991 "Applying the Boundary Element Technique to the Solution of Heat Radiation Problems in Cavities Filled by a Nongray Emitting-Absorbing Medium," *Numerical Heat Transfer*, Part A, Vol. 20, pp. 41-64.

BILGER, R., 1975 "Turbulent Diffusion Flames", *Progress in Energy and Combustion Science*, Vol. 1, pp. 87.

BILGER, R.W., 1980 "Turbulent Flows with Nonpremixed Reactants," *Topics in Applied Physics, Turbulent Reacting Flows,* Ed. by P.A. Libby and F.A. Williams, Springer-Verlag, New York.

BROOKS, A.N. and HUGHES, T.J.R., 1982 "Streamline Upwind/Petrov-Galerkin Formulations for Convection Dominated Flows with Particular Emphasis on the Incompressible Navier-Stokes Equations," *Comp. Meth. Appl. Mech. Eng.,* Vol. 32, pp. 199-259.

BUSNAINA, A.A., ZHENG, X. and SHARIF, M.A.R., 1991 "A Modified Skew Upwind Scheme for Fluid Flow and Heat Transfer Computations," *Appl. Math. Modelling,* Vol. 15, pp. 425-432.

BURNS, P.J., LOEHRKE, R.I., DOLAGHAN, J.S., and MALTBY, J.D., 1992 "Photon Tracing in Axisymmetric Enclosures," HTD-Vol. 203, *Developments in Radiative Heat Transfer*, ASME paper, pp. 93-100.

CALHOON, W.H., ROACH, R.L., 1993 "A New Upwind Procedure for the Incompressible Navier-Stokes Equations on Non-staggered Grids," *AIAA 93-0538, 31st Aerospace Sciences Meeting & Exhibit*, Jan. 11-14, Reno, NV.

CANT, R.S., ROGG, B., and BRAY, K.N.C., 1990 "On Laminar Flamelet Modelling of the Mean Reaction Rate in a Premixed Turbulent Flame," *Combust. Sci. and Tech.*, Vol. 69, pp. 53-61.

CARLSON, B.G. and LATHROP, K.D., 1968 "Transport Theory-the Method of Discrete Ordinates," *Computing Methods in Reactor Physics*, edited by Greenspan et al., Gordon and Breach, New York, pp. 171.

CARVALHO, M.G., DURAO,D.F.G. and PEREIRA, J.C.F., 1987 "Prediction of the Flow, Reaction and Heat Transfer in an Oxy-Fuel Glass Furnace," *Eng. Comput.-Int. J. Comput. Aided Eng. Software*, Vol. 4, pp. 23-34.

CARVALHO, M.G., OLIVEIRA, P. and SEMIAO, V., 1988 "A Three-Dimensional Modelling of an Industrial Glass Furnace," *J. of the Institute of Energy,* September, pp. 143-156.

CARVALHO, M.G., COELHO, P.J., 1990 "Numerical Prediction of an Oil-Fired Water Tube Boiler," *Eng. Comput.-Int. J. Comput. Aided Eng. Software*, Vol. 7, pp. 227-234.

CARVALHO, M.G., DURST, F. and PEREIRA, J.C.F., 1987 "Predictions and Measurements of Laminar Flow over Two-Dimensional Obstacles," *Appl. Math. Modelling*, Vol. 11, pp. 23-34.

CARVALHO,M.G., FARIAS, T. and FONTES, P., 1991 "Predicting Radiative Heat Transfer in Absorbing, Emitting, and Scattering Media Using the Discrete Transfer Method," HTD-Vol.160, *Fundamentals of Radiation Heat Transfer*, ASME, pp. 17-26.

CHAI, J.C., 1993 Personal Communication.

CHAI, J.C., LEE, H.S. and PATANKAR, S.V., 1993a "Radiation Heat Transfer Calculations Using a Control-Angle, Control-Volume-Based Discrete Ordinates Method," *AIAA-93-2731, Presented at the AIAA 28th Thermophysics Conference*, July 6-9, Orlando, FL.

CHAI, J.C., LEE, H.S. and PATANKAR, S.V., 1993b "Improved Treatment of Scattering Using the Discrete Ordinates Method," *UMSI 93/104*, July.

CHAI, J.C., LEE, H.S. and PATANKAR, S.V., 1993c "An Evaluation of Spatial Difference Practices for the Discrete-Ordinate Method," *UMSI 93/105*, July.

CHAI, J.C., LEE, H.S. and PATANKAR, S.V., 1993d "Ray Effect and False Scattering in the Discrete Ordinates Method," *UMSI 93/106*, July.

CHAI, J.C., LEE, H.S. and PATANKAR, S.V., 1993e "Treatment of Irregular Geometries Using a Cartesian-Coordinates-Based Discrete-Ordinates Method," HTD-Vol. 244, *Radiative Heat Transfer: Theory and Applications*, ASME, pp. 49-54.

CHAN, S.H., 1987 "Numerical Methods for Multidimensional Radiative Transfer Analysis in Participating Media," *Annu. Rev. Numer. Fluid Mech. and Heat Transfer*, Vol. 1, pp. 305-350.

CHATURVEDI, M.C., 1963 "Flow Characteristics of Axisymmetric Expansion," ASCE, *J. Hydraulic Div.*, Vol. 89, No. HY3, pp. 61-92.

CHANDRASEKHAR, S., 1960 *Radiative Transfer*, Dover, New York.

CHEN, J.Y., KOLLMANN, W., and DIBBLE, R.W., 1989 "PDF Modeling of Turbulent Nonpremixed Methane Jet Flames," *Combust. Sci. and Tech.*, Vol. 64, pp.315-346.

CHEN, C.-J., 1988, "Finite Analytic Method," in *Handbook of Numerical Heat Transfer*, pp. 723-746, Ed. by W.J. Minkowycz, E.M. Sparrow, G.E. Schneider, R.H. Pletcher, John Wiley & Sons, Inc., New York.

CHIENG, C.C. and LAUNDER, B.E., 1980 "On the Calculation of Turbulent Heat Transport Downstream from an Abrupt Pipe Expansion," *Numerical Heat Transfer*, Vol. 3, pp. 189-207.

CHIU, E.H., 1990 *Modelling of Radiative Heat Transfer in Participating Media by the Finite Volume Method*, Ph.D. Thesis, University of Waterloo, Dept. of Mech. Eng., Waterloo, Ontario, Canada.

CHORIN, A.J., 1976 "A Numerical Method for Solving Incompressible Viscous Flow Problems," *J. Comp. Phys.*, Vol. 2, pp. 12-26.

CHUNG, T.J., 1978 *Finite Element Analysis of Fluid Dynamics*, McGraw-Hill Book Co. Ltd., Toronto.

CHUNG, T.J., 1993 *Numerical Modeling in Combustion*, Chapter 6: Finite Element Methods in Turbulent Combustion, Edited by T.J. Chung, Taylor & Francis.

CHRISTIE, I., GRIFFITHS, D.F., MITCHELL, A.R. and ZIENKIEWICA, O.C., 1976 "Finite Element Method for Second Order Differential Equations with Significant First Derivatives," *Int. J. Numer. Methods Eng.*, Vol. 10, pp. 1389-1396.

COELHO, P.J. and PEREIRA,J.C.F., 1992 "Calculation of a Confined Axisymmetric Laminar Diffusion Flame Using a Local Grid Refinement Technique," HTD-Vol. 199, *Heat Transfer in Fire and Combustion Systems*, ASME, pp.159-165.

COELHO, P.J. and CARVALHO, M.G., 1993 "Application of a Domain Decomposition Technique to the Mathematical Modelling of a Utility Boiler," *Int. J. Numer. Methods Eng.*, Vol. 36, pp. 3401-3419.

COMINI, G. and DEL GIUDICE, S., 1985 "A (k-ϵ) Model of Turbulent Flow," *Numerical Heat Transfer*, Vol. 8, pp. 133-147.

CROUZEIX, M. and RAVIART, P.A., 1973 "Conforming and Non-Conforming Finite Element Methods for the Stationary Stokes Eq.," *RAIRO,* R3, pp.33-76.

DAVISON, B., 1957 *Neutron Transport Theory*, Oxford at the Clarendon Press.

DEMARCO, A.G. and LOCKWOOD, F.C., 1975 "A New Flux Model for the Calculation of Three Dimensional Radiation Heat Transfer," *La Rivista du Combustibili,* Vol. 5, pp. 184.

DOCHERTY, P. and FAIRWEATHER, M., 1988 "Predictions of Radiative Transfer from Nonhomogeneous Combustion Products Using the Discrete Transfer Method," *Combustion and Flame*, vol. 71, pp. 79-87.

DRIVER, D.M. and SEEGMILLER, H.L., 1985 "Features of a Reattaching Turbulent Shear Layer in Divergent Channel Flow," *AIAA J.*, Vol. 23, pp. 163-171.

DUNCAN, B.S., LIOU, W.W., and SHIH, T.H., 1993 "A Multiple-Scale Turbulence Model for Incompressible Flow," *AIAA 93-0086, 31st Aerospace Sciences Meeting & Exhibit*, Jan. 11-14, Reno, NV.

EDWARDS, D.K., 1976 "Molecular Gas Band Radiation," in: *Advances in Heat Transfer*, T.F. Irvine, Jr., J.P. Hartnrtt, eds., Academic Press, New York, Vol. 12, pp. 115-193.

ENGELMAN, M.S., 1991 *FIDAP Examples Manual,* Version 6.0.

ENGELMAN, M.S. and JAMNIA, M.-A., 1991 "Gray-Body Surface Radiation Coupled With Conduction and Convection for General Geometries," *Int. J. Numer. Methods Fluids*, Vol. 13, pp. 1029-1053.

ELKAIM, D., REGGIO, M. and CAMARERO, R., 1992 "Simulating Two-Dimensional Turbulent Flow by Using the k-ϵ Model and the Vorticity-Streamfunction Formulation," *Int. J. Numer. Methods Fluids*, Vol. 14, pp. 961-980.

ELKAIM, D., REGGIO, M. and CAMARERO, R., 1993 "Control Volume Finite-Element Solution of a Confined Turbulent Diffusion Flame," *Numerical Heat Transfer*, Part A, Vol. 23, pp. 259-279.

FAIRWEATHER, M., JONES, W.P. and LINDSTEDT, R.P., 1992 "Predictions of Radiative Transfer from a Turbulent Reacting Jet in a Cross-Wind," *Computer and Fluids*.

FAROUK, B. and SIDAWI, M.M., 1993 "Effects of Nitrogen Removal in a Natural Gas Fired Industrial Furnace: A Three Dimensional Study," HTD-Vol. 250, *Heat Transfer in Fire and Combustion Systems*, ASME, pp. 173-183.

FAVRE, A., 1969 "Statistical Equations of Turbulent Gases", *Problems of Hydrodynamics and Continuum Mechanics*, SIAM, pp.231-236.

FIVELAND, W.A., 1984 "Discrete Ordinates Solutions of the Radiative Transport Equation for Rectangular Enclosures," *J. of Heat Transfer*, Vol. 106, pp. 699-706.

FIVELAND, W.A., 1988 "Three Dimensional Radiative Heat Transfer Solution by the Discrete Ordinates Method," *Journal of Thermophysics and Heat Transfer*, Vol. 2, pp. 309-316.

FIVELAND, W.A., 1991 "The Selection of Discrete Ordinate Quadrature Sets for Anisotropic Scattering," HTD-Vol. 160, *Fundamentals of Radiation Heat Transfer*, ASME, pp. 89-96.

FIVELAND, W.A. and JESSEE, J.P., 1993 "A Finite Element Formulation of the Discrete-Ordinates Methods for Multidimensional Geometries," HTD-Vol. 244, *Radiative Heat Transfer: Theory and Applications*, ASME, pp.41-48.

FIVELAND, W.A. and WESSEL, R.A., 1986 "FURMO: A Numerical Model for Predicting Performance of Three-Dimensional Pulverized-Fuel Fired Furnaces,"

Presented at the Jt. AIAA/ASME Thermophysics and Heat Transfer Conference, Boston, Mass., 86-HT-35.

FLUENT, INC., 1993 *Introduction to the Renormalization Group Method and Turbulence Modeling*, Technical Memorandum, TM-107, Jan. 1993.

GARON, A., 1994 Personal Communication.

GHIA, U., GHIA, K.N. and SHIN, C.T., 1982 "High-Re Solutions for Incompressible Flow Using the Navier-Stokes Equations and a Multigrid Method," *J. of Comput. Physics*, Vol. 48, pp. 387-411.

GLASSNER, A.S., 1989 *An Introduction to Ray Tracing*, Academic Press, New York.

GOODY, R.M., 1964 *Atmospheric Radiation*: Part 1 - Theoretical Basis, The Clarendon Press, Oxford.

GORDON, S. and MCBRIDE, B.J., 1971 "Computer Program for Calculation of Complex Chemical Equilibrium Composition, Rocket Performance, Incident and Reflected Shock and Chapman Jouguent Detonations", *NASA*-sp 273.

GORNER, K. and DIETZ, U., 1993 "Calculations of Radiative Exchange by the Monte-Carlo Method. Theory and Applications to Industrial Combustion Systems," *International Chemical Engineering*, Vol. 33, No. 2, pp. 165-177.

GOSMAN, A.D., PUN, W.M., RUNCHAL, A.K., SPALDING, D.B. and WOLFSHTEIN, M., 1969 *Heat and Mass Transfer in Recirculating Flows*, Academic Press Ltd., New York.

GOSMAN, A.D. and LOCKWOOD, F.C., 1973 "Incorporation of a Flux Model for Radiation into a Finite-Difference Procedure for Furnace Calculation," *14th Symp. (Int.) on Combustion*, pp. 661-671.

GOSMAN, A.D. and LOCKWOOD, F.C. and SALOOJA, A.P., 1978 "The Prediction of Cylindrical Furnaces Gaseous Fueled with Premixed and Diffusion Burners," *16th Symp. (Int.) on Combustion*, pp. 747-760.

GUPTA, R.P., WALL, T.F. and TRUELOVE, J.S., 1983 "Radiative Scatter by Fly Ash in Pulverized-Coal-Fired Furnaces: Application of the Monte Carlo Method to Anisotropic Scatter," *Int. J. Heat Mass Transfer*, Vol. 26, No. 11, pp. 1649-1660.

HAIDEKKER, A., 1991 *Radiation Modelling in Complex Three Dimensional Enclosures*, M.A.Sc. Thesis, Université du Québec à Chicoutimi, Chicoutimi, Québec, Canada.

HALL, C.A., CAVENDISH, J.C. and FREY, W.H., 1991 "The Dual Variable Method for Solving Fluid Flow Difference Equations on Delaunay Triangulations," *Computers Fluids*, Vol. 20, No. 2, pp. 145-164.

HARLOW, F.H. and WELCH, J.E., 1965 "Numerical Calculation of Time-Dependent Viscous Incompressible Flow of Fluid with Free Surface," *Phys. Fluids*, Vol. 8, pp. 2182-2189.

HAUTMAN, D.J., DRYER, F.L.,SCHUG, K.P. and GLASSMAN,I., 1981 "A Multi-Step Overall Kinetic Mechanism for Oxidation of Hydrocarbons," *Combust. Sci. Technol.*, Vol. 25, pp.219-235.

HEINRICH, J.C., HUYAKORN, P.S., ZIENKIEWICZ, O.C. and MITCHELL, A.R., 1977 "An "Upwind" Finite Element Scheme for Two-Dimensional Convective Transport Equation," *Int. J. Numer. Methods Eng.*, Vol. 11, pp. 131-143.

HEYWOOD, J.B., 1986 *Internal Combustion Engine Fundamentals*, McGill-Hill, NY.

HILL, D.L. and BASKHARONE, E.A., 1993 "A Monotone Streamline Upwind Method for Quadratic Finite Elements," *Int. J. Numer. Methods Fluids,* Vol. 17, pp.463-475.

HJERTAGER, B.H. and MAGNUSSEN, B.F., 1982 "Computer Simulation of Flow, Heat Transfer and Combustion in Three-Dimensional Furnaces," Arch. Combust., 2(1-2), pp.25-48.

HOOKEY, N.A., 1989 *A Control Volume Finite-Element Methods for Steady Two-dimensional Viscous Compressible Flows*, Ph.D. Thesis, McGill University, Montreal, Quebec, Canada.

HOOKEY, N.A. and BALIGA, B.R., 1988 "Evaluation and Enhancements of Some Control Volume Finite-Element Methods: Part II - Fluid Flow Problems," *Numerical Heat Transfer*, Vol. 14, pp. 273-293.

HOTTEL, H.C. and COHEN, E.S., 1958 "Radiant Heat Exchange in a Gas-FilledEnclosure: Allowance for Non-Uniformity of Gas Temperature," *AICHE J.*, Vol. 4, No. 1, pp. 3-14.

HOTTEL, H.C. and SAROFIM, A., 1967 *Radiative Transfer*, McGraw-Hill, NY.

HOWELL, J.R., 1968 "Application of Monte Carlo to Heat Transfer Problems," *Advances in Heat Transfer*, Vol. 5, pp. 1-54, Academic Press, New York.

HOWELL, J.R., 1988 "Thermal Radiation in Participating Media: The Past, the Present, and Some Possible Futures," *J. of Heat Transfer*, Vol. 110, pp. 1220-1226.

HSU, A.T., TSAI, Y-L.P. and RAJU, M.S., 1993 "A PDF Approach for Compressible Turbulent Reacting Flows," AIAA 93-0087, *31st Aerospace Sciences Meeting & Exhibit*, Jan. 11-14, Reno, NV.

HUGHES, T.J.R., LIU, W.K. and BROOKS, A., 1979 "Finite Element Analysis of Incompressible Viscous Flows by the Penalty Function Formulation," *J. Comp. Phys.*, Vol. 30, pp. 1-60.

HUGHES, T.J.R., 1987 "Recent Progress in the Development and Understanding of SUPG Methods with Special Reference to the Compressible Euler and Navier-Stokes Equations," *Int. J. for Numerical Methods in Fluids*, vol. 7, pp. 1261-1275.

HYDE, D.J. and TRUELOVE, J.S., 1977 "The Discrete Ordinates Approximation for Multi-Dimensional Radiant Heat Transfer in Furnaces," *AERE Report*, AERE-R 8502.

ISSA, R.I., 1985 "Solution of the Implicity Discretized Fluid Flow Equations by Operator-Splitting," *J. of Comp. Phys*, Vol. 62, pp. 40-65.

JAMALUDDIN, A.S. and SMITH, P.J., 1988a "Predicting Radiative Transfer in Rectangular Enclosures Using the Discrete Ordinates Method," *Combustion Science and Technology*, Vol. 59, pp. 321-340.

JAMALUDDIN, A.S. and SMITH, P.J., 1988b "Predicting Radiative Transfer in Axisymmetric Cylindrical Enclosures Using the Discrete Ordinates Method," *Combustion Science and Technology*, Vol. 62, pp. 173-186.

JAMALUDDIN, A.S. and SMITH, P.J., 1992 "Discrete-Ordinates Solution of Radiative Transfer Equation in Nonaxisymmetric Cylindrical Enclosures," *Journal of Thermophysics and Heat Transfer*, Vol. 6, pp.242-245.

JAMES, R.K. and EDWARDS, D.K., 1977 "Effect of Molecular Gas Radiation on a Planar, Two-Dimensional, Turbulent-Jet-Diffusion Flame," *J. of Heat transfer*, Vol. 99, pp. 221-226.

JAMNIA, M.-A., 1992 "Participating Gray Body Radiation Coupled with Conduction and Convection for General Geometries," HTD-Vol. 203, *Developments of Radiative Heat Transfer*, ASME, pp. 197-205.

JAYATILLEKE, C.L.V., 1969 "The Influence of Prandtl Number on the Resistance of the Laminar Sub-Layer to Momentum and Heat Transfer," *Progress in Heat and Mass transfer*, Vol. 1, pp. 193-199.

JESSEE, J.P., GANSMAN, R.F., and FIVELAND, W.A., 1993 "Calculation of Chemically Reacting Flows Using Finite Kinetics," HTD-Vol. 250, *Heat Transfer in Fire and Combustion Systems*, ASME, pp. 43-53.

JOHNSON, T.R., LOWES, T.M. and BEER, J.M., 1972 "Comparison of Calculated Temperatures and Heat Flux Distributions with Measurements in the Ijmuiden Furnace," *4th Symp. on Flames and Industry*, London.

JONES, W.P., 1979 "Models for Turbulent Flows with Variable Density and Combustion", *Prediction Methods for Turbulent Flows*, Lecture Series 1979-2, Von Karman Institute for Fluid Dynamics, Jan. 15-19.

JONES, W.P. and WHITELAW, J.H., 1982 "Calculation Methods for Turbulent Reacting Flows; A Review" *Combustion and Flame*, vol.48, pp.1-26.

KARKI, K.C., and PATANKAR, S.V., 1988 "Calculation Procedure for Viscous Incompressible Flows in Complex Geometries," *Numerical Heat Transfer*,Vol. 14, pp. 295-307.

KEE, R.J., MILLER, J.A., and JEFFERSON, T.H., 1980 "A General Purpose, Transportable, FORTRAN Chemical Kinetica Package," *Sandia National Laboratories Report*, SAND80-8003.

KENT, J.H. and BILGER, R.W., 1976 "The Prediction of Turbulent Diffusion Flame Fields and Nitric Oxide Formation", *Sixteenth Symposium (Intl) on Combustion*, pp. 1643-1656.

KHALIL, E.E., SPALDING, D.B. and WHITELAW, J.H., 1975 "The Calculation of Local Flow Properties in Two-Dimensional Furnaces," *Int. J. Heat Mass Transfer*, Vol. 18, pp. 775-791.

KHALIL, E.E., 1982 *Modelling of Furnaces and Combustors*, Abacus Press, Turnbridge Wells, U.K.

KIM, Y.M., 1987 *Finite Element Methods in Turbulent Combustion*, Ph.D. thesis, The University of Alabama in Huntsville.

KIM, Y.M. and CHUNG, T.J., 1989 "Turbulent Combustion Analysis with Various Probability Density Functions," *Proc. of 9th AIAA CFD Meeting*, Buffalo, New York, pp. 594-601.

KIM, T.K. and LEE, H.S., 1988 "Effects of Anisotropic Scattering on Radiative Heat Transfer in Two-Dimensional Rectangular Enclosures," *Int. J. of Heat and Mass Transfer*, Vol. 31, pp. 1711-1721.

KOBAYASHI, M.H., and PEREIRA, J.C.F., 1991 "Calculation of Incompressible Laminar Flows on a Nonstaggered, Nonorthogonal Grid," *Numerical Heat Transfer*, Part B, Vol. 19, pp.243-262.

LARSEN, M.E. and HOWELL, J.R., 1985 "The Exchange Factor Method: An Alternative Basis for Zonal Analysis of Radiating Enclosures," *ASME, J. of Heat Transfer,* Vol. 107, pp. 936-942.

LATHROP, K.D., 1968 "Ray Effects in Discrete Ordinates Equations," *Nuclear Science and Engineering*, Vol. 32, pp. 357-369.

LAUNDER, B.E. and SPALDING, D.B., 1974 "The Numerical Computation of Turbulent Flow," *Comp. Meth. Appl. Mech. Eng.*, Vol. 3, pp. 269-289.

LEONARD, B.P., 1979 "A Stable and Accurate Convective Modelling Procedure Based on Quadratic Upstream Interpolation," *Comp. Meth. Appl. Mech. Eng.*, Vol. 19, pp. 59-98.

LEWIS, M.H. and SMOOT, L.D., 1981 "Turbulent Gaseous Combustion, Part I: Local Species Concentration Measurements", *Combustion and Flame*, Vol. 42, pp. 183-196.

LIEW, S.K., BRAY, K.N.C., and MOSS, J.B., 1981 "A Flamelet Model of Turbulent Non-Premixed Combustion," *Combust. Sci. and Tech.*, Vol. 27, pp.69-73.

LIEW, S.K., BRAY, K.N.C., and MOSS, J.B., 1984 "A Stretched Laminar Flamelet Model of Turbulent Nonpremixed Combustion," *Comb. and Flame*, Vol. 56, pp.199-213.

LISIENKO, V.G., MALIKOV, G.K. and MALIKOV, YU.K., 1992 "Zone-Node Method for Calculating Radiant Gas Flows in Complex Geometry Ducts," *Numerical Heat Transfer*, Part B, Vol. 22, pp. 1-24.

LIU, C., LIU, Z., and MCCORMICK, S., 1993 "Multigrid Methods for Numerical Simulation of Laminar Diffusion Flames," *AIAA 93-0236, 31st Aerospace Sciences Meeting & Exhibit*, Jan. 11-14, Reno, NV.

LOCKWOOD, F.C., EL-MAHALLAWY, F.M. and SPALDING, D.B., 1974 "An Experimental and Theoretical Investigation of Turbulent Mixing in a Cylindrical Furnace," *Combustion and Flame*, Vol. 23, pp. 283-293.

LOCKWOOD, F.C. and NAGUIB, A.S., 1975 "The Prediction of the Fluctuations in the Properties of Free, Round-Jet, Turbulent, Diffusion Flames" *Combustion and Flame*, Vol. 24, pp. 109-124.

LOCKWOOD, F.C. and SHAH, N.G., 1978 "Evaluation of an Efficient Radiation Flux Model for Furnace Prediction Procedures," *Proc. 6th Int. Heat Transfer Conference*, Toronto.

LOCKWOOD, F.C. and SHAH, N.G., 1981 "A New Radiation Solution Method for Incorporation in General Combustion Prediction Procedures," *18th Symp.(Int.) on Combustion*, pp. 1405-1414.

LOCKWOOD, F.C. and SPALDING, D.B., 1971 "Prediction of a Turbulent Duct Flow with Significant Radiation," *Proc. Thermodynamics Colloquium, Société Française de Physique*, Evian.

LOWES, T.M., BARTELDS, H, HEAP, M.P., MICHELFELDER, S. and PAI, B.R., 1973 "The Prediction of Radiant Heat Transfer in Axi-symmetrical Systems," Doc. Nr. G02/a/25, International Flame Research Foundation (IFRF),IJmuiden, The Netherlands.

MAJUMDAR, S., 1988 "Role of Underrelaxation in Momentum Interpolation for Calculation of Flow with Nonstaggered Grids," *Numerical Heat Transfer*, Vol. 13, pp. 125-132.

MALISKA, C.R. and RAITHBY, G.D., 1984 "A Method for Computing Three-Dimensional Flows Using Non-Orthogonal Boundary-Fitted Co-ordinates," *Int. J. Numer. Meth. Fluids*, Vol. 4, pp. 519-537.

MAGNUSSEN, B.F. and HJERTAGER, B.H., 1976 "On Mathematical Modelling of Turbulent Combustion with Special Emphasis on Soot Formation and Combustion", *Sixteenth Symposium (Intl) on Combustion,* pp. 719-729.

MANOUZI, H. and FORTIN, M., 1991 "A Treatment of Wall Boundaries for Turbulent Flows by the Use of a Transmission Finite Element Method," *Int. J. Numer. Methods Eng.*, Vol. 31, pp. 113-126.

MASSON, C., SAABAS, H.J. and BALIGA, B.R., 1994 "Co-located Equal-Order Control-Volume Finite-Element Method for Two-Dimensional Axisymmetric Incompressible Fluid Flow," *Int. J. Numer. Methods Fluids*, Vol. 18, pp. 1-26.

MCKENTY, F., 1992 *Modèles de Combustion pour la Simulation Numérique D'Ecoulements Réactifs en Atmosphère Confinée*, Ph.D Thesis, Ecole Polytechnique, Montreal, Quebec, Canada.

MCKENTY, F., MENG, F.L., CAMARERO, R., 1993 "Comparative Study of Four Combustion Models for the Simulation of Turbulent Methane-Air Flames Using the Control Volume Finite Element Method," ASME, *The 1993 International Joint Power Generation Conference & Exposition*, Kansas City, Missouri.

MCMURTRY, P.A., and GIVI, P., 1989 "Direct Numerical Simulations of Mixing and Reaction in a Nonpremixed Homogeneous Turbulent Flow," *Combustion and Flame*, Vol. 77, pp. 171-185.

MENG, F.L., MCKENTY, F., ELKAIM, D. and CAMARERO, R., 1992 "Predicting Radiative Heat Transfer in Two-Dimensional Rectangular and Axisymmetric Enclosures Using the Discrete Transfer Method," *Advanced Computational Methods*

in Heat Transfer II, Vol. 1: Conduction, Radiation and Phase Change, pp. 161-180.

MENG, F.L., MCKENTY, F. and CAMARERO, R., 1993 "Radiative Heat Transfer by the Discrete Transfer Method Using an Unstructured Mesh," HTD-Vol. 244, *Radiative Heat Transfer: Theory and Applications*, ASME. pp.55-66.

MENGÜÇ, M.P. and VISKANTA, R., 1985 "Radiative Transfer in Three Dimensional Rectangular Enclosures Containing Inhomogeneous, Anisotropically Scattering Media," *J. Quant. Spectrosc. Radiat. Transfer*, Vol.33, No.6, pp. 533-549.

MENTER, F.R., 1992 "Influence of Freestream Values on K-ω Turbulence Model Predictions," *AIAA J.*, Vo. 30, No. 6, pp. 1657-1659.

MICHELFELDER, S., 1976 *Beitrag zur Berechung des Abbrands und der Wärmeübertragung von nichtleuchtenden Gasflammen*, Dissertation, University of Stuttgart, Stuttgart, Federal Republic of Germany.

MICHELFELDER, S. and LOWES, T.M., 1974 "Report on the M-2 Trials," *IFRF Report*, Doc. No. F36/a/4.

MILLER, J.A., and BOWMAN, C.T., 1989 "Mechanism and Modeling of Nitrogen Chemistry in Combustion," *Prog. Energy Combust. Sci.*, 15, pp. 287-338.

MILLER, T.F., and SCHMIDT, F.W., 1988 "Use of a Pressure-Weighted Interpolation Method for the Solution of the Incompressible Navier-Stokes Equations on a Nonstaggered Grid System," *Numerical Heat Transfer*, Vol. 14, pp. 213-233.

MITCHELL, R.E., SAROFIM, A.F., and CLOMBURG, L.A., 1980 "Experimental and Numerical Investigation of Confined Laminar Diffusion Flames," *Combust. and Flame*, Vol. 37, pp. 227-244.

MODEST, M.F., 1975 "Radiative Equilibrium in a Rectangular Enclosure Bounded by Gray Walls," *J. Quant. Spectrosc. Radiat. Transfer*, Vol. 15, No. 6, pp. 445-461.

MODEST, M.F. and SIKKA, K.K., 1991 "The Stepwise Gray P-1 Approximation for Multi-Dimensional Radiative Transfer in Molecular Gas-Particulate Mixtures," HTD-Vol. 160, *Fundamentals of Radiation Heat Transfer*, ASME, pp.97-103.

MORGAN, K., HUGHES, T.G. and TAYLOR, C., 1977 "Investigation of a Mixing Length and a Two-Equation Turbulence Model Utilizing the Finite Element Method," *Appl. Math. Modelling*, Vol. 1.

MORGAN, K., HUGHES, T.G. and TAYLOR, C., 1979 "The Analysis of Turbulent, Free-Shear, and Channel Flows by the Finite Element Method," *Comp. Meth. Appl. Mech. Eng.*, Vol. 19, pp.117-125.

MUKHOPADHYAY, A., SUNDARARAJAN, T., and BISWAS, G., 1993 "An Explicit Transient Algorithm for Predicting Incompressible Viscous Flows in Arbitrary Geometry," *Int. J. Numer. Methods Fluids*, Vol. 17, pp. 975-993.

MURTHY, J.Y. and CHOUDHURY, D., 1992 "Computation of Participating Radiation in Complex Geometries," HTD-Vol. 203, *Developments in Radiative Heat Transfer*, ASME, pp. 153-160.

NARAGHI, M.H.N. and CHUNG, B.T.F. and LITKOUHI, B., 1988 "A Continuous Exchange Factor Method for Radiative Exchange in Enclosures with Participating Media," *J. of Heat Transfer*, Vol. 110, pp. 456-462.

NICOLAIDES, R.A., 1989 "Flow Discretization by Complementary Volume Techniques," AIAA paper 89-1978, *Proceedings of 9th AIAA CFD Mtg.*, Buffalo, NY.

NICOLAIDES, R.A., 1991 "Covolume Algorithms," *Proc. 4th Inter. Symp. Num. Meth. CFD*, Davis, CA.

NIKJOOY, M., SO, R.M.C., and PECK, R.E., 1988 "Modelling of Jet- and Swirl-stabilized Reacting Flows in Axisymmetric Combustors," *Combust. Sci. and Tech.*, Vol. 58, pp. 135-153.

NORRIS, L.H. and REYNOLDS, W.C., 1975 "Turbulent Channel Flow with a Moving Wavy Boundary," Rept. No. FM-10, Stanford University, Dept. Mech. Eng..

O'BRIEN, E.E., 1980 "The Probability Density Function (pdf) Approach to Reacting Flows," *Topics in Applied Physics, Turbulent Reacting Flows,* Ed. by P.A. Libby and F.A. Williams, Springer-Verlag, New York.

PAGE, M., GARON, A. and CAMARERO, R., 1989 "LUSS: Sous-Programmes pour la Résolution d'un Système d'Equations Algébriques Stockées en Ligne de Ciel," EPM/RT-89/13, Ecole Polytechnique, Montreal, Canada.

PAI, B.R., MICHELFELDER, S. and SPALDING, D.B., 1978 "Prediction of Furnace Heat Transfer with a Three-Dimensional Mathematical Model," *Int. J. Heat Mass Transfer*, Vol. 21, pp. 571-580.

PATANKAR, S.V. and SPALDING, D.B., 1972 "A Calculation Procedure for Heat, Mass and Momentum Transfer in Three-Dimensional Parabolic Flows," *Int. J. Heat Mass Transfer*, Vol. 15, pp. 1787-1806.

PATANKAR, S.V. and SPALDING, D.B., 1974 "Simultaneous Predictions of Flow Patterns and Radiation for Three-Dimensional Flames," *Heat Transfer in Flames*, pp. 73-94. N.H. Afgan and J.M. Beer, eds., Scripta Book Company, Washington, D.C.

PATANKAR, S.V., 1980 *Numerical Heat Transfer and Fluid Flow*, Hemisphere Publishing Corporation, Washington.

PATANKAR, S.V., 1981 "A Calculation Procedure for Two-Dimensional Elliptic Situations," *Numerical Heat Transfer*, Vol. 4, pp. 409-425.

PATEL, M.K., MARKATOS, N.C., 1986 "An Evaluation of Eight Discretization Schemes for Two-Dimensional Convection-Diffusion Equations," *Int. J. for Numerical Methods in Fluids*, Vol. 6, pp. 129-154.

PATEL, V.C., RODI, W. and SCHEUERER, G., 1985 "Turbulence Models for Near-Wall and Low-Reynolds-Number Flows: A Review," *AIAA J.*, Vol. 23, pp. 1308-1319.

PERIC, M., KESSLER, R. and SCHEUERER, G., 1988 "Comparison of Finite-Volume Numerical Methods with Staggered and Colocated Grids," *Computers & Fluids*, Vol. 16, No. 4, pp.389-403.

POLLARD, A. and SIU, L. W. A., 1982 "The Calculation of Some Laminar Flows Using Various Discretisation Schemes," *Comp. Meth. Appl. Mech. Eng.*, Vol. 35, pp. 293-313.

POPE, S.B., 1976 "The Probability Approach to the Modelling of Turbulent Reactive Flows", *Combustion and Flame*, vol.27, pp. 299.

PRAKASH, C., PATANKAR, S.V., 1985 "A Control Volume-Based Finite-Element Method for Solving the Navier Stokes Equations Using Equal-Order Velocity-Pressure Interpolation," *Numerical Heat Transfer*, Vol. 8, pp. 259-280.

PRAKASH, C., 1986 "An Improved Control Volume Finite-Element Method for Heat and Mass Transfer, and for Fluid Flow Using Equal-Order Velocity-Pressure Interpolation," *Numerical Heat Transfer*, Vol.9, pp. 253-276.

RADHAKRISHNAN, K., 1988, "Fast Algorithm for Calculating Chemical Kinetics in Turbulent Reacting Flow," *Combust. Sci. and Tech.*, Vol. 58, pp.155-176.

RAITHBY, G.D.,TORRANCE, K.E., 1974 "Upstream-Weighted Differencing Schemes and Their Application to Elliptic Problems Involving Fluid Flow," *Computers and Fluids*, Vol. 2, pp. 191-206.

RAITHBY, G.D., 1976a "A Critical Evaluation of Upstream Differencing Applied to Problems Involving Fluid Flow," *Comp. Meth. Appl. Mech. Eng.*, Vol. 9, pp. 75-103.

RAITHBY, G.D., 1976b "Skew Upstream Differencing Schemes for Problems Involving Fluid Flow," *Comp. Meth. Appl. Mech. Eng.*, Vol. 9, pp. 153-164.

RAITHBY, G.D. and Chui, E.H., 1990 "A Finite-Volume Method for Predicting Radiant Heat Transfer in Enclosures with Participating Media," *J. of Heat Transfer*, Vol. 112, pp. 415-423.

RATZEL III, A.C. and HOWELL, J.R., 1983 "Two-Dimensional Radiation in Absorbing Emitting Media Using the P-N Approximation," *J. of Heat Transfer*, Vol. 105, pp. 333-340.

RAZZAQUE, M.M., KLEIN, D.E. and HOWELL, J.R., 1983 "Finite Element Solution of Radiative Heat Transfer in a Two-Dimensional Rectangular Enclosure with Gray Participating Media," *J. of Heat Transfer*, Vol. 105, No. 4, pp.933-934.

RAZZAQUE, M.M., KLEIN, D.E. and HOWELL, J.R., 1984 "Coupled Radiative Conductive Heat Transfer in a Two-Dimensional Rectangular Enclosure with Gray Participating Media Using Finite Elements," *J. of Heat Transfer*, Vol.106, No.3, pp. 613-619.

REDDY, J. N., 1982 "On Penalty Function Methods in the Finite-Element Analysis of Flow Problems," *Int. J. Numer. Methods Fluids*, Vol. 2, pp. 151-171.

REGGIO, M., and CAMARERO, R., 1986 "Numerical Solution Procedure for Viscous Incompressible Flows," *Numerical Heat Transfer*, Vol. 10, pp. 131-146.

RHIE, C.M., and CHOW, W.L., 1983 "Numerical Study of the Turbulent Flow Past an Airfoil with Trailing Edge Separation," *AIAA J.*, Vol. 21, No.11, pp. 1525-1532.

RICE, J.G., SCHNIPKE, R.J., 1985 "A Monotone Streamline Upwind Finite Element Method for Convection-Dominated Flows," *Comp. Meth. Appl. Mech. Eng.*, Vol. 48,

pp. 313-327.

RICE, J.G., SCHNIPKE, R.J., 1986 "An Equal-Order Velocity-Pressure Formulation That Does Not Exhibit Spurious Pressure Modes," *Comp. Meth. Appl. Mech. Eng.*, Vol. 58, pp. 135-149.

RICHARDSON, J.N., HOWARD, H.C. and SMITH, R.W., 1953 "The Relation Between Sampling-Tube Measurements and Concentration Fluctuations in a Turbulent Gas Jet," *Fourth Symposium (Intl) on Combustion.*

RICHTER, W. and BAUERSFELD, G., 1974 "Radiation Models for Use in Complete Mathematical Furnace Models," in Proceedings International Flame Research Foundation (IFRF), 3rd Members Conference, IJmuiden, The Netherlands, Ch. II.

RICHTER, W. and QUACK, R., 1974 "A Mathematical Model of A Low-Volatile Pulverised Fuel Flame," *Heat Transfer in Flames*, N.H. Afgan and J.M. Beer, Eds., Scripta Book Company, Washington, D.C..

RIDA, S., 1993 *Méthode de Volumes Finis pour la Simulation Numérique D'Ecoulements Turbulents sur des Maillages non Structurés,* M.Sc.A Thesis, Ecole Polytechnique, Montréal, Québec, Canada.

ROACHE, P.J., 1976 *Computational Fluid Dynamics*, Hermosa, Albuquerque.

RODI, W., 1991 "Some Current Approaches in Turbulence Modelling," *AGARD-AR-291*, July.

RODI, W. and SCHEUERER, G., 1986 "Scrutinizing the k-ϵ Model Under Adverse Pressure Gradient Conditions," *J. Fluids Eng.*, Vol. 108, pp. 174-179.

ROGG, B., BEHRENDT, F., and WARNATZ, J., 1986 "Turbulent Non-Premixed Combustion in Partially Premixed Diffusion Flamelets with Detailed Chemistry," *Twenty-First Symposium (Int.) on Combustion/The Combustion Institute*, pp. 1533-1541.

SAABAS, H.J., 1991 *A Control Volume Finite Element Method for Three-Dimensional, Incompressible, Viscous Fluid Flow,* Ph.D. Thesis, McGill University, Montreal, Quebec, Canada.

SALTIEL, C. and NARAGHI, M.H.N., 1990 "Analysis of Radiative Heat Transfer in Participating Media Using Arbitrary Nodal Distribution," *Numerical Heat Transfer*, Part B, Vol. 17, pp. 227-243.

SALTIEL, C.J. and NARAGHI, M.H.N., 1991 "An Exchange Factor Method for Analysis of Radiative Heat Transfer in Nonhomogeneous Media," *HTD-Vol. 160, Fundamentals of Radiation Heat Transfer*, ASME 1991, pp. 55-68.

SANCHEZ, A. and SMITH, T.F., 1992 "Surface Radiation Exchange for Two-Dimensional Rectangular Enclosures Using the Discrete-Ordinates Method," *Journal of Heat Transfer*, Vol. 114, pp.465-472.

SCHNEIDER, G.E. and RAW, M.J., 1986 "A Skewed, Positive Influence Coefficient Upwinding Procedure for Control-Volume-Based Finite-Element Convection-Diffusion Computation," *Numerical Heat Transfer*, Vol. 9, pp. 1-26.

SCHNEIDER, G.E. and RAW, M.J., 1987 "Control Volume Finite-Element Method for Heat Transfer and Fluid Flow Using Colocated Variables - 1. Computational Procedure," *Numerical Heat Transfer*, Vol. 11, pp. 363-390.

SCHNEIDER, G.E. and KARIMIAN, S.M.H., 1992 "Advances in Control-Volume-Based Finite Element Methods for Compressible Flows," *International Conference on Computational Engineering Science*, Dec. 17-22, Hong Kong.

SHAH, N.G., 1979 *New Method of Computation of Radiant Heat Transfer in Combustion Chambers*, Ph.D. Thesis, Imperial College, University of London, England.

SHARIF, M.A.R. and BUSNAINA, A.A., 1988 "An Investigation into the Numerical Dispersion Problem of the Skew Upwind Finite Difference Scheme," *Appl. Math. Modelling*, Vol. 12, pp. 98-108.

SHARMA, L.K. and OSTERMIER, B.J., 1987 "Flowfield Characteristics of an Axi-symmetric 180-degree Turnaround Duct," *Proc. of the 5th SSME CFD Workshop*, NASA/MSFC, Huntsville, Alabama, April 21-23.

SHYY, W., and VU, T.C., 1991 "On the Adoption of Velocity Variable and Grid System for Fluid Flow Computation in Curvilinear Coordinates," *J. Comp. Phys.*, Vol. 92, pp. 82-105.

SHEMIRANI, F., JAMBUNATHAN, K., 1992 "Conservation Monotone Streamline Upwind Formulation Using Simplex Elements," *Int. J. for Numerical Methods in Fluids*, vol. 14, pp. 1245-1257.

SIDDALL, R.G. and SELCUK, N., 1974 "The Application of Flux Methods to Prediction of the Behavior of a Process Gas Heater," *Heat Transfer in Flames*, N.H. Afgan and J.M. Beer, eds., Scripta Book Company, Washington, D.C., pp. 191-200.

SIEGEL, R. and HOWELL, J.R., 1981 *Thermal Radiation Heat Transfer*, Second Edition, McGraw Hill, New York, London, pp. 453.

SHIH, T.M., TAN, C.H. and HWANG, B.C., 1989 "Equivalence of Artificial Compressibility Method and Penalty-Function Method," *Numerical Heat Transfer*, Part B, Vol. 15, pp. 127-130.

SMITH, K.M., COPE, W.K. and VANKA, S.P., 1993 "A Multigrid Procedure for Three-Dimensional Flows on Non-orthogonal Collocated Grids," *Int. J. Numer. Methods Fluids*, Vol. 17, pp.887-904.

SMITH, P.J. and SMOOT, L.D., 1981 "Turbulent Gaseous Combustion Part II: Theory and Evaluation for Local Properties", *Combustion and Flame*, vol.42, pp.277-285, 1981.

SPALDING, D.B., 1971a "Concentration Fluctuations in a Round Turbulent Free Jet", *Chemical Engineering Science*, Vol.26, pp.95-107.

SPALDING, D.B., 1971b "Mixing and Chemical Reaction in Steady Confined Turbulent Flames", *Thirteenth Symposium (Int.) on Combustion*, pp. 649-657.

SPALDING, D.B., 1972 "A Novel Finite Difference Formulation for Differential Expressions Involving Both First and Second Derivatives," *Int. J. Numer. Meth. Eng.*, Vol. 4, pp. 551-559.

SPALDING, D.B., 1980 "Mathematical Modelling of Fluid Mechanics, Heat Transfer and Mass Transfer Processes," Imperial College, London, Mechanical Eng. Department, Report No. HTS/80/1.

SPEZIALE, C.G., ABID, R. and CLAY ANDERSON, E., 1992 "Critical Evaluation of Two-Equation Models for Near-Wall Turbulence," *AIAA J.*, Vol. 30, No. 2, pp.324-331.

SPEZIALE, C.G. and THANGAM, S., 1992 "Analysis of an RNG Based Turbulence Model for Separated Flows," *Int. J. Eng. Sci.*, Vol. 30, No. 10, pp.1378-1388.

STEWARD, F.R. and CANNON, P., 1971 "The Calculation of Radiative Heat Flux in a Cylindrical Furnace Using the Monte Carlo Method," *Int. J. Heat Mass Transfer,* Vol. 14, pp. 245-262.

TAN, Z.Q., 1989 "Radiative Heat Transfer in Multi-dimensional Emitting, Absorbing, and Anisotropic Scattering Media: Mathematical Formulation and Numerical Method," *J. of Heat Transfer*, Vol. 111, pp. 141-147.

TANIGUCHI, H., 1969 "The Radiative Transfer of Gas in a Three Dimensional System Calculated by Monte Carlo Method," *Bull. JSME*, Vol. 12, pp.67-78.

TAYLOR, P.B. and FOSTER, P.J., 1974 "The Total Emissivities of Luminous and Non-Luminous Flames," *Int. J. Heat Mass Transfer*, Vol. 17, pp. 1591-1605.

THIART, G.D., 1990 "Finite Difference Scheme for the Numerical Solution of Fluid Flow and Heat Transfer Problems on Nonstaggered Grids," *Numerical Heat Transfer*, Part B, Vol. 17, pp. 43-62.

THOMASSET, F., 1981 *Implementation of Finite Element Methods for Navier-Stokes Equations*, Springer-Verlag, New York.

THOMPSON, J.F. and WARSI, Z.U.A. and MASTIN, C.W., 1985 *Numerical Grid Generation Foundations and Applications*, North-Holland, New York.

TRUELOVE, J.S., 1974 "Mathematical Modelling of Radiant Heat Transfer in Furnaces," *AERE Report*, AERE-R7817.

TRUELOVE, J.S., 1988 "Three-Dimensional Radiation in Absorbing-Emitting-Scattering Media Using the Discrete-Ordinate Approximation," *J. Quant. Spectrosc. Radiat. Transfer,* Vol. 39, No. 1, pp. 27-31.

TURKEL, E., 1987 "Preconditioned Methods for Solving the Incompressible and Low Speed Compressible Equations," *J. of Computational Physics*, Vol. 72., pp. 277-298.

VAN DOORMAAL, J.P. and RAITHBY, G.D., 1984 "Enhancements of the SIMPLE Method for Predicting Incompressible Fluid Flows," *Numerical Heat Transfer*, Vol. 7, pp. 147-163.

VAN DOORMAAL, J.P., TURAN,A., and RAITHBY, G.D., 1987 "Evaluation of New Techniques for the Calculation of Internal Recirculating Flows," *AIAA-87-0059, AIAA 25th Aerospace Science Meeting*, Reno, Nevada, Jan. 12-15.

VAN DRIEST, E.R., 1956 "On Turbulent Flow Near a Wall," *Journal of the Aeronautical Sciences*, Vol. 23, pp. 1007-1011.

VISKANTA, R. and MENGÜÇ, 1987 "Radiation Heat Transfer in Combustion Systems," *Progress in Energy and Combustion Science*, Vol. 13, No. 2, pp. 97-160.

VOS, J.B., 1987 "Calculating Turbulent Reacting Flows Using Finite Chemical Kinetics," *AIAA Journal*, Vol. 25, No.10, pp. 1365-1372.

WAKIL, N.El and SACADURA,J.F., 1992 "Some Improvements of the Discrete Ordinates Methods for the Solution of the Radiative Transport Equation in Multidimensional Anisotropically Scattering Media," HTD-Vol. 203, *Developments in Radiative Heat Transfer*, ASME, pp. 119-127.

WARE, J.M., and M. Berzins, 1992 "Finite Volume Techniques for Time-Dependent Fluid-Flow Problems," *Advances in Computer Methods for Partial Differential Equations VII*, R.Vichnevetsky, D. Knight and G. Richter (Editors), IMACS.

WESTPHAL, R.V., JOHNSTON, J.P. and EATON, J.K., 1984 "Experimental Study of Flow Reattachment in a Single-Sided Sudden Expansion," NASA Contractor Report 3765, Report MD-41, Stanford University.

WESTBROOK, C.K., and DRYER, F.L., 1981 "Simplified Reaction Mechanisms for the Oxidation of Hydrocarbon Fuels in Flames," *Combust. Sci. and Tech.*, Vol. 27, pp.31-43.

WILCOX, D.C., 1988 "Reassessment of the Scale-Determining Equation for Advanced Turbulence Models," *AIAA J.*, Vol. 26, No.11, pp. 1299-1310.

WILCOX, D.C., 1993a "A Two-Equation Turbulence Model for Wall-Bounded and Free-Shear Flows," *AIAA 93-2905, AIAA 24th Fluid Dynamics Conference*, July 6-9,

Orlando, FL.

WILCOX, D.C., 1993b "Comparison of Two-Equation Turbulence Models for Boundary Layers with Pressure Gradients," *AIAA J.*, Vol. 31, No.8, pp. 1414-1421.

WILLIAMS, F.A., 1965 *Combustion Theory*, Addison-Wesley, Reading. Mass..

WU, H.L. and FRICKER, N., 1971 "An Investigation of the Behaviour Swirling Jet Flames in a Narrow Cylindrical Furnace," *2nd Membery Conference of the IFRF.*

YAKHOT, V. and ORSZAG, S.A., 1986 "Renormalization Group Analysis of Turbulence, I. Basic Theory," *J. Sci. Comput.*, Vol. 1, pp.3-51.

YUEN, W.W., MA, A.K. and TAKARA, E.E., 1992 "Evaluation of Radiative Heat Transfer Using the Generalized Zonal Method and the Absorption Mean Beam Length Concept," HTD-Vol. 203, *Developments in Radiative Heat Transfer*, ASME, pp. 265-273.

ZHU, J. and RODI, W., 1992 "Computatiuon of Axisymmetric Confined Jets in a Diffuser," *Int. J. Numer. Meth. Fluids*, Vol. 14, pp. 241-251.

ZUERCHER, J.W., and ROZON, B.J., 1993 "Validation of a Two-Layer Turbulence Model Using Channel, Step and Turnaround Duct Data," *AIAA 93-3028, AIAA 24th Fluid Dynamics Conference*, July 6-9, Orlando, FL.

Appendix A: Integration of Pressure in Axisymmetric Coordinate

Substituting Eq. (4.29) into Eq. (4.28), it gives:

$$\int_{\Omega_c} r\nabla P dV = \sum_{j=1}^{4} r_j P_j \vec{n}_j s_j - \begin{pmatrix} 0 \\ \int_{\Omega_c} P dV \end{pmatrix} \tag{A.1}$$

when splitting Eq. (A.1) into theirs respective half co-volume, it becomes:

$$\int_{\Omega_c} r\nabla P dV = \sum_{j=1}^{2} r_j P_j \vec{n}_j s_j - \begin{pmatrix} 0 \\ A_{Lc} P_L \end{pmatrix} + \sum_{j=3}^{4} r_j P_j \vec{n}_j s_j - \begin{pmatrix} 0 \\ A_{Rc} P_R \end{pmatrix} \tag{A.2}$$

where j = 1,2,3 and 4 represent the midpiont of integration faces, A_{Lc} and A_{Rc} are the area of the left and right half co-volume, and P_L and P_R are pressure of the left and right elements, respectively.

Considering the integration (A.2) of left half co-volume, as shown in Figure A.1, it can be rewritten as following:

$$\int_{\Omega_{Lc}} r\nabla P dV = \begin{pmatrix} P_L r_1 n_{x1} s_1 \\ P_L r_1 n_{y1} s_1 \end{pmatrix} + \begin{pmatrix} P_L r_2 n_{x2} s_2 \\ P_L r_2 n_{y2} s_2 \end{pmatrix} - \begin{pmatrix} 0 \\ A_{Lc} P_L \end{pmatrix} \tag{A.3}$$

According to the geometry depicted in Figure A.1, the normals of each faces can be written as follows:

$$\begin{cases} s_1\vec{n}_1 = -\Delta y_1\vec{i} + \Delta x_1\vec{j} \\ s_2\vec{n}_2 = -\Delta y_2\vec{i} - \Delta x_2\vec{j} \\ s_0\vec{n}_0 = \Delta y_0\vec{i} + \Delta x_0\vec{j} \end{cases} \tag{A.4}$$

with the radius relations:

$$\begin{cases} r_1 = r + \frac{1}{2}\Delta y_1 + \Delta y_2 \\ r_2 = r + \frac{1}{2}\Delta y_2 \\ r_0 = r + \frac{1}{2}\Delta y_0 \end{cases} \tag{A.5}$$

Next, we want to derive the geometric relation between the integration face j=1,2 and the co-volume side 0. Mathematically, we want to verfy the following relations is held or not:

$$r_1\vec{n}_1 s_1 + r_2\vec{n}_2 s_2 + r_0\vec{n}_0 s_0 \stackrel{?}{=} 0 \tag{A.6}$$

or the equivalent x- and y-components form of Eq.(A.6) as:

$$r_0\Delta y_0 - r_1\Delta y_1 - r_2\Delta y_2 \stackrel{?}{=} 0 \tag{A.7a}$$

Relation of (A.7a)

Substituting the radius relations (A.5) into Eq.(A.7a), we have:

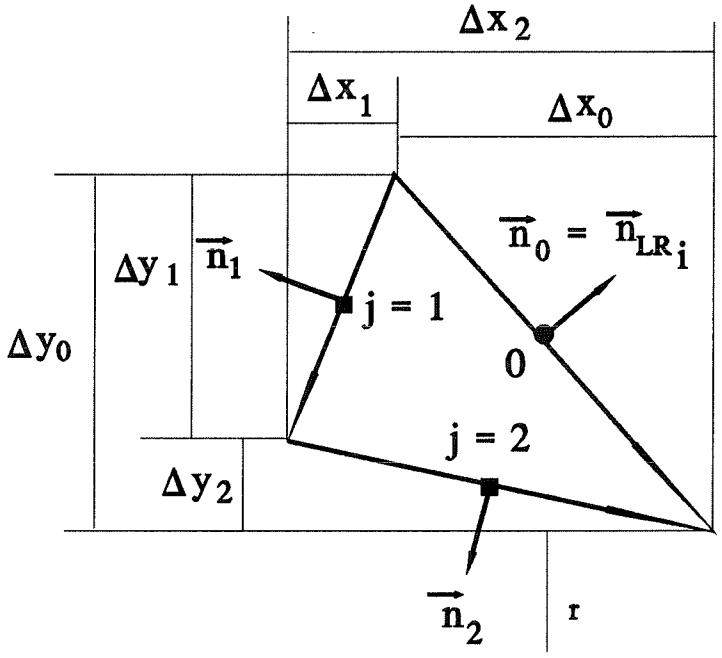

Figure A.1: Left half co-volume used in the derivation of pressure integration for an axisymmetric coordinate

$$\begin{aligned} r_0 \Delta y_0 &= (r+\frac{1}{2}\Delta y_0)\Delta y_0 \\ &= r(\Delta y_1+\Delta y_2)+\frac{1}{2}(\Delta y_1+\Delta y_2)^2 \end{aligned} \tag{A.8a}$$

and

$$\begin{aligned} -r_1\Delta y_1 - r_2\Delta y_2 &= -(r+\frac{\Delta y_1}{2}+\Delta y_2)\Delta y_1 - (r+\frac{\Delta y_2}{2})\Delta y_2 \\ &= -r(\Delta y_1+\Delta y_2)-\frac{1}{2}(\Delta y_1+\Delta y_2)^2 \end{aligned} \tag{A.8b}$$

Summing the relations (A.8a) and (A.8b), then the relation (A.7a) is held.

Relation of (A.7b)

$$\begin{aligned} r_0\Delta x_0 &= (r+\frac{\Delta y_1}{2}+\frac{\Delta y_2}{2})(\Delta x_2-\Delta x_1) \\ &= r(\Delta x_2-\Delta x_1)+\Delta x_2\frac{\Delta y_1}{2}+\Delta x_2\frac{\Delta y_2}{2}-\Delta x_1\frac{\Delta y_1}{2}-\Delta x_1\frac{\Delta y_2}{2} \end{aligned} \tag{A.9a}$$

$$\begin{aligned} r_1\Delta x_1-r_2\Delta x_2 &= (r+\frac{\Delta y_1}{2}+\Delta y_2)\Delta x_1-(r+\frac{\Delta y_2}{2})\Delta x_2 \\ &= -r(\Delta x_2-\Delta x_1)-\Delta x_2\frac{\Delta y_2}{2}+\Delta x_1\frac{\Delta y_1}{2}+\Delta x_1\Delta y_2 \end{aligned} \tag{A.9b}$$

Summing the relations Eq. (A.9a) and (A.9b), then we have:

$$r_0\Delta x_0+r_1\Delta x_1-r_2\Delta x_2 = \frac{\Delta x_1\Delta y_2}{2}+\frac{\Delta x_2\Delta y_1}{2} \tag{A.10}$$

Then the equation (A.7b) is not held.

The area of the left co-volume is:

$$\begin{aligned} A_{Lc} &= \frac{1}{2}|-\Delta x_2\Delta y_0+\Delta y_2\Delta x_0| \\ &= \frac{1}{2}|-\Delta x_2(\Delta y_1+\Delta y_2)+\Delta y_2(\Delta x_2-\Delta x_1)| \\ &= |-\frac{\Delta x_1\Delta y_2}{2}-\frac{\Delta x_2\Delta y_1}{2}| \end{aligned} \tag{A.11}$$

then Eq. (A.10) becomes:

$$r_0\Delta x_0 + r_1\Delta x_1 - r_2\Delta x_2 = A_{Lc} \tag{A.12}$$

Substituting Eq. (A.7a) and (A.12) into Eq. (A.3), then it becomes:

$$\int_{\Omega_{Lc}} r\nabla P dV = -r_0\vec{n}_0 s_0 P_L \tag{A.13}$$

Similar result is obtained for right hand side integration of the co-volume, it gives:

$$\int_{\Omega_{Rc}} r\nabla P dV = r_0\vec{n}_0 s_0 P_R \tag{A.14}$$

Summing Eq. (A.13) and (A.14), we have:

$$\int_{\Omega_c} r\nabla P dV = r_0\vec{n}_0 s_0 (P_R - P_L) \tag{A.15}$$

Eq. (A.15) is used in the derivation of the pressure-velocity coupling relation for obtaining the pressure algebraic equation.